Calcul optimal pour la modélisation de la dynamique naturelle des plages sableuses et la conception d'ouvrages de défense du littoral à faible impact anthropique

Megan Cook

THÈSE POUR OBTENIR LE GRADE DE DOCTEUR
DE L'UNIVERSITÉ DE MONTPELLIER

En Sciences de la Terre et de l'Eau

École doctorale GAIA

Unité de recherche UMR 5243 - Géosciences

Calcul optimal pour la modélisation de la dynamique naturelle des plages sableuses et la conception d'ouvrages de défense du littoral à faible impact anthropique

Présentée par Megan Cook

Le 10 décembre 2021

Sous la direction de Frédéric Bouchette et Bijan Mohammadi

Devant le jury composé de

Frédéric Bouchette	MCF HDR	Université de Montpellier	Invité
Rodolphe Cattin	PR	Université de Montpellier	Examinateur
France Floc'h	MCF HDR	Université de Bretagne Occidentale	Examinatrice
Nicolas Fraysse	Ingénieur	BRLi	Invité
François James	PR	Université d'Orléans	Président du jury
Bijan Mohammadi	PR	Université de Montpellier	Co-directeur
Damien Sous	MCF HDR	Université de Toulon	Rapporteur
Marissa Yates	CR HDR	Laboratoire d'Hydraulique Saint-Venant	Rapporteure

UNIVERSITÉ DE MONTPELLIER

Résumé

Les travaux de cette thèse portent sur l'application de la théorie de l'optimisation en zone littorale à travers trois études.

La première concerne une application classique d'ingénierie côtière. La problématique porte sur le ré-aménagement d'un port dans le but d'agrandir sa surface exploitable et simultanément réduire l'agitation des vagues, en l'occurrence, le port de La Turballe en France. Pour ce faire, l'introduction d'une digue et d'un môle a été proposée, dont les dimensions font l'objet d'une étude par optimisation.

Une deuxième étude, qui est le cœur de la thèse, concerne une nouvelle approche pour décrire la dynamique littorale des plages sableuses par la théorie de l'optimisation. Un nouveau modèle morphodynamique est développé, basé sur l'hypothèse que le profil bathymétrique d'une plage varie au cours du temps afin de minimiser une certaine quantité hydrodynamique. Le modèle numérique qui découle de cette théorie a été entièrement développé lors de la thèse, et est baptisé Opti-Morph. Les résultats numériques montrent le potentiel d'un modèle morphodynamique basé sur la théorie de l'optimisation, et ce malgré un modèle hydrodynamique simple. Opti-Morph a aussi l'avantage d'être rapide, robuste et de faible complexité.

La troisième étude cherche à coupler les deux études précédentes, c'est-à-dire une analyse d'ingénierie par optimisation couplée avec la réponse morphodynamique, décrite par Opti-Morph. Ici, nous cherchons à déterminer la position optimale d'un géotube le long du profil cross-shore, tout en tenant compte de la réponse morphodynamique de la plage. Les résultats numériques montrent non seulement l'emplacement optimal de géotubes, mais démontrent également l'efficacité d'Opti-Morph face à ces structures artificielles et son potentiel en tant qu'outil d'ingénierie côtière.

Mots-clés : optimisation, ingénierie côtière, dynamique littorale, morphodynamique, modélisation numérique, Opti-Morph, aménagement portuaire, hydrodynamique, analyse du trait de côte, brise-lames

Abstract

The work of this thesis focuses on the application of optimization theory in coastal areas by the means of three studies.

The first concerns a classic coastal engineering application. The problem focuses on the redesign of a port in order to increase its exploitable surface and simultaneously reduce the agitation of the waves, in our case, the port of La Turballe in France. To do this, the introduction of a jetty and a mole was proposed, the dimensions of which will be the subject of an optimization study.

A second study, which is at the heart of this thesis, concerns a new approach in describing the coastal dynamics of sandy beaches through optimization theory. A new morphodynamic model is developed, based on the assumption that the seabed at the coast varies over time in order to minimize a certain hydrodynamic quantity. The numerical model resulting from this theory was entirely developed during the thesis, and is called Opti-Morph. The numerical results demonstrate the potential of a morphodynamic model based on optimization theory, despite a simple hydrodynamic model. Opti-Morph also has the advantage of being fast, robust, and of low complexity.

The third study aims to combine the two previous studies, that is a coastal engineering analysis by optimization coupled with the morphodynamic response of the seabed, described by Opti-Morph. Here, we seek to determine the optimal position of a geotube along the cross-shore profile, while taking into account the morphodynamic response of the seabed. The numerical results not only describe the optimal location of geotubes, but also demonstrate the effectiveness of Opti-Morph with regards to these man-made structures and its potential as a coastal engineering tool.

Keywords: optimization, coastal engineering, coastal dynamics, morphodynamics, numerical modelling, Opti-Morph, harbour design, hydrodynamics, shoreline analysis, breakwaters

Cette thèse a été financée par BRL ingénierie.

To my grandad Jack

Remerciements

I would like to start by expressing my gratitude to my Ph.D. advisors Frédéric Bouchette and Bijan Mohammadi for their guidance, advice, and their hands-on mentoring. Thank you for always making time for my questions and remarks, and for all the lessons you imparted, both regarding my Ph.D. work and general life lessons.

I also wish to thank my industrial supervisor, Nicolas Fraysse, for his leadership and support. I am immensely grateful to BRLi for financing my Ph.D. You gave me the opportunity to pursue a subject I love, and apply it to a real-life, practical project. Your faith in me is greatly appreciated.

I wish to thank the jury for participating in my Ph.D. defense. Thank you to Damien Sous and Marissa Yates for their thorough report, their interesting remarks, and necessary corrections. Thank you to François James, for presiding the jury and offering many interesting comments. Thank you also to France Floc'h and Rodolphe Cattin. Your questions during the defense were both interesting and useful.

I wish to thank everyone at BRLi who helped and guided me in this work, both on the La Turballe project and the design of Opti-Morph. A special thanks to Nicolas Proust, Gaetan Dufour and Ludovie Le Coz.

Thank you also to the BRL administrative staff for their assistance with the BRLi administration, including Olivia Schetrit Belmar, Marine Toniutti, and Laëtitia Paska. Thank you to Fabienne Roussie for her help with the ANRT registration and for making sure all the paperwork was attended to in a timely manner. Thank you also to Hélène Ournat, Sophie Cazanave-Pin, Pauline Passera, Cendrine Jay-Allemand, and all the others from the University of Montpellier for their assistance with the university administration.

Furthermore, I wish to thank Benoît Ildefonse, Serge Lallemand and Fabrice Grosbeau for their kindness and professionalism throughout the three years I was at the Geosciences laboratory.

Thank you to everyone I met at GLADYS. I have learnt so much about oceans, coasts, and beaches from the interesting discussions we had at the Vercors retreats. The WAWA workshop, organized by GLADYS offered an alternative, more practical vision of coastal morphodynamics, and allowed me to better understand the data I was working with and the manner it was gathered. A special shoutout goes out to Samuel Meulé, who not only offered many different suggestions concerning this manuscript but also carried out the XBeach modeling used for comparative purposes throughout the work.

Thank you to my fellow Ph.D. / Postdoc colleagues, Léa, Manon, Abder, Rémi, Marie, Enora, Adeline, and so forth. A shoutout also goes to my office colleagues Oswald and Timothée. I wish you luck in your future endeavours. Thank you to Thomas, Virginie, MC, and Tiziano for the good times we spent in the interns' office as well as Louis, Ronan, and Garance, for their remarks, questions, and corrections with regards to my manuscript and final defense presentation. I wish you all the best in your Ph.D. adventure!

I wouldn't be here today without the love and support from my amazing parents Louise and Lee. You have always been there for me and always inspired me to do my best.

Thank you to my nan Freda and grandad Jack, who knew I could do it before I did! Thank you also to my Gdad Ben and nan Judy for bestowing me with the maths genes!

Thank you to my good friends Marwa and Mohammad. We can always count on you and I hope we stay good friends. I wish you and your adorable family all the best.

And last, but not least I wish to thank my future husband André Harnist without whom I would not be here today. Thank you for your love, your support, and your patience. This marks the end of an adventure and I hope to have many more with you.

Table des Matières

Liste des Symboles

La liste suivante décrit l'ensemble des symboles utilisés dans la suite du document.

Chapitre 1

α Extension de la digue (m)

β Largeur ajoutée au môle (m)

η Amplitude des vagues (m)

η_{i} Amplitude des vagues incidentes (m)

η_{r} Amplitude des vagues réfléchies (m)

γ Longueur entre l'extrémité du mur existant et l'épi (m)

γ_{ab} Coefficient d'absorption/réflexion des frontières (m)

Λ Frontière délimitant le port (m)

Λ_{i} Frontière décrivant l'entrée du port (m)

Λ_{o} Frontière décrivant la sortie du port (m)

Λ_{w} Frontière solide du port (m)

$\mathcal{E}_n$ Énergie surfacique totale des vagues associée au scénario de forçage n (m)

$\mathcal{J}$ Fonction de coût globale à minimiser (J)

$\mathcal{J}_n$ Fonction de coût locale associée au scénario de forçage n (J)

$\mathcal{P}$ Fonction de poids (-)

Ω Domaine d'étude du port (m^2)

ψ Paramétrisation du port (m)

ρ Densité de l'eau ($kg.m^{-3}$)

σ Pulsation de l'onde (s^{-1})

θ Angle de propagation (rad)

$\vec{k}$ Vecteur d'onde (m^{-1})

a_n Amplitude des vagues associée au scénario de forçage $n(m)$

$a_{\max}$ Amplitude maximale des vagues (m)

a_{i} Composante spatiale de l'amplitude des vagues incidentes (m)

$a_{\mathrm{i}}(n)$ Amplitude des vagues forçant le système associée au scénario de forçage n (m)

a_{r} Composante spatiale de l'amplitude des vagues réfléchies (m)

f Fréquence des vagues (s^{-1})

g Accélération gravitationnelle ($m.s^{-2}$)

k Nombre d'onde (m^{-1})

$K(\mathcal{P})$ Fonction de poids intégrée sur le domaine (m^2)

N Nombre de scénarios de forçage considéré dans l'étude (-)

n Indice du scénario de forçage (-)

Chapitre 2

α Coefficient de transition pour la condition de bord

γ Critère de déferlement (-)

Λ Excitation sédimentaire par les vagues de surface (-)

$\mathcal{J}$ Fonction de coût à minimiser ($J.m^{-1}$)

Ω Domaine d'étude (m)

Ω_{B} Zone de déferlement (m)

Ω_{S} Zone de shoaling (m)

Ψ Ensemble des paramètres physiques définissant le profil bathymétrique (m)

ψ Élévation du fond (m)

ψ_0 Élévation du fond initial (m)

ρ_w Densité de l'eau ($kg.m^{-3}$)

σ Pulsation de l'onde (s^{-1})

Υ Mobilité sédimentaire ($m.s.kg^{-1}$)

φ Fonction d'atténuation de la vitesse orbitale (-)

C Vitesse de phase des vagues ($m.s^{-1}$)

C_0 Vitesse de phase des vagues forçantes ($m.s^{-1}$)

C_g Vitesse de groupe des vagues ($m.s^{-1}$)

d Direction de descente (J)

d_w Distance maximale de dépendance spatiale des vagues (m)

E Énergie des vagues forçantes cumulée en temps ($J.m^{-1}.s^{-1}$)

g Accélération gravitationnelle ($m.s^{-2}$)

H Hauteur des vagues (m)

h Profondeur de l'eau (m)

H_0 Hauteur des vagues forçantes (m)

h_0 Niveau moyen de l'eau (m)

H_0^w Hauteur des vagues pondérée en espace (m)

k Nombre d'onde (m^{-1})

K_S Coefficient de shoaling (-)

M_slope Pente maximale du profil bathymétrique (-)

n Rapport entre C et C_g (-)

T Temps maximal de la simulation (s)

w Fonction de poids (-)

$x_{\max}$ Point de la côte situé au-delà du trait de côte (m)

Chapitre 3

$\mathcal{J}$ Fonction de coût pour la réponse morphodynamique $(J.m^{-1})$

$\mathcal{J}_{\mathrm{G}}$ Fonction objective pour le déploiement de géotube basé sur la position du trait de côte (m)

Ω Domaine d'étude (m)

Ω_{G} Domaine de positions possible de déploiement de géotube (m)

ψ Élévation du fond (m)

ρ_{w} Densité de l'eau $(kg.m^{-3})$

$\tilde{\mathcal{J}}_{\mathrm{G}}$ Fonction objective pour le déploiement de géotube basé sur l'énergie des vagues $(J.m^{-1}.s^{-1})$

$d(S_{\mathrm{G}}, h_0)$ Distance verticale entre le sommet du géotube et le niveau d'eau (m)

g Accélération gravitationnelle $(m.s^{-2})$

H Hauteur des vagues (m)

h_0 Niveau moyen de l'eau (m)

M_{slope} Pente maximale du profil bathymétrique (-)

T Temps maximal de la simulation (s)

x_{G} Distance entre le trait de côte et le géotube (m)

$x_{\mathrm{G}}^{\max}$ Distance maximale de déploiement de géotube par rapport au trait de côte (m)

$x_{\max}$ Point de la côte situé au-delà du trait de côte (m)

x_{S} Position du trait de côte (m)

Chapitre 4

$(t_p)_{p\in[0,N_T]}$ Discrétisation de l'intervalle de temps $[0, T]$ (-)

$(x_p)_{p\in[0,N_\Omega]}$ Discrétisation du domaine Ω (-)

α Paramètre de déferlement (-)

α_{w} Paramètre de transition pour les conditions de bords (-)

β Paramètre de précision pour la contrainte de stock sableux (-)

χ_{AD} Terme d'anti-dissipation des vagues (-)

γ Indice de déferlement des vagues (-)

$\mathcal{E}$ Énergie potentielle des vagues ($J.m^{-1}$)

$\mathcal{E}_{\mathrm{B}}$ Énergie potentielle des vagues dans la zone de déferlement ($J.m^{-1}$)

$\mathcal{E}_{\mathrm{S}}$ Énergie potentielle des vagues dans la zone de shoaling ($J.m^{-1}$)

$\mathcal{J}$ Fonction de coût à minimiser ($J.m^{-1}$)

$\mathcal{J}_{\mathrm{pen}}$ Fonction de coût incorporant le terme de pénalisation pour la contrainte de stock sableux ($J.m^{-1}$)

Ω Domaine d'étude (m)

Ω_{B} Zone de déferlement (m)

Ω_{S} Zone de shoaling (m)

Ψ Ensemble des paramètres définissant le profil bathymétrique (m)

ψ Élévation du fond (m)

ψ_0 Élévation du fond initial (m)

ψ_t Évolution du profil bathymétrique en temps ($m.s^{-1}$)

ρ_{w} Densité de l'eau ($kg.m^{-3}$)

σ Pulsation de l'onde (s^{-1})

Υ Mobilité sédimentaire ($m.s.kg^{-1}$)

φ Fonction d'atténuation de la vitesse orbitale (-)

a_{AD} Premier paramètre dans le terme d'anti-dissipation (-)

B Élévation du substrat rocheux (m)

b_{AD} Deuxième paramètre dans le terme d'anti-dissipation (-)

C Vitesse de phase des vagues ($m.s^{-1}$)

C_0 Vitesse de phase des vagues forçantes ($m.s^{-1}$)

C_g Vitesse de groupe des vagues ($m.s^{-1}$)

C_sand Différence entre le stock sableux initial et actuel (-)

d Direction de descente (J)

d_win Distance maximale de dépendance spatiale des vagues (m)

g Accélération gravitationnelle ($m.s^{-2}$)

H Hauteur des vagues (m)

h Profondeur de l'eau (m)

H_0 Hauteur des vagues forçantes (m)

h_0 Niveau moyen de l'eau (m)

H_0^w Hauteur des vagues pondérée en espace (m)

k Nombre d'onde (m^{-1})

K_S Coefficient de shoaling (-)

L Longueur d'onde (m)

M_slope Pente maximale du profil bathymétrique (-)

n Rapport entre la vitesse de phase et la vitesse de groupe (-)

N_Ω Nombre de points dans la discrétisation de Ω (-)

N_T Nombre de points dans la discrétization de l'intervalle de temps $[0, T]$ (-)

T Temps maximal de la simulation (s)

T_0 Période de l'onde (m)

w Fonction de poids (-)

x_B Position du (premier) déferlement le long du profil cross-shore (m)

x_max Point de la côte situé au-delà du trait de côte (m)

x_S Position du trait de côte (m)

Introduction

L'optimisation est une science qui permet de trouver la forme optimale à quelque chose vis-à-vis d'un critère, généralement une valeur réelle, que l'on calcule à partir d'une expression représentant l'état du système. On l'appelle fonctionnelle, ou encore fonction de coût. L'expression de la fonction de coût est choisie de telle sorte que pour trouver la forme optimale, on doit la minimiser (alternativement, la faire tendre vers une valeur particulière). Pour illustrer l'idée de l'optimisation, on utilise souvent l'image de l'aile d'avion : on cherche la forme la plus adaptée d'une aile pour réduire la traînée et maximiser la portance. Une fonction de coût reformulant correctement cet objectif est par exemple le rapport de la traînée sur la portance. La théorie de l'optimisation a souvent été à l'origine de développements industriels majeurs dans des disciplines à fort potentiel technologique (aéronautique, robotique, trains, ponts & chaussées). Pour tout problème basé sur une telle approche, il va de soi que le choix de la fonctionnelle est crucial pour espérer trouver une forme réellement optimale par rapport au problème posé.

1 Contexte de la Thèse

A l'Université de Montpellier, les laboratoires Géosciences-Montpellier et l'Institut de Mathématiques A. Grothendieck en partenariat avec l'entreprise BRLi travaillent depuis 2007 sur la formulation d'une théorie de l'optimisation adaptée au domaine de l'hydromorphodynamisme littoral, des développements numériques basés sur cette théorie et conçus pour inventer des systèmes optimaux de protection du littoral contre la submersion, l'érosion littorale, l'impact des vagues contre les ouvrages, etc. Les chercheurs et les ingénieurs adoptent des points de vue du type *soft-engineering* (modifier le comportement naturel finement, sans chercher à s'opposer très frontalement à la nature) ou de *reverse environmental engineering* (décortiquer comment le système naturel fonctionne, modifier par contrôle optimal un aspect de sa dynamique assez éloigné du problème mais bien compris, et laisser la nature résoudre le problème d'elle-même). En pratique, ce partenariat a jusqu'à présent réussi à (i) formuler et valoriser certains aspects théoriques, (ii) développer un premier ensemble d'outils numériques pour réaliser le calcul optimal, (iii) appliquer la démarche complète à plusieurs cas simples, validés en

canal à houle et bassins à houle dans des conditions contrôlées, (iv) mise en œuvre de manière totalement opérationnelle du principe de dimensionnement optimal d'ouvrages de protection littorale, dans le cadre de projets financés par l'état, l'Europe et les collectivités. Ces derniers développements ont notamment été menés sur le lido de Sète (façade méditerranéenne) où des géotubes furent déployés selon les recommandations du calcul optimal.

La compréhension de l'hydro-morphodynamisme littoral (comment les vagues et le sable se comportent en zone de plage) et le développement d'outils et concepts liés à l'aménagement littoral et portuaire sont au cœur de la stratégie de spécialisation de la région Occitanie. Ce projet a permis à la région de renforcer sa position de leader international sur le sujet de l'innovation en matière de systèmes de protection du littoral, notamment grâce à l'export du savoir-faire acquis par BRLi et la valorisation scientifique de l'Université de Montpellier sur le sujet.

L'ambition du partenariat fut de lancer une seconde phase de développement R&D autour de cette thématique après les succès prometteurs rencontrés. Il est important de constater que les travaux académiques liés à ce sujet ont été valorisés en début d'activité, mais sous exploités depuis 2009. Les objectifs généraux furent donc à la fois de finaliser certains développements déjà bien avancés, et de continuer à progresser sur tous les aspects du sujet. Pour mieux organiser les travaux, le partenariat découpa son activité en trois axes de développement décrits ci-dessous.

1.1 Axe 1 : Développement Théorique

L'objectif est de franchir une seconde étape dans l'approche théorique du calcul optimal en zone littorale en modélisant dans un même mouvement la forme des ouvrages de protection d'une plage et ses transformations morphologiques. Il s'agit de créer un nouvel outil capable de trouver la meilleure forme à un problème de protection du littoral alors même que le modèle est en train de prédire comment le sable se déplace. Une telle idée est très innovante car elle permet de contourner deux points épineux en génie côtier : (i) actuellement, aucun modèle numérique de morphodynamique littorale n'était capable de prédire correctement la dynamique sédimentaire d'un système sans efforts de paramétrisation substantiels. Ceci fut dû à un manque de connaissance théorique sur la physique complexe du transport sédimentaire de plage ; les premiers tests de modélisation de la morphodynamique par optimisation paraissaient efficaces dans la prédiction du profil du fond de la plage, sans recours à une paramétrisation lourde ; (ii) l'outil d'optimisation s'intéresse dans un même mouvement aux questions de submersion marine et d'érosion du littoral, les deux problématiques étant souvent intimement liées et au cœur des préoccupations des décideurs et des gestionnaires du littoral. En général, ces deux problèmes sont traités séparément.

1.2 Axe 2 : Développement Opérationnel

L'outil de calcul optimal qui fut utilisé pour les projets comme le lido de Sète et la plage de Tel Aviv, était certes efficace, mais son développement restait fragile, confidentiel, et basé sur des développements théoriques. L'objectif est d'implémenter une version robuste de l'outil d'optimisation, suffisamment claire pour pouvoir être mise dans les mains d'ingénieurs moins spécialisés que les utilisateurs actuels. Il se peut que le transfert de compétence de la recherche vers l'ingénierie pose problème du fait d'une écriture des outils numériques trop obscure et réservée à un public très averti. L'ambition est que les approches par calcul optimal deviennent la future référence en matière d'aménagement littoral.

1.3 Axe 3 : Validation Lourde In-situ et en Milieu Contrôlé

Les développements théoriques de l'Axe 1 et la mise en place d'un nouvel outil opérationnel dans l'Axe 2 nécessitent des exercices récurrents de validation en conditions réalistes. L'objectif est de réaliser ces validations sur deux sites distincts : (i) un site sur les secteurs de l'Espiguette et Port-Camargue, pour gérer les aspects d'ensablement portuaire et de submersion littorale en contexte ouvert ; (ii) un site sur le secteur de Béziers incluant Port-la-Nouvelle. Ces deux zones sont au cœur des préoccupations à la fois des scientifiques et de la région Occitanie. En effet, des mesures récurrentes furent relevés dans le cadre du SOLTC (www.soltc.org) et de GLADYS (www.gladys-littoral.org), et Port-Camargue et Port-la-Nouvelle sont deux lieux emblématiques de la stratégie de développement d'éco-cités portuaires en façade Méditerranée. La validation consiste à (i) réaliser systématiquement sur ces deux sites des tests en condition réelle de chaque fonctionnalité développée, et (ii) confronter l'optimiseur à la donnée métrologique de terrain (acquise dans le cadre de la plateforme GEPETO GLADYS/ SOLTC) dans différentes conditions de forçages météo-marins.

1.4 Objectifs de la Thèse

L'objectif général de la thèse est de participer au développement de l'approche du calcul optimal appliqué à la dynamique littorale. Plutôt que de s'investir dans les pistes actuelles en cours de finalisation ou valorisation, nous avons travaillé à refondre l'approche du calcul optimal appliqué au littoral, en profitant du recul dont l'équipe dispose sur la question désormais, et avec l'ambition de généraliser l'approche et la rendre opérationnelle dans un même temps. Les travaux de thèse sont essentiellement inscrits dans les Axes 1 et 2 sus-mentionnés.

2 Modélisation Mathématique du Littoral

Cette section présente les formalismes mathématiques utilisés pour modéliser les dynamismes littoraux selon une approche par optimisation.

On note $\psi : \Omega \subset \mathbb{R}^2 \rightarrow \mathbb{R}^+$ la bathymétrie qui est une fonction du temps et de l'espace, et $\boldsymbol{U}$ les variables hydrodynamiques qui nous intéressent, que ce soit l'état d'agitation de l'eau, la hauteur des vagues ou toute autre grandeur représentant les caractéristiques du fluide. On considère une fonction de coût $\mathcal{J}(\psi, \mathcal{U}(\psi))$ que nous souhaitons minimiser pour prédire d'une part le mouvement du sable et de l'autre définir les formes d'ouvrage de défense. La fonctionnelle peut intégrer des effets mémoires en portant sur $\mathcal{U}(\psi) = \{\boldsymbol{U}(\psi, \tau, x, y), \tau \in [t-T, t], (x, y) \in \Omega\}$.

Les modèles de type Saint-Venant sont un cas générique et seront utilisés dans la suite pour illustrer les concepts et les méthodes autour du calcul optimal et la dynamique bathymétrique.

2.1 Calcul Optimal Appliqué à la Dynamique Littorale

Pour fixer les idées, considérons $\boldsymbol{U}$ solution des équations de Saint Venant : $\boldsymbol{U} = {}^{\mathrm{t}}(h, h\boldsymbol{u})$ avec $\boldsymbol{u} = {}^{\mathrm{t}}(u, v)$ des vitesses moyennées verticalement où h est la profondeur d'eau. Le problème s'écrit :

$$\boldsymbol{U}_t + F(\boldsymbol{U}, \psi) = 0 \tag{1}$$

où

$$F(\boldsymbol{U}, \psi) = \begin{pmatrix} \nabla.(h\boldsymbol{u}) \\ \nabla.(h\boldsymbol{u} \otimes \boldsymbol{u}) + gh\nabla(h + \psi) \end{pmatrix}, \tag{2}$$

et soumis à des conditions initiales et aux limites.

La bathymétrie, qu'il s'agisse du sable ou des géotubes, aura sa propre dynamique suivante :

$$\begin{cases} \psi_t = -\lambda_{\mathrm{f}} \nabla_\psi \mathcal{J}(\psi, \mathcal{U}(\psi)), \\ \psi(t=0) = \psi_0, \end{cases} \tag{3}$$

où ψ_0 est donnée. Lorsqu'il s'agira de sable, $\lambda_{\mathrm{f}} > 0$ modélise la mobilité du fond. De même, λ_{f} tend vers zéro pour un fond dur ou pour une structure rigide.

La fonctionnelle peut être de la forme :

$$\mathcal{J}(\psi, \mathcal{U}(\psi)) = \int_{t-T}^{t} j(\psi, \boldsymbol{U}(\psi, \tau)) \mathrm{d}\tau \tag{4}$$

où j est une fonctionnelle à minimiser et T désigne la fenêtre temporelle d'interaction entre le fond et les vagues qui ont des échelles de dynamique temporelle différentes.

Dans ces travaux, la dynamique bathymétrique est vue comme le résultat d'une interaction entre un fluide et une structure souple : le fond sableux. Notre postulat fondamental est qu'en période de reconstruction, durant l'été par exemple, le fond

s'adapte à l'état de la mer de sorte à minimiser l'énergie de la houle, ou bien d'autres quantités qu'il faudra étudier. On postule aussi que cette adaptation prend place par petits déplacements de sable. Il s'agira de lier la vitesse de ce déplacement ψ_t à la vitesse orbitale et d'utiliser notre connaissance de cette dernière pour définir une borne supérieure pour le déplacement. Ce problème est donc un problème de transport optimal sous contrainte.

Suivant les travaux de thèse de A. Bouharguane [10], cette thèse doit améliorer la formalisation et quantification de ce postulat.

2.1.1 Fonctionnelles et Contraintes

Les vagues transportent difficilement la matière, mais ce sont de bonnes transporteuses d'énergie. Il est donc naturel de penser que si le postulat est juste, l'adaptation du fond à la houle aura pour objectif une diminution de cette énergie. Savoir minimiser l'énergie de la houle en optimisant les structures de défense est aussi utile pour la défense du littoral et la lutte contre son érosion. Cette énergie est aussi responsable de la mise en suspension du sable via la vitesse orbitale.

Considérons, par exemple, une fonctionnelle intégrant l'énergie mécanique de la houle ainsi qu'une contrainte sur les déplacements du sable modélisés par un terme de pénalisation à mémoire par rapport à l'état du fond $\psi(t-T)$ en début de la fenêtre de dépendance temporelle évoquée $[t-T, t]$:

$$\mathcal{J}_{\mathrm{f}}(\psi) = \int_{t-T}^{t} \int_{\Omega} \left(\frac{1}{2} \rho_{\mathrm{w}} g \eta^2 + \rho_{\mathrm{s}} g (\psi(\tau) - \psi(t-T))^2 \right) \mathrm{d}\tau \mathrm{d}\Omega, \tag{5}$$

où ρ_{w} et ρ_{s} sont les densités de l'eau et du sable, λ_{f} le paramètre de la mobilité, et ρ_{s} est le second paramètre qui décrit un site particulier. Ici, η est la déviation de la houle par rapport à une moyenne temporelle basse fréquence évaluée sur la fenêtre de dépendance temporelle T; η est une fonction du temps, de l'espace et de la bathymétrie :

$$\eta(x, y, \psi, t) = h(x, y, \psi, t) - \frac{1}{T} \int_{t-T}^{t} h(x, y, \psi, \tau) \mathrm{d}\tau \tag{6}$$

D'autres propositions sont possibles pour la fonctionnelle, par exemple, dans la fonctionnelle (5), on peut considérer l'amplitude A de l'onde plutôt que l'élévation :

$$A(x, y, \psi) = \max_{t \in [t-T, t]} \eta(x, y, \psi, t) \tag{7}$$

et la fonction de coût à minimiser devient :

$$\mathcal{J}_{\mathrm{f}}(\psi) = \int_{\Omega} \frac{1}{2} \rho_{\mathrm{w}} g A^2 \mathrm{d}\Omega + \int_{t-T}^{t} \int_{\Omega} \rho_{\mathrm{s}} g (\psi(\tau) - \psi(t-T))^2 \, \mathrm{d}\tau \mathrm{d}\Omega. \tag{8}$$

Un intérêt de $\mathcal{J}_{\mathrm{f}}$ est sa differentiabilité.

2.1.2 Conservation du Sable

Indépendamment du modèle utilisé pour la dynamique bathymétrique, il est intéressant de considérer la question de la quantité globale de sable mobilisable. Ce point différencie l'expérience en bassin d'une situation en mer ouverte. En effet, en bassin la quantité globale du sable pendant une expérience est en général donnée et conservée pendant l'expérience. Ceci impose une contrainte supplémentaire à prendre en compte par le modèle de bathymétrie :

$$\int_{\Omega'} \psi_t \mathrm{d}\omega = 0 \ \text{ ou } \ \int_{\Omega'} \psi \mathrm{d}\omega = C \text{ (donnée)}. \tag{9}$$

La dynamique gouvernée par (3) sera donc différente en présence de cette contrainte. C'est une des différences par rapport aux expériences en soufflerie aéronautique où ce type de contrainte n'est pas présent. Ainsi, un modèle basé sur une expérience en bassin pourrait ne pas donner le même résultat en mer ouverte.

2.2 Optimisation d'Ouvrages de Défense Littorale

En plus de caractériser l'évolution du fond marin, on peut aussi optimiser l'emplacement d'une structure. Soit $\mathcal{S}$ la paramétrisation de l'ouvrage et ψ celle du fond naturel. Nous pouvons avoir une nouvelle fonctionnelle $\mathcal{J}_\mathrm{s}(\psi+\mathcal{S}, \mathcal{U}(\psi+\mathcal{S}))$ et la minimiser en même temps que la fonctionnelle du fond naturel $\mathcal{J}_\mathrm{f}$ (décrite plus haut). Le système complet s'écrit :

$$\begin{cases} \psi_t = -\lambda_\mathrm{f} \nabla_\psi \mathcal{J}_\mathrm{f}(\psi+\mathcal{S}, \mathcal{U}(\psi+\mathcal{S})), \quad \psi(t=0) = \psi_0 \text{ donnée}, \\ \mathcal{S}_t = -\lambda_\mathrm{s} \nabla_\mathcal{S} \mathcal{J}_\mathrm{s}(\psi+\mathcal{S}, \mathcal{U}(\psi+\mathcal{S})), \quad \mathcal{S}(t=0) = \mathcal{S}_0 \text{ donnée}, \\ \boldsymbol{U}_t + F(\boldsymbol{U}, \psi) = 0, \ \text{ soumises aux conditions initiales et aux limites}, \\ \mathcal{U}(\psi+\mathcal{S}) = \{\boldsymbol{U}(\psi, \mathcal{S}, \tau, x, y), \tau \in [t-T, t], (x,y) \in \Omega\}. \end{cases} \tag{10}$$

Le terme λ_s est le pas de descente et n'a pas nécessairement de sens physique.

Pour un tel problème, la caractérisation de l'hydrodynamique (sur l'exemple de Saint-Venant) prend en compte la présence des ouvrages $\mathcal{S}$:

$$F(\boldsymbol{U}, \psi+\mathcal{S}) = \begin{pmatrix} \nabla.(h\boldsymbol{u}) \\ \nabla.(h\boldsymbol{u}\otimes\boldsymbol{u}) + gh\nabla(h+\psi+\mathcal{S}) \end{pmatrix}. \tag{11}$$

3 Organisation de la Thèse

Le premier chapitre est consacré à l'optimisation d'ouvrages d'ingénierie côtière, sans prendre en compte la réponse de la bathymétrie. Cette étude offre un cadre de travail sur l'utilisation de méthodes d'optimisation dans la recherche d'ouvrages de protection. Le sujet d'étude est le réaménagement du port de La Turballe (France) dont le but est

d'agrandir la surface exploitable du port tout en réduisant l'agitation des vagues longues. Ici, la fonction de coût à minimiser sera une fonction de l'énergie des vagues au sein du port et des contraintes supplémentaires sont ajoutées pour assurer la viabilité de la solution finale. En annexe se trouve un guide explicatif détaillant les différentes étapes dans la recherche de l'aménagement portuaire de La Turballe par optimisation.

Au deuxième chapitre, nous abordons le principe d'optimisation pour la morphodynamique littorale présenté précédemment. Dans cette première étude, nous excluons la notion d'ouvrage de protection côtière, pour se concentrer entièrement sur la réponse morphodynamique de la plage. Un nouveau modèle hydrodynamique, mieux adapté que les équations de Saint-Venant définies en Section 2.1, fut développé pour répondre aux besoins de la problématique. La fonction de coût choisie pour caractériser la morphodynamique littorale reprend la notion d'énergie des vagues évoquée en Section 2.1.1. La fenêtre de dépendance temporelle fut quant à elle, omise de ces premiers développements. Plusieurs contraintes s'ajoutent au problème d'optimisation dans le but d'offrir plus de physique au modèle. Ceci inclut la contrainte de conservation de sable de la Section 2.1.2. Un modèle numérique fut développé en parallèle des recherches théoriques et des simulations numériques ont été effectuées. Ce modèle appelé Opti-Morph fut intégralement conçu pendant la thèse. L'objectif était de créer un outil efficace, rapide et robuste, utilisable par les ingénieurs spécialisés dans le domaine littoral.

Le Chapitre 3 offre une première approche à la stratégie de couplage entre l'optimisation de la forme du profil bathymétrique et l'optimisation d'ouvrages, évoqués en Section 2.2. Nous considérons l'exemple du positionnement d'atténuateur de vagues le long d'un profil cross-shore. La fonction de coût associée à l'évolution du profil de plage reste l'énergie des vagues, pendant que celle associée à la position de brise-lame concerne l'érosion côtière. Nous réutilisons le modèle Opti-Morph pour la réponse morphodynamique. Pour simplifier, nous avons étudié le problème des brise-lames par une méthode directe, possible grâce à la rapidité et faible complexité d'Opti-Morph.

Enfin, un guide explicatif du modèle numérique Opti-Morph est présenté au Chapitre 4, et offre une description plus détaillée du modèle. Un guide d'utilisation et deux exemples d'application sont aussi fournis. Ce guide fut rédigé pour faciliter l'utilisation du modèle en accord avec les objectifs de l'Axe 2 de la Section 1.

Chapitre 1

Optimisation d'Ouvrages Littoraux

Ce premier chapitre est consacré à l'utilisation de l'optimisation dans le cadre d'un problème d'ingénierie classique, l'aménagement portuaire. Ces travaux furent réalisés dans le but d'accompagner les études effectuées par les ingénieurs de BRLi pour le projet du port de La Turballe en France.

Ces travaux ont fait l'objet d'un article, accepté pour publication par le journal *China Ocean Engineering*, intitulé "Optimal port design minimizing standing waves with a posteriori long term shoreline sustainability analysis", cf. [22].

1.1 Résumé en Français

1.1.1 Introduction

La théorie de l'optimisation est un outil efficace dans le réaménagement des ports. Avec le nombre croissant d'activités commerciales et économiques qui s'y installent, les ports se voient contraints d'élargir leur zone de surface afin d'accueillir cette hausse d'activité. Ce réaménagement peut s'accompagner d'un deuxième objectif, tel que la réduction de l'agitation de l'eau au sein du port. Ce dernier se fait généralement par l'introduction de structures de protection portuaire supplémentaires comme les digues, les brise-lames et les môles. Cependant, répondre à un de ces deux objectifs peut nuire au succès de l'autre. En effet, l'augmentation de la surface exploitable du port peut entraîner une hausse de l'agitation des vagues ou, à l'inverse, la réduction de l'agitation résulte d'un port dont la surface n'est pas suffisamment grande. Par conséquent, la conception d'un port n'a pas de solution triviale. De plus, le grand nombre de transformations géométriques possibles peut rendre l'approche d'ingénierie classique difficile et chronophage ; de nombreuses simulations numériques exploratoires sont nécessaires, elles-mêmes forcées par une large gamme de différentes conditions météorologiques et maritimes. Ces travaux ont ainsi pour but d'approfondir l'investigation des réaménagements portuaires au travers

de la théorie d'optimisation.

Dans ce chapitre, nous développons un modèle d'optimisation capable de déterminer les configurations portuaires optimales, par rapport à une fonction de coût prédéterminée. En modifiant cette fonction objectif, les conditions de forçage ou les paramètres du modèle, les utilisateurs peuvent explorer rapidement les différentes configurations portuaires optimales. Cet outil permet également aux utilisateurs de confirmer leurs hypothèses initiales ou obtenir des résultats innovants et non-intuitifs. Le modèle présenté ci-dessous est basé sur la minimisation de l'énergie des ondes longues. Une présentation générale du modèle hydrodynamique et du modèle d'optimisation est décrite dans la suite avec une application au port de La Turballe.

1.1.2 Modèle Hydrodynamique

Le calcul de configuration optimale de port par rapport à la minimisation de l'agitation de l'eau nécessite un modèle hydrodynamique capable de modéliser l'état de l'eau. Ainsi, nous développons une modèle capable de fournir les variations du niveau d'eau au sein du port, dont les observations préalables ont montré sont principalement dû aux seiches et aux ondes stationnaires à basse fréquence. Ce modèle hydrodynamique doit également être capable de prendre en compte les différents scénarios météorologiques et océanographique observés au large, ainsi que des caractéristiques d'absorption/réflexion des structures au sein du port.

On considère un bassin semi-fermé de profondeur d'eau relativement constante. On note Ω le domaine du bassin et Λ son contour. Ce dernier est partitionné en trois sous-ensembles : Λ_i l'entrée du port, Λ_w les bords solides et Λ_o les sorties, le cas échéant. L'agitation du port est directement contrôlée par des vagues apparaissant à son entrée Λ_i, et aucun apport d'énergie est possible depuis les autres frontières; les structures solides formant la frontière Λ_w sont considérées infranchissable et aucun échange d'énergie ne peut la traverser. De plus, aucune énergie ne peut apparaître au niveau de la frontière du flux sortant Λ_o. Certains ports, notamment celui de La Turballe, sont connus pour être contrôlés par les oscillations de basse fréquence ou seiches (cf. [99]) et dépendent uniquement de l'énergie fournie à son entrée et de sa géométrie. Par conséquent, un modèle basé sur les équations de Helmholtz est plus approprié pour décrire les processus hydrodynamiques au sein du port.

Pour simplifier, nous nous plaçons dans le cadre de la théorie linéaires des vagues. De la même manière que [57], une onde de surface est considérée comme la somme d'une onde incidente et d'une onde réfléchie :

$$\eta = \eta_i + \eta_r. \tag{1.1}$$

L'onde incidente η_i est définie par :

$$\eta_i(x,t) = a_i(x)e^{-i\sigma t} \tag{1.2}$$

où la composante spatiale a_i est définie par :

$$a_\mathrm{i}(x) = a_\mathrm{max} e^{-i\vec{k}x}. \tag{1.3}$$

Ici, σ est la fréquence des vagues (s^{-1}), a_max est l'amplitude de la vague (m), et $\vec{k} = k(\cos(\theta), \sin(\theta))$ est le vecteur d'onde, avec k le nombre d'onde et θ l'angle de propagation. L'onde réfléchi η_r est définie par :

$$\eta_\mathrm{r}(x,t) = a_\mathrm{r}(x) e^{-i\sigma t} \tag{1.4}$$

où le composant spatial a_r satisfait l'équation de Helmholz suivant :

$$\begin{cases} k^2 a_\mathrm{r} + \Delta a_\mathrm{r} = 0 & \text{over } \Omega \\ a_\mathrm{r} = 0 & \text{on } \Lambda_\mathrm{i} \\ a_\mathrm{r} = -\gamma_\mathrm{ab} a_\mathrm{i} & \text{on } \Lambda_\mathrm{w} \\ \nabla a_\mathrm{r} \cdot \vec{n} = 0 & \text{over } \Lambda_\mathrm{o} \end{cases}. \tag{1.5}$$

Les conditions aux bords caractérisent le comportement des vagues au contact avec les différents types de bords. Sur les bords forçants Λ_i, le champ d'ondes totales est composé uniquement du champ d'ondes incidentes puisque aucune réflexion ne se produit. Sur les bords solides Λ_w, une certaine partie de l'énergie des ondes est réfléchie/absorbée au contact avec le mur. Cette propriété réfléchissante est directement liée aux caractéristiques physiques du bord. On introduit donc le coefficient de réflexion/absorption $\gamma_\mathrm{ab} \in [0, 1]$. Pour $\gamma_\mathrm{ab} = 1$, on a réflexion totale, et $\gamma_\mathrm{ab} = 0$, on a une absorption totale. Les bords de flux sortant n'ont pas d'influence directe sur le champ d'onde dans Ω, mais l'énergie peut quitter le domaine à travers ces bords. On applique donc la condition aux limites de Neumann homogène sur Λ_o : $\nabla a_\mathrm{r} \cdot \vec{n} = 0$, où $\vec{n}$ est le vecteur normal extérieur unitaire et $\cdot$ représente l'opérateur de produit scalaire.

L'équation différentielle partielle elliptique stationnaire qui caractérise les ondes réfléchies, avec des conditions aux limites de Neumann et Dirichlet, est résolue par la méthode des éléments finis. Cette méthode a été choisie car elle permet l'utilisation d'un maillage irrégulier avec des éléments de différentes tailles et géométries, ainsi que la possibilité d'adaptation du maillage. Étant donné qu'un port peut présenter des bords complexes, cette méthode était le choix naturel. Les ondes incidentes en revanche sont calculées analytiquement.

1.1.3 Modèle d'Optimisation pour la Réduction de l'Agitation Portuaire

Le problème d'optimisation considéré ici pour l'aménagement portuaire concerne la minimisation de l'agitation des grandes vagues au sein du port tout en tenant compte des différents scénarios de forçage qui peuvent être observés. La configuration portuaire

finale devrait réduire l'agitation des vagues que ce soit en présence de beau temps ou de tempêtes. Une priorité est donnée aux conditions de vagues sévères, car des endommagements plus importants sont observés lors des tempêtes. Ainsi, dans cette étude, nous priorisons la minimisation des vagues de plus grande amplitude. Dans un premiers temps, nous définissons des fonctions de coût associées à chaque scénario de forçage. Ces fonctions de coût sont dites *locales*. Ensuite, nous combinons astucieusement ces fonctions de coût locales, pour former une fonction de coût *globale*. Cette dernière fera l'objet de la minimisation.

Soit ψ la paramétrisation du port modifiable lors la recherche de la configuration optimale, et dont on cherche la valeur optimale. Le domaine Ω varie en fonction de la paramétrisation ψ et est donc noté $\Omega(\psi)$ par la suite. Soit N le nombre total de scénarios de forçage considérés. On associe à chaque scénario un indice $n \in \{0, ..., N\}$. Pour un scénario de forçage n donné, on définit la fonction de coût locale $\mathcal{J}_n$ par :

$$\mathcal{J}_n(\psi) = \frac{1}{K(\mathcal{P})} \frac{1}{|\Omega(\psi)|} \int_{\Omega(\psi)} \mathcal{E}_n(\psi, \boldsymbol{x})\, \mathcal{P}(\boldsymbol{x})\, \mathrm{d}\boldsymbol{x} \tag{1.6}$$

où $|\Omega(\psi)|$ est la surface du domaine $\Omega(\psi)$ associé à la paramétrisation ψ du port. La quantité $\mathcal{E}_n(\psi, \boldsymbol{x}) = \frac{1}{2}\rho g (a_n(\psi, \boldsymbol{x}))^2$ est l'énergie surfacique totale définie sur le domaine $\Omega(\psi)$ et associée au scénario de forçage n et à la paramétrisation du port ψ. Ici, ρ est la densité de l'eau, g est l'accélération gravitationnelle et $a_n(\psi)$ est l'amplitude des vagues calculées sur $\Omega(\psi)$ et associées à n et ψ. La fonction $\mathcal{P}$ est la fonction de pondération spatiale, avec $K(\mathcal{P}, \Omega(\psi)) = \int_{\Omega(\psi)} \mathcal{P}(\boldsymbol{x})\, \mathrm{d}\boldsymbol{x}$. La fonction de pondération spatiale permet de prioriser la minimisation de l'agitation sur certaines zones privilégiées du port, telles que les zones de forte circulation ou les zones d'accostage.

La fonction de coût globale $\mathcal{J}$ est une combinaison linéaire des fonctions de coût locales, où les coefficients scalaires sont déterminés par l'énergie des vagues aux bords forçants du domaines Λ_i. Soit $a_\mathrm{i}(n)$ l'amplitude des ondes entrantes (définies sur Λ_i) et associées au scénario de forçage n, la fonction de coût globale est définie par :

$$\mathcal{J}(\psi) = \frac{\displaystyle\sum_{n=1}^{N} a_\mathrm{i}(n) \mathcal{J}_n(\psi)}{\displaystyle\sum_{n=1}^{N} a_\mathrm{i}(n)}. \tag{1.7}$$

Le choix de cette fonction de coût globale garantit qu'une priorité est donnée à la minimisation des fonctions de coût locales associées aux scénarios de forçages les plus extrêmes. En effet, plus l'amplitude à l'entrée du port $a_\mathrm{i}(n)$ est importante, plus une priorité est donnée à la minimisation de $\mathcal{J}_n(\psi)$ dans la minimisation de $\mathcal{J}(\psi)$.

1.1.4 Application au Port de La Turballe

Situé sur la côte Atlantique de la France, le port de La Turballe abrite une large gamme d'activités maritimes, dont la pêche, la plaisance, la réparation navale, le trafic de passagers, ainsi que les activités liées au parc éolien off-shore de Saint-Nazaire. Le département de la Loire-Atlantique souhaite réaménager le port pour augmenter sa surface exploitable afin d'accommoder la hausse des activités. Ainsi, l'objectif du projet est de modifier la géométrie du port en agrandissant sa surface, tout en réduisant l'agitation de l'eau, limitant ainsi les dégâts soumis aux bateaux amarrés. Grâce à l'ingénierie classique, il a été établi que le meilleur plan d'action était par l'intermédiaire d'une digue et d'un môle pour provoquer un effet d'entonnoir à l'entrée du port. Les dimensions de ces structures seront déterminées à l'aide de la théorie de l'optimisation pour assurer une agitation minimale au sein du port. D'autres contraintes s'ajoutent au problème pour garantir des résultats pratiques, concernant entre autres l'emplacement de la môle, le positionnement de la digue, et les dimensions des deux structures. Par exemple, nous considérons que le môle ait une largeur minimale de 30 m et que la digue ait une longueur minimale de 350 m. Les structures doivent également être suffisamment élevées pour être considérées comme infranchissable par les vagues. Chaque structure est caractérisée par le coefficient d'absorption γ_{ab}, que nous fixons à 1 pour étudier le scénario le plus critique, i.e. les bords sont entièrement réfléchissants.

Soit $\psi = (\alpha, \beta)$ l'ensemble des paramètres définissant le réaménagement du port, où α caractérise la largeur ajoutée au môle et β représente la longueur ajoutée à la digue. Le choix de ces paramètres découle de l'expertise des ingénieurs portuaires. Les contraintes se traduisent par une limitation sur les valeurs des dimensions des deux structures : la largeur totale du môle doit mesurer entre 30 m et 180 m, alors que la longueur totale de la digue doit mesurer entre 350 m et 550 m.

Le problème d'optimisation devient donc : *Trouver* $\psi = (\alpha, \beta)$ *tel que* $\mathcal{J}(\psi)$ *est minimal de sorte que :* $0 \leq \alpha \leq 150$ *et* $0 \leq \beta \leq 200$.

Nous omettons les modifications du fond sableux dans le modèle d'optimisation.

1.1.5 Résultats

Les résultats numériques montrent que cette étude de solution optimale à deux degrés de liberté admet un minimum global unique de $\mathcal{J}(\psi)$ qui correspond à un prolongement de la digue de 107 m et un élargissement du môle de 90 m.

Une étude sur l'état énergétique de l'eau au sein du port fut réalisée en fonction des différents scénarios de forçage. Les valeurs des fonctions de coût locales $\mathcal{J}_n$ ont été comparées pour chaque configuration de port considérée ainsi que pour la configuration optimale. On observe que l'énergie associée à la configuration optimale se situe parmi les énergies les plus faibles pour chaque scénario de forçage, ce qui montre que le minimum de la fonction de coût globale $\mathcal{J}$ équivaut au minimum de chacune des fonctions de coût

locales $\mathcal{J}_n$. Dans chaque cas, la solution optimale réduit considérablement la quantité d'énergie dans le port.

Ce travail démontre que l'optimisation numérique peut être un outil rapide et efficace dans l'identification de solutions portuaires optimales.

1.1.6 Discussion

La solution optimale réduisant au maximum l'agitation de l'eau au sein du port peut toutefois s'avérer inadaptée si elle engendre des effets indésirables sur son environnement. Il est donc nécessaire de réaliser des études supplémentaires sur la configuration optimale. À titre d'exemple, une étude fut menée afin de déterminer l'impact morphologique de la nouvelle configuration sur le littoral environnant. Des simulations numériques long-terme ont été appliquées au port de La Turballe par le biais du modèle numérique GenCade [44]. Les résultats d'une simulation de 30 ans montrent que l'installation de la digue et du môle déterminés par la recherche d'optimum n'a pas d'effet sur le trait de côte et donc n'impacte pas la dynamique littorale environnante.

1.1.7 Annexe : Guide Explicatif du Modèle Numérique

Une annexe fut écrite pour détailler les étapes du modèle d'optimisation, avec chaque section correspondant à une étape dans le workflow. Nous illustrons le modèle à l'aide de l'exemple du port de La Turballe (France), pour une problématique autre que celle présentée auparavant. Cette dernière concernait l'ajout d'une digue et d'un môle dont leurs dimensions furent étudiées dans la recherche d'optimum. Ici, nous étudions la longueur de la digue et la position d'un épi le long d'un mur existant. Ceci nécessite entre autres, la redéfinition de l'espace de paramétrisation du port. Ces deux études furent l'objet d'un rapport fourni aux responsables du projet de La Turballe. La solution retenue fut la deuxième : un réaménagement portuaire par l'introduction d'une digue et d'un épi (voir www.loire-atlantique.fr).

1.2 Introduction

When designing a port, an extensive study should be conducted to ensure a smooth functioning of services, improve the experience of its users, and provide sufficient protection of the port. This study on the port, its structural components and its users should combine different approaches such as risk identification methods and extensive surveys of the site [62, 115, 2, 74, 51], the development of design criteria on the different components of the harbour [108, 60, 111, 3] and numerical and physical simulations [118, 117, 114, 71, 43, 94, 23, 46]. We present a method by optimization to supplement these standard procedures.

The term optimization in the field of coastal dynamics refers to the transformation of the natural seabed or the geometric and rheological properties of artificial structures present in ports or at the coast and leads to the minimization of a scalar quantity. This quantity, named cost function and denoted $\mathcal{J}$, is representative of the state of the system and is generally associated with certain physical quantities, such as those related to waves or currents. Applications of optimization theory to coastal dynamics already exist in literature. The work by [57] sought to minimize the L^2 norm of the water waves free surface elevation in the design of harbours or offshore breakwaters, and [54] and [11] used this approach when designing coastal protection structures while minimizing the effect of beach erosion. Other examples of optimal design of coastal structures include [124, 107, 70, 127, 15]. Alternatively, [81], [12], and [79] used optimization theory as a tool in the modeling of the dynamics of seabeds in shallow waters. A general presentation of the methods used here can be found in [59, 82, 83], and we refer to these documents for the theoretical bases of optimization theory and its applications to coastal systems and coastal management.

It is indisputable that a model based on optimization theory can be an invaluable tool for the development or updating of port configurations. Ports and harbour are generally extended to accommodate the increasing number of commercial and economical activities. Ports are enlarged to increase their exploitable surface area. This increase can be achieved with a second objective in mind. For instance, as well as increasing the surface area, one may also wish to reduce the agitation of the water within the port by introducing additional port protection, using jetties, breakwaters and groins. However, the increase in exploitable surface area may cause an increase in agitation or, conversely, the decrease of wave agitation may cause a decrease in surface area. Therefore, the design of a port has no trivial solution. Additional difficulties include the large number of geometric transformations considered in such a study; therefore employing a classic engineering approach could be difficult and time-consuming, requiring a large number of exploratory numerical simulations forced by a large range of different weather and sea conditions.

The work presented here was prompted by the desire to further the investigation in the redesign of ports via the introduction of optimal theory. The introduction of optimal theory in a management port operation originates from a successful operation that consisted in the deployment on the coast of Sète (France) of a geotube [58].

With the intention of accompanying the engineers with their analysis on harbor protection, we devise a tool, based on the concept of port agitation minimization. and capable of identifying pertinent port configurations. This work was conducted in the case of La Turballe port (France), but is valid for any semi-enclosed harbour with relatively constant water depth. This tool should in no way substitute the classical approach to port design performed by the experts in the field but is intended to offer suggestions on possible configurations. Oftentimes, numerical modeling of port configurations is costly,

both in time and resources, and consequently, the number of simulations is restricted. The tool presented here offers a rapid, cost-efficient, and user-friendly resource designed to assist traditional approaches. This optimization model is capable of indicating optimal harbor designs in very little time, with regards to a predetermined objective function. Modifying the objective function, forcing conditions, and/or parameters surrounding the optimization model allows users to explore different harbor configurations in a short span of time. The resulting port designs can, and should, be subject to further investigation so as to evaluate their effectiveness, this being achieved using a more classical engineering approach. This tool also allows users to give credence to their initial hypotheses and may provide unorthodox results not necessarily envisioned by the experts.

This paper presents one such study where the focus is on the minimization of long wave energy within La Turballe port, situated in North-Western France. The parameters are chosen with the aim of depicting a worst-case scenario.

We begin this paper with the hydrodynamic model used in the minimization of port agitation. Here, we use a variation of the Helmholtz equation applied to a port configuration because the control of wave/wave interactions, seiches and resonance phenomena is preeminent in the design of this inner port, in so far as gravity waves are efficiently fully dissipated at the entrance. Obviously, the hydrodynamic model must deal with different forcing conditions and returns water oscillation amplitudes. The next section is devoted to the concept of optimization theory applied to coastal engineering, and more specifically to the extension of ports, with the main objective to increase the exploitable surface area and minimize the agitation of the water within the port. In the third section, we apply this theory to the practical case of La Turballe port in North-Western France and a discussion of the long term shoreline sustainability can be found in the final section.

1.3 Hydrodynamic Model for Port Agitation

In order to calculate the optimal port configuration with regards to the minimization of water oscillations within the port, a hydrodynamic model capable of modeling the relevant water level fluctuations is required. Generally, water level in ports can be driven by tide, very low frequency waves, infra-gravity waves, waves or wind waves depending upon the context. Here, we know from historical experience that classic gravity waves are efficiently attenuated at the port entrance, but may transfer part of their energy to the inner port in the form of seiches and various standing low frequency waves. In addition, the model should be able to take into account the different weather and deep sea scenarios observed off the coast, as well as the absorption/reflection characteristics of the structures within the harbour.

The model can be applied to any port verifying the required conditions (semi-enclosed basin with a forcing boundary and roughly constant water depth). We illustrate

this model on the case of the old port of La Rochelle, as a generic port. This example was chosen because it illustrates the three different boundary conditions we are able to consider with this model. The realistic application that follows in Section 1.5 doesn't present all the boundary conditions presented here, so hasn't been used as an illustration.

The model was designed with the application of La Turballe in mind (see Section 1.5), that is a port with input waves arriving with no angle of incidence.

1.3.1 Settings

We define the domain Ω as the area occupied by water within the port. The domain is a closed, compact subdomain of $\mathbb{R}^2$. We denote Λ the boundary of Ω, which is be partitioned into 3 subsets $(\Lambda_i, \Lambda_w, \Lambda_o)$. We denote Λ_i the boundary over which the incoming forcing is present. Forcing is given in the form of wave agitation at the entrance of the port, where the influx of energy arises. We denote Λ_w the borders of the domain representing the walls of the port. These walls are associated with an absorption/reflection coefficient in order to take into account the behavior of the waves when they reach the solid borders of the port. Finally, we denote Λ_o the boundary of Ω over which an outflux of energy is observed. This occurs when an outlet is present in the port, as is the case of the old port of La Rochelle (France). The different types of boundaries of Ω are illustrated by Figure 1.1.

Port agitation is directly controlled by waves appearing at its entrance at Λ_i, and no influx of energy is possible from the other borders; the solid structures forming the boundary Λ_w are considered impassible and no exchange of energy can cross it. Furthermore, no energy can appear from the outflux boundary Λ_o. As such, the hydrodynamic model we consider is limited to the inside of the port with local forcings at its entrance.

Some ports, and especially the one at La Turballe, are known to be controlled by low frequency oscillations or seiches (cf. [99] driven solely by the energy provided at the port entrance and the geometry of the port. Therefore a model based on the Helmholtz equations is more suitable to describe the hydrodynamic processes within the port than a theory based on wave propagation.

1.3.2 Helmholtz Model

For simplicity purposes, we place ourselves in the setting of linear wave theory, which provides a first order description of the gravity waves on the surface of the water.

Similar to [57], we consider a surface wave to be the sum of an incident wave and a reflected wave:

$$\eta = \eta_i + \eta_r \tag{1.8}$$

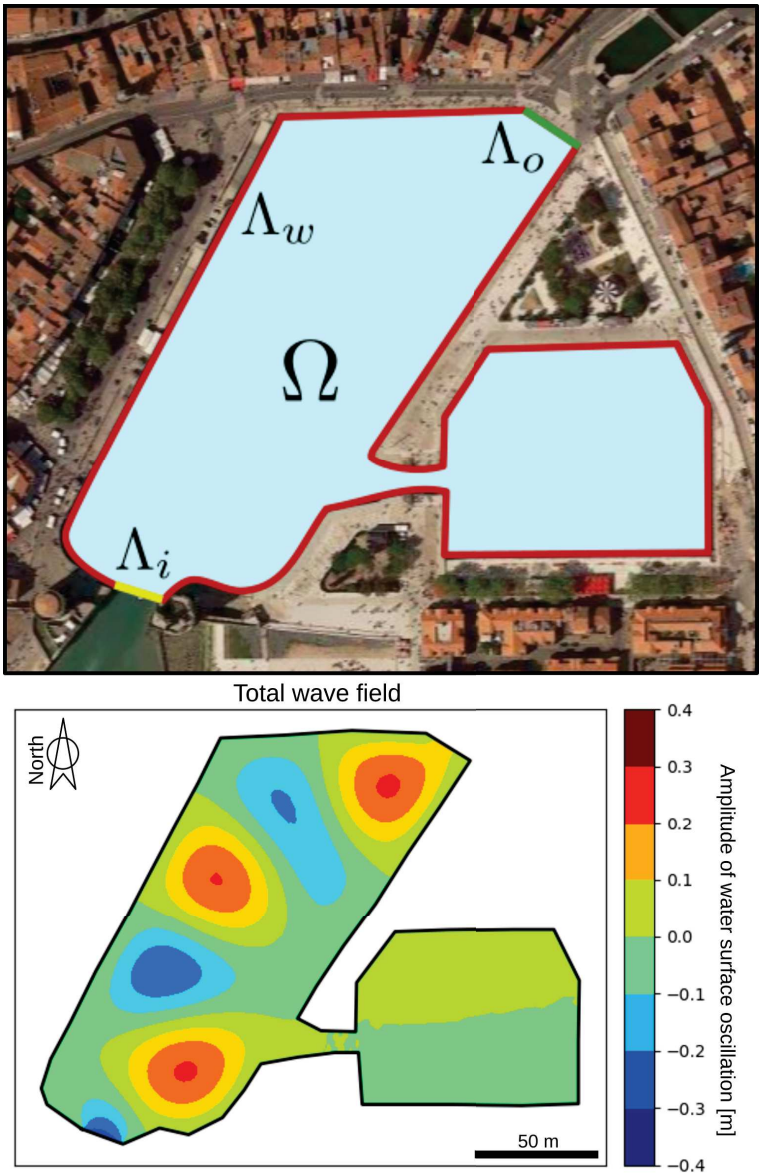

Figure 1.1: *Top:* Illustration of the domain Ω and its borders on the old port of La Rochelle (France). The red borders depict the walls of the port, characterized by absorption and reflection. The yellow border indicates an influx of energy, depending on outer wave conditions. The green border indicates an outflux of energy, where the energy flux driven by dynamics of the water surface exits the port domain through the existing channel. *Bottom:* Numerical result of the hydrodynamic model applied to the La Rochelle configuration. The plot represents the resulting total wave field $\eta = \eta_\mathrm{i} + \eta_\mathrm{r}$ forced by incoming fair-weather waves at an angle $110°$ through Λ_i, and fully transformed to standing long waves within the port.

The incident wave η_{i} is simply defined by:

$$\eta_{\mathrm{i}}(x,t) = a_{\mathrm{i}}(x)e^{-i\sigma t} \tag{1.9}$$

where the spatial component a_{i} is defined by

$$a_{\mathrm{i}}(x) = a_{\max}e^{-i\vec{k}x} \tag{1.10}$$

Here, σ is the wave frequency, $a_{\max}$ is the amplitude of the water surface oscillation for this given frequency, and $\vec{k} = k(cos(\theta), \sin(\theta))$ is a wave number vector, with k the wave number and θ the angle of propagation of the wave. The wave number k is calculated over the domain using the linear dispersion equation (1.11). Practically, a shallow water approximation can be used as port standing waves are of very significant wave length with respect to mean water depth; h is water depth and g is gravitational acceleration.

$$\sigma^2 = gk\tanh(kh) \tag{1.11}$$

The reflected wave is defined by:

$$\eta_{\mathrm{r}}(x,t) = a_{\mathrm{r}}(x)e^{-i\sigma t} \tag{1.12}$$

We suppose the spatial component a_{r} of the reflected wave satisfies the following Berkhoff equation [7]:

$$\nabla\cdot(CC_g\nabla a) + \sigma^2\frac{C_g}{C}a = 0 \tag{1.13}$$

where C and C_g are respectively the phase velocity and the group velocity of the wave.

Assuming constant depth within the port and $C_g = \frac{1}{2}C$, and noting that $C = \frac{\sigma}{k}$, equation (1.13) can be simplified to yield the following Helmholtz equation:

$$k^2a + \Delta a = 0 \tag{1.14}$$

1.3.3 Eigen Mode and Domain Resonance

Solving Helmholtz equation can also be seen as looking for the eigen modes of the Laplace operator in the domain Ω under some boundary conditions:

$$-\Delta u_\lambda = \lambda u_\lambda \qquad + \quad b.c. \tag{1.15}$$

where $(\lambda(\Omega), u_\lambda(\Omega))$ are the eigen couple functions of the domain Ω which is variable in a context of shape optimization.

In situation where $|\lambda(\Omega)| = ||\vec{k}||^2$, the solution of equation (1.15) is an eigenmode of the Laplace operator. Exciting therefore this mode by a relevant incoming wave forcing will result to an infinite increase of the wave agitation in the basin and subsequently of the corresponding energy. We will address how to deal efficiently with this issue in the optimization section.

1.3.4 Boundary Conditions

Boundary conditions need to be associated with equation (1.14) for the reflected wave field a_r.

On forcing boundaries Λ_i, the total wave field is composed solely of the incident wave field since no reflection occurs. This yields $\eta = \eta_i$ and therefore $a_r = 0$ over Λ_i.

On solid borders Λ_w, a certain portion of the energy of the waves is reflected/absorbed when contact with this boundary is made. This reflective property is directly linked to the physical characteristics of the boundary. In the case of vertical rigid walls, almost all of the energy is reflected. On mild slope boundaries, more energy is absorbed/dissipated; the reflected wave field on these boundaries is equal to a portion of the incident wave field. Over Λ_w, we have $\eta_r = -\gamma_{ab}\eta_i$, where $\gamma_{ab} \in [0, 1]$ is a reflection/absorption coefficient. For $\gamma_{ab} = 1$, the border shows total reflection and $\gamma_{ab} = 0$ the border shows total absorption. This also yields $a_r = -\gamma_{ab}a_i$ over Λ_w.

Outlet borders have no direct influence of the wave field within Ω, but energy can leave the domain via this boundary. We therefore apply the homogeneous Neumann boundary condition over Λ_o: $\nabla a_r \cdot \vec{n} = 0$, where $\vec{n}$ is the outer unit normal and $\cdot$ represents the inner product operator.

1.3.5 Numerical Strategy

The incident wave field is calculated analytically using (1.10), whereas the reflected wave field satisfies:

$$\begin{cases} k^2 a_r + \Delta a_r = 0 & \text{over } \Omega \\ a_r = 0 & \text{on } \Lambda_i \\ a_r = -\gamma_{ab} a_i & \text{on } \Lambda_w \\ \nabla a_r \cdot \vec{n} = 0 & \text{over } \Lambda_o \end{cases} \tag{1.16}$$

This time-independent elliptic partial differential equation which includes Neumann and Dirichlet boundary conditions is solved using a finite element method. This method was chosen because it allows the use of irregular grids with elements of different sizes and geometries, as well as the possibility of mesh adaptation. Given that a port may present intricate details and complex boundaries, a finite element method was a natural choice. Such a finite element method requires a weak formulation of the considered problem. In our case, the weak formulation of the Helmholtz problem (1.16) reads:

Find a_r such that

$$\int_\Omega k^2 a_r v = \int_\Omega \nabla a_r \nabla v + \int_{\Lambda_w} \gamma_{ab}(\nabla a_i \cdot \vec{n}) v \tag{1.17}$$

for all test functions v of the same nature as a_r. We use piecewise linear finite element functions to numerically determine the solution of (1.17) over a triangular adapted mesh.

Figure 1.1 illustrates the resulting field of the water surface oscillations within the La Rochelle port with the boundary conditions described previously and in the case of fair weather incoming conditions. We observe the arrival of energy over the forcing boundary Λ_i as well as the presence of bumps and nodes within the port resulting from the interactions of wave oscillations with the boundary walls. We also observe an output of energy at Λ_o where the energy leaves the domain Ω of the port and enters the adjoining canal.

1.4 Optimal design model

Using the previously described hydrodynamic model, we consider the following optimization approach in the design of ports based on agitation minimization.

1.4.1 Application to Port Configuration

We set ψ as the set of parameters defining the possible transformations of the port. Examples include the dimensions of a groin, the angle of a jetty or width of the entrance. The values of these parameters are modifiable and are used to determine the optimal configuration of the port with regard to the minimization of the cost function. Given that ψ determines the shape of the port, it is clear that the domain Ω varies in relation to ψ. Therefore, the computational domain of the hydrodynamic model changes at each step of the optimization method.

The optimization problem consists of minimizing the global agitation of long waves within the port while taking into account the different forcing scenarios that can be observed. The design of the port should reduce long wave agitation whether in the presence of fair weather or storms offshore. It is clear that priority should be given to the minimization of severe wave conditions over calmer ones, since greater damage is observed in stormy conditions. In this study, the frequency of occurrence of a given wave scenario is discarded and instead we focus on the minimization of waves of greater amplitude. Let N be the total number of forcing scenarios considered in the study of the port design. We associate each scenario with an index $n \in \{0, ..., N\}$. In order to incorporate these different forcing scenarios, we define the local cost functions $\mathcal{J}_n$ associated to a given scenario n and combine them in a purposeful manner to form the global function $\mathcal{J}$ to be minimized.

1.4.2 Choice of Cost Function

For a given forcing scenario n, we consider the following local cost function:

$$\mathcal{J}_n(\psi) = \frac{1}{K(\mathcal{P})} \frac{1}{|\Omega(\psi)|} \int_{\Omega(\psi)} \mathcal{E}_n(\psi, \boldsymbol{x})\, \mathcal{P}(\boldsymbol{x})\, \mathrm{d}\boldsymbol{x} \tag{1.18}$$

where ψ is the parameterization of the port modifiable in the search of an optimal configuration and $|\Omega(\psi)|$ is the surface area of $\Omega(\psi)$. The quantity $\mathcal{E}_n(\psi, \boldsymbol{x}) = \frac{1}{2}\rho g (a_n(\psi, \boldsymbol{x}))^2$ is the total surface energy defined over the domain Ω and associated with the forcing scenario n and the configuration ψ of the port. Here, ρ is the density of the water, g is the gravitational acceleration and $a_n(\psi)$ the amplitude of the waves calculated over $\Omega(\psi)$ associated with the forcing scenario n and the configuration ψ of the port. The function $\mathcal{P}$, named spatial weight function, enables us to prioritize the minimization of the agitation over certain preferred zones of the port, with $K(\mathcal{P}, \Omega(\psi)) = \int_{\Omega(\psi)} \mathcal{P}(\boldsymbol{x})\, \mathrm{d}\boldsymbol{x}$. In practice, these zones are defined by traditional port engineers in order to focus the minimization of agitation in zones nearby mooring stations for boats or in which high maritime circulation is expected. Examples of spatial weight functions include $\mathcal{P}_0(\boldsymbol{x}) = 1$, where no zone is prioritized over another, or alternatively

$$\mathcal{P}_1(x, y) = \exp(-A((x - x_a)^4 + (y - y_a)^4)) \tag{1.19}$$

where a circular zone within the port is considered a priority, the center of which is given by the coordinates (x_a, y_a) and A defines its radius.

The global cost function $\mathcal{J}$ is a linear combination of the local cost functions defined by (1.18), where the scalar coefficients are determined by the wave energy at the forcing boundary. Let $a_{\mathrm{i}}(n)$ be the amplitude of the incoming waves (defined on Λ_{i}) associated with the forcing scenario n, the global cost function to be minimized in the search of the optimal solution is defined as:

$$\mathcal{J}(\psi) = \frac{\sum_{n=1}^{N} a_{\mathrm{i}}(n) \mathcal{J}_n(\psi)}{\sum_{n=1}^{N} a_{\mathrm{i}}(n)} \tag{1.20}$$

The choice of this global cost function ensures priortity is given to the minimization of the local cost functions associated with the more extreme weather scenarios. These scenarios have the ability to cause the most damage within the port, so it is natural to design a glocal cost function capable of prioritizing the more severe weather conditions.

1.4.3 Numerical Strategy

Figure 1.2 illustrates the numerical strategy put in place in the search of the optimal port configuration. The model explores the different port configurations allowed by the user.

For each forcing scenario, wave agitation is calculated using the hydrodynamic model presented in Section 1.3. This includes calculating the incident wave analytically and solving the Helmholtz equation with a PDE solver for the reflected waves. The local cost function (1.18) can then be determined. Once all the local cost functions have been calculated, it is then possible to determine the global cost function $\mathcal{J}$ (1.20). It is then possible to determine the optimal port configuration with regards to $\mathcal{J}$, which concludes the simulation.

1.4.4 Managing Resonance

We mentioned the necessity of making sure the solution of the Helmholtz equation is not an eigenmode of the Laplace operator in the domain as these situations lead to artificially high level of wave energy in the basin and therefore the functional.

Obviously, one cannot imagine computing, at each iteration of an optimization procedure, all the eigenmodes of the Laplace operator for the corresponding domain to make sure the corresponding energy level is not artificially driven by some resonance phenomenon. This would increase dramatically the computation time and is thus opposite to the optimization philosophy.

An alternative method must be set to control resonance efficiently. The method chosen aims to reducing the energy of the port in the case of an energy exceeding a given threshold, here 10^5 J, which is by far a maximum energy that could be observed in the port. This simple method assumes that any huge amount of energy observed in the port must be due to numerical resonance and therefore must be reduced to secure more realistic results.

Resonance is not often observed in real basin because wave-wave interactions reduce the concentration of energy on one specific frequency, preventing this situation from occurring. However, the hydrodynamical model of this study is based on many superimposed computations of the linear Helmholtz equation forced by monochromatic waves, which does not account for non-linear processes, which explains the possible high energy levels to control.

1.5 Application to La Turballe port

In this section, we have applied the previous optimization strategy to the port of La Turballe (France). The present work accompanies a more traditional engineering approach in finding the best configuration satisfying all parties involved. Contrarily to the port preciously mentioned, this port doesn't possess an outlet boundary.

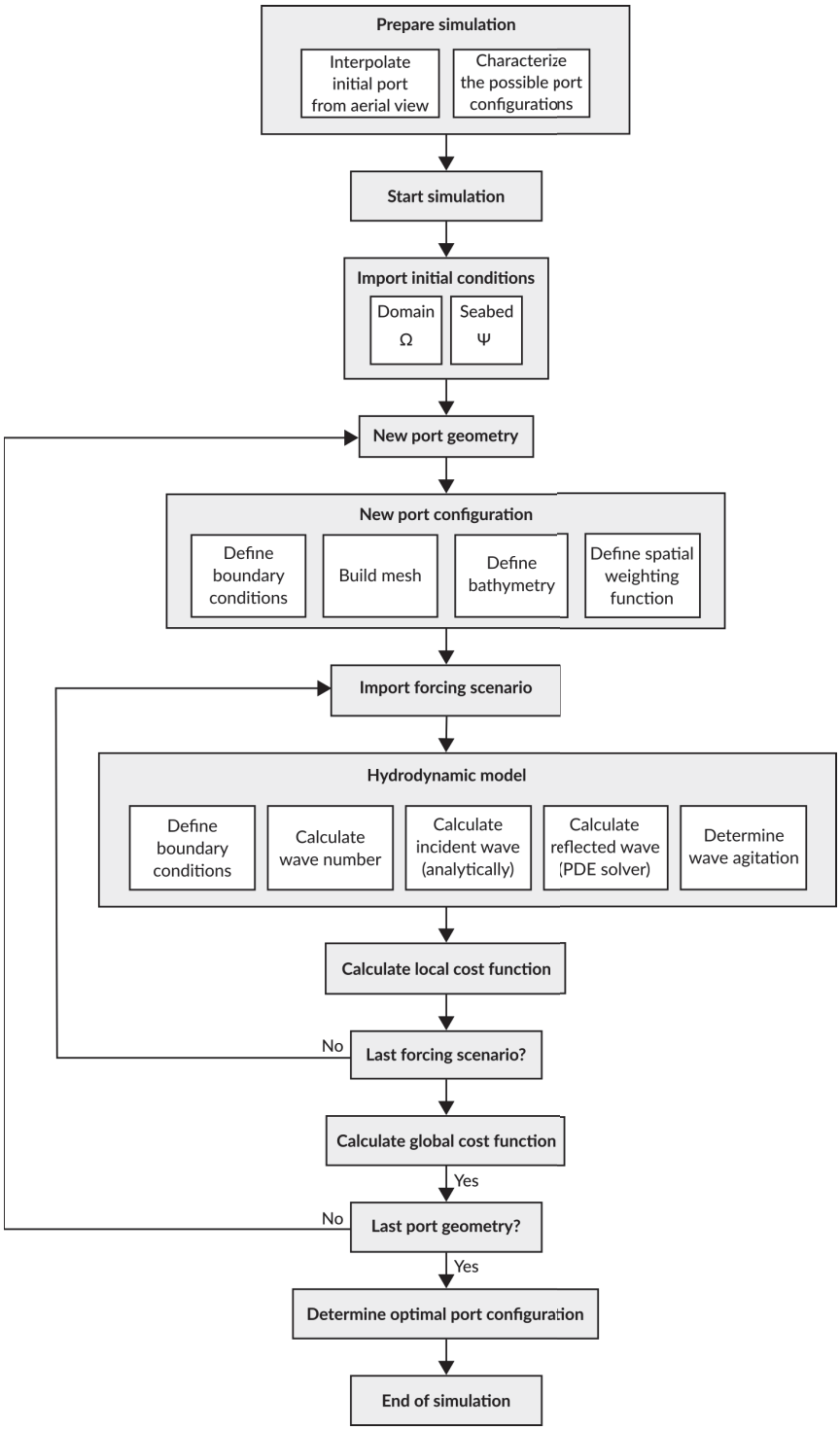

Figure 1.2: Numerical strategy applied to the search of the optimal configuration of La Turballe port

1.5.1 Presentation of the Port

Situated along the Atlantic coast in the North-West of France, the port of La Turballe is home to a wide range of maritime activities, including the presence of a marina, numerous fishing facilities as well as a ship repair services. With the increase of these activities and the arrival of others, the department of Loire-Atlantique wishes to increase the available surface area of the port. This project accompanies the plan of introducing an offshore wind turbine farm, since its maintenance center is expected to be installed at the La Turballe port. Its expansion is therefore crucial for the well-being of users of the port. The objective of the project is to expand the port in such a way that the agitation within the port is reduced, thereby reducing the damages to moored boats. Damages caused by excessive agitation within the port include sinking, stranding, collisions, and overturning. The aim of this study is to alter the geometry of the port while verifying the following conditions: the surface area of the port must be increased and the agitation of the long waves within the port must be reduced.

Usually, waves customarily arrive nearby a port with some incidence (cf. [123, 8, 90]. However, in light of the orientation of the port of La Turballe with regard to the mean orientation of the coast and the incoming wave spectrum in this area, no direct waves can enter the port. Furthermore, the large rounded jetty head located at the seaward side of the port entrance reflects any direct incoming waves. It also drives a significant diffraction pattern of any incoming wave forcing that result in the scattering of the wave field towards the shore, but not in the direction of the inner port. This claim is supported by observational data of said port. Therefore the only source of external energy generating port agitation is not that of the direct wave spectrum, but the energy resulting from the transformation of a part of the wave spectrum into low frequency oscillations at the port entrance. This is the primary reason why the dimensioning of La Turballe is a question of low frequency agitation, and not a problem relative to the direct impact of oceanic waves. To handle this classic situation in harbours, we shoaled the deep water wave conditions towards the port entrance, calculated the energy brought by the waves at this point, and we fed our model directly with an equivalent wave forcing representative of such energetic conditions assuming that the totality of energy associated with the incoming waves is transferred by diffraction and wave spectrum transformation to the port entrance.

1.5.2 Setting

Through classic engineering, it was established that the best course of action was through the installation of a jetty and a mole to produce a bottleneck effect at the entrance of the port. As illustrated in Figure 1.3, the jetty extends in an east-western direction to form a basin. The mole is attached to the existing structure occupied by parking facilities.

The dimensions of these structures will be determined using optimization theory

Figure 1.3: Illustration of La Turballe port. *Left:* The port in its initial state. *Right:* The port with the two additional structures considered in this study: mole A and jetty B.

to ensure minimal agitation within the port. However, certain constraints are imposed in order to guarantee practical results. These constraints include the location of the mole along the existing wall, the dimensions of the mole, the location of the jetty (the extremity must be fixed to the existing port and cannot be installed in waters deeper than 5.5 m) and the dimensions of the jetty. The structures must also be sufficiently elevated to be considered impassable by wave overtopping. Each structure is characterized by the absorption factor γ_{ab} defined in (1.16). In order to investigate the most critical scenario, we consider the boundaries to be fully reflective by setting $\gamma_{ab} = 1$.

The bathymetric properties within the port have been observed to be stable, with a depth ranging between 1.5 m and 3.5 m. We therefore omit the changes to the seabed from the optimization simulation.

In order to conduct this study, we were provided with wave scenarios that were deemed representative of the forcing conditions of the port. These scenarios were given in the form of statistical data of the directional waves (significant wave height, peak period, average direction, etc...) and did not include the probability of occurrence of each scenario. Given the nature our study which prioritizes the minimization of extreme weather waves (with the introduction of the weighted global cost function), the probability of occurrence of each scenario is irrelevant. This data could not be used in its initial state in the optimization process, because it was attained at different depths surrounding the port. This results in forcing scenarios that cannot be easily compared. The idea is therefore to propagate the wave conditions to the entrance of the port in a classic manner and using a regional wave simulation tool, TELEMAC [50, 38]. Certain assumptions involving the nature of the waves and the configuration of the port were

made to simplify the calculations, but have no consequences on the results aside from a slight increase in wave agitation. Since this study was conducted for a worst-case scenario, it makes no difference if a little more energy enters the port. This guarantees additional security on the final port configuration.

This process ultimately provided the study with twenty-eight different forcing scenarios, representing conditions ranging from fair weather to severe storms. These scenarios are given in the form of 3 parameters: the frequency, angle and amplitude of the incoming wave $(f, \theta, a_{\max})$. These are then plugged into the hydrodynamic model presented in Section 1.3, noting that $\omega = 2\pi f$, to calculate the wave field over the domain.

By way of illustration, fair weather conditions resemble $(f, \theta, a_{\max}) = (0.00373, 1.47, 0.344)$, whereas the more extreme conditions are of the like of $(f, \theta, a_{\max}) = (0.0261, 1.25, 3.75)$. Some scenarios may exceed the operating limit given by the ship mooring stability conditions [96]. The inclusion of these scenarios ensures port stability, in so far as possible, even in the most extreme forcing scenarios.

1.5.3 Parameterization of the Port

For illustrative purposes, we present the search for the optimal configuration of the port using two degrees of freedom only. We define the set of parameters by $\psi = (\alpha, \beta)$, where α represents the width added to the mole A along the existing wall and β represents the length of the extension of the jetty B. Figure 1.4 illustrates the definitions of α and β. The choice of these parameters originate from the expertise of classic port engineering, and incorporates the required design constraints. The total width of mole A must measure between $30\,m$ and $180\,m$, whereas the length of the jetty must measure between $350\,m$ and $550\,m$.

The optimization problem becomes: *Find* $\psi = (\alpha, \beta)$ *such that* $\mathcal{J}(\psi)$ *is minimal and the following constraints are met:* $0 \leq \alpha \leq 150$ *and* $0 \leq \beta \leq 200$.

Following the discussion with the industrial experts leading the study of the redesign of La Turballe port, it was established that the minimization of wave agitation should be concentrated in the South basin of the port. This choice is natural given the dense network of boats and the plan to add a dock and/or wharf to this area. Therefore, the cost function $\mathcal{J}$, defined by (1.18), features the spatial weighting function $\mathcal{P}_1$. This function, defined by (1.19), is illustrated in Figure 1.5 over $\Omega(\psi)$ for a given parameterization ψ of the port.

1.6 Results

In this section, we present the results of the hydrodynamic model presented in Section 1.3 applied to the port of La Turballe, as well as the results of the optimization calculations.

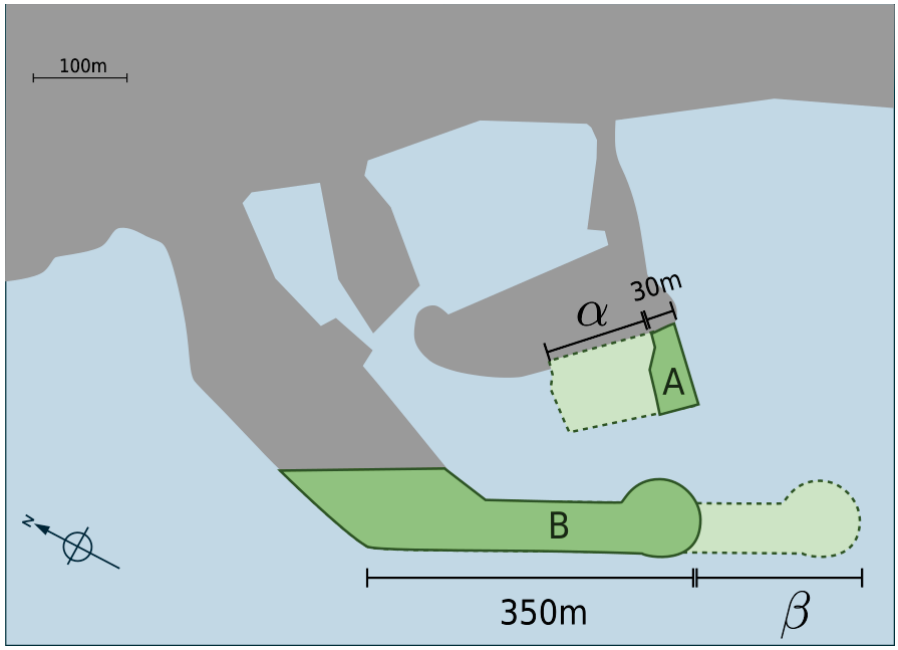

Figure 1.4: Illustration of the two degrees of freedom (α and β) used in the search of the optimal solution.

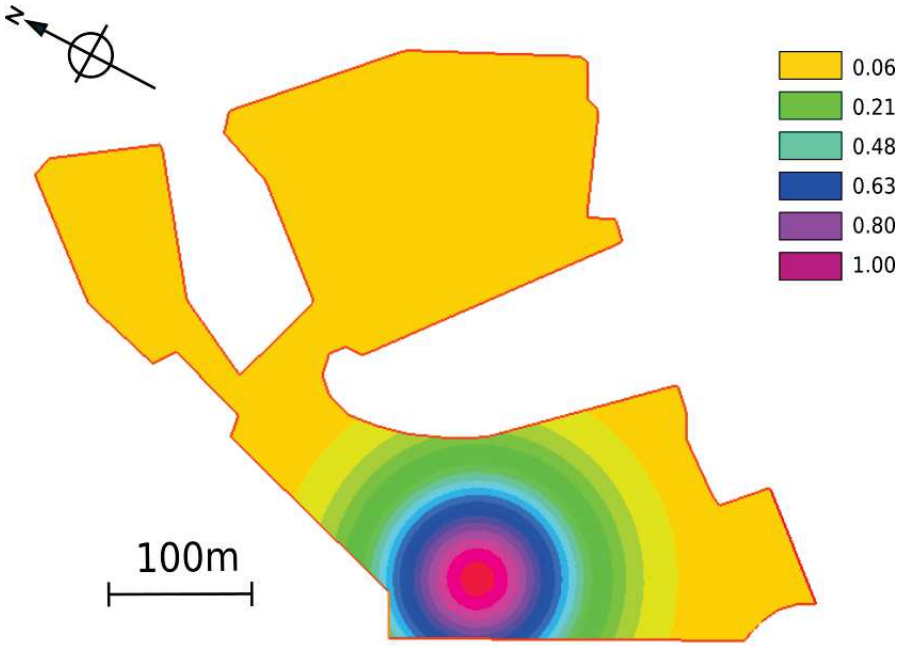

Figure 1.5: Spatial weight function $\mathcal{P}_1$ defined over $\Omega(\psi)$ for a given parameterization ψ of the La Turballe port.

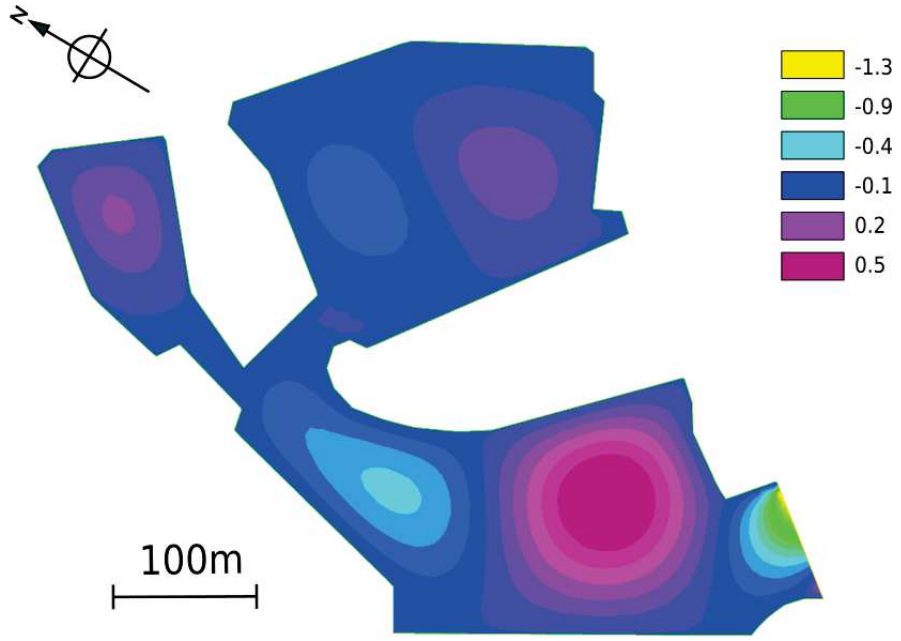

Figure 1.6: Oscillation of waves within the port of La Turballe, for a given parameterization of the port. The wave field results from forcing conditions associated with scenario $n = 23$ and characterized by $(f, \theta, a_{\max}) = (0.0186, 1.25, 1.50)$.

1.6.1 Hydrodynamic Simulations

Figure 1.6 illustrates the amplitude of the wave field within the La Turballe port under moderately severe weather conditions. We observe that the energy originates from the forcing boundary at the entrance of the port. Crest and troughs are observed as the waves propagate throughout the port reacting to the solid borders and show signs of seiche-like behavior.

1.6.2 Optimization Simulations

The local cost function associated with forcing scenario $n = 4$ is given by Figure 1.7. Here the forcing conditions, given by $(f, \theta, a_{\max}) = (0.0261, 1.47, 0.172)$, depict fair weather conditions. Several local minima are observed, which demonstrates the necessity of adopting an optimizing program capable of detecting a global minimum. Otherwise, problems may occur, especially if the number of design parameters is increased.

Figure 1.8 represents the values of the cost function $\mathcal{J}$ (1.20) with respect to the parameters α and β. The minimum of $\mathcal{J}$ is marked by a cross and is located away from the borders. Despite the presence of several local minima in one forcing scenario, the linear combination of scenarios that form the global cost function leads to a unique

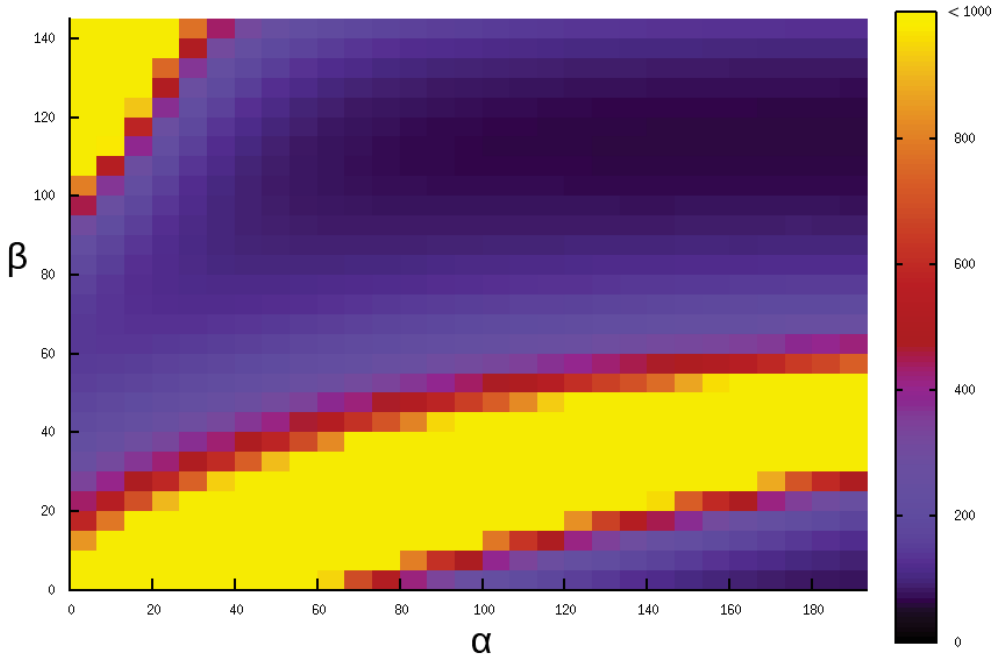

Figure 1.7: The local cost function $\mathcal{J}(\alpha, \beta)$ where only one forcing scenario is considered. There are several local minima located at the dark purple regions of the graph.

global minimum. This may differ depending on the choice of parameters ψ. We deduce that the study of the optimal solution with two degrees of freedom provides the following result: $\alpha^* = 90$ and $\beta^* = 107$. We notice great variability of the solution over the α axis, whereas over β, the function is relatively independent. This suggests that the decrease of wave agitation within the port is greatly influenced by dimensions of the mole and less so by the extension of the jetty.

The corresponding configuration is given in Figure 1.9. The jetty is extended by $107\,m$ and the mole is widened by $90\,m$.

1.6.3 Energetic State of the Port

Figure 1.10 represents the values of the local cost function $\mathcal{J}_n$ with regard to the 28 different forcing scenarios here represented on the X-axis by their reference number. Each point plotted on the figure corresponds to the value of the function $\mathcal{J}_n$ calculated for a given configuration of the port and a given forcing scenario n.

We therefore have a graphical representation of the set of the values of the functional $\mathcal{J}_n$ for all scenarios and all configurations explored by optimization simulation. Along a vertical line (i.e. for a given forcing scenario), we see the values of $\mathcal{J}_n$ for the scenario n, according to the different configurations. The lowest point corresponds to the local

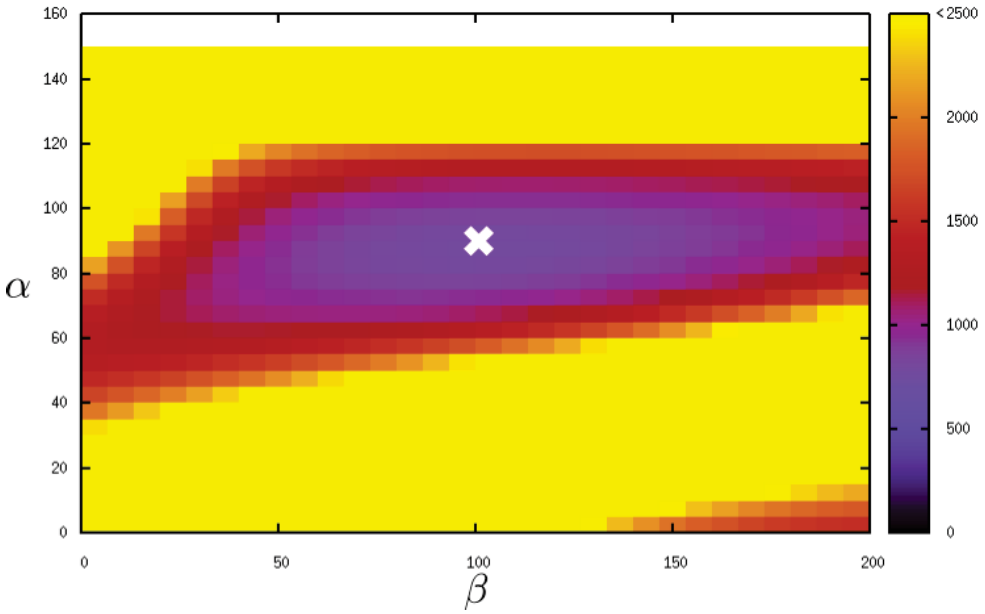

Figure 1.8: The cost function $\mathcal{J}(\alpha, \beta)$. The optimal solution is indicated by a cross. In this case, we have a unique global optimum and a local minimum.

optimal configuration for this forcing scenario. The red marker indicates the energy $\mathcal{J}_n$ associated with the configuration (α^*, β^*) for each of the forcing scenarios. For each of the 28 cases, this marker is situated in the lower range of the possible values, showing that the minimum of the global cost function $\mathcal{J}$ is equivalent to the minimum of each of the local cost functions $\mathcal{J}_n$.

In each case, the optimal solution has significantly reduced the quantity of energy within the port. Let us take the example of scenario 4. The energy within the port can potentially be in the order of $10^5\,J$; this corresponds to a wave height of $4.5\,m$. The optimal configuration, marked by a red point, results in an energy of $58\,J$, which corresponds to a wave height of $0.12\,m$. This reduction of $4.38\,m$ in wave height demonstrates the efficiency of the optimization model in determining the best configuration of the port. Considering that the lowest possible energy of the port for scenario 4 is $33\,J$, which corresponds to a wave height of $0.082\,m$, we can conclude that the optimization model provides a quasi-optimal solution for this forcing scenario. This reasoning can be applied to each forcing scenario, which leads us to conclude that the optimization model provides a solution which reduces the agitation in the port for all types of forcing conditions.

Figure 1.9: The inner border (red) of the optimal configuration of the port, resulting from the minimization of energy. We observe an extended jetty and a wide mole.

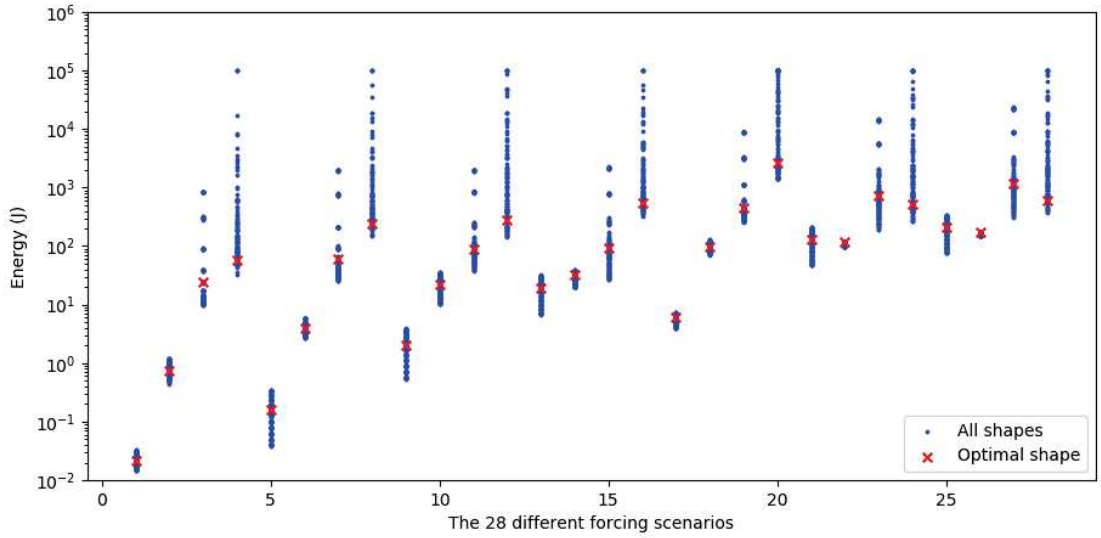

Figure 1.10: Analysis of the efficiency of the global optimal solution where the parameters are limited to 2 degrees of freedom $(\alpha;\beta)$ and forced by the 28 scenarios. The diagram represents the variation of the global cost function $\mathcal{J}$ with regard to the forcing scenario and for each possible port configurations (red markers correspond to the values of $\mathcal{J}$ associated with each parameterization of the port, green corresponds to the values of $\mathcal{J}$ associates to the global optimal solution).

1.7 Discussion

Despite finding an optimal solution to reduce the agitation of the water within the port whilst increasing its exploitable surface area, the solution may be deemed unfit if it has an undesirable effect on its environment. A study has therefore been conducted so as to determine the morphological impact of the new configuration on the surrounding shoreline. Depending on the results, the optimal solution may or may not be retained.

1.7.1 GenCade Model

The study of the morphological effect of the newly designed port was modeled by GenCade [44], a numerical model developed by the CIRP and the Regional Sediment Management Program which combines the engineering processes of GENESIS [45] and the long-term, regional transport processes of Cascade [18].

This model simulates the evolution of the shoreline and the transport of sand over time. Capable of incorporating different engineering structures, such as jetties, breakwaters, and seawalls as well as other activities such as beach nourishment, this model is often used to determine the consequences of introducing man-made structures to the

coastal environment. Examples of this model being applied to the study of shoreline dynamics include [35, 109, 36].

1.7.2 Setup

GenCade was applied to an area surrounding La Turballe port, covering a distance of over 5 km. Two set of simulations were conducted in order to compare the evolution of the shoreline with and without the jetty and mole studied in Section 1.5. Figure 1.11 shows the two initial shoreline conditions used in the simulation. The blue line indicates the shoreline with the newly determined jetty and mole whereas the red delimits the shoreline in its actual state. Characteristic forcing conditions of the area were applied over the duration of 30 years.

The aim of this simulation was to confirm that the redesign of the port has little influence of the surrounding shoreline to the long term. We cannot compare simulation with field data since the simulations are purely forecasts. We set the Gencade model with typical parameters for the beaches surrounding La Turballe, and a comparison was performed with and without the port transformation. The modeling of the long term shoreline dynamics is relative on account of Gencade using a purely linear formalism (Pelnard Considère equation, cf. [95], but does provide a trend.

1.7.3 Results

Figure 1.12 shows the results of two simulations conducted by GenCade, in the area surrounding the port. Beyond this area, no changes to the shoreline are observed, arguing that the new layout of the port only impacts the surrounding shoreline within a 150 m radius, and no long term impact can be expected. In the vicinity of the port, two areas of discrepancy can be observed. The first is located in the area where the beach reaches the port. However, the difference between the two configurations does not exceed 15 m over the 30-year period. The second zone of interest is situated on the border of the jetty exposed to the ocean waves. Here, a difference of several meters is observed. Given that this border is a solid wall and cannot vary over time, the discrepancy can be explained as the result of numerical inaccuracy against such solid boundary condition. Given the results provided by GenCade, we can conclude that redesigning the port to include a jetty and mole does not impact the shoreline dynamics of the surrounding area.

1.8 Conclusion

This work describes a full textbook case of port engineering redesign by optimization theory combined with a posteriori management of an environmental question. The concepts and a comprehensive methodology are presented on the very classic port of La

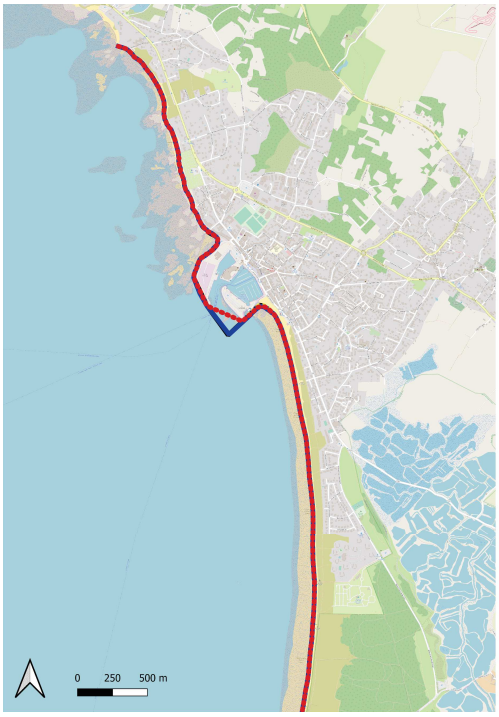

Figure 1.11: The two initial shoreline conditions of La Turballe port.

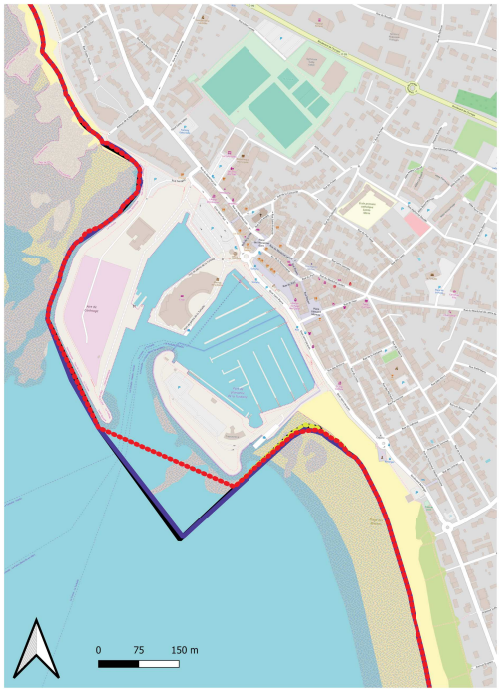

Figure 1.12: Results of the long term morphodynamic simulation with and without the proposed structures. The simulations without the redesign of the port are given by the dotted lines: yellow is the initial shoreline and red is the shoreline after the 30-year simulation. The simulations incorporating the redesign of the port are given by the solid lines: black is the initial shoreline and blue is the shoreline after the 30-year simulation.

Rochelle; then a realistic application is performed for the redesign of La Turballe port. The optimal solution presented in Section 1.5 where an elongated jetty and a widened mole is preferred is determined by optimization theory.

The motivation behind this numerical model is not to determine the ultimate port design, which would require extensive verification and validation procedures, but to provide a description of a new rapid and cost effective optimization tool, with an application to La Turballe port. This tool was designed to accompany classical engineering approaches and should not be the sole component of the port design study; the Verification and Validation (V&V) component is undeniably required when approving a new port design. However, this is beyond the scope of the numerical work presented here. In this paper, we demonstrate that the rapidity and adaptiveness of the model allows the engineers in charge to focus on practical solutions efficiently. They should subsequently perform a thorough V&V of the considered port configurations.

The final redesign of the port promoted by the procedure satisfies the constraints imposed, is a good solution for any incoming forcing considered and thus delineates the best solution ever. This solution is consistent with classic engineering. Despite the calculations being centered on the minimization of wave agitation and the increase of exploitable surface area, the optimal solution also has the advantage of having no significant impact on the surrounding shoreline dynamics. This work demonstrates that numerical optimization may be quick and efficient in the identification of port solutions consistent with classic engineering even in the context of complex problems.

1.A Appendix: La Turballe Workflow

This appendix was written to detail the workflow of the shape optimization model. This model was developed in collaboration with BRLi for the purpose of accompanying engineers and project managers in the search of the optimal positions and/or dimensions of coastal protection structures such as breakwaters, jetties, moles and groynes. The following is based on the model diagram depicted in Figure 1.13. Each section of this report corresponds to a step of the workflow. We illustrate the model using the example of La Turballe port (France). In the study conducted in Section 1.5, we were interesting in the addition of a mole and a jetty at the entrance of the port. A second study was conducted with the idea of adding a groyne and a jetty. This second project is the subject of the following workflow. Both studies were presented to the project managers for further discussions.

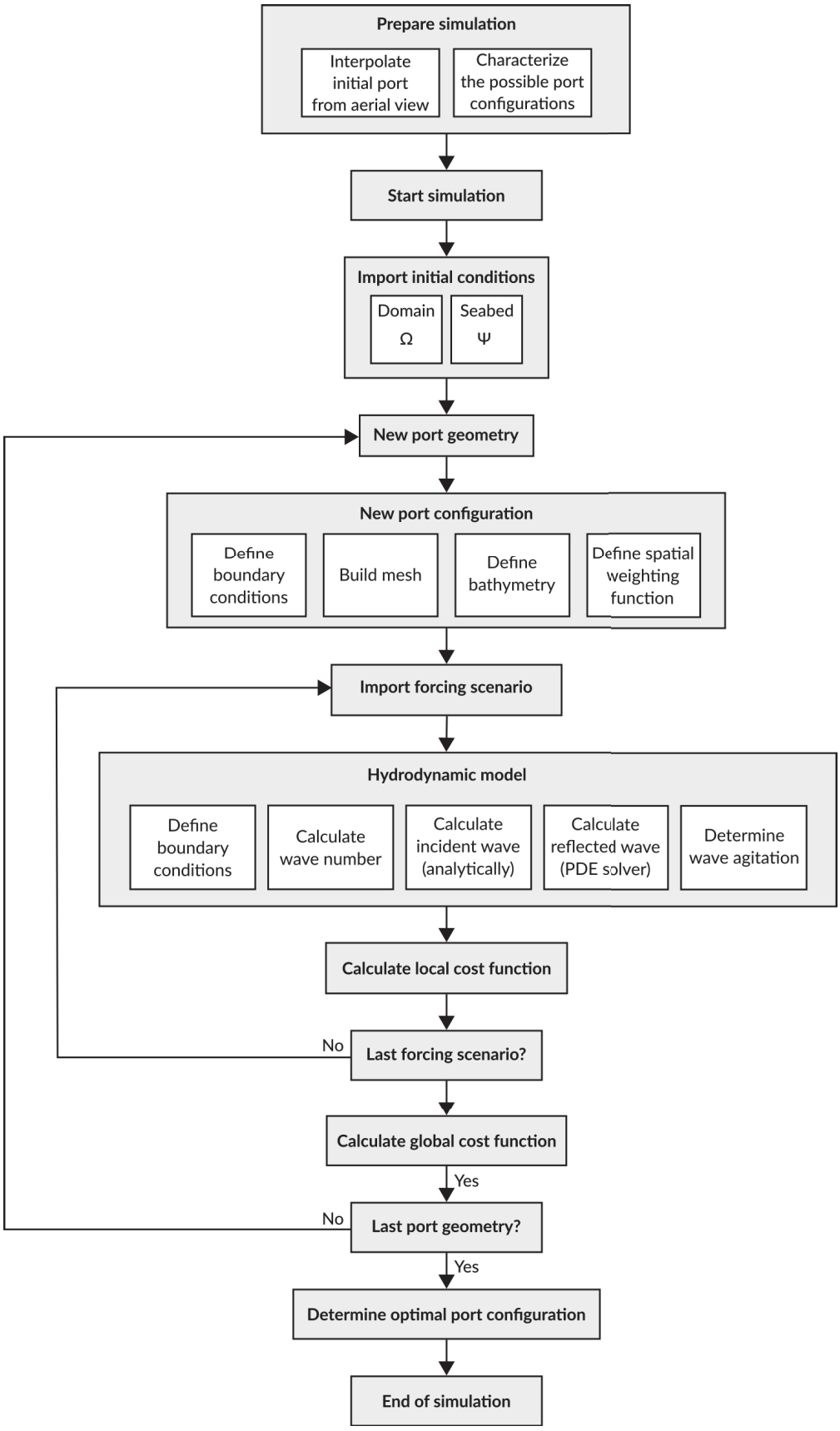

Figure 1.13: Workflow of the numerical model used to find the optimal configuration of La Turballe port

Step 0: Establish topic of study

Before starting the simulation, the user must first establish the topic of study. This includes the type of land mass (e.g. islands, ports, beaches), the parameters used in the optimization problem (e.g. position and/or dimensions of protection structures) and the quantity to be minimized (e.g. wave energy, agitation, coastal erosion). The study illustrating this report is that of the port of La Turballe, situated in North-Western France. The department of Loire-Atlantique plans to enlarge the port to accommodate the increasing commercial, fishing and other activities appearing there. The objective of this study is to increase the surface area of the port using structures such as jetties and groynes, while at the same time, limiting the wave energy entering the port. This second condition originates from observations made by the users and managers of the port; during extreme weather, dangerously large waves arrive at the port and cause significant damage to the moored boats and nearby equipment.

Step 1: Prepare simulation

Interpolate initial port from aerial view

Using satellite imagery provided by Google Maps, we extracted the outline of the port. Thirty-four points delimiting the port were used in this simulation. These points are stored in a two-columned file and will be given at the start of the simulation.

Figure 1.14: Aerial view of current configuration of La Turballe port

Characterize the possible port configurations

During discussions with BRLi, it was established that adding a groyne and a jetty to the existing port configuration could be a possible solution, in order to protect the port and offer more exploitable surface area. For illustrative purposes, we present the search for the optimal configuration of the port using only two degrees of freedom. We define the set of parameters by $\psi = (\beta, \gamma)$, where β characterizes the jetty and γ characterizes the groyne. Certain constraints are imposed in order to guarantee practical results; these originate from the expertise of classic port engineering. Constraints include the location and dimensions of the structures. The structures must also be sufficiently elevated to be considered impassable by wave over-topping.

Groyne: The parameter γ represents the position of the groyne, more precisely the distance between the groyne and the edge of the existing wall as illustrated by Figure 1.15.

Characteristics:

- The groyne extends perpendicularly from the port wall.
- The width of the groyne is fixed at $30\,m$.
- The length of the groyne is fixed at $100\,m$.
- The groyne must be located between $0\,m$ and $130\,m$ from the existing edge.

Figure 1.15: Parameter γ defining the groyne

Jetty: The parameter β represents the length of the extension of the jetty as illustrated by Figure 1.16.

Characteristics:

- The extremity of the jetty is fixed to the port, but the jetty itself can be extended freely towards the south.
- The jetty cannot be installed in waters where the depth exceeds 5.5 m.
- The jetty must measure between 120 m and 550 m.
- The distance between the groyne and jetty cannot be under 60 m.

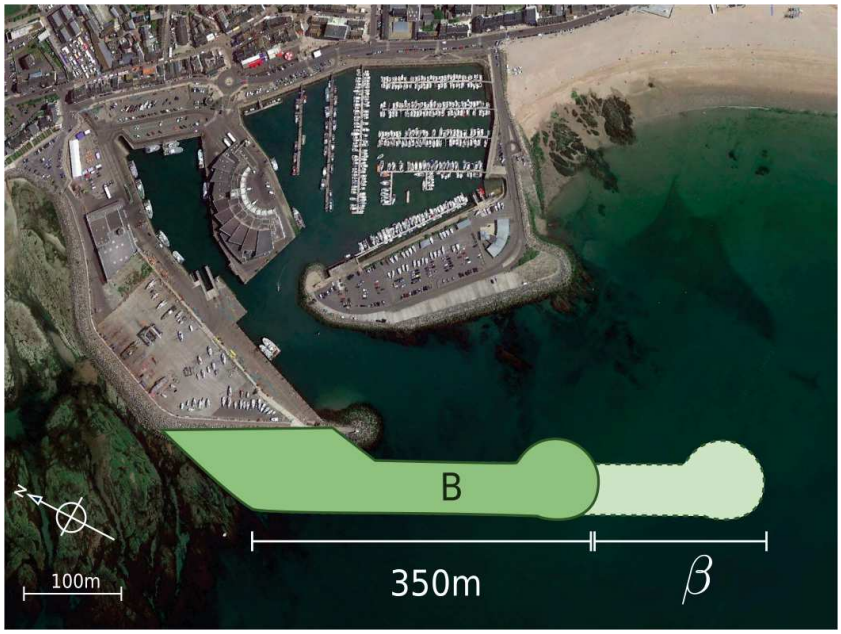

Figure 1.16: Parameter β defining the jetty

Step 2: Start simulation

Once the simulation has been prepared and the input files have been defined, the user can then run the simulation. The following steps describe the workflow performed by the numerical model.

Step 3: Import initial conditions

Domain

The outline of the port is given at the entry of the model in the form of the (x, y) coordinates. The simulation requires a closed domain of study, so the model itself adds

the desired groyne and jetty and closes the domain in such a manner that the forcing boundary is clearly defined.

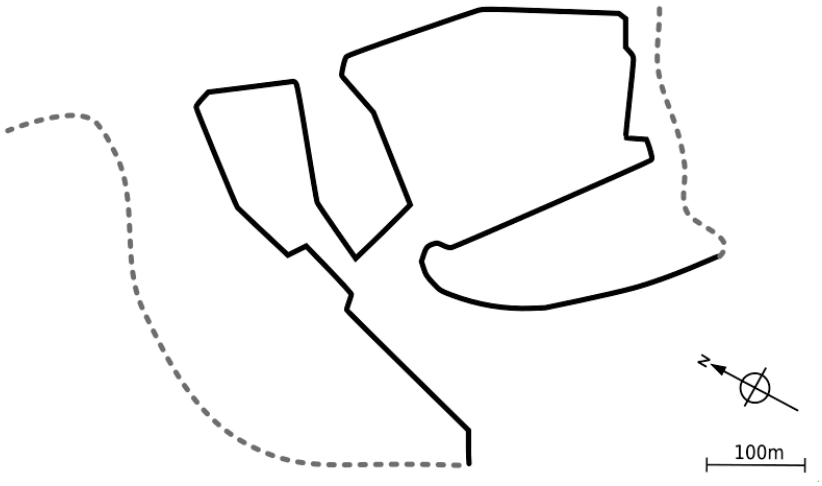

Figure 1.17: Example of port outline given in input of the model

Seabed

It is also possible to import the bathymetric characteristics of the port.

Figure 1.18: Bathymetric data within the port

The bathymetric properties within the port of La Turballe have been observed to be stable, with a depth ranging between 1.5 m and 3.5 m. Changes over time to the seabed have been omitted from the optimization simulation. For a more complex sea floor, it is possible to import the bathymetric data, and interpolate over the mesh. However, given the simplicity of the seabed and for time saving purposes, the bathymetry here will be defined analytically.

Step 4: New port geometry

Adopting a given value of the parameters $\psi = (\beta, \gamma)$ generates a new configuration of the port and is fed into the optimization model.

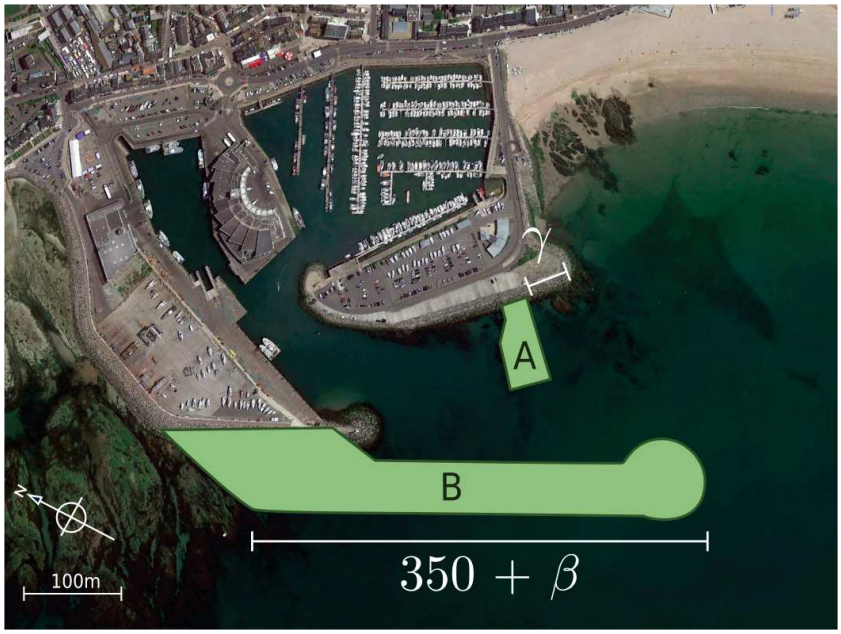

Figure 1.19: Example port configuration, defined by the parameters (β, γ)

Given that the domain Ω varies for each port geometry, the mesh, bathymetric function and wave field must be recalculated for each loop, i.e. for each variation of the couple (β, γ).

Step 5: New port configuration

Define boundary conditions

We define the domain Ω as the area occupied by water within the port. The domain is a closed, compact sub-domain of $\mathbb{R}^2$. We denote Λ the boundary of Ω, which is partitioned

into 3 subsets ($\Lambda_i, \Lambda_w, \Lambda_o$). We denote Λ_i the boundary over which the incoming forcing is present, Λ_w the boundary of the domain representing the walls of the port and Λ_o the boundary over which an outflux of energy is observed. The different types of boundaries present at La Turballe port are illustrated by Figure 1.20; there is no outlet border.

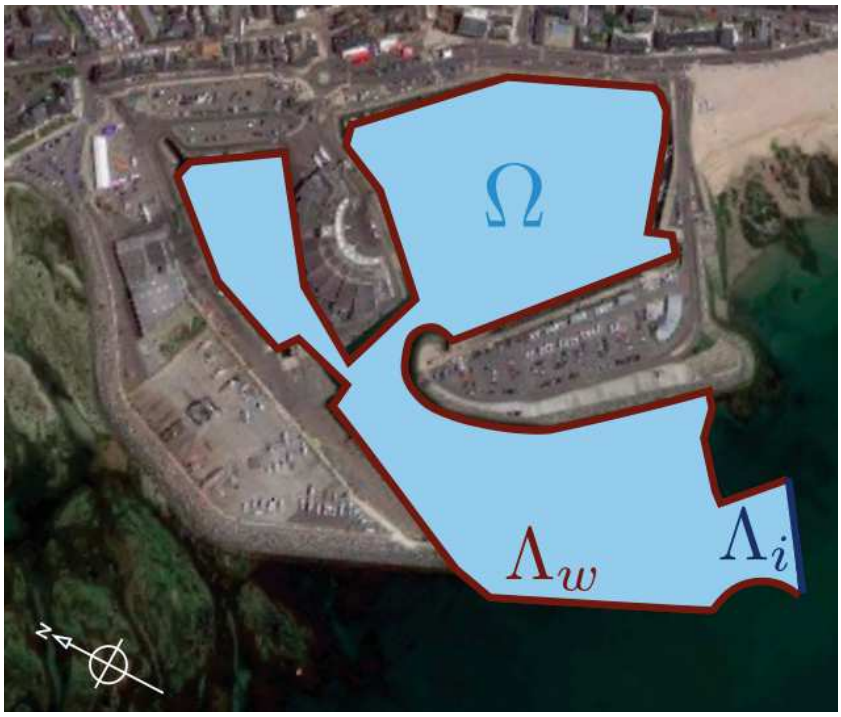

Figure 1.20: Illustration of the domain Ω with the different boundary types: Ω is the domain of the hydrodynamic study (light blue), Λ_i is the set of borders responsible for the influx of energy (dark blue) and Λ_w is the set of borders corresponding to the solid walls of the port (red).

Build mesh

The mesh used in this model is a non structured, triangular isotropic mesh, adapted to the shape of the domain Ω (cf. Figure 1.21). It is also generated to incorporate the different boundary types. The mesh is recalculated for each explored solution which guarantees more precise calculations by the hydrodynamic model.

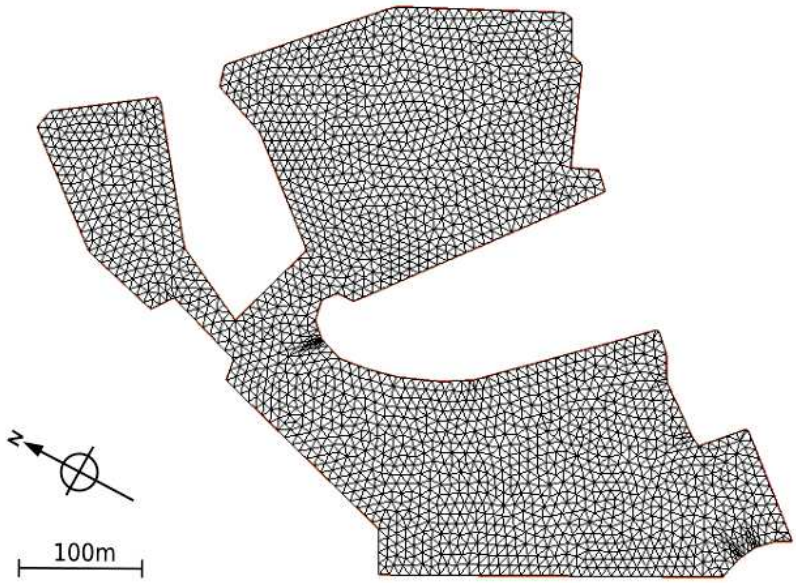

Figure 1.21: Mesh used in the hydrodynamic simulation (here, Nb of Triangles = 4288, Nb. of Vertices = 2315)

Define bathymetry

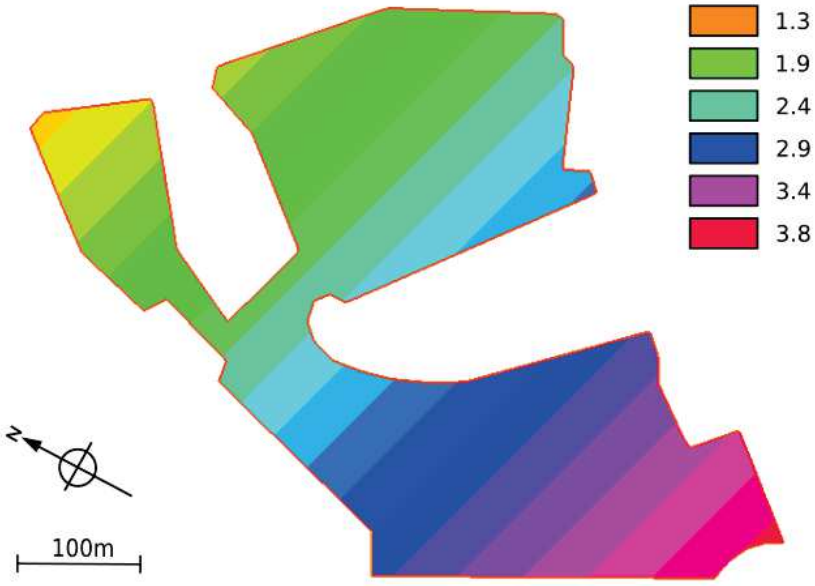

Figure 1.22: Analytical function defining the seabed over the port domain

As mentioned previously, the seabed here is defined simply as a linear function over the domain. This choice was taken in an effort to save time; the seabed would have had to be interpolated over each new port configuration. Here, it is defined analytically and illustrated by Figure 1.22.

Define spatial weighting function

The spatial weighting function allows the user to prioritize certain zones of the port where they would like the minimization of wave energy to be focused. These zones are typically surrounding mooring stations or zones in which high maritime circulation is expected. Examples of spatial weighting functions include

$$\mathcal{P}_0(x) = 1, \tag{1.21}$$

where no zone is prioritized, and

$$\mathcal{P}_1(x, y) = \exp(-A((x - x_a)^4 + (y - y_a)^4)) \tag{1.22}$$

where a circular zone within the port is considered a priority, the center of which is given by the coordinates (x_a, y_a) and A defines its radius (cf. Figure 1.23).

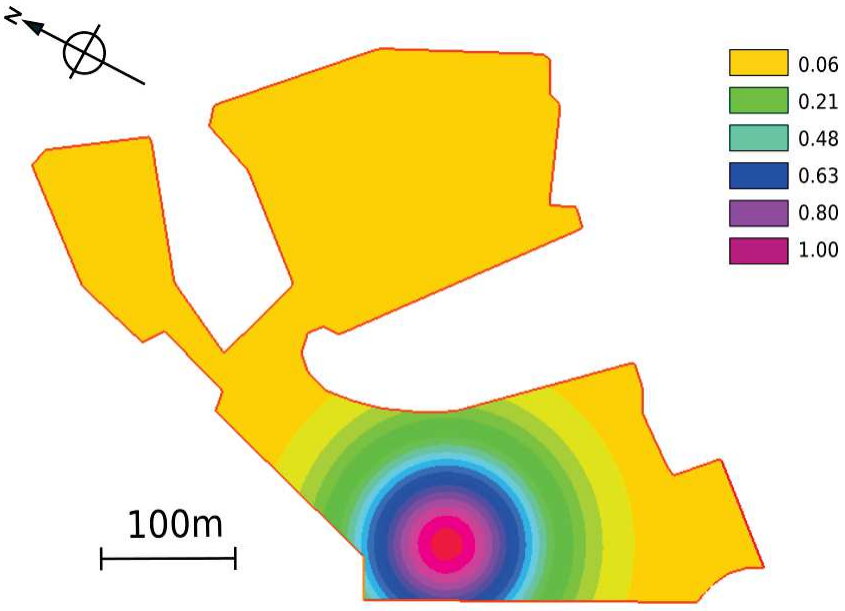

Figure 1.23: Example of spatial weighting function

Step 6: Import forcing scenario

Forcing is given in the form of wave agitation at the entrance of the port, where the influx of energy originates. In our example, 28 different forcing scenarios were provided

for the study, representing conditions ranging from fair weather to severe storms. These scenarios are given in the form of 3 parameters: the frequency, angle and amplitude of the incoming wave $(f, \theta, a_{\max})$, cf. Table 1.1. For each forcing scenario, we apply the hydrodynamic model, and then define a local cost function.

Case nb.	f	θ	$a_{\max}$
1	0.003730333266735	245.738	0.17206
2	0.011190999800205	245.738	0.17206
3	0.018651666333675	245.738	0.17206
4	0.026112332867145	245.738	0.17206
5	0.003730333266735	248.278	0.297345
6	0.011190999800205	248.278	0.297345
7	0.018651666333675	248.278	0.297345
8	0.026112332867145	248.278	0.297345
9	0.003730333266735	250.684	0.49606
10	0.011190999800205	250.684	0.49606
11	0.018651666333675	250.684	0.49606
12	0.026112332867145	250.684	0.49606
13	0.003730333266735	257.133	0.63832
14	0.011190999800205	257.133	0.63832
15	0.018651666333675	257.133	0.63832
16	0.026112332867145	257.133	0.63832
17	0.003730333266735	242.439	0.87658
18	0.011190999800205	242.439	0.87658
19	0.018651666333675	242.439	0.87658
20	0.026112332867145	242.439	0.87658
21	0.003730333266735	258.572	1.496755
22	0.011190999800205	258.572	1.496755
23	0.018651666333675	258.572	1.496755
24	0.026112332867145	258.572	1.496755
25	0.003730333266735	258.774	1.87653
26	0.011190999800205	258.774	1.87653
27	0.018651666333675	258.774	1.87653
28	0.026112332867145	258.774	1.87653

Table 1.1: Forcing table containing the 28 different forcing scenarios used in the simulation

Step 7: Hydrodynamic model

The aim of this hydrodynamic model is to provide the height of the waves (and therefore energy) within the port, in a short amount of time. Considering that this tool has been developed in order to aide engineers in designing protection structures, it is critical that the numerical simulations can be performed while discussions are underway, and to do so, results of the simulations must be produced rapidly.

For simplicity purposes, we place ourselves in the setting of linear wave theory. The hydrodynamic model developed here, is based on the assumption that a surface wave η can be described as the sum of an incident wave η_{i} and a reflected wave η_{r}.

Define boundary conditions

On forcing boundaries Λ_{i}, the total wave field is composed solely of the incident wave field since no reflection occurs. This yields $\eta = \eta_{\mathrm{i}}$ over Λ_{i}.

On solid borders Λ_{w}, a certain portion of the energy of the waves is reflected/absorbed when contact with this boundary is made. This reflective property is directly linked to the physical characteristics of the boundary. In the case of vertical rigid walls, almost all of the energy is reflected. On mild slope boundaries, more energy is absorbed/dissipated; the reflected wave field on these boundaries is equal to a portion of the incident wave field. Over Λ_{w}, we have $\eta_{\mathrm{r}} = -\gamma_{\mathrm{ab}}\eta_{\mathrm{i}}$, where $\gamma_{\mathrm{ab}} \in [0, 1]$ is a reflection/absorption coefficient. For $\gamma_{\mathrm{ab}} = 1$, the border shows total reflection and $\gamma_{\mathrm{ab}} = 0$ the border shows total absorption.

Outlet borders can also be implemented but are not present in this simulation.

Calculate wave number

Before calculating wave agitation, we first need the wave number k across the domain. We use the linear dispersion equation:

$$\sigma^2 = gk \tanh(kh) \tag{1.23}$$

where σ is the wave frequency, h is water depth and g is gravitational acceleration. A shallow water approximation can be used here because the wave length of standing waves inside the port are significantly greater than the mean water depth.

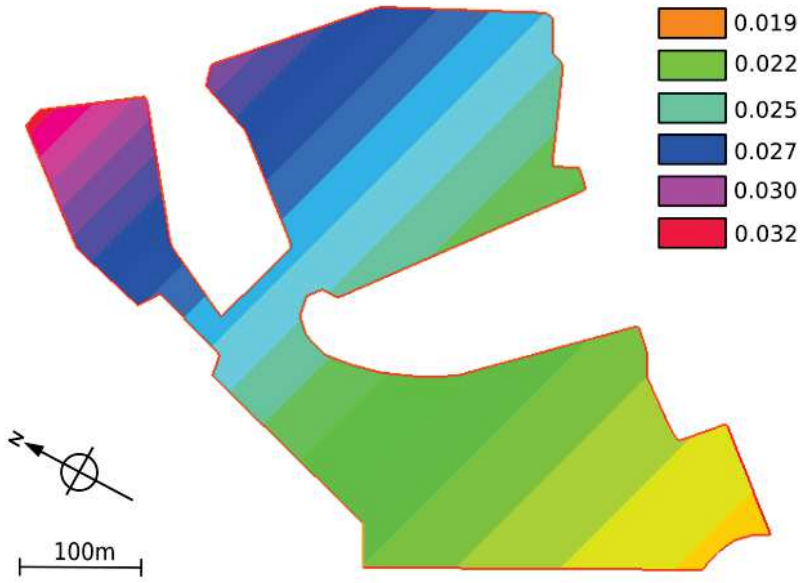

Figure 1.24: Example of wave number field calculated over the port domain

Calculate incident wave

The incident wave η_{i} is defined analytically by:

$$\eta_{\mathrm{i}}(x,t) = a_{\mathrm{i}}(x)e^{-i\sigma t} \tag{1.24}$$

where the spatial component a_{i} is defined by:

$$a_{\mathrm{i}}(x) = a_{\max}e^{-i\vec{k}x} \tag{1.25}$$

with $a_{\max}$ the amplitude of the water surface oscillation for this given frequency, and $\vec{k} = k(\cos(\theta), \sin(\theta))$ the wave number vector. Here, θ is the angle of propagation of the wave and k is the previously calculated wave number.

ℹ Note that the angle of the waves given in the input file does not correspond to the angle used in the definition of $\vec{k}$; we take $\theta = 2\pi - \theta_{\mathrm{input}}\pi/180 - \theta_{\mathrm{north}}$, where θ_{input} is the angle given in the forcing input file and θ_{north} is the angle from north.

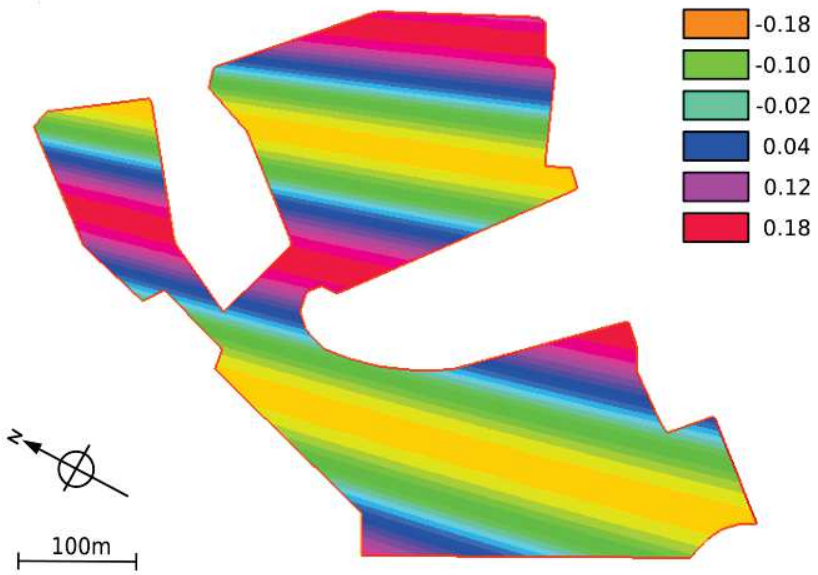

Figure 1.25: Example of incident wave field, with $(\theta, f, a_{\max}) = (245.738, 0.0186, 0.172)$

Calculate reflected wave

The reflected wave is defined by:

$$\eta_{\mathrm{r}}(x,t) = a_{\mathrm{r}}(x)e^{-i\sigma t}. \tag{1.26}$$

We suppose the spatial component a_{r} of the reflected wave satisfies the following Helmholtz under the assumption that the water depth is sufficiently flat:

$$k^2 a + \Delta a = 0. \tag{1.27}$$

Incorporating the previous boundary conditions, the reflected wave field satisfies:

$$\begin{cases} k^2 a_{\mathrm{r}} + \Delta a_{\mathrm{r}} = 0 & \text{over } \Omega \\ a_{\mathrm{r}} = 0 & \text{on } \Lambda_{\mathrm{i}} \\ a_{\mathrm{r}} = -\gamma_{\mathrm{ab}} a_{\mathrm{i}} & \text{on } \Lambda_{\mathrm{w}} \end{cases}. \tag{1.28}$$

This time-independent elliptic partial differential equation which includes Dirichlet boundary conditions is solved using a finite element method. This method was chosen because it allows the use of irregular grids with elements of different sizes and geometries, as well as the possibility of mesh adaptation. Given that a port may present intricate details and complex boundaries, a finite element method was a natural choice. Such a finite element method requires a weak formulation of the considered problem. In our case, the weak formulation of the Helmholtz problem (1.28) reads:

Find a_r such that

$$\int_\Omega k^2 a_r v = \int_\Omega \nabla a_r \nabla v + \int_{\Lambda_w} \gamma_{ab} (\nabla a_i \cdot \vec{n}) v \tag{1.29}$$

for all test functions v of the same nature as a_r. We use piecewise linear finite element functions to numerically determine the solution of (1.29) over a triangular adapted mesh.

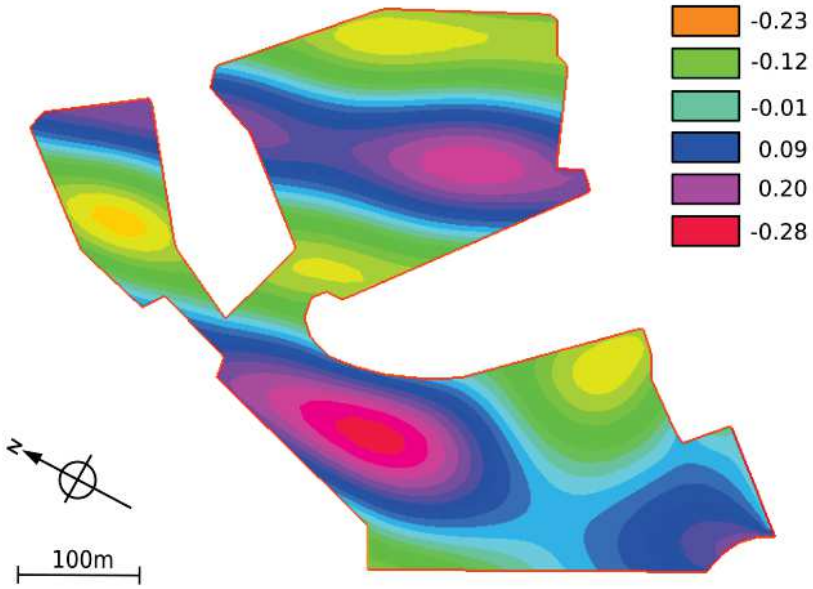

Figure 1.26: Example of reflected wave field, resulting from the resolution of the Helmholtz equation, with $(\theta, f, a_{max}) = (245, 0.0186, 0.172)$

Determine wave agitation

Having calculated η_i and η_r over Ω, we can now determine the total wave agitation field by setting

$$\eta = \eta_i + \eta_r. \tag{1.30}$$

This quantity is used to calculate the local cost functions used in the energy minimization simulation.

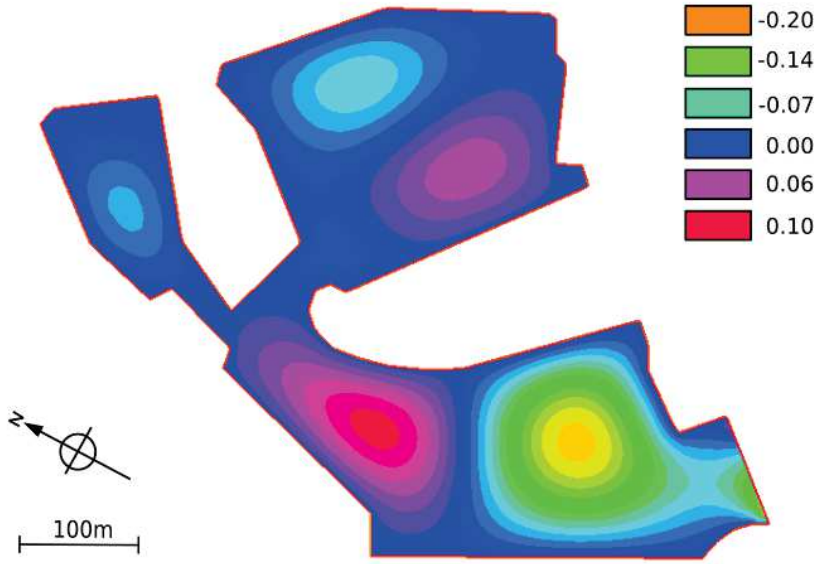

Figure 1.27: Example of wave field provided by the hydrodynamic model, with $(\theta, f, a_{\max}) = (245, 0.0186, 0.172)$

Step 8: Calculate local cost function

For a given forcing scenario n, we consider the following local cost function:

$$\mathcal{J}_n(\psi) = \frac{1}{K(\mathcal{P})} \frac{1}{|\Omega(\psi)|} \int_{\Omega(\psi)} \mathcal{E}_n(\psi, x)\, \mathcal{P}(x)\, \mathrm{d}x \tag{1.31}$$

where ψ is the parameterization of the port modifiable in the search of an optimal configuration and $|\Omega(\psi)|$ is the surface area of $\Omega(\psi)$. The quantity $\mathcal{E}_n$ is the total surface energy defined over the domain Ω and associated with the forcing scenario n and the configuration ψ of the port. It is defined by:

$$\mathcal{E}_n(\psi, x) = \frac{1}{2} \rho g (a_n(\psi, x))^2 \tag{1.32}$$

where ρ is the density of the water, g is the gravitational acceleration and $a_n(\psi)$ the amplitude of the waves calculated over $\Omega(\psi)$ associated with n and ψ. The function $\mathcal{P}$, is the spatial weighting function defined in Step 6, with $K(\mathcal{P}, \Omega(\psi)) = \int_{\Omega(\psi)} \mathcal{P}(x)\, \mathrm{d}x$.

The local cost function $\mathcal{J}_n(\psi)$ is calculated for a given parameterization ψ and a given forcing scenario n. Once all the forcing scenarios have been explored, a global cost function associated with the parameterization ψ is determined. As such, the term *local* indicates the use of one forcing scenario and has nothing to do with spacial locality.

Step 9: Check last forcing scenario condition

If the last forcing condition has not yet been reached, go to Step 7 to apply the hydrodynamic model and calculate the associated local cost function with a new forcing condition. Otherwise, continue to Step 11, to determine the global cost function using the previous local cost functions.

Step 10: Calculate global cost function

The global cost function $\mathcal{J}$ is a linear combination of the local cost functions defined by Equation (1.31), where the scalar coefficients are determined by the wave energy at the forcing boundary. Let $a_{\mathrm{i}}(n)$ be the amplitude of the incoming waves (defined on Λ_{i}) associated with the forcing scenario n, the global cost function to be minimized in the search of the optimal solution is defined as:

$$\mathcal{J}(\psi) = \frac{\sum_{n=1}^{N} a_{\mathrm{i}}(n)\mathcal{J}_n(\psi)}{\sum_{n=1}^{N} a_{\mathrm{i}}(n)}. \tag{1.33}$$

Step 11: Check last port geometry condition

If the last port geometry has not yet been reached, go to Step 5 with a new port geometry. The forcing conditions will be explored once again, the hydrodynamic model will be applied over this new domain and the local and global cost functions are calculated. Otherwise, continue to Step 13 to establish the optimal port configuration.

Step 12: Determine optimal port configuration

Having explored all the possible port geometries and having calculated the global cost function for each of them, we are able to determine the optimal port configuration for wave energy minimization. This minimum is obtained using a simple optimization model, or can be represented on a 2-dimensional graph (this is possible because this simulation only contains two degrees of freedom). A problem with a greater number of parameters is still possible but the cost function is more difficultly represented. Figure 1.28 represents the value of the global cost function for the set of parameters $\psi = (\beta, \gamma)$.

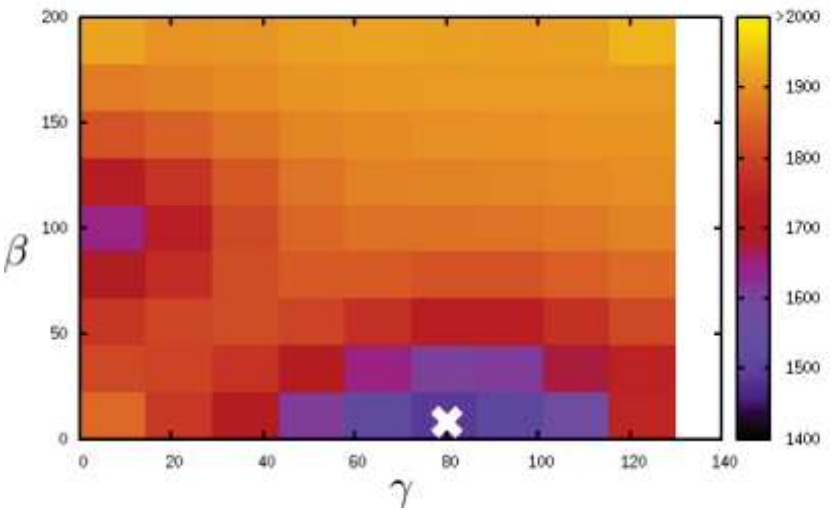

Figure 1.28: Global cost function with regard to the parameters (β, γ)

The minimum of the global cost function $\mathcal{J}$ is given by:

$$\boxed{\beta^* = 0 \text{ and } \gamma^* = 91.}$$

The best solution is the configuration where the groyne is located at 91 m from the edge and the length of the jetty measures 350 m. This corresponds to the configuration shown in Figure 1.29.

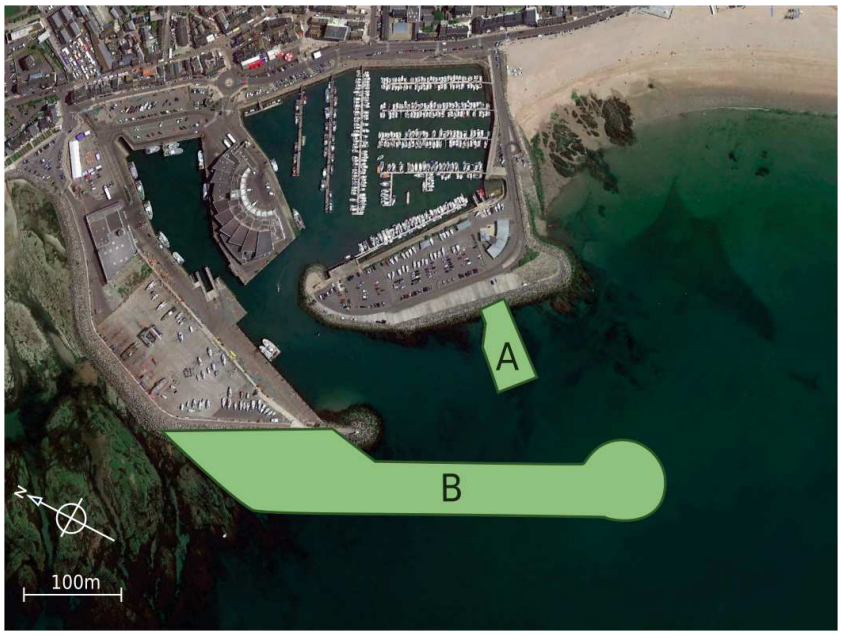

Figure 1.29: Final configuration resulting from the optimization model

Step 13: End of simulation

The end results of this simulation were presented to BRLi, as well as the municipality of Loire-Atlantique and aided in the decision of the redesign of La Turballe port. Construction began December 2020.

The advantage of the method presented here is the possibility of representing the global cost function $\mathcal{J}$ with regards to the parameters β and γ. This allows the user to open a discussion about the possible final results. The user may prefer not to use the optimal configuration associated with the global minimum and adopt a configuration associated with a local minimum for reasons not incorporated in the model, such as costs of construction, surface area, estimated revenue or boat mooring space. It is worth noting that these characteristics can be included in the shape optimization model by redefining the cost function.

Chapitre 2

Calcul Optimal Appliqué à la Dynamique Littorale

Ce chapitre concerne le développement d'un nouveau modèle hydro-morphodynamique, nommé Opti-Morph et basé sur la théorie d'optimisation. Nous cherchons à développer un modèle numérique rapide, robuste et de faible complexité, capable de simuler l'évolution du profil bathymétrique.

Ces travaux ont fait l'objet d'un article, soumis pour publication au journal *Geophysical Research Letters*, intitulé "Opti-Morph, a new platform for sandy beach dynamics by constrained wave energy minimization", cf. [21].

2.1 Résumé en Français

2.1.1 Introduction

Les modèles numériques morphodynamiques sont des outils essentiels pour comprendre et prédire l'évolution du profil bathymétrique et de la morphologie des plages en zone littorale. Le nouveau modèle Opti-Morph développé lors de la thèse et décrit dans ce chapitre est basé sur la théorie d'optimisation. Jusqu'à présent, l'optimisation a surtout été utilisée dans l'étude des ouvrages de protection littorale, tels que les ports (cf. Chapitre 1) ou les brise-lames (cf. Chapitre 3).

Dans le prolongement des travaux théoriques de [11, 81, 12, 79], Opti-Morph décrit l'évolution du fond sableux en prenant en compte le couplage entre les processus morphodynamiques et hydrodynamiques. L'hypothèse fondamentale de ce modèle affirme que le fond sableux s'adapte pour minimiser une certaine quantité hydrodynamique. Le choix de cette quantité définit la force motrice derrière l'évolution morphologique des fonds sableux. Ce problème d'optimisation est soumis à un certain nombre de contraintes, permettant une description plus précise des processus morphodynamiques.

Dans le but de valider Opti-Morph, nous comparons les résultats de la simulation numérique avec des données expérimentales obtenues dans une expérience physique de canal à houle. Nous comparons également Opti-Morph à un deuxième modèle hydro-morphodynamique littoral numérique, XBeach [103], afin d'évaluer sa performance par rapport aux modèles hydro-morphodynamiques existants. Opti-Morph a l'avantage supplémentaire d'être un modèle numérique rapide, robuste et de faible complexité.

2.1.2 Modèle Hydrodynamique

L'évolution en temps du profil bathymétrique est basé sur l'hypothèse que le fond évolue afin de minimiser une certaine quantité hydrodynamique. Ainsi, un modèle hydrodynamique fournissant une description de l'état des vagues de surface est indispensable. Le modèle présenté ci-dessous détermine la hauteur significative des vagues, noté H le long du profil cross-shore.

Soit $\Omega := [0, x_{\max}]$ le domaine du profil cross-shore, où $x = 0$ est un point arbitraire en eaux profondes, et $x_{\max}$ est un point arbitraire au-delà du trait de côte. Le domaine Ω est divisé en deux sous-ensembles disjoints : la zone de shoaling Ω_S et la zone de déferlement Ω_B.

La hauteur des vagues H sur Ω_S est basée sur l'équation de shoaling (2.1), où H_0 est la hauteur des vagues en eau profonde et K_S est un coefficient de shoaling.

$$H(x,t) = H_0(t)K_S(x,t) \tag{2.1}$$

Toutefois, au lieu de considérer que les vagues dépendent uniquement de la hauteur des vagues au large H_0, on considère que la hauteur d'une vague dépend des vagues en amont. Par ailleurs, plus on remonte en amont du domaine, plus cette influence s'amoindrit, jusqu'à ce qu'aucune influence ne soit détectée. Cette distance maximale est appelée la distance maximale de dépendance spatiale des vagues et est notée d_w.

Ainsi, le terme H_0 de l'équation de shoaling (2.1) devient H_0^w défini par (2.2), où w est la fonction de poids avec $w(0) = 1$ (dépendance totale pour les vagues proches) et $w(d_w) = 0$ (dépendance nulle pour les vagues distantes).

$$H_0^w(x,t) = \frac{1}{\int_{x-X}^{x} w(x-y)\mathrm{d}y} \int_{x-X}^{x} w(x-y)H(y)K(y)\mathrm{d}y \tag{2.2}$$

En utilisant le critère de déferlement de Munk [84] pour définir la hauteur de vagues en zone de déferlement Ω_B, nous définissons la hauteur des vagues le long du profil

cross-shore par :

$$H(x,t) = \begin{cases} \left[(1-\alpha(x))H_0(t) + \alpha(x)H_0^w(x,t)\right] K_{\mathrm{S}}(x,t) & \text{si } x \in \Omega_{\mathrm{S}} \text{ et } x < d_{\mathrm{w}} \\ H_0^w(x,t)K_{\mathrm{S}}(x,t) & \text{si } x \in \Omega_{\mathrm{S}} \text{ et } x \geq d_{\mathrm{w}} \\ \gamma h(x,t) & \text{si } x \in \Omega_{\mathrm{B}} \end{cases} \quad (2.3)$$

où $\alpha(x) = \dfrac{x}{d_{\mathrm{w}}}$ sur $[0, d_{\mathrm{w}}]$ permet la gestion des condition aux bords.

2.1.3 Modèle Morphodynamique basé sur l'Optimisation de l'Énergie des Vagues

On note $\psi : \Omega \times [0,T] \times \Psi \to \mathbb{R}^+$ l'élévation du fond sableux où $[0,T]$ est l'intervalle de temps considéré lors de la simulation et Ψ est l'ensemble des paramètres physiques décrivant les caractéristiques du fond. On suppose que le fond varie au cours du temps afin de minimiser une fonction de coût $\mathcal{J}$. Nous supposons que cette fonction de coût est définie comme l'énergie potentielle des vagues en zone de shoaling, définie pour tout $t \in [0,T]$ par :

$$\mathcal{J}(\psi,t) = \frac{1}{16}\int_{\Omega_{\mathrm{S}}} \rho_{\mathrm{w}} g H^2(\psi,x,t)\mathrm{d}x \qquad [J.m^{-1}] \quad (2.4)$$

où H désigne la hauteur des vagues calculée par le modèle hydrodynamique susmentionné, ρ_{w} est la densité de l'eau ($kg.m^{-3}$), et g désigne l'accélération gravitationnelle ($m.s^{-2}$). Dans le but de décrire l'évolution du profil bathymétrique ψ, dont l'état initial est donné par ψ_0, nous supposons que ψ, dans son effort pour minimiser $\mathcal{J}$, vérifie la dynamique suivante :

$$\begin{cases} \psi_t = \Upsilon \,\Lambda\, d \\ \psi(t=0) = \psi_0 \end{cases} \quad (2.5)$$

où ψ_t est l'évolution en temps du fond sableux ($m.s^{-1}$), Υ est la mobilité sédimentaire ($m.s.kg^{-1}$), Λ est l'excitation du fond sableux par les vagues, et d est la direction de descente indiquant la manière dont le fond sableux varie.

Dans des configurations sans contrainte, on a $d = -\nabla_\psi \mathcal{J}$, qui par sa définition, indique la direction d'un minimum local de $\mathcal{J}$ par rapport à ψ.

Néanmoins, des contraintes sont ajoutées au modèle pour incorporer plus de physique et fournir des résultats plus réalistes. Les forces motrices de l'évolution morphologique du profil bathymétrique sont décrites par la minimisation de la fonction de coût $\mathcal{J}$ alors que les processus secondaires sont exprimés par des contraintes. Deux contraintes physiques ont été adoptées par la suite : (i) une contrainte de pente sableuse, qui empêche le sable de présenter des pentes irréalistes et (ii) la contrainte de stock sableux, obligeant

la quantité de sable dans un bassin expérimental à rester constante au cours du temps. Cette dernière est nécessaire pour vérifier et valider le modèle numérique dans des simulations de canal à houle.

La première contrainte se traduit par :

$$\left|\frac{\partial \psi}{\partial x}\right| \leq M_{\text{slope}} \tag{2.6}$$

où le paramètre M_{slope} représente l'angle de talus critique du sable, tandis que la deuxième s'écrit :

$$\int_{\Omega} \psi(t,x)\mathrm{d}x = \int_{\Omega} \psi_0(x)\mathrm{d}x \qquad \forall t \in [0,T] \tag{2.7}$$

pour garantir que le stock sableux reste constant au cours du temps.

Pour conclure, le problème d'optimisation gouvernant l'évolution en temps du fond sableux s'écrit de la forme :

Pour chaque temps $t \in [0,T]$, trouver la forme du fond sableux $\psi \in \Psi$ de telle sorte que l'énergie des vagues $\mathcal{J}$ soit minimale, tout en vérifiant les contraintes de pente (2.6) *et de stock sableux* (2.7).

Le modèle numérique qui découle de cette théorie fut baptisé Opti-Morph.

2.1.4 Application Numérique

Dans l'optique de valider le modèle Opti-Morph, le profil bathymétrique produit par le modèle numérique est comparé à des données expérimentales. Une série d'expériences en laboratoire dans un canal à houle a été réalisée. Mesurant $36\,m$ de long, $0.55\,m$ de large et $1.3\,m$ de profondeur, ce canal est équipé d'un batteur, de jauges mesurant la hauteur de l'eau et de jauges à ultrasons mesurant la topographie sédimentaire. Le fond mobile fut soumis à des séries de vagues représentant des conditions de tempête. Une fois le modèle hydrodynamique validé pour garantir un apport énergétique hydrodynamique comparable, les modèles numériques Opti-Morph et XBeach furent appliqués à la configuration du canal à houle. Les résultats montrent une concordance qualitative entre Opti-Morph et les données expérimentales : la barre naturelle s'affaisse, le plateau présente peu de variations et les profils coïncident à la côte. Cependant Opti-Morph, ainsi que XBeach, n'étaient pas en mesure de prédire l'avancée de la barre vers la côte. Ces résultats montrent qu'un modèle morphodynamique basé sur la minimisation de l'énergie des vagues a du potentiel dans le cas de simulations à court terme.

2.1.5 Discussion

Dans cette section, nous cherchons à analyser la robustesse d'Opti-Morph ainsi qu'étudier le comportement long-terme de ce modèle numérique. Dans son état actuel, Opti-Morph nécessite deux hyper-paramètres : le paramètre de mobilité Υ et le paramètre

de pente maximale M_{slope}. Des simulations furent effectuées avec une variation de ±50% de chacun de ces paramètres. Les résultats montrent peu de variations au profil bathymétrique, d'où la robustesse d'Opti-Morph. Une étude sur le comportement long-terme d'Opti-Morph fut également réalisée, la question principale étant de savoir si ce modèle numérique est capable de créer un état d'équilibre après avoir été soumis à un grand nombre d'événements répétés. Cinq scénarios de forçage d'une durée de 2 ou 6 jours furent appliqués au même profil initial et dans les mêmes conditions paramétriques. Les résultats finaux montrent des comportements morphodynamiques typiques et illustrent le potentiel d'Opti-Morph.

2.2 Introduction

Optimization theory is the study of the evolution of a system while searching systematically for the minimum of a function derived from physical properties of the system. In this paper, we have applied this approach to coastal dynamics, with our primary objective to simulate the interactions between the waves and seabed. Continuing the work of [11, 81, 12, 79] and using mathematical optimization theory, we have designed a model that describes the evolution of the seabed while taking into account the coupling between morphodynamic and hydrodynamic processes. This study focuses on a theoretical and numerical approach to the modeling of this coupling, based on the assumption that the seabed adapts to minimize a certain wave-related function. The choice of this function determines the driving force behind the morphological evolution of the seabed. This optimization problem is subjected to a certain number of constraints, allowing for a more accurate description of the morphodynamic evolution.

This study is accompanied by the development of a numerical hydro-morphodynamic model, which has the advantages of being fast, robust, and of low complexity. The model was given the name *Opti-Morph*.

The paper starts with a description of the simple hydrodynamic model used to calculate the driving forces behind the morphodynamic processes. Then, we provide a description of the morphodynamic model (Opti-Morph) based on wave-energy minimization. With the purpose of validating Opti-Morph, we compare the results of the numerical simulation with that of experimental data acquired in a flume experiment. We also compared the model to another nearshore hydro-morphodynamic model, XBeach [103], to see how it fares against existing hydro-morphodynamic models. XBeach is considered to be quite a reputable model in the coastal dynamic community [128, 14, 122].

2.2.1 State of the Art

Numerical models of morphodynamic processes are seen as a valuable tool for understanding and predicting the evolution of the sediment and morphology over time in

coastal areas. Different morphodynamic models exist in the literature, ranging from empirical models [26, 41, 63, 106] to process-based models. The latter can be sorted into several categories, such as i) profile evolution models [65, 66, 87], which use only cross-shore transport, ii) 2D morphological models [34, 67, 17, 126, 120, 72, 119, 61, 89, 103], which use depth-averaged wave and current equations to model the sediment transport while neglecting the vertical variations of wave-derived parameters, as well as iii) 3D and quasi-3D models [104, 69, 105, 13, 129, 30, 31], which determine the sediment evolution using both horizontal and vertical variations of the wave-derived parameters.

The Opti-Morph model described in this paper is based on optimal control. In the past, the use of optimization theory has primarily been used in the design of coastal defense structures, whether in the design of ports and offshore breakwaters [57, 54].

Optimal control has already been envisaged for the modeling of shallow water morphodynamics, based on the assumption that the seabed acts as a flexible structure and adapts to a certain hydrodynamic quantity [81, 11]. These pioneering studies were based on somewhat theoretical developments with no direct relationship with real case studies. In this work, we continue along with the objective of producing a physically robust numerical morphodynamic model based on optimal control and validating it using experimental and numerical data.

2.2.2 Hypotheses

Opti-Morph is based on a certain number of assumptions. Since the model is based on the minimization of a cost function, certain hypotheses must be made regarding the choice of this function. This function, which originates from a physical quantity, must be directly linked to the elevation of the seabed. At present, we set the quantity to be minimized as the energy of shoaling waves. This implies that the seabed reacts to the state of the waves by minimizing the energy of shoaling waves. Other assumptions assess the behavior of seabed and originate from general observations. Sediment transport is influenced by the orbital velocity of water particles [113], which leads to greater sediment mobility in shallower waters. Another natural observation concerns the slope of the seabed, which cannot be overly steep without an avalanching process occurring [100]. Finally, in an experimental flume configuration, the quantity of sand must remain constant over time, with no inflow or outflow of sand to alter the sandstock.

2.3 Theoretical Developments

2.3.1 Modeling Framework

For the sake of simplicity, we present the principle of morphodynamics by optimization in a one-dimensional setting. This enables us to compare the numerical results based

on this theory with experimental flume data. However, no assumptions were made regarding the dimension of the problem, and as a result, it is straightforward to extend this theory to a two-dimensional configuration.

We consider a coordinate system composed of a horizontal axis x and a vertical axis z. We denote $\Omega := [0, x_{\max}]$ the domain of the cross-shore profile of the active coastal zone, where $x = 0$ is a fixed point in deep waters where no significant change in bottom elevation can occur, and $x_{\max}$ is an arbitrary point at the shore beyond the shoreline, as shown by Figure 2.1. The elevation of the seabed is a one-dimensional positive function, defined by: $\psi : \Omega \times [0, T] \times \Psi \to \mathbb{R}^+$ where $[0, T]$ is the duration of the simulation (s) and Ψ is the set of physical parameters describing the characteristics of the seabed. In order to model the evolution over time of ψ and given the assumption that the seabed ψ changes over time in response to the energy of shoaling waves, a description of the surface waves is needed.

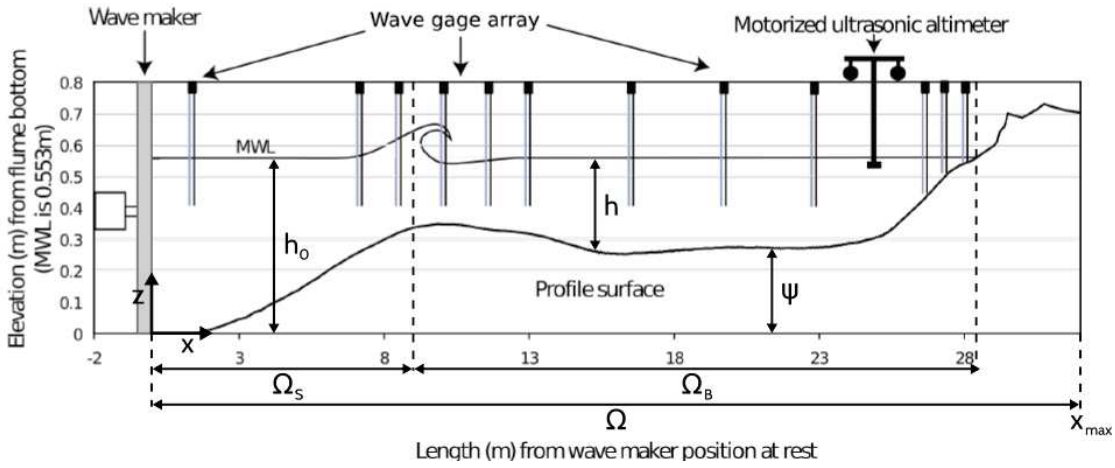

Figure 2.1: Diagram of a cross-shore profile in the case of an experimental flume.

2.3.2 Hydrodynamic Model

The literature on hydrodynamic models is vast [85]. However, as our main focus in this work is on the morphodynamic part of the approach, we present the procedures with a simple hydrodynamic model based on the linear wave theory [27]. More sophisticated models may be applied insofar as the model can be linearized for sensitivity analysis and that the corresponding numerical implementation has a significantly short run-time. This model has the advantage of expressing wave height as an explicit function of the seabed, which leads to rapid calculations of the morphodynamic model.

Let h be the depth of the water from a mean water level h_0 (cf. Figure 2.1). Ocean waves, here assumed monochromatic, are characterized by phase velocity C, group

velocity C_g, and wavenumber k, determined by the linear dispersion relation (2.8), where σ is the pulsation of the waves and g is the gravitational acceleration.

$$\sigma^2 = gk\tanh(kh) \tag{2.8}$$

We define Ω_S as the time-dependent subset of Ω over which the waves shoal and Ω_B the subset of Ω over which the waves break, cf. Figure 2.1. Munk's breaking criterion [84] enables us to define $\Omega_S(t) = \left\{x \in \Omega, \frac{H(x,t)}{h(x,t)} < \gamma\right\}$ and $\Omega_B(t) = \left\{x \in \Omega, \frac{H(x,t)}{h(x,t)} \geq \gamma\right\}$, where γ is a wave breaking index.

$$H(x,t) = H_0(t)K_S(x,t) \tag{2.9}$$

The height of the waves H over the cross-shore profile is inspired by the shoaling equation (2.9), where $H_0(t)$ is the deep water wave height and K_S is a shoaling coefficient, given by

$$K_S = \left(\frac{1}{2n}\frac{C_0}{C_g}\right)^{\frac{1}{2}} \tag{2.10}$$

where C_0 is the deep water wave velocity, and:

$$n = \frac{C}{C_g}, \quad C = C_0\tanh(kh), \quad C_g = \frac{1}{2}C\left(1 + \frac{2kh}{\sinh(2kh)}\right). \tag{2.11}$$

Instead of considering that waves depend solely on offshore wave height H_0, this model suggests that shoaling waves are decreasingly influenced by seawards waves. The greater the distance, the less effect it has on the present wave height. As such, we introduce a weighting function w. Assuming that the maximal distance of local spatial dependency of a wave is denoted d_w, the weighting function over the maximal distance d_w is given by $w : [0, d_w] \to \mathbb{R}^+$ such that $w(0) = 1$, $w(d_w) = 0$ and decreases exponentially.

Equation (2.9) for shoaling wave height becomes equation (2.12), where H_0^w is defined by (2.13).

$$H(x,t) = H_0^w(x,t)K_S(x,t) \tag{2.12}$$

$$H_0^w(x,t) = \frac{1}{\int_{x-X}^{x} w(x-y)\mathrm{d}y}\int_{x-X}^{x} w(x-y)H(y)K(y)\mathrm{d}y \tag{2.13}$$

Equation (2.12) applies only to the shoaling, nearshore-dependent waves of Ω_S, significant wave height over the cross-shore profile $H : \Omega \to \mathbb{R}^+$ is defined by (2.14), where $\alpha(x) = \frac{x}{d_w}$ over $[0, d_w]$ to allow a smooth transition between offshore and nearshore-dependent waves.

$$H(x,t) = \begin{cases} \left[(1-\alpha(x))H_0(t) + \alpha(x)H_0^w(x,t)\right]K_S(x,t) & \text{if } x \in \Omega_S \text{ and } x < d_w \\ H_0^w(x,t)K_S(x,t) & \text{if } x \in \Omega_S \text{ and } x \geq d_w \\ \gamma h(x,t) & \text{if } x \in \Omega_B \end{cases} \quad (2.14)$$

2.3.3 Morphodynamic Model by Wave Energy Minimization

The evolution of the seabed is assumed to be driven by the minimization of a cost function $\mathcal{J}$. Recalling the hypotheses made in Section 2.2.2 , the shape of the seabed is determined by the minimization of the potential energy of shoaling waves, for all $t \in [0,T]$:

$$\mathcal{J}(\psi,t) = \frac{1}{16}\int_{\Omega_S} \rho_w g H^2(\psi,x,t)\mathrm{d}x \qquad [J.m^{-1}] \quad (2.15)$$

where H denotes the height of the waves over the cross-shore profile, ρ_w is water density ($kg.m^{-3}$), and g is the gravitational acceleration ($m.s^{-2}$). In order to describe the evolution of the seabed, whose initial state is given by ψ_0, we assume that the seabed ψ, in its effort to minimize $\mathcal{J}$, verifies the following dynamics:

$$\begin{cases} \psi_t = \Upsilon \, \Lambda \, d \\ \psi(t=0) = \psi_0 \end{cases} \quad (2.16)$$

where ψ_t is the evolution of the seabed over time $[m.s^{-1}]$, Υ is the abrasion of sand ($m.s.kg^{-1}$), Λ is the excitation of the seabed by the water waves, and d is the direction of the descent, which indicates the manner in which the seabed changes. The approach involves two parameters with clear physical interpretation. The first Υ takes into account the physical characteristics of the sand and represents the mobility of the sediment. At the present time, we consider Υ to be a measure of sand mobility expressed in $m.s.kg^{-1}$. Further explanation of the nature of this parameter will be given at a later stage of the model's development. The second parameter Λ is a local function which represents the influence of the water depth on the seabed and is defined using an orbital velocity damping function [113]:

$$\begin{array}{rccc} \varphi: & \Omega \times [0,h_0] & \longrightarrow & \mathbb{R}^+ \\ & (x,z) & \longmapsto & \dfrac{\cosh(k(x)(h(x)-(h_0-z)))}{\cosh(k(x)h(x))} \end{array} \quad (2.17)$$

In unconstrained circumstances, for instance, if a total sand volume constraint does not need to be enforced, we set $d = -\nabla_\psi \mathcal{J}$, which indicates a direction for local minimization of $\mathcal{J}$ with regards to ψ. The calculation of $\nabla_\psi \mathcal{J}$ is described in Appendix 2.A.1. However, constraints are added to the model to incorporate more physics and deliver

more realistic results. Driving forces behind the morphological evolution of the seabed are described by the minimization of the cost function $\mathcal{J}$. Secondary processes are expressed by constraints. In the interest of simplicity, we have adopted two physical constraints though more can be introduced if necessary. The first concerns the slope of the seabed. Depending on the composition of the sediment, the slope of the seabed is bounded by a grain-dependent threshold M_{slope}[27]. This is conveyed by the following constraint on the local bathymetric slope:

$$\left|\frac{\partial \psi}{\partial x}\right| \leq M_{\text{slope}} \tag{2.18}$$

The dimensionless parameter M_{slope} represents the critical angle of repose of the sediment, and varies between 0.2 and 0.6 [1].

A second example concerns the sandstock in the case of an experimental flume. This constraint states that the quantity of sand in a flume must be constant over time, as given by (2.19), contrarily to an open-sea simulation where sand can be transported between the onshore and the offshore zones [49, 98].

$$\int_{\Omega} \psi(t,x)\mathrm{d}x = \int_{\Omega} \psi_0(x)\mathrm{d}x \qquad \forall t \in [0,T] \tag{2.19}$$

This constraint is necessary for verifying and validating the numerical model with physical simulations.

2.4 Numerical Application

In this section, we present the numerical results produced by the Opti-Morph model. For validation purposes, the resulting seabed is compared to experimental data acquired during a flume tank experiment. We also conduct a comparative analysis between the physical seabed, the seabed produced by Opti-Morph and the seabed produced by XBeach, with the aim of assessing how Opti-Morph holds up against existing hydro-morphodynamic models. A brief description of the experiment is provided, as well the XBeach model.

2.4.1 Description of the Experiment

The experimental observations presented here were collected as part of the COPTER project and a series of laboratory wave-flume experiments were performed in order to investigate the morphodynamic impact of introducing solid geotextile tubes to the Hatzuk (Israel) seafloor [9]. We use the data collected without tubes to describe the natural evolution of the seabed over time.

A glass flume measuring 36 m long, 0.55 m wide and 1.3 m deep is equipped with a wave-maker and gauges measuring the height of the water. Artificial particles are placed inside the flume representing the mobile sea bottom and an ultrasonic gauge is used to measure the sedimentary topography.

The experimental seabed, described in Figure 2.1 is subjected to a 30-minute storm climate, with a significant wave height and period of $H_s = 135\,mm$ and $T_s = 2.5\,s$. Time and length scale ratio are set to $1/3$ and $1/10$ respectively to that of the field.

2.4.2 XBeach Model

XBeach is an open-source process-based model developed by Deltares, UNESCO-IHE, and Delft University of Technology to simulate the hydro-morphodynamic processes in coastal areas.

In brief, XBeach uses four interconnected modules to model near-shore processes [25]. The two hydrodynamic modules consist of the short wave module and the flow module. The first is based on wave action equations [53], and incorporates breaking, dissipation [101], and wave current interactions, while the latter is governed by shallow water equations [5, 116]. One of the two morphodynamic modules is the sediment transport module based on the equilibrium sediment concentration equation [112] and a depth-averaged advection-diffusion equation [37]. The other is the morphology module which concerns seabed transformations such as the evolution of the seabed and avalanching.

In order to configure the XBeach model for the experimental flume setting, we refer to the XBeach user manual [102]. The domain Ω is defined over 32 m with a uniform subdivision of 320 cells. The incoming wave boundary condition is provided using the JONSWAP wave spectrum [48], with a significant wave height of $H_{m0} = 0.015\,m$ and a peak frequency at $f_p = 0.4 s^{-1}$. The breaker model uses the Roelvink formulation [101], with a breaker coefficient of $\gamma = 0.4$, a power $n = 15$, and a wave dissipation coefficient of 0.5. These parameters were calibrated using the hydrodynamic data produced during the physical flume experiment. Concerning sediment parameters, the $D50$ coefficient is set as 0.0006, and the porosity is 2650 $kg.m^{-3}$. No other parameters such as bed friction or vegetation were applied. The model is set to run for a period of 1800 s, as a short-term simulation.

2.4.3 Hydrodynamic Validation

This section is devoted to the comparison of the two numerical hydrodynamic models to the experimental wave data obtained in the experimental flume of Section 2.4.1. Mean wave height profiles were calculated over the short-term storm simulation, for both Opti-Morph and XBeach, and compared to the mean wave height of the experimental model. The latter was calculated using the measures taken by the gauges of the flume.

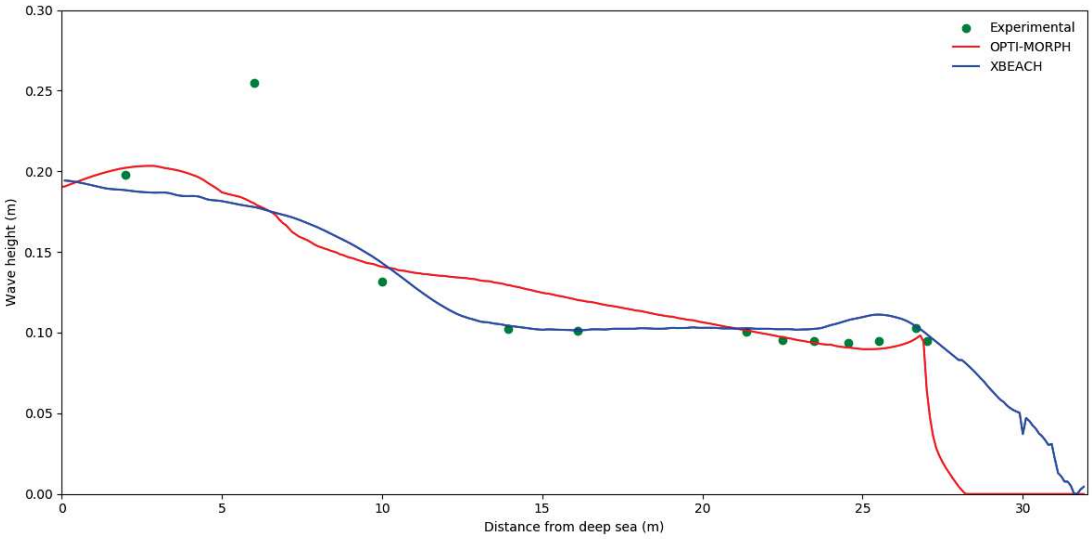

Figure 2.2: Comparison of mean wave height over a storm simulation. The green points correspond to the mean wave height provided by the gauges of the flume experiment. The mean wave height determined by Opti-Morph (red) and XBeach (blue) also appear. The non-zero wave height beyond the shoreline as presented by XBeach is due to wave set-up, which Opti-Morph doesn't include.

Figure 2.2 shows that the hydrodynamic module of both Opti-Morph (red) and XBeach (blue) are both comparable with respect to the experimental measurements (green) excluding, as is often the case, the second point at $x = 6\,m$. XBeach demonstrates a close qualitative fit over the 10-22 m section of the flume, whereas Opti-Morph excels at the coast (21-27 m), with a near-perfect fit with the experimental data. Despite the simplicity of the hydrodynamic model used by Opti-Morph, the resulting wave height is of the same order of magnitude over the cross-shore profile than that measured during the flume experiment, which indicates that the resulting seabeds are comparable with regard to the forcing energy driving the morphodynamic response.

2.4.4 Numerical Results of the Morphodynamic Simulations

The Opti-Morph model was applied to the configuration of the COPTER experiment of Section 2.4.1, and the resulting beach profile is shown by the red profile, in Figure 2.3.A. The main observation is the decrease of 2.5 cm in height of the sandbar, at $x = 9\,m$. We observe a slight decrease of the seabed adjacent to the wave-maker, and a slight increase at the plateau, situated at 15-25 m. No mobility is observed at the coast.

When comparing the results provided by Opti-Morph (red), with that of XBeach (blue) and the experimental data (green), as shown on Figure 2.3.A, we observe that

the red seabed profile provided by the Opti-Morph model shows a general quantitative agreement when compared to the experimental data, as does the XBeach morphological module. In fact, both models produce profiles close to the experimental data over the plateau located at 15-25 m from the wave-maker (Fig. 2.3.C). At the shore, Opti-Morph matches the experimental data whereas XBeach shows a vertically difference of up to 3cm at $x = 27\,m$ (Fig. 2.3.D). Discrepancies on the part of both models occur in the area surrounding the tip of the sandbar, as both Opti-Morph and XBeach fail to predict the advancing of the sandbar (Fig. 2.3.B); the experimental data show that the height of the sandbar remains unchanged with regards to the initial profile. Both sandbars have a height of $0.375\,m$, however, the sandbar resulting from the experimental simulation has advanced towards the coast, an occurrence that neither numerical model was able to predict.

As such, this new model based on wave-energy minimization shows potential when compared to XBeach, in the case of short-term simulations.

2.5 Discussion

2.5.1 Parameter Robustness Analysis

One of the advantages of the Opti-Morph model is the low number of morphodynamic hyper-parameters required. At the present time, Opti-Morph requires two hyper-parameters: the mobility parameter Υ and the maximal slope parameter M_{slope}. Here, an assessment on these parameters is conducted. In Figure 2.3.E, three simulations were performed in identical settings with changes made solely to the mobility parameter. Initially, this parameter Υ has a value of 5×10^{-6}, $m.s.kg^{-1}$. Figure 2.3.E shows no significant difference despite a 50% increase ($\Upsilon = 7.5 \times 10^{-6}\,m.s.kg^{-1}$) (orange) or decrease ($\Upsilon = 2.5 \times 10^{-6}\,m.s.kg^{-1}$) (light blue) of Υ with regard to the baseline seabed profile (black). Similar conclusion can be deduced for the maximal slope parameter M_{slope}, whose reference value here is 0.2. The corresponding parameter of XBeach is *wetslp*, described in the XBeach manual as the critical avalanching slope under water, and is also set to 0.2. In Figure 2.3.F, we observe little difference between the reference seabed (black), the seabed resulting from a 50% increase ($M_{\text{slope}} = 0.3$) (orange) and the seabed resulting from a 50% decrease ($M_{\text{slope}} = 0.1$) (light blue). The only apparent discrepancy can be found at $x = 28\,m$, where the seabed is at its steepest, and therefore the sand slope constraint is more prone to be active. The reduction of the critical angle of repose results naturally in a less steep slope. The robustness of Opti-Morph in relation to both the mobility parameter and the slope parameter, despite a significant increase or decrease of their value, is apparent. Further simulations show that the robustness of these parameters is not specific to this particular flume configuration, but can be observed regardless of the initial configuration.

2.5.2 Long-term Simulations

This section is devoted to the long-term behavior of Opti-Morph, the main question being, is this numerical model capable of creating an equilibrium state after being subjected to a great number of repeated events. Five forcing scenarios, lasting either 2 or 6 days, were applied to the same initial seabed in the same parametric configuration. The current Opti-Morph code is in Python. Typically, using time-steps of 1 s simulating a day of forcing requires about 1.5 hours on a 2GHz PC computer. Each time iteration gathering the steps presented in this paper requires therefore about 63 ms. An analysis of the resulting seabeds is performed as well as their behavior throughout the simulation. The latter is achieved through a comparative study of four time-series', focusing on: (1), the vertical evolution of seabed elevation at the tip of the sandbar; (2), the vertical evolution of seabed elevation at a point of the plateau; (3), the distance between the wave-maker and the onset of the seabed; and (4), the location of the shoreline position.

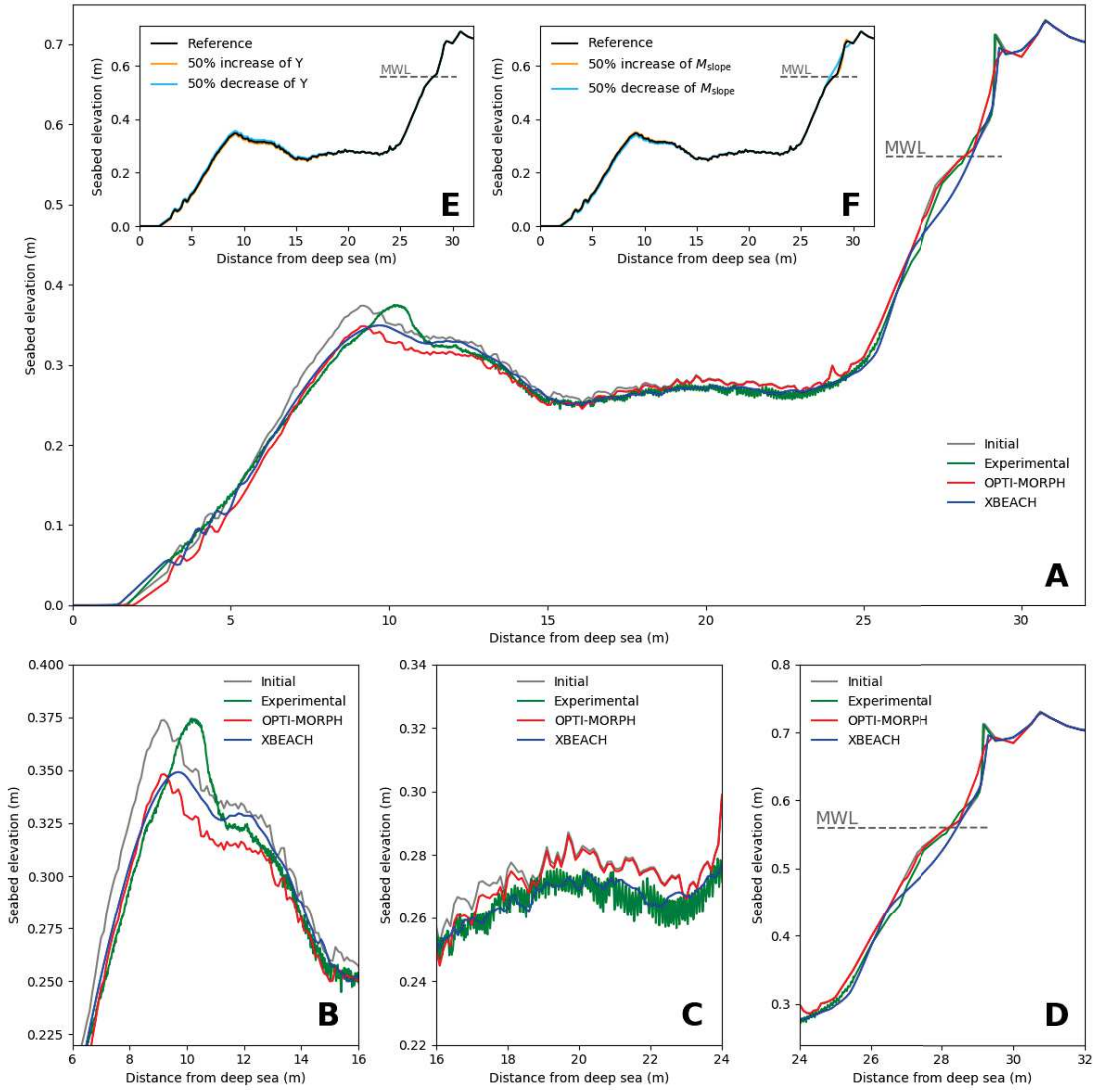

Figure 2.3: **A.** Results of the numerical simulation calculated over the initial seabed (gray) using the XBeach morphodynamic module (blue) and the Opti-Morph model (red). These are compared with the experimental data acquired during the COPTER project (green). The mean water level is denoted MWL and is set at $0.56\,m$. **B.** Zoomed in view of the sandbar, located between $6\,m$ and $16\,m$. **C.** Zoomed in view of the plateau, located between $16\,m$ and $24\,m$. **D.** Zoomed in view at the shoreline, located between $24\,m$ and $32\,m$. **E.** Robustness analysis of the mobility parameter Υ. The reference profile is depicted in black. The orange (resp. light blue) profile is the result of a 50% increase (resp. decrease) in mobility, with all other parameters remaining the same. **F.** Robustness analysis of the maximal sand slope parameter M_{slope}. The reference profile is depicted in black. The orange (resp. light blue) profile is the result of a 50% increase (resp. decrease) of M_{slope} , with all other parameters remaining the same.

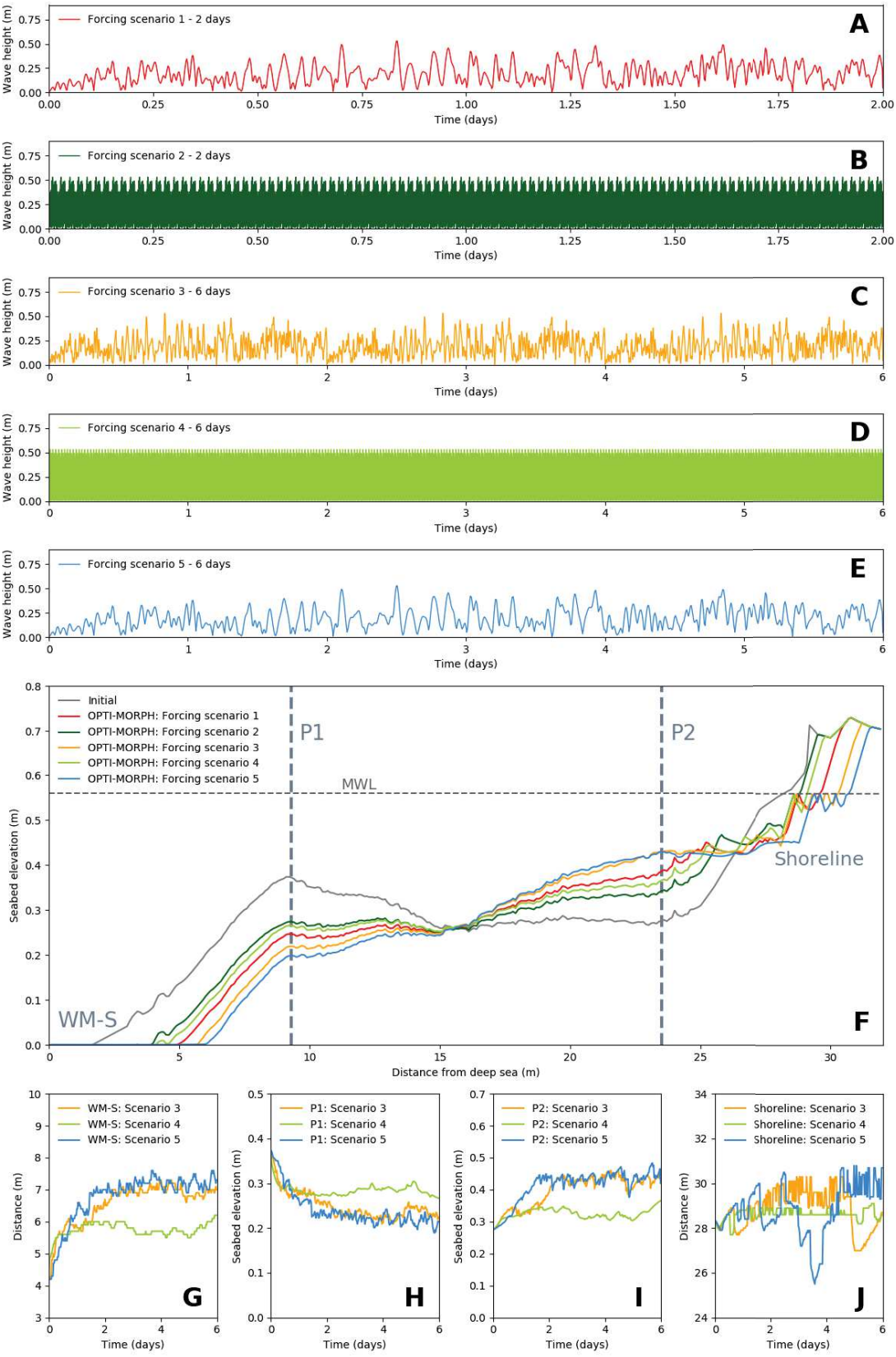
Forcing scenario 1 - 2 days
A
Forcing scenario 2 - 2 days
B
Forcing scenario 3 - 6 days
C
Forcing scenario 4 - 6 days
D
Forcing scenario 5 - 6 days
E
Wave height (m)
Time (days)
Initial
OPTI-MORPH: Forcing scenario 1
OPTI-MORPH: Forcing scenario 2
OPTI-MORPH: Forcing scenario 3
OPTI-MORPH: Forcing scenario 4
OPTI-MORPH: Forcing scenario 5
P1
P2
MWL
Shoreline
WM-S
F
Seabed elevation (m)
Distance from deep sea (m)
WM-S: Scenario 3
WM-S: Scenario 4
WM-S: Scenario 5
G
P1: Scenario 3
P1: Scenario 4
P1: Scenario 5
H
P2: Scenario 3
P2: Scenario 4
P2: Scenario 5
I
Shoreline: Scenario 3
Shoreline: Scenario 4
Shoreline: Scenario 5
J
Distance (m)

Figure 2.4: Long-term simulations of Opti-Morph. **A.** Forcing wave height for scenario 1, composed of several long-term events over a 2-day period. **B.** Forcing wave height for scenario 2, composed of numerous short-term events over a 2-day period. **C.** Forcing wave height for scenario 3, composed of several long-term events over a 6-day period. **D.** Forcing wave height for scenario 4, composed of numerous short-term events over a 6-day period. **E.** Forcing wave height for scenario 5, composed of few long-term events over a 6-day period. **F.** Seabeds resulting from the different forcing scenarios produced by Opti-Morph. Two points of interest have be identified: P1 located at $x = 9.3\,m$ and P2 located at $x = 20.1\,m$. **G.** Evolution of the distance, devoid of sediment, between the wave-maker (located at $x = 0\,m$) and the seabed (WM-S), regarding forcing scenarios 3, 4, and 5. **H.** Vertical evolution of seabed elevation at P1, driven by the 6-day forcing scenarios 3, 4, and 5. **I.** Vertical evolution of seabed elevation at P2, driven by the 6-day forcing scenarios 3, 4, and 5. **J.** Evolution of shoreline position, driven by the 6-day forcing scenarios 3, 4, and 5.

Applying Opti-Morph over a longer time-series leads to the results of Figure 2.4. The two 2-day forcing scenarios are shown in Figures 2.4.A and 2.4.B. In both cases, we observe that the resulting seabeds of Figure 2.4.F are subjected to the destruction of the sandbar and have a tendency to evolve progressively towards an equilibrium beach profile [92]. Simulations over a 6-day period were conducted to confirm this tendency. These scenarios are depicted in Figures 2.4.C, 2.4.D, and 2.4.E, and the resulting seabeds given in Figure 2.4.F show once again the destruction of the sandbars, the elevation of the plateau, and erosion at the shoreline. Furthermore, all three tend towards an equilibrium state. This is confirmed by the four time-series analysis presented in Figures 2.4.G, 2.4.H, 2.4.I, and 2.4.J. The vertical elevation of the seabed at both points P1 and P2 show initial variations over the first 2 days: a decrease in the case of P1 (cf. Figure 2.4.H) and an increase in the case of P2 (cf. Figure 2.4.I). However, both studies show a stabilization of the seabed elevation over the last 4 days of the 6-day period. Similar conclusions can be drawn regarding the length of the zone containing no sediment adjacent to the wave-maker (cf. Figure 2.4.G). An initial increase between 2 and 3 meters can be observed, with stability achieved in the later stages of the simulations. Finally, Figure 2.4.J shows the evolution of the shoreline position. Initially found at $x = 28.3\,m$, all scenarios provoke a retreat of the shoreline: $0.4\,m$ in scenario 3, $0.3\,m$ in scenario 4, and $2\,m$ in scenario 5. The shorelines of the latter two converge, whereas scenario 3 shows an abrupt advance of the shoreline at day 5, with an attempt to return back to its stable state of $x = 30\,m$. This tendency to evolve towards an equilibrium state indicates the presence of storm-like conditions; the seabed has been flattened, the sandbar has been destroyed and erosion can be observed at the coast [40].

The comparisons made between the two 2-day simulations and the three 6-day simulations, in this given configuration, also reveal the little influence heritage has on

the morphodynamic response. Both scenarios 1 and 2 have a comparable cumulative incoming wave energy density $E = \frac{1}{16}\int_0^T \rho g H_0^2 \mathrm{d}t$ of $0.0591\, J.m^{-2}$. The resulting seabeds evolve towards similar profiles (reduction of the sandbar, increase of elevation of the plateau, and erosion at the coast), despite two very different forcing conditions. Similar conclusions can be drawn regarding the 6-day simulations, where the cumulative energy density of all three is equal to $0.177\, J.m^{-2}$.

2.6 Conclusion

Opti-Morph shows potential as a fast, robust, and low complexity morphodynamic model involving only two hyper-parameters. Despite using a basic hydrodynamic model for the description of the complex coupling of hydrodynamic and morphodynamic processes, we can nevertheless observe that a numerical model based on an optimization theory works effectively, with comparable results to a state of the art hydro-morphodynamic model requiring the tuning of dozens of hyper-parameters. Long-term simulations also show typical morphodynamic behavior, with the tendency of the seabed to evolve towards an equilibrium state. These results demonstrate the tremendous potential of Opti-Morph, a constrained energy minimization morphodynamic model.

2.A Mathematical Developments

In this section, we detail some of the mathematical results needed in the implementation of the Opti-Morph model, specifically the calculation of the gradient of the cost function $\mathcal{J}$ (Eq. (2.15)) with regard to the bathymetry ψ, which in turn requires the gradient of the wave height function (Eq. (2.14)) with regard to ψ. With the current choice of hydrodynamic model, this can be achieved analytically. With more sophisticated hydrodynamic models this is not always possible. In these cases, if the source code of the model is available, the calculation of the gradient can be performed using automatic differentiation of programs [42, 47] directly providing a computer program for the gradient.

2.A.1 Gradient of the Cost Function with respect to the Bathymetry

Opti-Morph requires the evaluation of gradient of the functional $\mathcal{J}$ with respect to the bathymetry ψ, denoted $\nabla_\psi \mathcal{J}$. For a general functional of the form $\mathcal{J}(\psi(x), H(\psi(x)))$ involving dependencies with respect to the bathymetry and hydrodynamic quantities H, this sensitivity can be expressed using the chain rule:

$$\nabla_\psi \mathcal{J} = \nabla_\psi \mathcal{J} + \nabla_H \mathcal{J}\, \nabla_\psi H \tag{2.20}$$

where $\nabla_\psi H$ requires the linearization of the hydrodynamic model, and ψ is a parametric representation of the bathymetry.

2.A.2 Gradient of the Wave Height with respect to the Bathymetry

This section is devoted to the calculation of the gradient of the wave height H, given by (2.14), with regards to the seabed elevation ψ and denoted $\nabla_\psi H$. Being as $h = h_0 - \psi$, the derivation of the third line of (2.14) with regards to ψ is immediate. The calculation of the gradient of the first line of (2.14) is analogous to that of the second. It remains to differentiate the second line of (2.14) with regards to ψ. Observing that the chain rule yields for all $x, t \in \Omega_S \times [0, T]$ with $x \geq d_w$,

$$\nabla_\psi H(x,t) = H_0^w(x,t)\nabla_\psi K_S(x,t) + \nabla_\psi H_0^w(x,t)K_S(x,t), \tag{2.21}$$

and that the term $\nabla_\psi H_0^w(x,t)$ can be determined iteratively, using $\nabla_\psi H_0 = 0$, it remains to determine $\nabla_\psi K_S(x,t)$. Injecting the definitions of n, C and C_g, given in (2.11), yields

$$K_S = \left[\tanh(kh)\left(1 + \frac{2kh}{\sinh(2kh)}\right)\right]^{-1/2}. \tag{2.22}$$

For the sake of simplicity, let $U = \tanh(X)\left(1 + \dfrac{2X}{\sinh(2X)}\right)$ with $X = kh$. Equation (2.22) becomes

$$\nabla_\psi K_S = -\frac{1}{2}\, U^{-3/2}\, \nabla_\psi U, \tag{2.23}$$

and we have

$$\nabla_\psi U = 2\nabla_\psi X \frac{\cosh^2(X) - X\sinh(2X)}{\cosh^4(X)}, \tag{2.24}$$

with $\nabla_\psi X = h\nabla_\psi k + k\nabla_\psi h = h\nabla_\psi k - k$. Moreover, differentiating both sides of the dispersion equation (2.8) by ψ gives

$$k_\psi = \frac{k^2}{\cosh(kh)\sinh(kh) + kh}. \tag{2.25}$$

Combining (2.23),(2.24), and (2.25), we obtain $\nabla_\psi K_S$, and therefore $\nabla_\psi H$.

Chapitre 3

Couplage entre Structure Rigide et Réponse Morphodynamique

Dans ce chapitre, nous cherchons à coupler deux problèmes d'optimisation littoraux : trouver le meilleur emplacement d'un géotube le long du profil cross-shore tout en considérant la réponse morphodynamique du fond, calculée par Opti-Morph.

Ces travaux ont fait l'objet d'une pré-publication, intitulé "Application of Opti-Morph: Optimized beach protection by submerged geotextile tubes", cf. [19].

3.1 Résumé en Français

3.1.1 Introduction

Cette étude détaille l'analyse numérique de l'emplacement des géotubes, en cherchant à répondre à la question suivante : Où placer le géotube le long du profil cross-shore pour minimiser l'érosion à la côte ? Pour ce faire, deux problèmes d'optimisation doivent être posés. Le premier concerne l'emplacement des géotubes et nécessite la définition d'une fonction objectif et de contraintes. Le deuxième concerne la réponse morphodynamique du fond sableux. Pour simuler l'évolution morphodynamique, et la prendre en compte dans la recherche de la position optimale de géotubes, nous utilisons Opti-Morph, qui est également basé sur un problème d'optimisation. Nous définissons donc un deuxième problème d'optimisation, avec sa propre fonction de coût et et ses propres contraintes. Étant donné ses temps de simulation courts et sa faible complexité, Opti-Morph est idéal pour étudier la position optimale de ces brise-lames en tenant compte de la réponse morphodynamique de la plage.

3.1.2 Optimisation de la Position du Géotube

La recherche de l'emplacement optimal du géotube dépend du choix de la fonction objectif à minimiser ou à maximiser. Plusieurs fonctions objectifs peuvent être envisagées en fonction de l'objectif principal du déploiement, qu'il soit environnemental, financier ou physique. Dans cette étude, nous cherchons à minimiser la position du trait de côte, afin de limiter l'érosion et favoriser l'accrétion.

Certaines contraintes liées à l'introduction de tubes géotextiles sur le littoral sont prises en compte dans la recherche de la position optimale. Ces contraintes permettent d'exclure certaines positions jugées inacceptables. Par exemple, les géotubes ne peuvent pas être installés dans une eau trop profonde car le déploiement d'une telle structure, ainsi que son entretien, s'avéreront trop difficiles et coûteux. Inversement, ils ne peuvent pas être installés trop près de la côte car ils risquent d'être endommagés par les usagers de la plage. La topographie du fond et la présence de flore marine protégée peut également restreindre les zones de déploiement possibles.

3.1.3 Réponse Morphodynamique par Optimisation

La théorie centrale derrière le modèle Opti-Morph est l'hypothèse que le fond marin évolue naturellement dans un effort de minimiser l'état énergétique des vagues de surface. Ceci est réalisé grâce à la minimisation d'une fonction de coût hydro-morphodynamique ; cette minimisation est considérée comme la force motrice de la réponse morphodynamique. Les phénomènes secondaires aux processus morphodynamiques sont considérés comme des contraintes, et permettent d'incorporer d'avantage de physique dans le modèle.

Dans cette étude, la fonction de coût qui gouverne le modèle Opti-Morph est la même que celle du Chapitre 2, c'est-à-dire l'énergie potentielle des vagues dans la zone de shoaling.

3.1.4 Couplage des Problèmes d'Optimisation

Deux problèmes d'optimisation ont été définis et doivent être résolus simultanément : (P1) le positionnement du géotube le long du profil cross-shore et (P2) la réponse morphodynamique des fonds marins réalisée par Opti-Morph. Cela nécessite un traitement adapté pour leur résolution.

Compte tenu du faible temps d'exécution et de la complexité d'Opti-Morph pour résoudre (P2), il est possible de résoudre (P1) en utilisant une méthode d'optimisation directe.

3.1.5 Résultats Numériques

Cette section est consacrée aux résultats numériques des deux problèmes d'optimisation : la recherche de la position optimale du géotube pour une érosion côtière minimale et la réponse morphodynamique naturelle du fond marin.

Nous considérons un profil de plage cross-shore 1D avec un profil bathymétrique linéaire, ainsi qu'un scénario de forçage simple de 20 jours caractérisé par une tempête simplifiée. Une étude de la fonction objectif pour la problématique (P1) fut réalisée, avec l'identification du minimum. Nous pouvons ainsi déduire la position optimale du géotube pour minimiser la position du trait de côte ; un déploiement de géotube à l'emplacement optimal entraînerait une réduction conséquente sur l'érosion côtière.

La réponse morphodynamique le long du profil cross-shore fut de même analysée. Opti-Morph est capable de produire des résultats morphodynamiques réalistes face au déploiement de géotubes submergés, avec la formation d'une barre, l'apparition d'un creux et le déplacement du trait de côte. Ces phénomènes varient en fonction de l'emplacement du géotube. En effet, plus le géotube est positionné près de la côte, moins le profil bathymétrique varie, et inversement, plus le géotube est déployé en eaux profondes, plus le fond marin se comporte comme si aucun géotube n'avait été introduit.

3.1.6 Discussion

Dans cette section, nous analysons (i) le comportement du modèle hydrodynamique utilisé par Opti-Morph face aux géotubes, (ii) l'effet des géotubes sur le déferlement, le trait de côte et l'énergie des vagues, et (iii) les résultats d'un changement de fonction objective dans l'étude de la position optimale de géotube.

Une comparaison de la hauteur des vagues le long du profil cross-shore fut réalisée en fonction de la position du géotube. Les résultats montrent que le modèle hydrodynamique pourtant simple d'Opti-Morph est capable de gérer les géotubes submergés. Les vagues se comportent comme prévu : on observe le shoaling avant le géotube, le déferlement au dessus des structures, puis une diminution progressive de la hauteur des vagues jusqu'à la côte.

L'analyse de l'effet des géotubes sur le déferlement, le trait de côte et l'énergie des vagues illustre plusieurs phénomènes auxquels on peut s'attendre du déploiement des géotubes : (a) les vagues passent au-dessus des géotubes sans déferlement lorsqu'elles sont petites ; (b) le déferlement a lieu au dessus des géotubes lorsque les vagues sont suffisamment importantes ; (c) plus le géotube est profond, moins il a d'influence sur les vagues ; (d) le déferlement prématuré induit par les géotubes entraîne une diminution de l'énergie des vagues et ainsi moins d'érosion du littoral.

Pour finir, une nouvelle étude sur le positionnement des géotubes fut réalisée avec une autre fonction objectif afin de démontrer l'adaptabilité de cette approche dans la recherche de la position optimale d'un géotube.

3.2 Introduction

The question of coastal protection is of crucial importance, and breakwaters are a typical example of means to approach this. Designed to absorb/dissipate the energy of incoming waves and therefore reduce coastal erosion, breakwaters date back to the Roman Empire and have been used for coastal protection ever since [33]. Different types of breakwaters exist depending on whether they are emerged, floating [24] or submerged [86]. Examples include rubble-mound, caissons, pontoons, and geosynthetic tubes. The nature of the considered breakwater depends on many factors such as wave conditions, water depth, characteristics of the seabed foundations, cost of construction and maintenance, as well as visual and environmental impacts. Different characteristics of the breakwater need to be studied. This includes length and width of the structure, orientation, and location with regard to the shoreline, shape. Given the many parameters surrounding the design of breakwaters, i.e. length, width, shape, location, orientation, etc., it is natural to consider numerical simulations to accompany the investigation.

This paper details the numerical study of submerged breakwaters made of geotextile material. For the sake of simplicity, this study focuses on one breakwater parameter: its location along the cross-shore profile. The objective is to determine the optimal position of a geotextile tube for minimal beach erosion along the cross-shore profile and to do so, optimization methods are required.

The use of optimization methods for coastal protection can easily be found in the literature, such as [57, 22] for the protection of ports, [125, 121] in the case of the design of seawalls, and [29, 32, 16] for the study of breakwaters. Geotextile tubes, or geotubes, have already been the subject of an optimization study on a static background [55, 56], where the authors sought the optimal shape of these coastal protection structures. Here, we search for the optimal location of the seabed, while taking into account the morphodynamic response of the seabed, the latter being determined by the numerical model, Opti-Morph [21].

Opti-Morph is a new morphodynamic model, based on the theory that shallow-water seabeds react to the surface waves and evolves in an effort to minimize a certain hydrodynamic quantity. This concept was first formulated in the works of [11, 81, 12, 79], in a somewhat theoretical context. The numerical model Opti-Morph was then developed (cf. [21]), in an effort to apply this concept to experimental and in situ configurations and validate the theory. Advantages of this numerical model include its low number of hyperparameter and their robustness, its fast simulation times. The work of [21] demonstrates the potential of this up-and-coming morphodynamic model, with both short-term and long-term simulations.

This paper presents the potential of this new morphodynamic model, by applying it to the problem of the positioning of submerged geotextile tubes. First, we define the optimization problem regarding the position of the breakwater for optimal coastal protection, with the definition of the domain, the objective function, and constraints.

Next, we offer a brief description of the Opti-Morph model, which is based on wave energy optimization and thus requires the definition its own cost function. A description of the coupling of both optimization problems is approached in section 3.5 before presenting the numerical results.

3.3 Geotube Position Optimization

3.3.1 Description

Geotextile tubes are made from high-strength geosynthetic fabric and are increasingly used in coastal and riverine applications. They are often filled hydraulically with a slurry of sand and water, although many other materials have been used. Sand-filled flexible tubes of geotextile material are used for their ability to allow water to pass through but maintain the sand within. Geotextiles tubes are for coastal protection by the means of revetments, protection dykes, groynes, and offshore breakwaters [68, 64], the latter being the focus of this study. Like other types of offshore emerged breakwaters, geotextile tubes are designed to dissipate the waves by creating local shallow water conditions forcing waves to prematurely break, thus, ensuring less energy arrives at the coast and in doing so protecting the shoreline from erosion. Geotextile tubes have been deployed all over the world, on account of their low costs and less ecological and environmental impact [73, 110], having little effect on the local marine fauna and flora. Their easy installation and maintenance, with potentially locally sourced materials and their low visual impact also play a role in their increasing popularity.

One such example is the introduction of submerged geotextile breakwaters on the Northern coast of Yucatan, Mexico [4, 39]. Beaches were sustaining erosion of approx. $1\,m$ per year, with many beaches being almost fully eroded. Several geotextile tubes were installed $10\,m$ and $30\,m$ from the shoreline with promising results. Similarly, geotextile tubes were deployed for the coastal protection of Young-Jin beach on the east coast of Korea [93, 91]. The situation was so critical shoreline roads and other public properties were being damaged. Eight geotubes tubes were deployed along the beach at $90\,m$–$100\,m$ from the shoreline, with a water depth of $3\,m$. Field monitoring shows an extension of up to $7.6\,m$ of the shoreline and an accumulation of sand around the areas covered by the geotextile tube. On the Lido of Sète, France, on the Mediterranean Sea, submerged geotextile tubes were also installed [6, 55]. Here, they were deployed approximately $350\,m$ from the beach with a depth of $4\,m$ and induced an important enlargement of the beach. Extensive studies were made prior to the installation. In particular, the location of the geotubes with regards to the coastline. In the three previous examples, the position of the structures ranges between $10\,m$ and $350\,m$ from the shore.

Here, we study the optimal location of the geotube using a numerical model. To do so, we must define the quantity to be minimized as well as the physical constraints that

arise.

3.3.2 Geotube Deployment Objective Function

The search for the optimal geotube location depends on the choice of the cost function, or objective function to be minimized or maximized. Several cost functions can be considered depending on the main objective of the deployment, whether it's environmental, financial or physical (e.g. limiting beach erosion or reducing wave energy). It may also be a combination of several factors. In this study, we seek to minimize the position of the shoreline, in order to prevent erosion and encourage accretion. For illustrative purposes, we consider one geotube parameter, its location along the cross-shore profile, but additional parameters can be incorporated if desired.

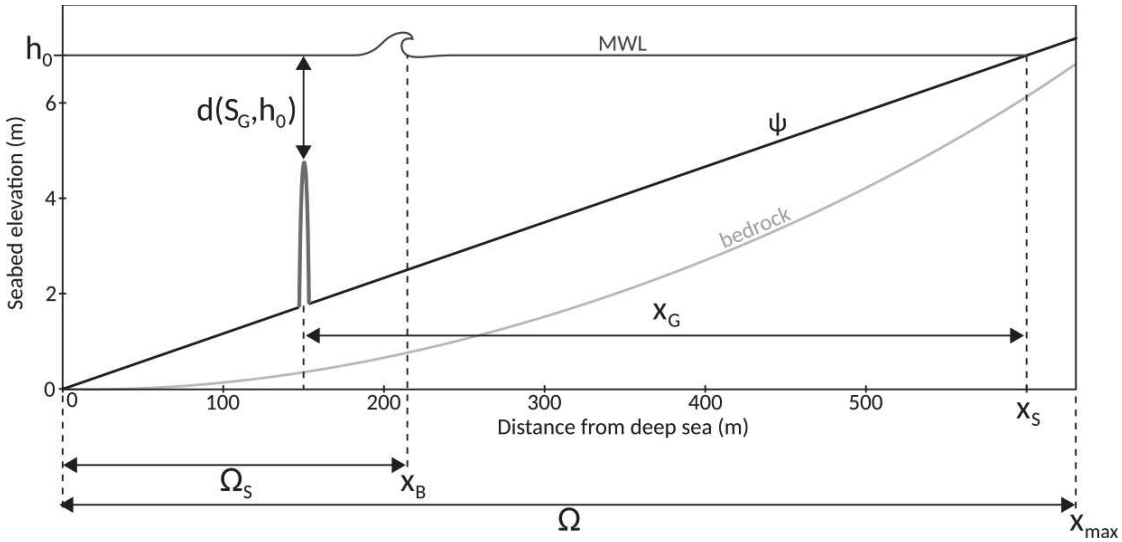

Figure 3.1: Diagram of the cross-shore profile featuring a geotube

Let $\Omega = [0, x_{\max}]$ be the domain of the cross-shore profile, where $x = 0\,m$ is an arbitrary point situated in deep waters and $x_{\max}$ is a point located beyond the shoreline, as shown in Figure 3.1. Let ψ be the elevation of the seabed, and $x_G \in \Omega_G$ the location of the geotube, where Ω_G is the zone of feasible deployment. We define the geotube deployment objective function as the final position of the shoreline $x_S \in \Omega$:

$$\mathcal{J}_G(x_G) = x_S(t = T, x_G) \qquad (m) \tag{3.1}$$

where $[0, T]$ is the time interval considered for the morphodynamic response. This function is to be minimized in the search of the optimal geotube location.

3.3.3 Constraints

Certain constraints associated with the introduction of geotextile tubes need to be considered in the search for the optimal position. These constraints are used to exclude certain positions which are deemed unacceptable. For instance, geotextile tubes cannot be installed in too deep a water because the deployment of such a structure, as well as its maintenance, will prove to be too difficult and expensive. The topography of the seabed may also limit the choice of position, with sharp rock or debris that may damage the tubes. Protected marine flora may also restrict the feasible zones of deployment. Furthermore, one should avoid installing geotextile tubes in shallow waters where they risk being damaged by beach users, in particular the keels of ships which can cause lesions to the geotextile material.

As such, in this study, we impose that the geotextile tubes must be set: (i) close enough to the shore to allow for easy deployment/maintenance; (ii) such that the vertical distance between them and the water surface measures at least $1\,m$. For illustrative purposes, topographical constraints have not been included, but can easily be added if necessary.

3.4 Morphodynamic Response by Wave Optimization

3.4.1 Description

Opti-Morph is a new hydro-morphodynamic model developed to simulate the dynamics of sandy beaches and designed to be robust, of low complexity, and have remarkably low execution times. For this reason, Opti-Morph is a natural choice of morphodynamic model regarding problems relating to coastal engineering. This model, first presented in [21] is used here in the study of the optimal location of geotubes. The central theory behind the Opti-Morph model is the assumption that the seabed evolves naturally in an attempt to minimize the energetic state of the surface waves. This is achieved through the minimization of a hydro-morphodynamic cost function, this minimization is deemed the driving force behind the morphodynamic response. Constraints are added to the model for increased realism; phenomena that are secondary to the morphodynamic processes are considered constraints.

3.4.2 Hydro-morphodynamic Cost function

The hydro-morphodynamic cost function driving the Opti-Morph model is the same as that of [21], i.e. the potential energy of shoaling waves:

$$\mathcal{J}(\psi,t) = \frac{1}{16}\int_{\Omega_S} \rho_w g H^2(\psi,x,t)\mathrm{d}x \qquad (J.m^{-1}) \tag{3.2}$$

for all $t \in [0, T]$, where Ω_S is a time-dependent subset of Ω over which the waves shoal (see Figure 3.1), H denotes the height of the waves over the cross-shore profile (m), ρ_w is water density ($kg.m^{-3}$) and g is the gravitational acceleration ($m.s^{-2}$).

3.4.3 Constraints

In the works of [21], two constraints are mentioned: (i) a sandstock constraint, which ensures that the quantity of sand in a closed basin remains constant over time and (ii) a slope constraint preventing the seabed from being unrealistically steep. In the aforementioned work, Opti-Morph was applied to a flume configuration and thus required the presence of a sandstock constraint to guarantee that the quantity of sand remains constant over time. Given the open-sea setting of this study, a sandstock constraint is not required but is used here to limit the displacement of sand between the deep waters and the nearshore zone. The slope constraint remains the same, with a limit of the slope of the seabed by a quantity relative to the critical angle of repose of the sediment. This constraint prevents impossibly steep slopes from forming, which would lead to unrealistic results.

3.5 Coupling

Two optimization problems have been defined and must be resolved simultaneously: the geotube positioning along the cross-shore profile and the morphodynamic response of the seabed performed by Opti-Morph. This requires special treatment for their resolution.

3.5.1 Optimization problem 1: Geotube Positioning

The first optimization problem concerns the optimal geotube position. This can be formulated as follows:

(P1): Find $x_G \in \Omega_G$ such that $\mathcal{J}_G(x_G)$ defined by (3.1) is minimal and subjected to two constraints:

- *(C1): $x_G < x_G^{max}$*
- *(C2): $d(S_G, h_0) < 1$*

where $x_G^{\max}$ (m) is the maximal distance from the coast for geotube deployment, and $d(S_G, h_0)$ (m) is the distance between the summit of the geotube S_G and the mean water level h_0 (cf. Figure 3.1).

Constraint (C1) prevents the geotube from being installed too far from the coast : geotubes cannot be deployed beyond a distance of $x_G^{\max}$ from the coast. Constraint (C2) ensures that the geotube is located deep enough to evade collision with boats and

other beach users which could potentially damage the tubes. Here, a minimum of 1 m is permitted between the geotube and the water surface.

3.5.2 Optimization problem 2: Morphodynamic Response of the Seabed

The second optimization problem determines the evolution of the shape of the seabed over the course of the simulation and can be summarized as:

(P2): For each $t \in [0, T]$*, find* $\psi \in \Psi$ *such that* $\mathcal{J}(\psi, t)$ *defined by* (3.2) *is minimal and subjected to the constraints:*

- *(C1'):* $\int_\Omega \psi(t, x)dx = \int_\Omega \psi(t = 0, x)dx \qquad \forall t \in [0, T]$
- *(C2'):* $\left|\frac{\partial \psi}{\partial x}\right| \leq M_{slope}$

where Ψ is the set of physical parameters describing the characteristics of the seabed and M_{slope} is a grain-dependent upper-bound of the seabed slope.

The constraint (C1') and (C2') describe the constraints mentioned in Section 3.4.3. The first is the sandstock constraint, which limits the sediment transfer between the nearshore zone and the deep sea. This is achieved by setting the sandstock as constant over the course of the simulation. Constraint (C2') ensures that the slope of the seabed cannot be overly steep by defining the upper-bound M_{slope}.

3.5.3 Workflow

Given the low run time and complexity of Opti-Morph to solve (P2), it is possible to solve (P1) using a direct optimization method. Other optimization methods such as a gradient descent method can be applied, if the morphodynamic model used is more complex and if only a small number of morphodynamic simulations can be performed. This study operates in a manner analogous to the search for an optimal port configuration in [22], but the morphodynamic response of the sandy seabed is now incorporated in the study.

Before launching the simulation, the parameterization of the Opti-Morph model must be defined, including the domain of the cross-shore profile Ω, the initial seabed $\psi_{|_{t=0}}$, the forcing conditions, and the parameters determining constraints. The set of all considered geotube positions must also be provided. For each position of geotubes, the morphodynamic response is calculated over time. The geotube deployment objective function $\mathcal{J}_G$ is then deduced. When the set of eligible positions has been explored, the value of x_G which minimizes $\mathcal{J}_G$ can then be determined. An explanatory diagram of the implementation strategy is given in Figure 3.2.

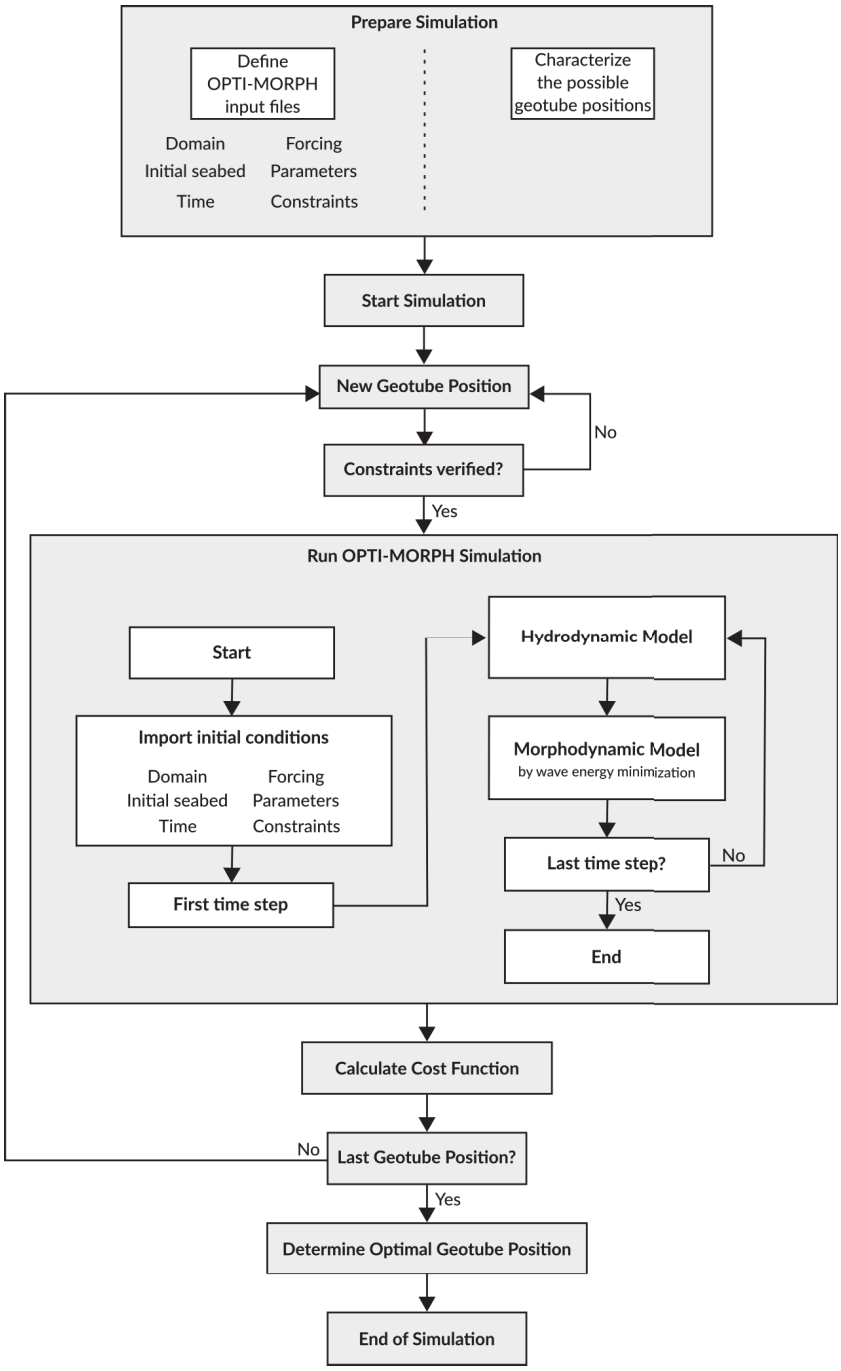

Figure 3.2: Diagram of the structure of the model capable of finding the optimal geotube position while incorporating the morphodynamic response of the seabed.

3.6 Application and Numerical Results

3.6.1 Setting

For simplicity, this study concerns a 1D cross-shore beach profile, although it can be easily adapted to the 2D case, once Opti-Morph has been extended to cater to 2 dimensional configurations. The initial seabed is a linear seabed measuring 600 m along cross-shore profile, similar to the seabed at Sète, France [6]. Bedrock features in the configuration as shown in Figure 3.1. The domain of the cross-shore profile is subdivided into 1 m long cells, allowing for a horizontal precision of 1 m over the 600 m domain. The mean water level (MWL) is set at 7 m. We consider a simple 20-day forcing scenario characterized by a rise-peak-fall storm over 6 days and fair weather conditions preceding and succeeding the storm. The sediment is considered fine sand with a critical angle of talus of 0.2. Geotubes are to be placed along the cross-shore and are defined by a width of 6 m and a height of 3 m. Constraints of problem $(P1)$ restrict the deployment of the geotextile tube to the interval $x_G \in (350, 495]$.

3.6.2 Results

This section is devoted to the numerical results of both optimization problems: the search for the optimal position of the geotube for minimal coastal erosion and the natural morphodynamic response of the seabed.

Figure 3.3.A illustrates the variations of the geotube deployment objective function $\mathcal{J}_G$ defined by Equation (3.1), with regard to the location of the geotube. We observe a piecewise constant function with erosion ranging between 2 m for $x_G = 351$ and 9 m for $x_G = 495\,m$. The optimum is located in the zone nearest the coast, over the 351 m-388 m plateau. As such, geotubes located anywhere between 351 m and 388 m from the coast induce the same retreat of the shoreline of 2 m. Given the downward trend of the objective function, it is natural to elect $x_G = 351\,m$ as the optimum for the remaining studies. The piecewise constant nature of the objective function is due to the 1 m precision of the discretization of the cross-shore domain Ω.

Figure 3.3.B illustrates the morphodynamic response of the seabed in relation to the different positions of the geotube. Four simulations were performed, with geotubes located at $x_G = 495\,m$ (blue), $x_G = 450\,m$ (green), $x_G = 400\,m$ (yellow), and $x_G = 351\,m$ (red), where the latter corresponds to an optimal geotube position. The value of the objective function $\mathcal{J}_G$ associated with each of the geotubes is labeled in Figure 3.3.A. A fifth simulation was also performed without geotube (black) for the purpose of providing a reference in the efficiency analysis of the geotubes.

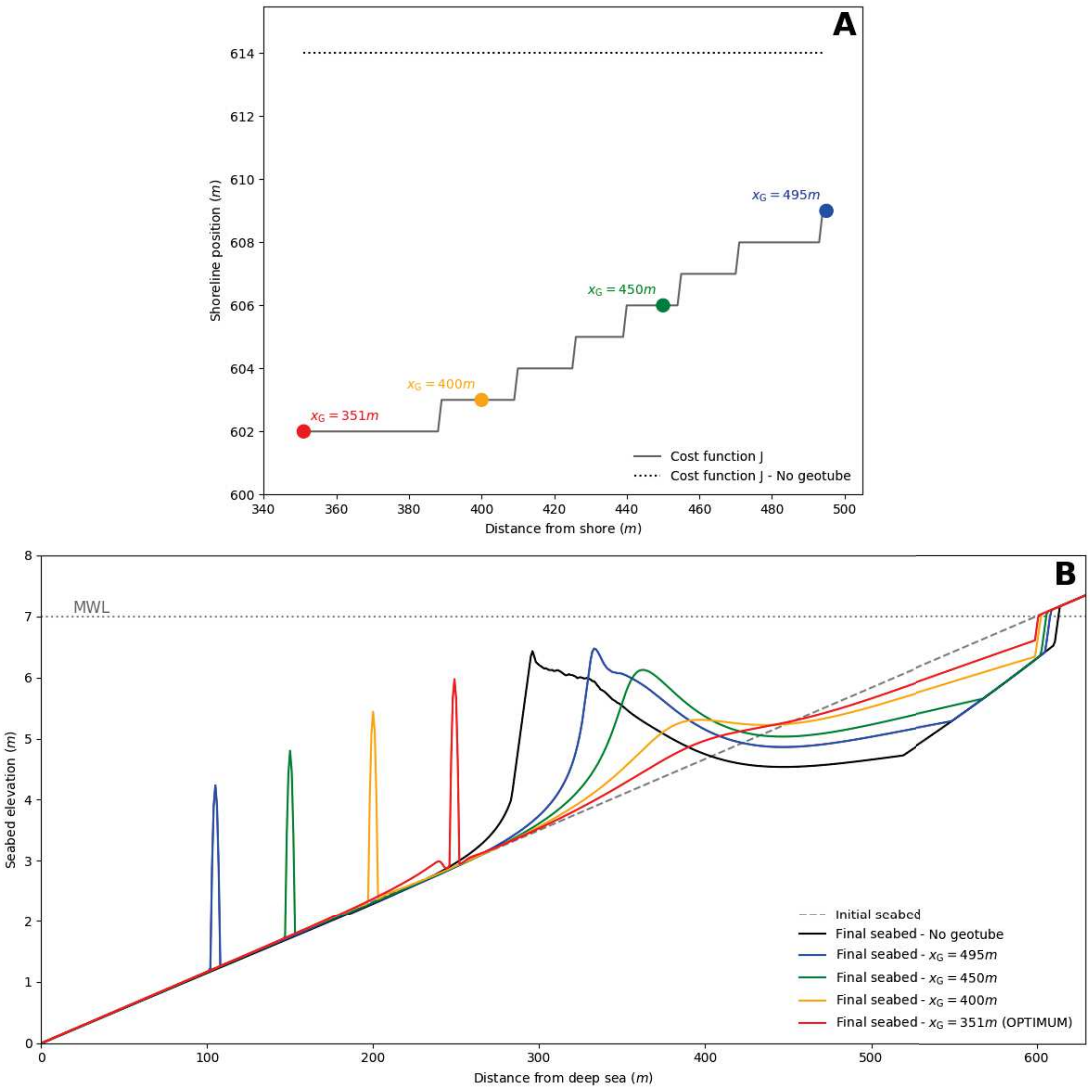

Figure 3.3: Results of the numerical search of the optimal geotube position via Opti-Morph. **A.** Variations of the geotube deployment objective function with regards to the distance between the geotube and the shoreline. The objective function calculated over a cross-shore profile with geotubes is also given as a reference. Four points are emphasized, corresponding to the four seabeds depicted in the second graphic. **B.** Final seabed profiles produced by the morphodynamic model Opti-Morph with varying geotube positions over the cross-shore profile.

At the end of the numerical simulation, each seabed features a sandbar, the height and location of which depend on the geotube position. A sandbar located at $x = 330\,m$ appears for a geotube deployed at $x_G = 495\,m$ (blue) with a height of $2.6\,m$. The closer

the geotube is to the shoreline, the smaller and closer the resulting sandbar is to the coast. For a geotube located 450 m (green) from the shoreline, the resulting sandbar measures 1.9 m and is located at $x = 360\,m$. For a geotube at $x_G = 400\,m$ (yellow), the sandbar measures 0.8 m in height, and for $x_G = 351\,m$ (red), it measures 0.3 m. The latter two are located at $x = 390\,m$. A trough proportional to the sandbar has also appeared near the coastline, and induces erosion at the coast. Limited by the bedrock, this trough has a depth of 1.1 m for $x_G = 495\,m$ and 0.4 m for $x_G = 351\,m$. The greatest displacement of sediment is observed for a seabed devoid of geotubes. A sandbar located at $x = 300\,m$ appears with a height of 3 m, as well as a 1.3 m deep trough.

Opti-Morph is capable of producing realistic results when dealing with submerged breakwaters. Indeed, the closer the geotube is positioned relative to the coast, the more wave energy is dissipated, and as such less seabed movement can be observed. For $x_G = 351\,m$, i.e. the optimal geotube, very little movement occurs, whereas for $x_G = 495\,m$, the shape of the seabed has undergone major transformation. Conversely, the further in deep waters the geotube is deployed, the more the seabed behaves as if no geotube has been introduced. This is due to the fact that in too deep a water, the geotube have little effect on the surface waves, allowing waves to pass with little to no attenuation, and as such, he energy hitting the shore is comparable to a configuration without geotubes. This can be observed by the final shape of the sandbar and trough for the deeper geotubes compared to the non-geotube configuration.

Furthermore, 3.3.B shows that the position of the geotube has a noticeable effect on the shoreline, with the red geotube inducing less erosion than those situated further seaward. This can be explained by the decrease of wave energy associated with the geotubes nearer the shore. According to Figure 3.3.A, deploying a geotube anywhere in the $[105, 250)$ zone has a positive effect on the shoreline, when compared to that without geotubes. Indeed, even in the worst case, with a geotube situated at $x_G = 495\,m$, the objective function is lesser ($\mathcal{J}_G(x_G = 495) = 609\,m$) than without any geotubes where the objective function is 614 m.

We notice an accumulation of sand at the foot of the $x_G = 351\,m$ geotube. The small trough is due to numerical inaccuracies; further developments are required on Opti-Morph to allow sand to build up against the solid structure. However, this accumulation of sand seaward of a geotube is often encountered in in situ observations of the behavior of the seabed following the deployment of a submerged breakwater [52].

3.7 Discussion

3.7.1 Effect of the Geotube on Wave Height

In this section, we analyze the behavior of the hydrodynamic model used by Opti-Morph. Figure 3.4 shows the height of the waves over the cross-shore profile at three

different points in time: (i) after 2 days (Fig. 3.4.A) to observe the wave height during fair-weather conditions before the storm, (ii) after 8.3 days (Fig. 3.4.B) at the peak of the storm, and (iii) 18.7 days (Fig. 3.4.C) after the storm has occurred and the fair-weather conditions have returned. For each of the three points of time, the wave height associated to five different morphodynamic configurations is depicted. Black shows the wave height associated to a seabed without geotube. The blue, green and yellow profiles show the wave height corresponding to a seabed where a geotube has been deployed at $x_G = 495\,m$, $x_G = 450\,m$ and $x_G = 400\,m$ respectively, and the red corresponds to the optimal geotube position, for $x_G = 351\,m$.

Figure 3.4 demonstrates that the simple hydrodynamic model used by Opti-Morph is capable of handling underwater breakwaters, as shown by the fact that the waves behave as expected: (i) waves shoal prior to the geotube with an increase in wave height, (ii) geotubes trigger a breaking effect on the waves with a sharp drop of height, and (iii) after breaking, wave height decreases smoothly before reaching the coast. Furthermore, Figure 3.4 illustrates the different impact that geotubes have on the surface waves depending on the height of the latter. Indeed, we observe that geotubes have little impact on the small waves of Figures 3.4.A, and 3.4.C, with a drop of a few millimeters, whereas when the wave height is great, as in Figure 3.4.B, the drop can reach up to $2\,m$ (red). This behavior of the wave height is characteristic of cross-shore profiles containing a geotube.

In addition, geotubes in deeper waters have less effect on the waves as those in shallower waters. In Figure 3.4.B, the geotube located at $x_G = 495\,m$ induces as drop of $0.8\,m$ whereas the optimal geotube, located at $351\,m$ provokes a drop of over $2\,m$. This can also be illustrated using the transmission coefficient, K_t, described in [97, 64] as the ratio between the height of the waves prior to the geotube and posterior to the geotube, and used to describe the efficiency of submerged breakwaters. This coefficient ranges between 0 and 1, where 0 indicates no transmission (i.e. an impermeable structure) and 1 indicates complete transmission (i.e. the geotube has no impact on the surface waves). According to [64], a transmission coefficient lesser than 0.6 is required for the most effective submerged breakwaters.

At the apex of the storm, the optimal geotube has a transmission coefficient of $K_t = 0.20$. Geotubes located at $x_G = 495\,m$, $x_G = 450\,m$ and $x_G = 400\,m$ have a transmission parameter of $K_t = 0.68$, $K_t = 0.49$ and $K_t = 0.32$ respectively. In fact, K_t is inferior to 0.6 for all geotubes located between $351\,m$ and $475\,m$ from the coast. In other words, geotubes deployed beyond the $x = 475\,m$ threshold from the shoreline are deemed ineffective in reducing wave energy.

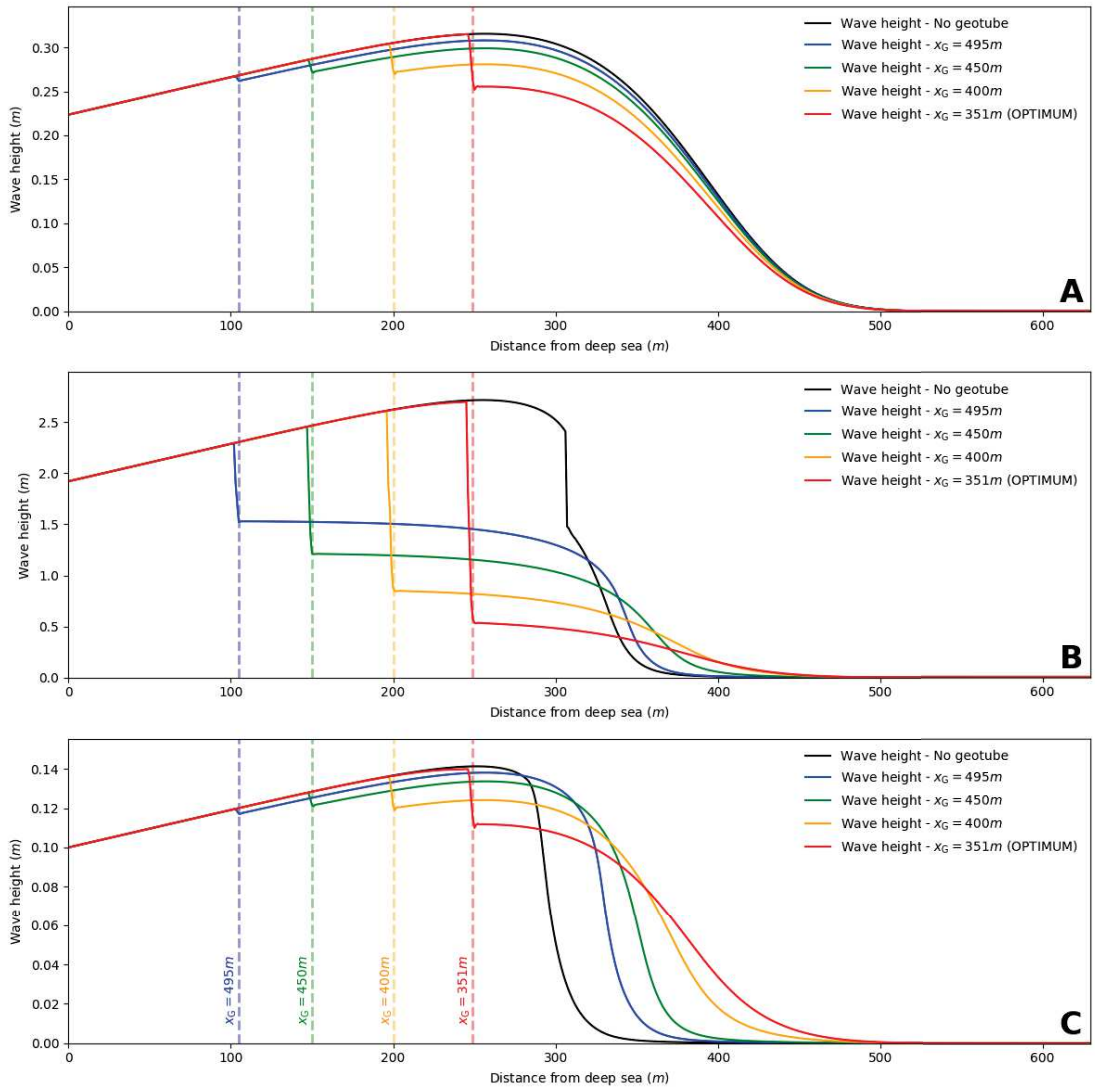

Figure 3.4: Wave height over the cross-shore profile associated with four geotube positions: $x_G = 495\,m$ (blue), $x_G = 450\,m$ (green), $x_G = 400\,m$ (yellow), and $x_G = 351\,m$ (red). Wave height relating to a seabed profile devoid of geotubes has also been given as a reference (black). **A.** Wave height prior to the storm at $t = 2\,days$. **B.** Wave height at the apex of the storm at $t = 8.3\,days$. **C.** Wave height posterior to the storm at $t = 18.7\,days$.

3.7.2 Time-dependent Geotube Analysis

The main purpose of introducing a geotube to the cross-shore profile is to provoke premature breaking of the greater waves, and thus reducing the energy of the waves and limiting coastal erosion. As such, this section is devoted to the analysis of these three physical quantities. Figure 3.5 shows the influence of geotubes on the breaking location, the energy of the waves, and the shoreline.

Figure 3.5.A shows the time-series of the forcing wave height in order to identify the different forcing conditions exerted on the beach profile. We can then analyze the effect of the storm on the breaking waves, energy, and shoreline position. Forcing wave height follows a Gaussian curve, the peak appearing at $t = 9$ days. After day 13, fair weather conditions return for the remaining 8 days of simulation. Figures 3.5.B, 3.5.C, and 3.5.D respectively show the evolution of the breaking point, energy of the waves, and shoreline associated with this forcing scenario, for seabeds without a geotube (black), with a geotube located at $x_G = 351\,m$ (red), $x_G = 400\,m$ (yellow), $x_G = 450\,m$ (green), and $x_G = 495\,m$ (blue).

Figure 3.5.B shows the evolution of the breaking point of the waves over the course of the simulation. All five profiles show breaking occurring at the coast at the beginning and end of the simulation, i.e. when the forcing wave height is minimal. This result is normal given that geotubes are expected to have little effect on smaller waves and greater effect on larger ones. In the case of the optimal geotube (red), we observe that breaking occurs at the site of the geotube (i.e. $x_G = 351\,m$) at day 5, and continues to break there up until day 11, that is when the forcing wave height exceeds $0.75\,m$. The geotube placed at $x_G = 400\,m$ (yellow) induces wave breaking as of day 5.8 and continues to do so until day 10.6; this corresponds to a forcing wave height exceeding $1\,m$. Similarly, the geotube placed at $x_G = 450\,m$ (green) induces wave breaking over the 6.5 - 10.3 day interval, which corresponds to a forcing wave height exceeding $1.2\,m$. Finally, in a configuration with a geotube placed at $x_G = 495\,m$ (blue), wave break at the site of the geotube from day 7.3 until day 10, when the forcing wave height exceeds $1.5\,m$. For another 0.5 days, waves breaking fluctuates between $340\,m$ and the shoreline. This corresponds to the sandbar which appeared over the course of the simulation as shown in Figure 3.3.B, and now acts as a natural submerged breakwater, prematurely breaking the waves before they hit the coast. This phenomenon is more observable for the configuration with no submerged structures (black). Here, breaking occurs at the coast up until day 7.3. Then, waves breaks at $x = 350\,m$, due to the appearance of the sandbar, which acts as a natural breakwater. Breaking continues to occur around this point, fluctuating often with the coast. Over the course of the simulation only 12% of the waves break away from the shoreline.

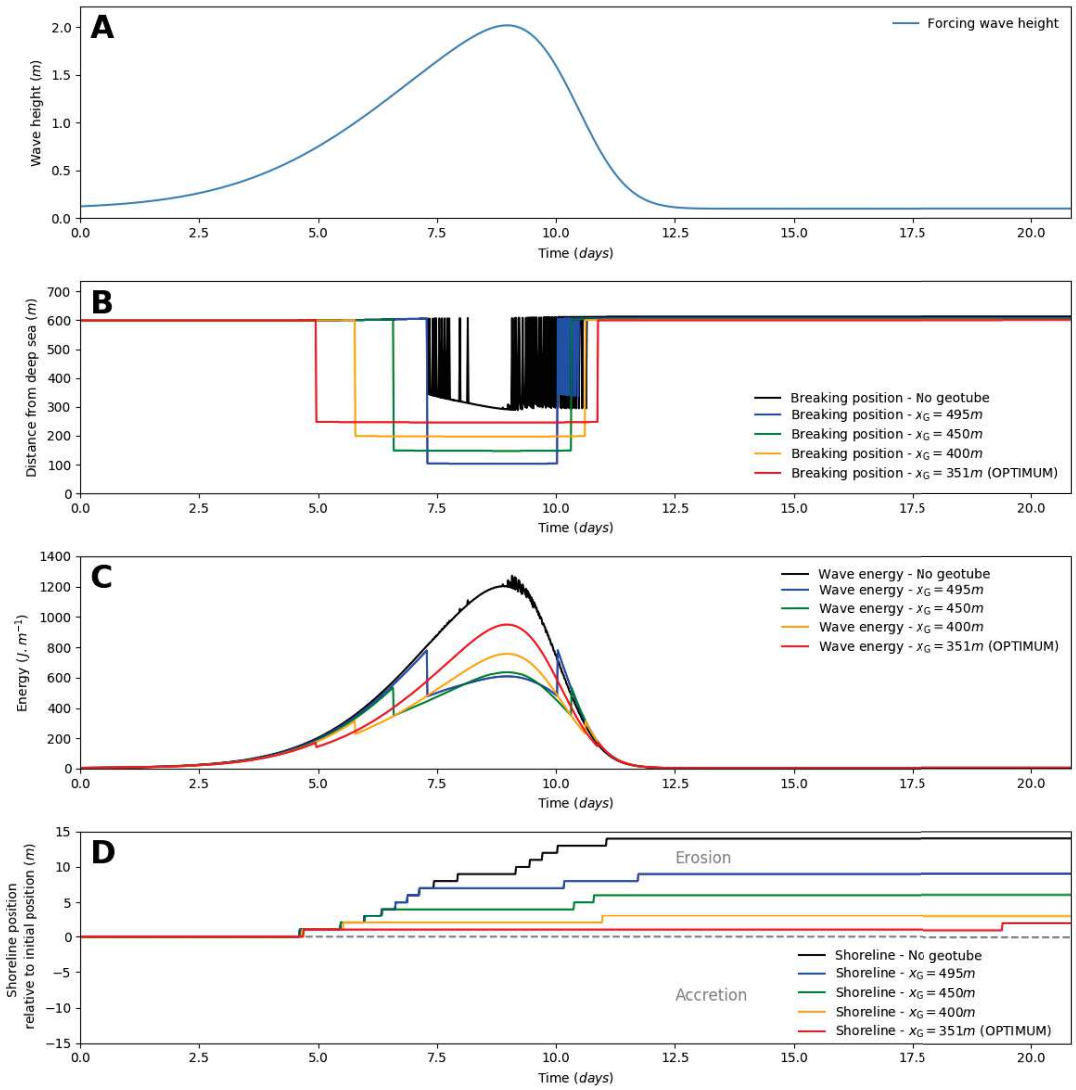

Figure 3.5: Time series of the wave breaking position, wave energy and shoreline position for different geotube configurations : $x_G = 351\,m$ (red), $x_G = 400\,m$ (yellow), $x_G = 450\,m$ (green), and $x_G = 495\,m$ (blue). The time series of the forcing wave height is also provided. **A.** Forcing wave height. **B.** Time series of the wave breaking position associated with different geotube locations. Should several breakings occur, the first event is retained. The breaking position associated to a seabed devoid of geotubes is also given (black). **C.** Time series of the energy of the waves associated with different geotube locations. The energy associated to a seabed devoid of geotubes is also given (black). **D.** Time series of the position of the shoreline relative to its initial location at $x = 600\,m$, and associated with different geotube locations. A positive value indicates erosion and a negative value indicates accretion. The breaking position associated to a seabed devoid of geotubes is also given (black).

Figure 3.5.C shows the evolution of the energy of surface waves over time, given by $E = \frac{1}{16}\int_{\Omega} \rho g H^2 \mathrm{d}x$ $(J.m^{-1})$. Before and after the geotubes take effect, all four energy profiles coincide with the energy profile associated with no geotubes. However, we observe a drop in energy when the wave height is sufficiently high to detect the geotube, i.e. at day 5 for the optimal geotube (red), day 6.5 for the geotube located at $x_G = 450\,m$ (green), day 5.8 for $x_G = 400\,m$ (yellow) and day 7.3 for the geotube located at $x_G = 495\,m$. Similar observations can be made after the storm peak, with a sharp rise of energy when the geotubes no longer affect the waves.

Energy reaches $1240\,J.m^{-1}$ at the apex of the storm in the case of no geotubes. This has been significantly reduced for all the geotube simulations. In fact, the geotube located at $x_G = 351\,m$ (resp. $400\,m$, $450\,m$ and $495\,m$) generates an apex energy of $950\,J.m^{-1}$ (resp. $755\,J.m^{-1}$, $635\,J.m^{-1}$ and $610\,J.m^{-1}$), this suggest a reduction of energy of $290\,J.m^{-1}$, $485\,J.m^{-1}$, $605\,J.m^{-1}$, and $630\,J.m^{-1}$ respectively.

Figure 3.5.D depicts the evolution of the shoreline. The shoreline remains constant over the first 4.6 days of the simulation, when the forcing wave height remains small ($0.6\,m$). The seabeds with geotubes closest to the shore experience relatively little erosion, varying from its initial position by $2\,m$ for $x_G = 351\,m$ and $3\,m$ for $x_G = 400\,m$. The greater the distance between the geotube and the shoreline, the greater the erosion. For $x_G = 450\,m$, we observe a retreat of $6\,m$ and $9\,m$ for $x_G = 495\,m$. In the case of no geotubes, the shoreline experiences the greatest retreat with a variation of $14\,m$. Once the storm has passed, and the height of the forcing waves is once again small, the shoreline remains stable over the subsequent period of the simulation.

Figure 3.5 shows unsurprising results when it comes to the influence of the geotubes on the breaking position, wave energy, and shoreline position, and demonstrates the potential of Opti-Morph. This model, with a simple approach to hydrodynamic processes, illustrates several phenomena one would expect of a geotube deployment. First, Figure 3.5.B shows that waves pass over the geotubes smoothly for smaller waves. Also, the further the geotube is from the coast, the greater the waves have to be for the geotube to take effect. When a geotube is detectable, breaking occurs directly above, demonstrating that it is the submerged breakwater which causes the premature breaking. Figure 3.5.C shows that any geotube capable of prematurely breaking the waves causes a reduction of energy. We observe that the geotube reducing the most energy is not the same as the one obtained during the optimal search (red). Based on this observation, we investigate which geotube location minimizes wave energy in the following section. Finally, 3.5.D demonstrates that premature breaking has a positive effect on the shoreline; breaking away from the coast over a long period of time leads to less erosion at the coast.

3.7.3 Alternative Geotube Deployment Objective Function

The adaptability of this approach in the search of the optimal geotube position is illustrated in this section. We perform the previous analysis, with the same constraints and

forcing conditions, but using a different geotube deployment objective function. The choice of cost function will depend on many factors, and as such flexibility with regard to its choice is preferred. Previously, the search of the optimal position is performed with regard to the position of the shoreline (cf. Eq. (3.1)). In this section, we choose to minimize the time-averaged energy of the surface waves, as mentioned in Section 3.7.2 and in Figure 3.5, where it was revealed that an optimal geotube in terms of minimal erosion is not necessarily equivalent to an optimal geotube in terms of energy.

Given that the geotextile tubes are designed to prematurely cause wave breaking and thus ensuring less energy arrives at the coast, in this study we seek to minimize the cumulative energy of the waves over the cross-shore profile.

As such, a new objective function is considered:

$$\tilde{\mathcal{J}}_{\mathrm{G}}(x_{\mathrm{G}}) = \frac{1}{16}\int_0^T \int_\Omega \rho g H^2(x,t,x_{\mathrm{G}})\mathrm{d}x\mathrm{d}t \qquad (J.m^{-1}.s^{-1}) \tag{3.3}$$

where ρ is water density ($kg.m^{-3}$), g is gravitational acceleration ($m.s^{-1}$), and H is the height of the surface waves (m).

Figure 3.6.A shows the variations of the objective function $\tilde{\mathcal{J}}_{\mathrm{G}}$ (cf. Eq. (3.3)) with regard to the location of the geotube. Contrarily to the results of Section 3.6.2, a unique minimum is observed at $x_{\mathrm{G}} = 435\,m$ (red point), this signifies that to achieve maximal energy reduction over the course of a storm, the best deployment location of a geotube is at $435\,m$ from the coast. This corresponds to a cumulative wave energy of $2.56\times10^8\,J.m^{-1}.s^{-1}$ Other geotube positions are also depicted; their color matching the color of the seabeds in Figure 3.6.B. The energy associated to a configuration without geotubes is also shown.

Figure 3.6.B shows the outcome of the seabed, after being subjected to a storm. Six profiles are presented, the same five as in Section 3.6.2 and the new optimal geotube position $x_{\mathrm{G}} = 435\,m$ (red). As the only difference between this and the previous study is the choice of objective function in geotube location optimization problem, the morphodynamic model produces the same results for the first five seabeds: for $x_{\mathrm{G}} = 495\,m$ (blue), $x_{\mathrm{G}} = 450\,m$ (green), $x_{\mathrm{G}} = 400\,m$ (yellow), and $x_{\mathrm{G}} = 351\,m$ (pink), as well as the configuration without geotube (black). The pink profile was previously featured in red because it corresponded to the optimal position in the previous study. The new addition is the seabed corresponding to the optimal geotube location with regard to wave energy, this is $x_{\mathrm{G}} = 435\,m$ (red). In this configuration, the formation of a sandbar can be observed at $x = 370\,m$, with a height of $1.5\,m$, as well as the creation of a trough whose depth reaches $0.9\,m$, stopped only by the now exposed bedrock. As with the previous study, all geotubes have a position influence on the reduction of wave energy: Figure 3.6.A shows that for all x_{G}, the associated value of the objective function is less than the energy without geotubes. However, the behavior of the waves and seabed tend towards a configuration without geotube when the geotubes are placed further towards

the deep sea.

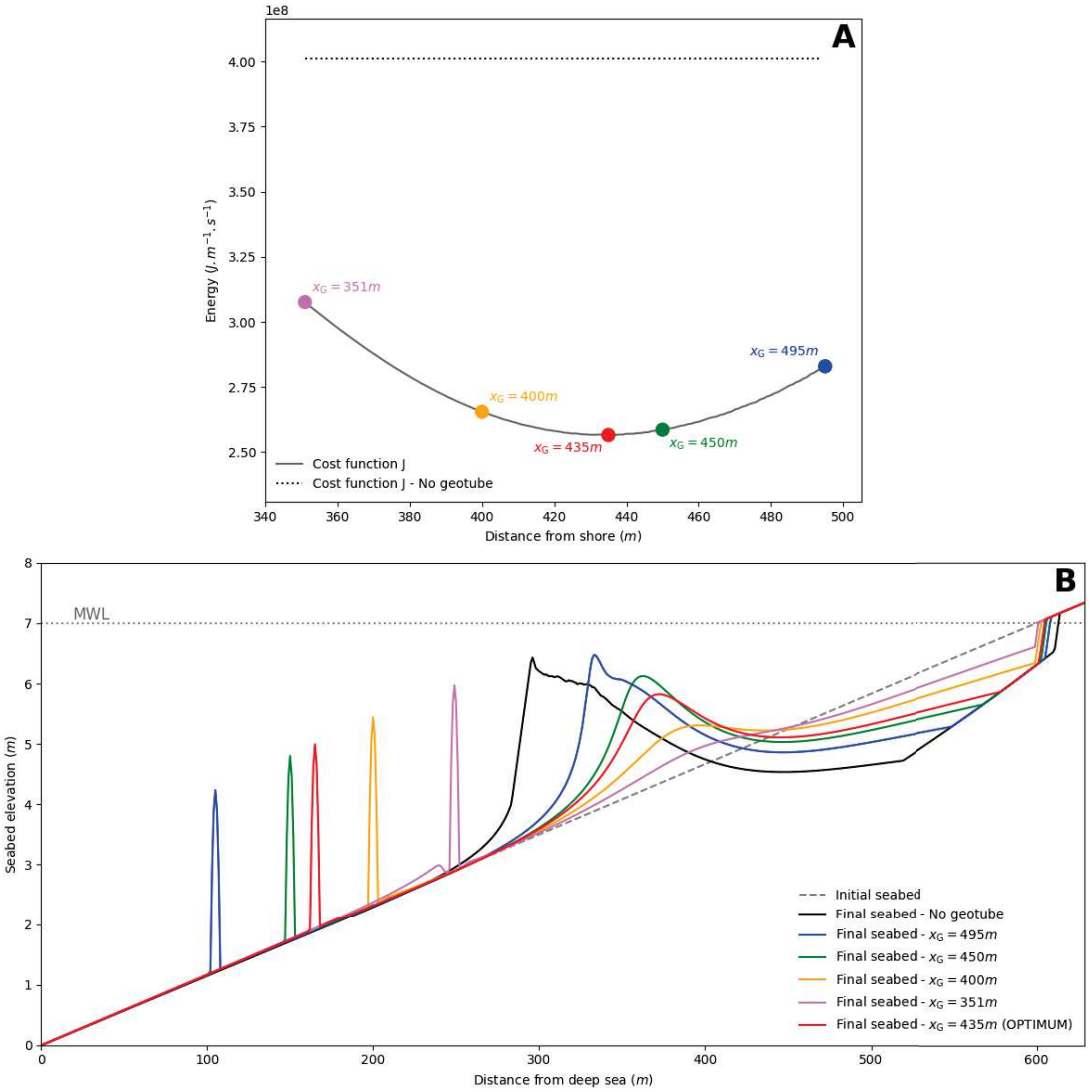

Figure 3.6: Results of the numerical search of the optimal geotube position via Opti-Morph. **A.** Variations of the geotube deployment objective function with regards to the distance between the geotube and the shoreline. The objective function calculated over a cross-shore profile with geotubes is also given as a reference. Five points are emphasized, corresponding to the five seabeds depicted in the second graphic. **B.** Final seabed profiles produced by the morphodynamic model Opti-Morph with varying geotube positions over the cross-shore profile : $x_G = 495\,m$ (blue), $x_G = 450\,m$ (green), $x_G = 400\,m$ (yellow) and $x_G = 351\,m$ (pink) and the optimal position at $x_G = 435\,m$ (red)

This study shows that the minimization of erosion of Section 3.6.2 differs from the minimization of cumulative energy of the waves calculated over the length of the domain. This is due to the manner in which the waves shoal and break. Breaking too early causes a small drop in wave height and thus generates large waves after the geotube. Breaking too late generates large waves prior to breaking at the geotube (with a considerable drop in wave height afterward). As such, the optimal geotube position relative to the energy across the totality of the domain can be found somewhere between these two scenarios.

The rapidity of Opti-Morph and the simplicity of the problem allows the use of a direct method to find the optimal position of the geotube. However, in more complex circumstances, an optimizer may be preferable. By way of illustration, the Nelder–Mead algorithm [88] was applied to this energy minimization problem, and the minimum of $\tilde{\mathcal{J}}_{\mathrm{G}}$ was found in 20 iterations, which corresponds to a run-time around four times quicker than the direct method.

3.8 Conclusion

This study was performed in an attempt to demonstrate the potential of the morphodynamic model, Opti-Morph. This model is capable of handling artificial structures such as geotextile breakwaters. We conducted an extensive search for the optimal geotube position, and thus solving two optimization problems simultaneously: the morphodynamic response by wave energy minimization and the optimal geotube position in terms of minimal coastal erosion. Further analyses were conducted to illustrate the influence of the geotube position on the waves. The resulting observations are coherent with expectations, demonstrating the potential of Opti-Morph for coastal engineering projects. In addition to this, Opti-Morph is fast, robust and of low-complexity which makes it an appealing tool for coastal engineering investigations.

Chapitre 4

Opti-Morph : Guide d'Utilisation

Dans ce chapitre, nous présentons le guide d'utilisation d'Opti-Morph, offrant une description complète du modèle, son implémentation et des exemples d'application.

Ce guide a été pré-publié, intitulé "Opti-Morph User Guide", cf. [20].

4.1 Résumé en Français

4.1.1 Introduction

Le modèle numérique hydro-morphodynamique Opti-Morph incarne une nouvelle approche dans la description de la morphodynamique côtière, basée sur la théorie de l'optimisation. Ce modèle repose sur l'hypothèse que le profil bathymétrique d'une plage sableuse évolue dans le temps afin de minimiser une certaine fonction, dite fonction de coût. Le choix de cette fonction dépend de ce qui est considéré comme la force motrice derrière la morphodynamique littorale. Ce problème d'optimisation est également soumis à un certain nombre de contraintes, permettant d'incorporer davantage de physique dans le modèle morphodynamique. Nous poursuivons les travaux pionniers de [11, 81] et [79], qui ont initié cette approche dans un contexte plus théorique.

Opti-Morph a été développé pour démontrer le potentiel d'une approche d'optimisation dans la modélisation de la dynamique côtière. Les principaux objectifs d'Opti-Morph sont :

- Production de résultats de simulation logique/naturaliste
- Adaptabilité face aux configurations en mer ou en canal
- Rapidité d'exécution
- Grande robustesse

- Facilité d'utilisation
- Adaptabilité du modèle hydrodynamique, de la fonction de coût et des contraintes
- Possibilité d'introduire des brise-lames submergés ou autres techniques d'ingénierie douce

Le modèle Opti-Morph est un outil destiné à toute personne souhaitant simuler l'évolution naturelle des profils bathymétriques côtiers et/ou étudier l'effet des dispositifs immergés artificiels sur le transport sédimentaire. À ce titre, cet outil peut être utilisé par les ingénieurs et les chefs de projet lors de la planification du déploiement de certains ouvrages de réduction des vagues et de leur influence sur le fond marin environnant.

Ce modèle peut également être utilisé dans un cadre académique pour étudier les forces motrices de la morphodynamique côtière. Le modèle a été développé de sorte que la mobilité du fond est entraînée par la minimisation d'une grandeur physique. Le choix de cette grandeur détermine quelles composantes hydro-morphodynamiques entraîne la mobilité du fond. L'énergie des vagues fut choisie dans cette étude, mais d'autres fonctions peuvent être explorées.

4.1.2 Formulations Théoriques

Le modèle Opti-Morph fonctionne en couplant un modèle hydrodynamique et un modèle morphodynamique. La base du modèle morphodynamique est la minimisation d'une fonction de coût liée aux vagues ; cette fonction de coût est fournie par le modèle hydrodynamique, ce qui démontre la relation étroite entre les processus hydrodynamiques et morphodynamiques.

Il existe actuellement sept modèles hydrodynamiques différents implémentés dans Opti-Morph. Ces modèles hydrodynamiques ont l'avantage de pouvoir calculer analytiquement le gradient de la hauteur des vagues par rapport à l'élévation du fond. Opti-Morph s'appuie fortement sur cette différenciation, et puisque l'un de ces principaux objectifs était d'obtenir des temps d'exécution rapides, il est naturel d'adopter des modèles hydrodynamiques qui soient également rapides. Ceci est réalisé en définissant analytiquement la hauteur des vagues par rapport au profil bathymétrique.

Les sept modèles hydrodynamiques sont présentés dans la suite. Ces modèles, et l'ordre dans lequel ils apparaissent, illustrent l'évolution du modèle au cours de son développement, le dernier étant le produit final. Ceci fut réalisé dans le but de répondre aux différents problèmes rencontrés pendant la phase de recherche. Chaque modèle a ses propres atouts, ils furent tous retenus afin de démontrer la simplicité du remplacement d'un modèle hydrodynamique par un autre.

Nous décrivons ensuite les formalismes théoriques gouvernant le modèle morphodynamique. L'hypothèse fondamentale gouvernant Opti-Morph stipule que le fond évolue en temps de manière à minimiser une certaine quantité, appelée fonction de coût. Le

choix de la fonction de coût dépend de ce qui est considéré comme la force motrice de la réponse morphodynamique du fond. Plusieurs fonctions de coût furent considérées, mais toutes dérivent de l'énergie des vagues. En d'autres termes, la forme du profil bathymétrique varie dans le but de minimiser l'énergie des vagues de surface à un instant donné. À chaque instant, le modèle indique la direction vers un minimum local de la fonction de coût par rapport à la paramétrisation du fond. Cette direction est nommée la direction de descente. Deux paramètres physiques limitent ou favorisent la mobilité des profils bathymétriques en fonction des propriétés du sédiment et de la profondeur de l'eau. De plus, des contraintes sont ajoutées à ce problème d'optimisation comme moyen d'incorporer des phénomènes physiques supplémentaires au modèle. Les contraintes sont considérées comme des processus secondaires par rapport à la minimisation de la fonction de coût, cette dernière étant considérée comme la force principale derrière la réponse morphodynamique. Trois contraintes sont incluses dans ce modèle : celles de la pente maximale, du stock sableux (dans le cas d'un canal à houle), et du substrat rocheux.

Dans le but d'illustrer la facilité de changer de fonction de coût (ou direction de descente), nous présentons sept options. Elles sont toutes basées sur l'énergie des vagues.

4.1.3 Modèle Numérique

Une description de l'implémentation est donnée par la suite, ainsi qu'une présentation de son utilisation. Un diagramme est fourni pour illustrer les différentes étapes d'Opti-Morph :

- Avant le lancement du modèle, les données initiales de la simulation ainsi que les paramètres du modèle doivent être définis. Cela inclut les données de forçage, le choix du modèle hydrodynamique, les données bathymétriques, le choix de la fonction de coût et les contraintes.

- L'utilisateur lance Opti-Morph. Les données initiales sont importées et le modèle est configuré.

- Pour chaque pas de temps, les données de forçage sont transmises au modèle hydrodynamique. Ce modèle calcule ensuite la hauteur des vagues sur le profil cross-shore et fournit ainsi la valeur de la fonction de coût (ou la direction de descente) utilisée par le module morphodynamique d'Opti-Morph.

- Le nouveau profil du fond est déterminé en minimisant la fonction de coût (ou en suivant la direction de descente). Des contraintes sont appliquées au fond avant ou après la minimisation, et le nouveau fond est retenu.

- Au pas de temps suivant, le modèle hydrodynamique reçoit la nouvelle condition de forçage ainsi que ce nouveau profil bathymétrique.
- Ce cycle se poursuit au cours de la simulation et illustre l'interaction complexe entre les processus hydrodynamiques et morphodynamiques.

Le modèle numérique Opti-Morph est implémenté en objet orienté. Cette structuration du modèle à l'aide de classes a été choisie afin de permettre flexibilité et créativité au sein du modèle. Chaque objet peut être considéré comme un bloc de construction qui peut être facilement modifié ou remplacé en fonction des intentions de l'utilisateur. Par exemple, un modèle hydrodynamique différent peut être implémenté et adapté au modèle Opti-Morph avec facilité. Il en va de même pour le choix de la fonction de coût : adopter une autre fonction de coût revient à implémenter la nouvelle fonction ainsi que son gradient et laisser le reste du modèle Opti-Morph inchangé.

Un guide d'utilisation est ensuite fourni avec des détails sur (i) l'environnement de travail nécessaire à l'exécution du code, (ii) la fonction main, avec un exemple détaillé, et (iii) les quatre fichiers d'entrée : les données bathymétriques, les forçages, les paramètres physiques et les paramètres de sortie.

4.1.4 Applications

Deux exemples sont fournis pour illustrer l'utilisation d'Opti-Morph. Dans un premier temps, nous considérons un profil bathymétrique décrit comme une simple fonction linéaire le long du profil cross-shore. Puis nous cherchons à introduire des structures immergées conçues pour limiter l'activité des vagues sur la côte.

4.2 Introduction

4.2.1 About

The numerical hydro-morphodynamic model presented here embodies a new approach to coastal morphodynamics, based on optimization theory. This model is based on the assumption that a sandy seabed evolves over time in order to minimize a certain wave-related function, the choice of which depends on what is considered the driving force behind coastal morphodynamics. This numerical model was given the name **Opti-Morph**, and has the advantages of being fast, robust, and requires very few input parameters.

Optimization theory has been widely used in the study of coastal zones, but is mainly applied in the development of protection structures [54, 57] and/or ports [22, 57]. Continuing the pioneering work of [11, 81] and [79], which put in motion the idea that morphodynamic processes can be described using optimization theory, we have

developed a numerical model that simulates the evolution of the seabed while taking into account the complex coupling between morphodynamic and hydrodynamic processes. Based on the assumption that the seabed adapts to minimize a certain hydrodynamic quantity, this optimization problem is also subjected to a certain number of constraints, allowing for a more accurate description of the morphodynamic evolution. First results can be found in [21], where this model was applied to a flume configuration and compared with physical data. A comparative analysis was also conducted between Opti-Morph and another numerical model for the purpose of evaluating the performance of Opti-Morph in comparison with existing hydro-morphodynamic models.

4.2.2 Expectations and Objectives

The main goal of Opti-Morph is to demonstrate the potential of using optimal control in the modeling of coastal dynamics by designing an adaptable, easy-to-use numerical model.

A non-exhaustive list of objectives considered during the initial development of Opti-Morph follows.

- ➔ Production of logical/naturalistic simulation results
- ➔ Adaptable to open-sea or flume configurations
- ➔ Low run times
- ➔ High robustness
- ➔ User-friendly (including inexperienced users)
- ➔ Adaptability of:
  - → hydrodynamic model
  - → cost function
  - → constraints
- ➔ Possibility of introducing submerged breakwaters or other soft engineering techniques

4.2.3 Target Audience

The Opti-Morph model is a tool intended for any person wishing to simulate the natural evolution of the coastal seabed in response to the incoming wave conditions, and/or to study the effect of man-made submerged devices on the sediment transport. As such

this tool can be used by engineers and project managers when planning the deployment of certain wave-reducing structures and their influence on the surrounding sediment.

This model can also be used in an academic setting to study the driving forces behind coastal morphodynamics. The model has been developed such that the mobility of the seabed is driven by the minimization of a cost function. The choice of cost function determines which coastal hydro-morphodynamic components drive the seabed mobility. The default cost function is wave energy but other functions can be explored if desired.

4.3 Processes and Theoretical Formulation

The Opti-Morph model operates by pairing a hydrodynamic and a morphodynamic model. The basis of the morphodynamic model is the minimization of a wave-related cost function; this cost function is provided by the hydrodynamic model, which demonstrates the close relation between the hydrodynamic and morphodynamic processes. In this first section, we will begin by describing the domain and definitions used throughout this document. The hydrodynamic model is then described with its various adaptations, followed by the theoretical description of the morphodynamic model. This includes the governing equations, the choice of cost function, and the introduction of the notion of constraints.

4.3.1 Domain and Definitions

We consider a coordinate system composed of a horizontal axis x and a vertical axis z. We denote $\Omega := [0, x_{\max}]$ the domain of the cross-shore profile, where $x = 0$ refers to an arbitrary fixed point in the deep water and $x_{\max}$ an arbitrary fixed point at the shore, beyond the coast. The elevation of the seabed is a one-dimensional positive function, defined by: $\psi : \Omega \times [0, T] \times \Psi \rightarrow \mathbb{R}^+$ where $[0, T]$ is the interval of time considered for the study, and Ψ is the set of physical parameters describing the shape of the seabed. Let h_0 be the mean water level (m) and h be the water depth (m), defined over the cross-shore profile by $h = h_0 - \psi$. We denote Ω_S the sub-domain of Ω over which the waves shoal and Ω_B the sub-domain of Ω over which the waves break. Let x_B denote the location of the breaking of the waves and let x_S be the shoreline position, that is when the seabed intersects with the mean water level h_0. Note that the breaking location and the shoreline position may vary over the course of the simulation, and as such x_B and x_S are both time-dependent. The same also goes for Ω_B and Ω_S. Time dependency of x_B, x_S, Ω_B and Ω_S have been omitted for clarity from the remainder of this document. The definitions and notations presented above are summarized in Figure 4.1.

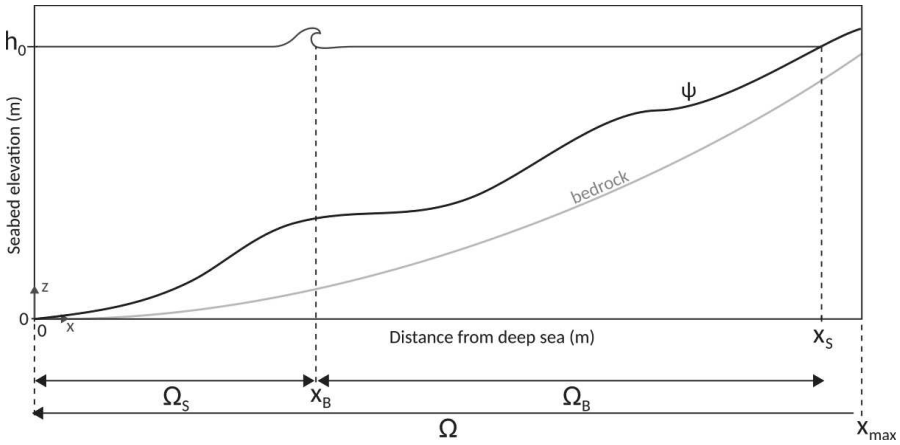

Figure 4.1: Illustration of the cross-shore profile where breaking occurs once at $x = x_B$

ℹ At the present time, Opti-Morph operates in a one-dimensional setting, depicting either the cross-shore profile of a sandy beach or a flume experiment. However, no assumptions were made regarding the choice of dimension in the theoretical development of this model, and as a result, it is straightforward to extend this theory to a two-dimensional configuration.

4.3.2 Hydrodynamic Model

4.3.2.1 Introduction

In order to model the evolution over time of the seabed ψ and given the assumption that ψ changes over time in response to the minimization of some hydrodynamic quantity, a hydrodynamic model capable of providing the necessary data is required, here the significant wave height over the cross-shore profile.

There are currently seven different hydrodynamic models associated with the Opti-Morph model. These hydrodynamic models have the advantage of being able to analytically calculate the gradient of wave height with respect to the seabed. Indeed, Opti-Morph relies heavily on this differentiation, and explicit formulas induce quick execution times. Considering that one of the main objectives of Opti-Morph is a rapid output time (cf. Section 4.2.2), it is natural for the associated hydrodynamic models to also have significantly fast execution times. This is achieved by providing wave height analytically with regard to the seabed ψ. Other hydrodynamic models can be integrated with ease, provided that the parameters and methods required by the morphodynamic model are still present. A model using a time-consuming differentiation method can be used but defeats the purpose of Opti-Morph which was designed to be quick and of low-complexity. Another solution would be to perform the calculation of the gradient

using automatic differentiation programs [42, 47]. This exceeds the initial scope of the Opti-Morph model, but may be implemented at some point in the future if needs be.

The seven hydrodynamic models presented below provide the significant wave height over the cross-shore profile as well as other wave-related data. They range in complexity, from the simplest model in 4.3.2.3 to the more complex in 4.3.2.3. In fact, the hydrodynamic models, and the order in which they appear, illustrate the evolution of the model over the course of its development, with the last being the final product. This was carried out in an attempt to address the different issues encountered during the research phase. Each model has its own merits and all have been retained in order to demonstrate the simplicity of replacing one hydrodynamic model with another. This evolution of the hydrodynamic model is showcased in Table 4.1.

Hydrodynamic model / Characteristics	**1** (4.3.2.3)	**2** (4.3.2.3)	**3** (4.3.2.3)	**4** (4.3.2.3)	**5** (4.3.2.3)	**6** (4.3.2.3)	**7** (4.3.2.3)
Shoaling	■	■	■	■	■	■	■
Breaking condition	■	■	■	■	■	■	■
Energy conservation		■					
Multiple wave-breaking			■	■	■	■	■
Handling submerged breakwaters				■	■	■	■
Dependency of seaward activity				■	■	■	■
Dependency of seaward activity with decreasing influence					■	■	■
Smooth transition of boundary conditions						■	■
Incorporation of anti-dissipative effect							■

Table 4.1: Defining characteristics of each of the featured hydrodynamic models

In the following sections, hydrodynamic models no. 1 to 7 are presented. All are based on the same principle derived from linear wave theory [28]. The processes shared by all of the models appear in the first section. Then, individual descriptions of the various hydrodynamic models are provided.

4.3.2.2 Shared Processes Between Hydrodynamic Models

Let H be the significant wave height over the cross-shore profile. We use the partition of $\Omega = \Omega_S \cup \Omega_B$ to define H: waves over the cross-shore profile are either shoaling (over Ω_S) or breaking (over Ω_B).

In order to determine H over the cross-shore profile, the following wave parameters are required:

- wavenumber k (m^{-1}): see Section 4.3.2.2
- phase velocity C $(m.s^{-1})$: see Section 4.3.2.2
- group velocity C_g $(m.s^{-1})$: see Section 4.3.2.2

ℹ All models also require the following input data:

- forcing wave height $t \longrightarrow H_0(t)$
- forcing wave period $t \longrightarrow T_0(t)$ (here assumed constant)
- a wave-breaking index γ

Wavenumber

The wavenumber is determined by the linear dispersion equation. Linear dispersion is given by:

$$\sigma^2 = gk \tanh(kh) \tag{4.1}$$

where $\sigma = \frac{2\pi}{T_0}$ is the wave pulsation (s^{-1}), $g \approx 9.81\, m.s^{-2}$ is the gravitational acceleration, and k is the wavenumber (m^{-1}). Recalling that $k = \frac{2\pi}{L}$, this equation states that waves with different wavelengths L (m) travel at different speeds C $(m.s^{-1})$. Here, we use it to determine the wavenumber k by using a recursive algorithm such as the Newton-Raphson method.

Phase Velocity

The phase velocity of a wave C $(m.s^{-1})$ is given by:

$$C(x,t) = C_0(t) \tanh(k(x,t)h(x,t)) \qquad \forall (x,t) \in \Omega \times [0,T] \tag{4.2}$$

where C_0 is the velocity of the forcing waves $(m.s^{-1})$, defined here by $C_0(t) = \frac{g}{2\pi} T_0(t)$ for all $t \in [0,T]$.

Group Velocity

The group velocity of a wave C_g $(m.s^{-1})$ is given by:

$$C_g = \frac{1}{2}C\left(1 + \frac{2kh}{\sinh 2kh}\right) \qquad \forall (x,t) \in \Omega \times [0,T] \tag{4.3}$$

Let n be is the ratio of the wave velocity with respect to the group velocity: $n = \frac{C_g}{C}$.

Wave Height

For all $x \in \Omega_S$ and $t \in [0,T]$, we define the shoaling wave height H_S as:

$$H_S(x,t) = H_0(t)K_S(x,t) \tag{4.4}$$

where H_0 is the height of the forcing waves and K_S is the shoaling coefficient (-) defined by Equation (4.5).

$$K_S(x,t) = \left(\frac{1}{2n(x,t)}\frac{C_0(t)}{C(x,t)}\right)^{1/2} \qquad \forall (x,t) \in \Omega_S \times [0,T] \tag{4.5}$$

Breaking Wave Height

The equations governing breaking wave height (over Ω_B) vary according to the choice of hydrodynamic model. However, all use the breaking condition first established by [84], which states that waves break when their height is too great with respect to the water depth. In other words, waves break when inequality (4.6) holds, where γ is a wave-breaking index. This parameter is set to 0.55 in the upcoming simulations (cf. Section 4.5).

$$\frac{H}{h} > \gamma \tag{4.6}$$

Using this wave-breaking condition, we can define Ω_S and Ω_B as:

$$\Omega_S(t) = \left\{x \in \Omega, \frac{H(x,t)}{h(x,t)} < \gamma\right\} \quad \text{and} \quad \Omega_B = \left\{x \in \Omega, \frac{H(x,t)}{h(x,t)} \geq \gamma\right\} \tag{4.7}$$

ℹ The domain over which H is defined as the disjoint union of Ω_S and Ω_B: $[0, x_S] = \Omega_S \cup \Omega_B$ and $\Omega_S \cup \Omega_B = \emptyset$.

4.3.2.3 Presentation of Hydrodynamic Models

Hydrodynamic Model No.1: Shoaling Model with Decreasing Exponential Breaking

Technical Features

Technical features

- **Code name:** shoaling_1run
- **Use:** Regular seabed
- **Advantages:** Very fast; Known wave-breaking type
- **Inconveniences:** One wave-breaking allowed; wave-breaking type must be known
- **Additional entry parameters:** α: wave-breaking parameter
- **Description:** Shoaling until breaking then decreasing exponentially with the alpha parameters describing the descent.
- **Governing equations:**

$$H(x,t) = \begin{cases} H_0(t)K_S(x,t) & \text{for } x \in [0, x_B] \\ H_S(x_B)\dfrac{e^{-\alpha(x-x_B)} - e^{-\alpha(x_S-x_B)}}{1 - e^{-\alpha(x_S-x_B)}} & \text{for } x \in [x_B, x_S] \end{cases}$$

for all $(x,t) \in \Omega \times [0,T]$, where α is user-defined.

⚠ Time dependency of x_B and x_S have been omitted for clarity.

Detailed Description

We assume that waves shoal the length of the cross-shore profile until the breaking condition (4.6) is first activated. This point is denoted x_B. From then on, waves break up until the shoreline x_S, decreasing in height until $H(x_B) = 0$. Breaking wave height is described as a simple decreasing exponential function from x_B to x_S: for all $x \in \Omega_B = [x_B, x_S]$, wave height is given by:

$$H(x,t) = H_S(x_B)\frac{e^{-\alpha(x-x_B)} - e^{-\alpha(x_S-x_B)}}{1 - e^{-\alpha(x_S-x_B)}} \tag{4.8}$$

where the parameter α determines the manner in which the waves break (cf. Figure 4.2).

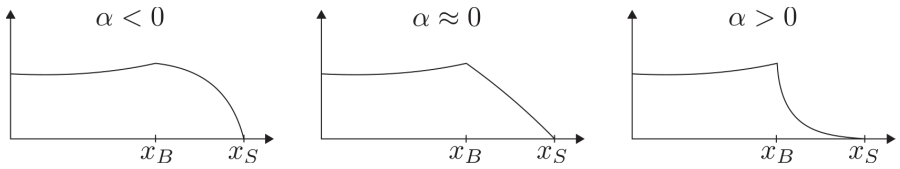

Figure 4.2: Different values of α alter the behavior of the breaking waves.

ℹ This function was designed such that the resulting wave height over the cross-shore profile Ω is a continuous function with zero wave height at the shoreline i.e.$H(x_{\mathrm{B}}) = H_{\mathrm{S}}(x_{\mathrm{B}})$ and $H(x_{\mathrm{S}}) = 0$.

Combined with the shoaling equation (4.4) over $\Omega_{\mathrm{S}} = [0, x_{\mathrm{B}}]$, Hydrodynamic model no.1 provides wave height over the cross-shore profile using the following definition:

$$H(x,t) = \begin{cases} H_{\mathrm{S}}(x,t) & \text{for } x \in [0, x_{\mathrm{B}}] \\ H_{\mathrm{S}}(x_{\mathrm{B}}) \dfrac{e^{-\alpha(x-x_{\mathrm{B}})} - e^{-\alpha(x_{\mathrm{S}}-x_{\mathrm{B}})}}{1 - e^{-\alpha(x_{\mathrm{S}}-x_{\mathrm{B}})}} & \text{for } x \in [x_{\mathrm{B}}, x_{\mathrm{S}}] \end{cases} \tag{4.9}$$

for all $x \in \Omega$ and $t \in [0, T]$.

Note that breaking may occur only once, and therefore Ω_{B} and Ω_{S} are both connected sets.

Illustration

An illustration of the the wave height provided by this model is given in Figure 4.3 on different types of seabeds.

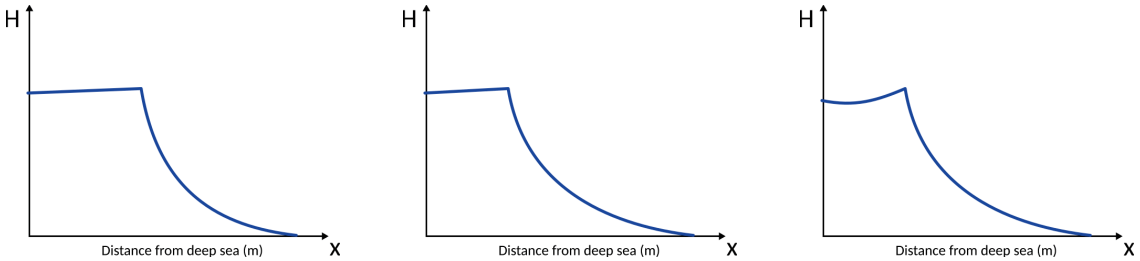

(a) Wave height calculated over a linear seabed

(b) Wave height calculated over a linear seabed with submerged breakwater

(c) Wave height calculated over an experimental seabed (with natural sandbar)

Figure 4.3: Illustration of Hydrodynamic model no.1 on different seabeds

All three examples of wave height look alike: waves shoal in the deeper waters then decrease exponentially to reach zero at the shore.

ℹ This model is recommended on all seabeds, on the condition that the user is content with having waves only breaking once along the cross-shore profile. It is also the faster of the models.

Hydrodynamic Model No.2: Shoaling Model with Decreasing Exponential Breaking and Energy Conservation

Technical Features

Technical features

- **Code name:** shoaling_2run
- **Use:** Regular seabed
- **Advantages:** Very fast; Guarantees conservation of wave energy between sediment displacement (for a same forcing condition)
- **Inconveniences:** One wave-breaking allowed
- **Additional entry parameters:** $\alpha_{t=0}$: initial breaking decrease parameter
- **Description:** Shoaling until breaking then decreasing exponentially with $\alpha(t)$ chosen for energy conservation.
- **Governing equations:**

$$H(x,t) = \begin{cases} H_0(t)K_S(x,t) & \text{for } x \in [0, x_B] \\ H_S(x_B)\dfrac{e^{-\alpha(t)(x-x_B)} - e^{-\alpha(t)(x_S-x_B)}}{1 - e^{-\alpha(t)(x_S-x_B)}} & \text{for } x \in [x_B, x_S] \end{cases}$$

for all $(x,t) \in \Omega \times [0,T]$, where α is determined to ensure conservation of wave energy between sediment displacement.

⚠ Time dependency of x_B and x_S have been omitted for clarity.

Detailed Description

This model is based on the principle of energy conservation. Given two wave height functions H_1 and H_2 originating from the same forcing H_0, we should have **conservation**

of energy, irrespective of the shape of the seabed. Therefore, the energy of the system should be the same before and after applying the morphodynamic model.

To achieve this, we implement the following workflow:

- **Step 1:** Apply Hydrodynamic model with user defined parameters
- **Step 2:** Apply Morphodynamic model
- **Step 3:** Apply Hydrodynamic model with parameters selected to ensure energy conservation

We adopt the previous hydrodynamic model from Section 4.3.2.3, but allow variations of the value of the parameter α to guarantee energy conservation. This implies that waves break differently depending on the forcing wave energy.

Step 1: In Step 1, the wave height over the cross-shore profile is set as:

$$H(x,t) = \begin{cases} H_{\mathrm{S}}(x) & \text{for } x \in [0, x_{\mathrm{B}}] \\ H_{\mathrm{S}}(x_{\mathrm{B}}) \dfrac{e^{-\alpha(x-x_{\mathrm{B}})} - e^{-\alpha(x_{\mathrm{S}}-x_{\mathrm{B}})}}{1 - e^{-\alpha(x_{\mathrm{S}}-x_{\mathrm{B}})}} & \text{for } x \in [x_{\mathrm{B}}, x_{\mathrm{S}}] \end{cases} \tag{4.10}$$

for all $x \in \Omega$ and $t \in [0, T]$. Here, H_{S} is once again given by the shoaling equation (4.4) and α is user-defined as a prediction of the type of breaking waves.

Step 2: The morphodynamic model is then applied which provides the new seabed elevation function ψ in response to the forcing conditions at time t.

Step 3: Here, we consider that waves break as per Equation (4.10), but α is no longer user-defined. We now need to determine the breaking parameter α such that energy is conserved.

Let $H_1, \mathcal{E}_1, x_{S_1}, x_{B_1}, \Omega_{S_1}$ and Ω_{S_1} (resp. $H_2, \mathcal{E}_2, x_{S_2}, x_{B_2}$, Ω_{S_2} and Ω_{S_2}) be the wave height, wave energy, shoreline and breaking point, shoaling zone and breaking zone before (resp. after) the morphodynamic changes.

Conservation of energy implies:

$$\mathcal{E}_1 = \mathcal{E}_2 \Rightarrow \frac{1}{16}\int_{\Omega} \rho_{\mathrm{w}} g H_1^2 = \frac{1}{16}\int_{\Omega} \rho_{\mathrm{w}} g H_2^2 \tag{4.11}$$

$$\Rightarrow \underbrace{\int_{\Omega} H_1^2}_{A} = \underbrace{\int_{\Omega_{S_2}} H_2^2 dx}_{B} + H_2(x_{B_2})^2 \int_{\Omega_{B_2}} \left(\frac{e^{-\alpha(x-x_{B_2})} - e^{-\alpha(x_{S_2}-x_{B_2})}}{1 - e^{-\alpha(x_{S_2}-x_{B_2})}} \right)^2 \mathrm{d}x \tag{4.12}$$

$$\Rightarrow \frac{A - B}{H^2(x_{B_2})} = \int_{\Omega_{B_2}} \left(\frac{e^{-\alpha(x-x_{B_2})} - e^{-\alpha(x_{S_2}-x_{B_2})}}{1 - e^{-\alpha(x_{S_2}-x_{B_2})}} \right)^2 \mathrm{d}x \tag{4.13}$$

⚠ Wave height over $\Omega \setminus (\Omega_S \cup \Omega_B)$ is zero.

The quantities A and B are easily calculated. Using a Newton-Raphson method, we can determine α such that Equation (4.13) holds, and therefore energy is conserved between morphodynamic changes.

To conclude, the Hydrodynamic Model no.2 provides wave height over the cross-shore profile using the following definition: For all $(x,t) \in \Omega \times [0,T]$

$$H(x,t) = \begin{cases} H_S(x) & \text{for } x \in [0, x_B] \\ H_S(x_B)\dfrac{e^{-\alpha(t)(x-x_B)} - e^{-\alpha(t)(x_S-x_B)}}{1 - e^{-\alpha(t)(x_S-x_B)}} & \text{for } x \in [x_B, x_S] \end{cases} \tag{4.14}$$

where $\alpha(t)$ is the time-dependent breaking parameter ensuring conservation of energy at time $t \in [0,T]$.

Illustration

An illustration of the the wave height provided by this model is given in Figure 4.4 on different types of seabeds.

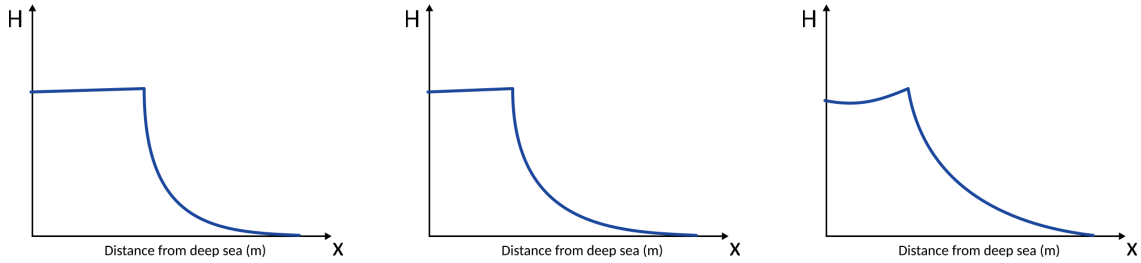

(a) Wave height calculated over a linear seabed

(b) Wave height calculated over a linear seabed with submerged breakwater

(c) Wave height calculated over an experimental seabed (with natural sandbar)

Figure 4.4: Illustration of Hydrodynamic model no.2 on different seabeds

Similar to before, all three examples of wave height look alike: waves shoal in the deeper waters then decrease exponentially to reach zero at the shore. The only difference is the value of α which differs over time.

ℹ This model is recommended on all seabeds, on the condition that the user is content with waves only breaking once across the cross-shore profile.

Hydrodynamic Model No.3: Global Shoaling Model with Munk's Breaking Condition

Technical Features

Technical features

- **Code name:** `shoaling_throughout`
- **Use:** Regular seabed
- **Advantages:** Very fast; Possibility of multiple wave-breakings
- **Inconveniences:** Not suitable for submerged breakwaters
- **Additional entry parameters:** -
- **Description:** Shoaling waves in shoaling zone(s) and waves based on Munk's breaking condition in breaking zones.
- **Governing equations:**

$$H(x,t) = \begin{cases} H_0(t)K_S(x,t) & \text{for } x \in \Omega_S \\ \gamma h(x,t) & \text{for } x \in \Omega_B \end{cases}$$

for all $(x,t) \in \Omega \times [0,T]$.

⚠ Time dependency of Ω_B and Ω_S have been omitted for clarity.

Detailed Description

As with the previous two models, the height of the waves over Ω_S is described by the shoaling equation (4.4). Over Ω_B, we set the height of the wave H as the tipping point condition between breaking and shoaling waves. That is, for all $(x,t) \in \Omega_S \times [0,T]$, breaking waves are defined as:

$$H(x,t) = \gamma h(x,t) \tag{4.15}$$

ℹ The sets Ω_S and Ω_B can now be non-connected, i.e. the shoaling zone (resp. breaking zone) can now be comprised of multiple disjoint sets (cf. Figure 4.5).

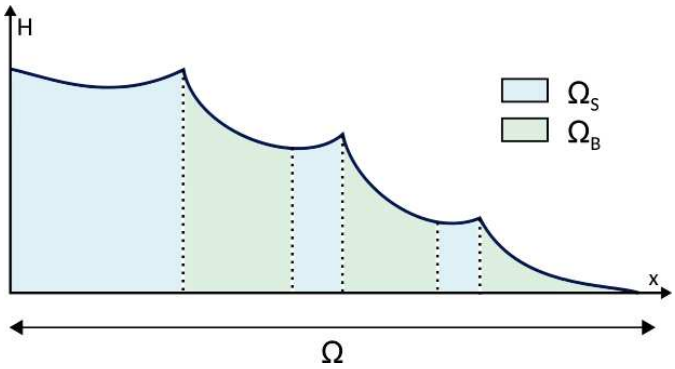

Figure 4.5: Multiple wave-breakings are now possible, which leads to Ω_S and Ω_B being potentially disconnected.

Therefore, Hydrodynamic model no.3 provides wave height over the cross-shore profile using the following definition:

$$H(x,t) = \begin{cases} H_0(t)K_S(x,t) & \text{for } x \in \Omega_S \\ \gamma h(x,t) & \text{for } x \in \Omega_B \end{cases} \tag{4.16}$$

Illustration

An illustration of the the wave height provided by this model is given in Figure 4.6 on different types of seabeds.

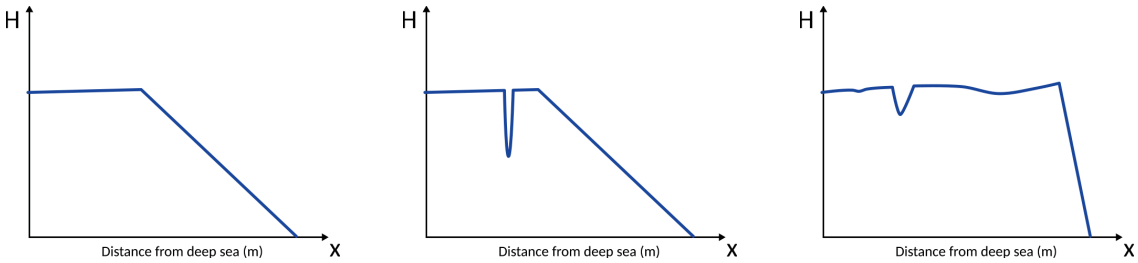

(a) Wave height calculated over a linear seabed

(b) Wave height calculated over a linear seabed with submerged breakwater

(c) Wave height calculated over an experimental seabed (with natural sandbar)

Figure 4.6: Illustration of Hydrodynamic model no.3 on different seabeds

When waves break, wave height closely follows the profile of the seabed, since over Ω_B, $H = \gamma(h_0 - \psi)$, by definition of h. As such, for a linear seabed, the breaking descent is linear (Fig. 4.6a). For the configuration with submerged breakwater, the shape of the structure is outlined (Fig. 4.6b). The structure triggers breaking but wave height quickly resumes it's previous state. This demonstrates that this model is not equipped to

manage underwater structures or any irregular seabed. This is also shown in Figure 4.6c, where the natural sandbar starts the breaking phenomenon, but wave height increases unrealistically once the sandbar has been passed. This model does however have the advantage of allowing multiple breakings. Breaking occurs twice in Figures 4.6b and 4.6c, once at the breakwater/sandbar and once further toward the coast.

ℹ This model is recommended on regular seabeds, but is unable to handle irregular seabed such as those with submerged breakwaters or natural sandbars.

Hydrodynamic Model No.4: Local Shoaling Model with Munk's Breaking Condition

Technical Features

Technical features

- **Code name:** shoaling_incremental
- **Use:** Regular or irregular seabeds
- **Advantages:** Very fast; Possibility of multiple wave-breakings
- **Inconveniences:** Unstable (due to the iterative nature of the model)
- **Additional entry parameters:** -
- **Description:** Local shoaling waves in shoaling zone(s) and waves based on Munk's breaking condition in breaking zones.
- **Governing equations:**

$$H(x,t) = \begin{cases} H(x-\varepsilon)K_S(x,t) & \text{if } x \in \Omega_S \\ \gamma h(x,t) & \text{if } x \in \Omega_B \end{cases}$$

for all $(x,t) \in \Omega \times [0,T]$.

⚠ Time dependency of Ω_B and Ω_S have been omitted for clarity.

Detailed Description

Instead of considering that a wave is spatially dependent on only the initial wave height, this model considers that wave height depends on the seaward activity of the waves. In a

configuration with a local sandbar or wave-breaking structure, waves determined by the previous model (Section 4.3.2.3) shoal up until the structure and then break when the structure is detected. However, once the waves move beyond the wave-breaking device, they resume a wave height similar to that before the structure, i.e. disregarding the encounter of the wave-breaking structure. In other words, the model doesn't register the loss of energy that took place at the submerged wave-breaker. This is due to the fact that the only spacial component influencing the wave height across the cross-shore profile is at $x = 0$ (by way of the term $H_0(t)$). This model amends this.

Instead of using wave height at the entry of the domain at each point x of the cross-shore profile Ω, we now use the previous seaward point of the domain discretization, located at $x - \varepsilon$. Therefore, shoaling waves, which were previously described by (4.4) is now defined by:

$$H(x,t) = H(x-\varepsilon)K_S(x,t) \tag{4.17}$$

for all $x \in \Omega_S$ and $t \in [0,T]$, where $x - \varepsilon$ is the previous point of the discretization.

With the same breaking process as before over Ω_B, i.e. Equation (4.15), wave height is now described by the following equation:

$$H(x,t) = \begin{cases} H(x-\varepsilon)K_S(x,t) & \text{for } x \in \Omega_S \\ \gamma h(x,t) & \text{for } x \in \Omega_B \end{cases} \tag{4.18}$$

for all $(x,t) \in \Omega \times [0,T]$.

⚠ Taking the previous point of the discretization guarantees that submerged breakwaters are taken into account. However, the iterative nature of the model leads to unstable results. Increasing ε would render the model more stable, but results in a poor management of the submerged breakwaters once again.

Illustration

An illustration of the the wave height provided by this model is given in Figure 4.7 on different types of seabeds.

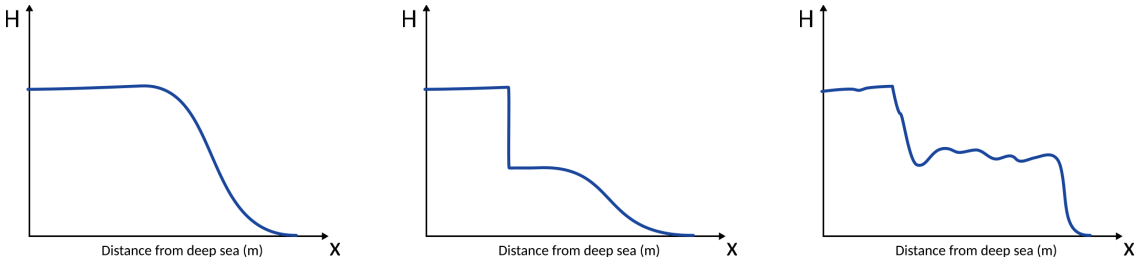

(a) Wave height calculated over a linear seabed

(b) Wave height calculated over a linear seabed with submerged breakwater

(c) Wave height calculated over an experimental seabed (with natural sandbar)

Figure 4.7: Illustration of Hydrodynamic model no.4 on different seabeds

Figure 4.7 shows that this model can handle the introduction of geotubes. The structure causes the waves to break prematurely. Wave height drops and shoaling resumes. This is also true for natural sandbars. Once the waves break, waves can once again shoal, allowing for multiple breakings if necessary.

ℹ This model is not recommended for Opti-Morph because of the unstable effect it has on the seabed.

Hydrodynamic Model No.5: Weighted Window Local Shoaling Model

Technical Features

Technical features

- **Code name:** shoaling_window
- **Use:** Regular or irregular seabeds
- **Advantages:** Fast; Possibility of multiple wave-breakings; Takes into account the effect of the seawards waves; Handles submerged breakwaters
- **Inconveniences:** Poor management of deep sea conditions
- **Additional entry parameters:** d_w: maximal distance of local spatial dependency of a wave
- **Description:** Seaward waves influence wave height with decreasing effect
- **Governing equations:**

$$H(x,t) = \begin{cases} H_0^w(x,t)K_S(x,t) & \text{for } x \in \Omega_S \\ \\ \gamma h(x,t) & \text{for } x \in \Omega_B \end{cases}$$

for all $(x,t) \in \Omega \times [0,T]$, where H_0^w is the weighted average of the seaward waves.

⚠ Time dependency of Ω_B and Ω_S have been omitted for clarity.

Detailed Description

Instead of considering that waves depend solely on offshore wave height H_0 as in 4.3.2.3, or a nearby seaward point as in 4.3.2.3, this model suggests that shoaling waves are decreasingly influenced by seawards waves. The greater the distance, the less effect it has of the present wave height. Let $d_w > 0$ be the maximal distance of local spatial dependency of a wave. Wave height at $x \in \Omega_S$ depends on the behavior of the wave height over the interval $[x - d_w, x)$ with a strong influence at the upper-bound and little to no influence at the lower-bound. As such, we introduce a weighting function w, defined

over $[0, d_w]$ and quantifies the influence of the seawards waves on the current wave. It is defined such that $w(0) = 1$, $w(d_w) = 0$ and decreases exponentially:

$$\begin{aligned} w : \quad [0, d_w] &\longrightarrow \mathbb{R}^+ \\ x &\longmapsto \exp\left(\ln(0.01)\left(\frac{x}{d_{win}}\right)^2\right) \end{aligned} \tag{4.19}$$

Figure 4.8: Weighting function w, equal to 1 closest to the present wave and decreases exponentially as the distance seaward increases

An illustration of the weighting function w is given in Figure 4.8. However, if breaking occurs, the history of the wave prior to breaking should not be relevant. This is to ensure that once the energy of the waves is lost due to breaking, it cannot be regained. The term H_0 in equation (4.4) (or the term $H(\cdot - \varepsilon)$ in (4.17)) is now replaced by a weighted average of the seaward wave height, denoted H_0^w and defined as:

$$H_0^w(x,t) = \frac{1}{\int_{x-X}^{x} w(x-y)\mathrm{d}y} \int_{x-X}^{x} w(x-y)H(y)K(y)\mathrm{d}y \tag{4.20}$$

where $X = \min(x, d_w, \mathrm{dist}(x, x_B))$. Introducing X ensures wave history is taking into account over the appropriate zone: $X = x$ indicates that the zone of local spatial dependency is cut off by the lower-bound of the domain, $X = d_w$ depicts wave dependency over the maximal distance, and $X = \mathrm{dist}(x, x_B)$ indicates that the zone of local spatial dependency is interrupted by waves breaking.

Shoaling waves are therefore described by:

$$H(x,t) = H_0^w(x,t)K_S(x,t) \tag{4.21}$$

for all $x \in \Omega_S$ and $t \in [0, T]$.

As such, wave height over the cross-shore profile Ω is given by:

$$H(x,t) = \begin{cases} H_0^w(x,t)K_S(x,t) & \text{for } x \in \Omega_S \\ \\ \gamma h(x,t) & \text{for } x \in \Omega_B \end{cases} \tag{4.22}$$

Illustration

An illustration of the the wave height provided by this model is given in Figure 4.9 on different types of seabeds.

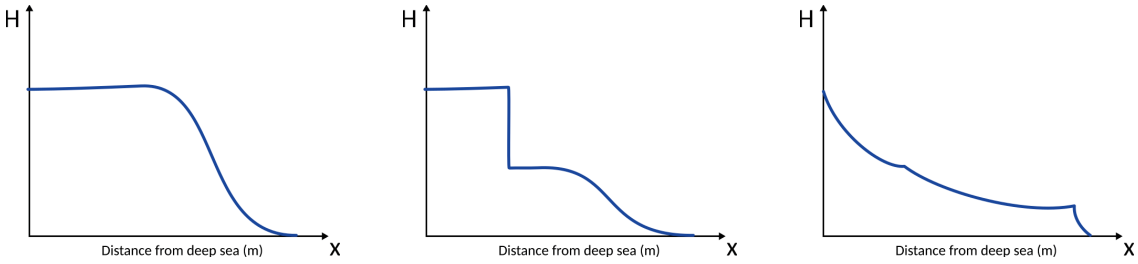

(a) Wave height calculated over a linear seabed

(b) Wave height calculated over a linear seabed with submerged breakwater

(c) Wave height calculated over an experimental seabed (with natural sandbar)

Figure 4.9: Illustration of Hydrodynamic model no.5 on different seabeds

Like before, this model can handle multiple breakings and the introduction of submerged breakwaters. In addition, it produces stable results. However, in some configurations, the poorly managed boundary conditions may cause a drop in wave height at deep-sea border (e.g. Fig. 4.9c). This may happen when $x = 0$ doesn't correspond to deep-sea conditions, a condition which is not always possible when applying the model to a flume configurations.

ℹ This model is recommended on regular seabeds, with and without submerged breakwaters. However, the user must proceed with caution when applying to an experimental setting.

Hydrodynamic Model No.6: Weighted Window Local Shoaling Model and Improved Boundary Conditions

Technical Features

Technical features

- **Code name:** shoaling_window_LC
- **Use:** Regular or irregular seabeds
- **Advantages:** Fast; Possibility of multiple wave-breakings; Takes into account the effect of the seawards waves; Handles submerged breakwaters; Proper handling of deep sea conditions
- **Inconveniences:** May lead to overly dissipative waves
- **Additional entry parameters:** d_{w}: maximal distance of local spatial dependency of a wave
- **Description:** Previous hydrodynamic model with linear combination of 6 equations for smoother boundary conditions
- **Governing equations:**

$$H(x,t) = \begin{cases} \left[(1-\alpha_{\mathrm{w}}(x))H_0(t) + \alpha_{\mathrm{w}}(x)H_0^w(x,t)\right] K_{\mathrm{S}}(x,t) & \text{if } x \in \Omega_{\mathrm{S}},\ x < d_{\mathrm{w}} \\ H_0^w(x,t)K_{\mathrm{S}}(x,t) & \text{if } x \in \Omega_{\mathrm{S}},\ x \geq d_{\mathrm{w}} \\ \gamma h(x,t) & \text{if } x \in \Omega_{\mathrm{B}} \end{cases}$$

for all $(x,t) \in \Omega \times [0,T]$, where H_0^w is the weighted average of the seaward waves and $\alpha_{\mathrm{w}}(x) = \dfrac{x}{d_{\mathrm{w}}}$ over $[0, d_{\mathrm{w}}]$.

⚠ Time dependency of Ω_{B} and Ω_{S} have been omitted for clarity.

Detailed Description

The boundary conditions of the previous model lead to unrealistic wave height over the lowermost part of the domain Ω. The weighting function w is provided with a very small number of points at the beginning of Ω, which may lead to an unreasonable drop in wave

height in deeper waters. To allow a smooth transition between offshore and nearshore-dependent waves, we adopt a linear combination of the initial shoaling equation (4.4) and the weighted shoaling equation (4.21) over the lowermost part of Ω.

Let α_w be the linear combination parameter combining both shoaling physics, defined by:

$$\begin{array}{rccc} \alpha_w : & [0, d_w] & \longrightarrow & [0,1] \\ & x & \longmapsto & \alpha_w(x) = \dfrac{x}{d_w} \end{array} \tag{4.23}$$

Over the deepest portion of Ω_S, more specifically, the interval $[0, d_w]$, shoaling wave height is defined such that the initial shoaling equation (4.4) prevails for x close to 0 and the weighted shoaling equation (4.21) dominates for x close to d_w. A smooth transition between models is achieved via the parameter α_w. The weighted shoaling equation (4.21) is also adopted over the remaining portion of Ω_S, beyond $x = d_w$.

Wave height over the shoaling zone Ω_S is therefore defined for all $x \in \Omega_S$ and $t \in [0, T]$ by:

$$H(x,t) = \begin{cases} \left[(1-\alpha_w(x))H_0(t) + \alpha_w(x)H_0^w(x,t)\right] K_S(x,t) & \text{if } x < d_w \\ H_0^w(x,t)K_S(x,t) & \text{if } x \geq d_w \end{cases} \tag{4.24}$$

Adopting the same wave height equation over Ω_B as before, with Equation (4.15), wave height over the cross-shore domain is defined for all $(x,t) \in \Omega \times [0,T]$ by:

$$H(x,t) = \begin{cases} \left[(1-\alpha_w(x))H_0(t) + \alpha_w(x)H_0^w(x,t)\right] K_S(x,t) & \text{for } x \in \Omega_S \text{ and } x < d_w \\ H_0^w(x,t)K_S(x,t) & \text{for } x \in \Omega_S \text{ and } x \geq d_w \\ \gamma h(x,t) & \text{for } x \in \Omega_B \end{cases} \tag{4.25}$$

Illustration

An illustration of the the wave height provided by this model is given in Figure 4.10 on different types of seabeds.

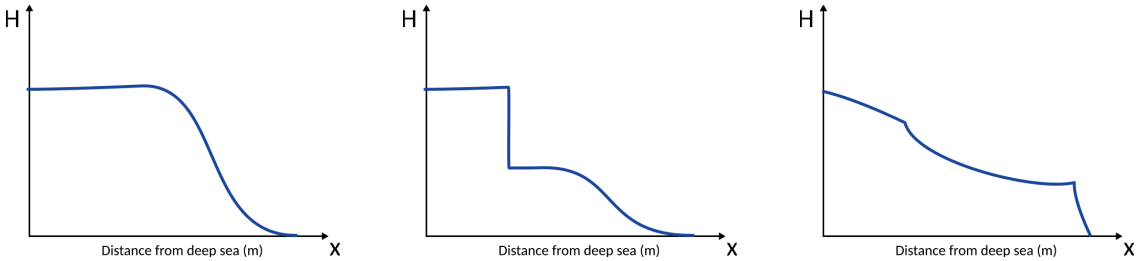

(a) Wave height calculated over a linear seabed

(b) Wave height calculated over a linear seabed with submerged breakwater

(c) Wave height calculated over an experimental seabed (with natural sandbar)

Figure 4.10: Illustration of Hydrodynamic model no.6 on different seabeds

Now that the boundary condition has been properly dealt with, we no longer observe the unusual drop at the beginning of the domain. Acceptable wave height is produced in all three settings.

ℹ This model is recommended on regular seabeds, with and without submerged breakwaters, as well as in experimental settings.

Hydrodynamic Model No.7: Weighted Window Shoaling Model with Anti-dissipative Effect

Technical Features

Technical features

- **Code name:** shoaling_window_LC_ADT
- **Use:** Regular or irregular seabeds
- **Advantages:** Fast; Possibility of multiple wave-breakings; Takes into account the effect of the seawards waves; Handles submerged breakwaters; Proper handling of deep sea conditions; Control of the dissipative effect of the waves;
- **Inconveniences:** TBA
- **Additional entry parameters:** d_{w}: maximal distance of local spatial dependency of a wave; a_{AD} and b_{AD}: anti-dissipative parameters
- **Description:** Previous hydrodynamic model with the possibility of including an anti-dissipative term.
- **Governing equations:**

$$H(x,t) = \chi_{\mathrm{AD}}(x) \begin{cases} \left[(1-\alpha_{\mathrm{w}}(x))H_0(t) + \alpha_{\mathrm{w}}(x)H_0^w(x,t)\right] K_{\mathrm{S}}(x,t) & \text{for } x \in \Omega_{\mathrm{S}},\ x < d_{\mathrm{w}} \\ H_0^w(x,t)K_{\mathrm{S}}(x,t) & \text{for } x \in \Omega_{\mathrm{S}},\ x \geq d_{\mathrm{w}} \\ \gamma h(x,t) & \text{for } x \in \Omega_{\mathrm{B}} \end{cases}$$

for all $(x,t) \in \Omega \times [0,T]$, where H_0^w is the weighted average of the seaward waves, $\alpha_{\mathrm{w}}(x) = \frac{x}{d_{\mathrm{w}}}$ over $[0, d_{\mathrm{w}}]$ and χ_{AD} is an anti-dissipative term.

⚠ Time dependency of Ω_{B} and Ω_{S} have been omitted for clarity.

Detailed Description

Depending on the required wave behavior, it may be necessary to limit the dissipation

of the waves. Indeed, one may discover that the hydrodynamic model of Section 4.3.2.3 dissipates too much energy over the cross-shore profile. This is especially relevant when comparing the numerical wave height with experimental data. For the purposes of allowing the user to calibrate the dissipation of the shoaling waves, we introduce the following anti-dissipative term χ_{AD}:

$$\chi_{\mathrm{AD}}(x) = \begin{cases} \left(1 + a_{\mathrm{AD}} \dfrac{x}{x_{\max}}\right)^{b_{\mathrm{AD}}} - \left(1 + a_{\mathrm{AD}} \dfrac{x_{\Omega_{\mathrm{S}}^-}(x)}{x_{\max}}\right)^{b_{\mathrm{AD}}} + 1 & \text{for } x \in \Omega_{\mathrm{S}} \\ 1 & \text{for } x \in \Omega_{\mathrm{B}} \end{cases} \tag{4.26}$$

where $x_{\Omega_{\mathrm{S}}^-}(x)$ is the lower-bound of the connected subset of Ω_{S} where x is found. The parameters a_{AD} and b_{AD} allow the user to define the manner in which the waves dissipate; a_{AD} determines the slope of χ_{AD} and b_{AD} its quadratic behavior. An example of the anti-dissipative term is given in Figure 4.11, with $b_{\mathrm{AD}} > 1$.

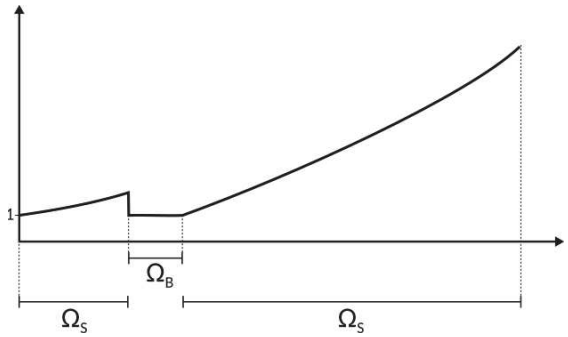

Figure 4.11: Example of the anti-dissipative term

ℹ Setting $(a_{\mathrm{AD}}, b_{\mathrm{AD}}) = (0, 1)$ disables the anti-dissipative effect.

Wave height over the cross-shore profile Ω is defined by:

$$H(x,t) = \chi_{\mathrm{AD}}(x) \begin{cases} \left[(1 - \alpha_{\mathrm{w}}(x))H_0(t) + \alpha_{\mathrm{w}}(x)H_0^w(x,t)\right] K_{\mathrm{S}}(x,t) & \text{for } x \in \Omega_{\mathrm{S}}, x < d_{\mathrm{w}} \\ H_0^w(x,t)K_{\mathrm{S}}(x,t) & \text{for } x \in \Omega_{\mathrm{S}}, x \geq d_{\mathrm{w}} \\ \gamma h(x,t) & \text{for } x \in \Omega_{\mathrm{B}} \end{cases} \tag{4.27}$$

for all $(x,t) \in \Omega \times [0,T]$.

This is the model used in the subsequent applications of Section 4.5.

Illustration

An illustration of the the wave height provided by this model is given in Figure 4.12 on different types of seabeds.

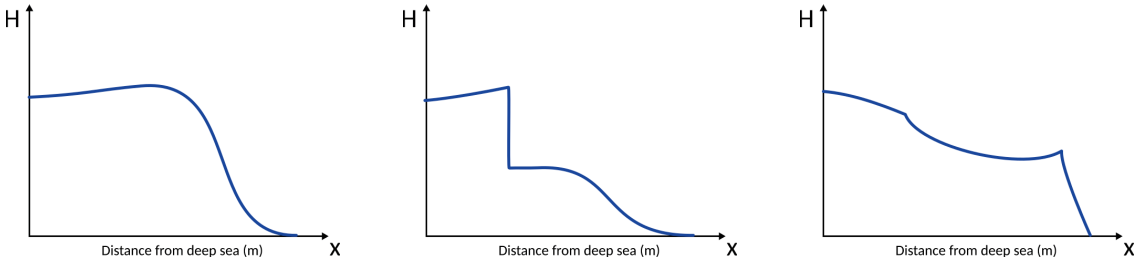

(a) Wave height calculated over a linear seabed

(b) Wave height calculated over a linear seabed with submerged breakwater

(c) Wave height calculated over an experimental seabed (with natural sandbar)

Figure 4.12: Illustration of Hydrodynamic model no.7 on different seabeds

With the proper choice of a_{AD} and b_{AD}, we can now calibrate the hydrodynamic model to fit the required profile. This is especially useful in the case of an experimental flume setting where wave height has been collected as part of the experiment.

ℹ This model is recommended on regular seabeds, with and without submerged breakwaters, as well as in experimental settings.

4.3.3 Morphodynamic Model by Wave Energy Minimization

4.3.3.1 Introduction

This section is devoted to the presentation of the Opti-Morph model. This one-of-a-kind morphodynamic model is based on optimization theory. The fundamental assumption governing Opti-Morph states that the seabed evolves over time so as to minimize a certain quantity, named cost function. The choice of cost function depends on what is considered the driving force behind the morphodynamic response to the seabed. Several cost functions have been considered, but all revolve around wave energy. In other words, the shape of the seabed varies in an effort to minimize the energy of the surface waves at that given time. At each time, the model indicates the direction to a local minimum of the cost function with regard to the parameterization of the seabed. Two physical parameters limit or encourage seabed mobility depending on the proprieties of the sediment and the depth of the water. Furthermore, constraints are added to this optimization problem as a means to incorporate additional physics to the model. Constraints are regarded as secondary processes in regards to the minimization of the cost function, which is deemed the primary force behind the morphodynamic response to the seabed. Three constraints

have been included in this model. The first concerns the maximal slope of the seabed, the second manages the sandstock of the profile in the case of an experimental flume, and the third concerns the presence of bedrock.

The optimization problem that Opti-Morph seeks to solve is:

For each $t \in [0, T]$*, find the shape of the seabed* $\psi(t) \in \Psi$ *such that the cost function* $\mathcal{J}(t)$ *is minimal, while subjected to constraints.*

This morphodynamic model is associated with one of the hydrodynamic models from Section 4.3.2, which provides the morphodynamic model with the necessary hydrodynamic quantities.

4.3.3.2 Governing Seabed Dynamics

In order to describe the evolution of the seabed, we assume that at each time $t \in [0, T]$, the seabed ψ, in its effort to minimize a certain energy related quantity $\mathcal{J}$, verifies the following dynamics over Ω:

$$\begin{cases} \psi_t(\cdot, t) = \Upsilon \Lambda d(\cdot, t) \\ \psi(\cdot, 0) = \psi_0(\cdot) \end{cases} \tag{4.28}$$

where ψ_t is the evolution of the seabed over time, Υ is the mobility of the sand $(m.s.kg^{-1})$, Λ is the excitation of the seabed by the water waves $(-)$, and d is the direction of descent (J).

Parameter Υ

The first parameter Υ takes into account the physical characteristics of the sand and represents the mobility of the sediment. For Υ great, as is the case with finer particles, the seabed may be submitted to significant change. For Υ close to zero, little mobility is observed, as is the case of a seabed composed of larger rocks. This parameter, expressed in $m.s.kg^{-1}$, may vary over the cross-shore profile. Further interpretation of the nature of this parameter will be provided in future works.

Parameter Λ

The second parameter Λ represents the influence of the water depth on the seabed and is defined using the orbital velocity damping function φ (cf. [113]):

$$\begin{array}{rccl} \varphi: & \Omega \times [0, h_0] & \longrightarrow & \mathbb{R}^+ \\ & (x, z) & \longmapsto & \dfrac{\cosh(k(x)(h(x) - (h_0 - z)))}{\cosh(k(x)h(x))} \end{array} \tag{4.29}$$

An illustration of the orbital velocity of the wave particles is given in Figure 4.13. This function describes the excitation of the water particles for a given location along the cross-shore profile and a given water depth. However, our interest lies in the excitation of

the seabed by the surface waves. Therefore, it is natural to consider the orbital damping function at $z = \psi(x)$. The parameter Λ of Equation (4.28) is therefore defined by:

$$\Lambda(x) = \varphi(x, \psi(x)) = \frac{1}{\cosh(k(x)h(x))} \tag{4.30}$$

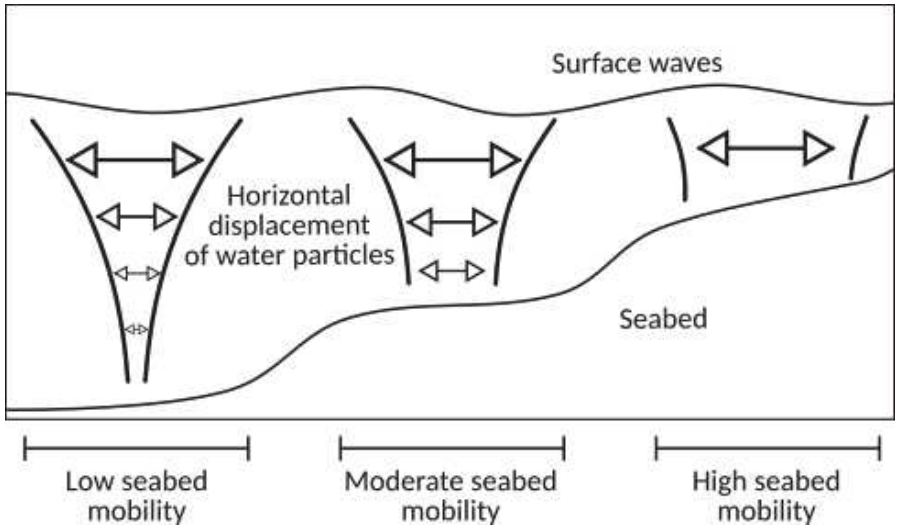

Figure 4.13: Illustration of the orbital velocity over the cross-shore profile

This parameter governs the manner in which the waves affect the seabed. In deeper waves, the surface waves have little to no effect on the seabed below. No movement should be observed of the seabed, and thus $\Lambda \simeq 0$ over this portion of the cross-shore profile. When the waves have a large impact on the seabed, e.g. at the coast, greater movement can be observed and as such we set $\Lambda \simeq 1$. An illustration of Λ is given in Figure 4.14.

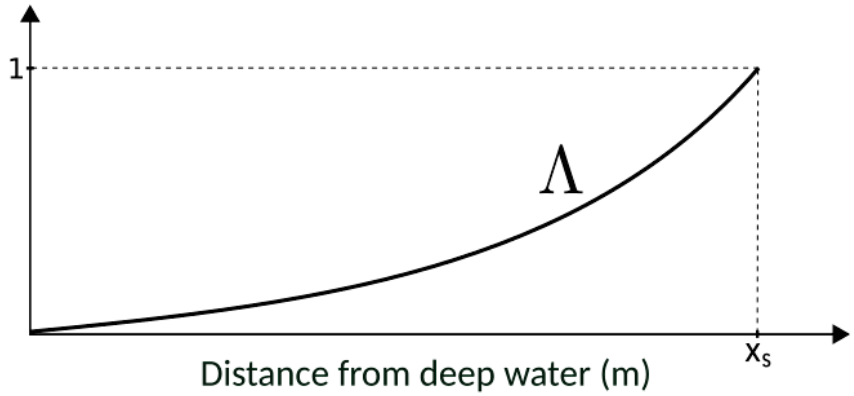

Figure 4.14: Variation of the parameter Λ over the cross-shore profile

Direction of Descent d:

The vector d is the direction of descent. In unconstrained circumstances, we set $d = -\nabla_\psi \mathcal{J}$, i.e. the direction indicating the minimum of the cost function $\mathcal{J}$ with regards to the seabed ψ. However, adding constraints changes the value of d, but increases the efficiency of the model, by incorporating more physics into the model. This results in a less optimal direction of descent but one that is capable of respecting the criteria required by the constraints, and as such produces more realistic morphodynamic results.

The following section explores the different cost functions / directions of descent implemented in Opti-Morph.

4.3.3.3 Choice of Direction of Descent

The term "cost function" is used for the quantity to be minimized and is noted $\mathcal{J}$. The term "direction of descent" is used for direction indicating the manner in which the seabed varies, and is denoted d. In the more simpler cases, $d = -\nabla_\psi \mathcal{J}$, but exploring other directions of descents leads to more complex formulations. It is not always possible to express the cost function $\mathcal{J}$ when exploring directions.

For the purpose of illustrating the simplicity of implementing a new cost function, seven different directions of descent have been considered. Modifying d modifies the physics behind the morphodynamic response of the seabed. These choices are shown in Table 4.2 and are all based on the energy of shoaling waves given by the following equation:

$$\mathcal{E}_S = \frac{1}{16}\int_{\Omega_S} \rho_w g H^2(\psi, x, t)\mathrm{d}x \tag{4.31}$$

where Ω_S is the shoaling zone, ρ_w is the density of the water ($kg.m^{-3}$), g is gravitational acceleration ($m.s^{-2}$), H is the height of the wave (m) and ψ is the elevation of seabed (m). We denote χ_{Ω_S} the characteristic function of the subset Ω_S of Ω.

The introduction of directions `CF1`, `CF2`, and `CF3` occurred while exploring the different possible dimensions of the cost function $\mathcal{J}$. Ultimately, it was decided to maintain a cost function expressed in $J.m^{-1}$, so `CF0` was retained. Directions `CF4`, `CF5`, and `CF6` were proposed in an attempt to combine two different physics depending on the location along the cross-shore profile. A simple well-chosen factor may be needed to ensure that d has a consistent dimension. All of the considered directions have been kept in order to demonstrate how easy it is to introduce a new cost function to the model but should be adopted with caution.

The first and simplest choice is `CF0` and is the one used in the subsequent applications of Section 4.5. The directions `CF5` and `CF6` are more complex and combines two physics to simulate the seabed evolution. More details can be found for these choices in sections 4.3.3.3 and 4.3.3.3.

Keyword	Definition	Commentary
`CF0`	$d = -\nabla_\psi \mathcal{E}_S \chi_{\Omega_S}$	Recommended
`CF1`	$d = -\frac{x_B}{x_S} \nabla_\psi \mathcal{E}_S \chi_{\Omega_S}$	
`CF2`	$d = -\frac{x_B^2}{x_S} \nabla_\psi \mathcal{E}_S \chi_{\Omega_S}$	
`CF3`	$d = -x_B \nabla_\psi \mathcal{E}_S \chi_{\Omega_S}$	
`CF4`	$d = -\frac{x_B}{x_S} \int_{\Omega_S} \nabla_\psi \mathcal{E}_S \chi_{\Omega_S}$	
`CF5`	$d = (1-\Lambda)$`CF2`$+\Lambda$`CF4`	where Λ is the excitation of the seabed
`CF6`	$d = (1-\Lambda)$`CF3`$+\Lambda$`CF4`	where Λ is the excitation of the seabed

Table 4.2: Table of the different directions of descent implemented in Opti-Morph

Cost Function based on $\mathcal{E}_S$

The evolution of the seabed is assumed to be driven by the minimization of a cost function $\mathcal{J}$, here described as the potential energy of shoaling waves:

$$\mathcal{J}(\psi, t) = \frac{1}{16} \int_{\Omega_S} \rho_w g H^2(\psi, x, t) \mathrm{d}x \tag{4.32}$$

Differentiating $\mathcal{J}$ with respect to ψ yields the direction of descent `CF0`. This direction was used in [21] and is currently the recommended choice of direction.

Cost Function combining two Physics

In this section, we suppose that two different physics govern the evolution of seabed based whether the waves act globally or locally on the seabed. Both physics are based on the potential energy of the waves over the cross-shore profile, given by Equation (4.31). However, unlike in Section 4.3.3.3, an explicit formulation of $\mathcal{J}$ is not possible.

As mentioned in Section 4.3.3.2 with the introduction of the Λ parameter, the seabed evolves differently in deep waters and at the coast. Therefore, we define two different

physics governing the seabed evolution depending on location across the cross-shore profile. We denote A_1 the gradient of the potential surface energy of the waves and A_2 the gradient of the mean value of A_1.

$$A_1(x,t) = -\nabla_\psi \mathcal{E}(x,t) \quad \forall (x,t) \in \Omega \times [0,T] \tag{4.33}$$

$$A_2(x,t) = -\frac{1}{x_B(t)} \int_{\Omega_S} \nabla_\psi \mathcal{E}(x,t) \mathrm{d}x \quad \forall (x,t) \in \Omega \times [0,T] \tag{4.34}$$

The mean value A_2 was chosen to represent the physics governing the seabed over the deeper waters since the seabed is affected in a global manner in this zone. The gradient of the potential surface energy A_1 will be used at the coast, where the waves have a local effect on the seabed. In order to differentiate the different zones of the cross-shore profile, the parameter Λ is used (cf. Equation (4.30)). We set the direction of descent as:

$$d = \Lambda A_1 + (1 - \Lambda) A_2 \tag{4.35}$$

The term A_1 is dominant near the coast (for a local effect) and the term A_2 is dominant in deep waters (for a global effect). The parameter Λ is used to weight these two physics.

ℹ Up to the multiplication of a constant, this approach is used for the directions `CF5` and `CF6`.

4.3.3.4 Constraints

As mentioned already, the driving force behind the morphodynamic response to the seabed is assumed to be the minimization of the energy of the shoaling waves. Any physical phenomenon deemed secondary to this mechanism is represented in the form of a constraint. Constraints are added to incorporate more physics into the model, and as such provide more realistic results. At the current stage of development, three constraints have been implemented, though more can be introduced if necessary. This includes a maximal slope constraint to prevent unrealistically steep seabeds, a sandstock constraint for flume configurations, and a bedrock constraint.

Maximal Sand Slope Constraint

The slope of the seabed is bounded by a grain-dependent threshold M_{slope} ([28]). If a slope becomes too steep and exceeds this threshold, avalanching occurs. The maximal sand slope constraint prevents the slope from exceeding this upper limitation and is conveyed by the following inequality:

$$\left| \frac{\partial \psi}{\partial x} \right| \leq M_{\text{slope}} \tag{4.36}$$

ℹ The parameter M_{slope} may vary over the cross-shore profile.

Sandstock Constraint

In the case of an experimental flume, the sediment composing the seabed cannot leave the confines of the tank over the course of the simulation. Also, sediment cannot be added during this period. Therefore, a sandstock constraint is introduced which asserts that the quantity of sand in a flume must be constant over time, contrarily to an open-sea simulation where the sediment can move freely between the limits of the domain. The sandstock constraint is therefore expressed by the following equation:

$$\int_\Omega \psi(x,t)\mathrm{d}x = \int_\Omega \psi(t=0,x)\mathrm{d}x \qquad \forall t \in [0,T] \tag{4.37}$$

ℹ This constraint is essential for validating the numerical model with experimental data.

ℹ The sandstock constraint is also applicable to an open-sea configuration when little to no transfer of sediment is observed between the deep sea and the nearshore area.

For a given time $t \in [0,T]$, we define $C_{\text{sand}}(t)$ as the difference between the current and initial sandstock:

$$C_{\text{sand}}(t) = \int_\Omega \left(\psi(x,t) - \psi(t=0,x)\right)^2 \mathrm{d}x \tag{4.38}$$

ℹ The exponent 2 ensures that $C_{\text{sand}} \geq 0$, while keeping C_{sand} differentiable.

The optimization problem becomes:
For each $t \in [0,T]$, find the shape of the seabed $\psi(t) \in \Psi$ such that the cost function $\mathcal{J}(t)$ is minimal, while maintaining $C_{\text{sand}}(t) = 0$.

Two methods can be adopted to ensure that the sandstock remains constant over time, the *penalization method* and/or the *feasible direction method*.

Penalization Method

This method consists of adding a penalty term to the cost function $\mathcal{J}$. So, instead of minimizing $\mathcal{J}$, we minimize both $\mathcal{J}$ and C_{sand} simultaneously. The new cost function $\mathcal{J}_{\text{pen}}$ is given by:

$$\mathcal{J}_{\text{pen}} = \mathcal{J} - \beta C_{\text{sand}} \tag{4.39}$$

where $\beta > 0$ is the sandstock constraint precision parameter and determines the importance of the conservation of the sand constraint. For β small, the constraint is largely ignored and the minimization of the $\mathcal{J}$ governs the evolution of the seabed. For β great, the sandstock constraint dominates the minimization method.

⚠ A simple well-chosen factor may be used to express $\mathcal{J}_{\text{pen}}$ as the same dimension as $\mathcal{J}$.

Feasible Directions

Another possible approach to incorporate the sand constraint into the morphodynamic model is to use the *feasible direction method*.

Since $C_{\text{sand}}(0) = 0$, we wish to minimize $\mathcal{J}$ while keeping C_{sand} constant. This equates to following the direction $\nabla_\psi \mathcal{J}$ while keeping $\nabla_\psi C_{\text{sand}} = 0$. In order to do so, we project the direction $\nabla_\psi \mathcal{J}$ onto the orthogonal of $\nabla_\psi C_{\text{sand}}$. Hence, the direction of descent d becomes:

$$d = \nabla_\psi \mathcal{J} - \left\langle \nabla_\psi \mathcal{J}, \frac{\nabla_\psi C_{\text{sand}}}{\|\nabla_\psi C_{\text{sand}}\|} \right\rangle \frac{\nabla_\psi C_{\text{sand}}}{\|\nabla_\psi C_{\text{sand}}\|} \tag{4.40}$$

This new direction of descent, illustrated by Figure 4.15, describes a less optimal path to the minimum of $\mathcal{J}$, but ensures that $\nabla_\psi C_{\text{sand}}(t) = 0$, i.e. $C_{\text{sand}}(t) = 0$, for all $t \in [0, T]$.

We can easily show that the new direction d and $\nabla_\psi C_{\text{sand}}$ are now orthogonal:

$$\left\langle d, \nabla_\psi C_{\text{sand}} \right\rangle = \left\langle \nabla_\psi \mathcal{J} - \left\langle \nabla_\psi \mathcal{J}, \frac{\nabla_\psi C_{\text{sand}}}{\|\nabla_\psi C_{\text{sand}}\|} \right\rangle \frac{\nabla_\psi C_{\text{sand}}}{\|\nabla_\psi C_{\text{sand}}\|}, \nabla_\psi C_{\text{sand}} \right\rangle = 0$$

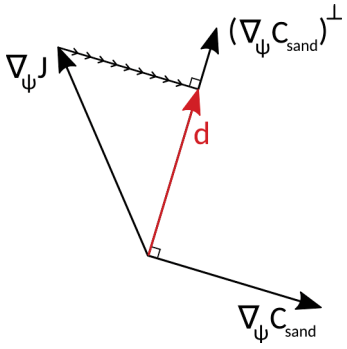

Figure 4.15: Illustration of the new direction of descent in $\mathbb{R}^2$: the direction $\nabla_\psi \mathcal{J}$ is projected onto the orthogonal of $\nabla_\psi C_{\text{sand}}$ to yield d.

ℹ The feasible direction method can also be used to guarantee that the total energy of the waves in conserved for a same forcing condition with regards to the evolution of the seabed, i.e. $\mathcal{E}(\psi_1, t) = \mathcal{E}(\psi_2, t)$ for all $\psi_1, \psi_2 \in \Psi$ and $t \in [0, T]$. All one needs to do is project $\nabla_\psi \mathcal{J}$ onto the common orthogonal vector of $\nabla_\psi C_{\text{sand}}$ and $\nabla_\psi \mathcal{E}$.

Bedrock Constraint

The third constraint concerns the existence of bedrock in the beach configuration. We assume bedrock to be a solid invariable feature to the cross-shore profile, with a layer of sediment covering it.

Let B be the elevation of the bedrock over Ω as in Figure 4.1. By definition, B remains constant over time and the seabed ψ cannot appear lower than the bedrock:

$$\psi(x,t) \geq B(x) \qquad \forall x \in \Omega, t \in [0,T] \tag{4.41}$$

In other words, the bedrock acts as a lower bound of the seabed elevation. Equality of Equation (4.41), for a given $x \in \Omega$, implies exposure of the bedrock.

4.4 Numerical Model

4.4.1 Presentation

In this section, we present the numerical model Opti-Morph and how to use it.

4.4.1.1 Workflow

Figure 4.16 illustrates the workflow of the Opti-Morph model, with the associated hydrodynamic model. Before launching the model, the user must first define the initial setting of the simulation. This includes the forcing data, the choice of hydrodynamic model, the seabed elevation data, the choice of cost function, and the constraints.

For each time step, the forcing data is provided to the hydrodynamic model. This model then calculates the wave height over the cross-shore profile and thus provides the cost function $\mathcal{J}$ (or direction of decent d) used by Opti-Morph's morphodynamic module. Using the imported sand characteristics, the new shape of the seabed is determined by minimizing the cost function $\mathcal{J}$ (or following the direction of descent d). Constraints are applied to the seabed either before or after the minimization takes place, and the new seabed is retained. At the next time step, the hydrodynamic model is fed a new forcing condition as well as the new seabed. This cycle continues over the course of the simulation, and illustrates the intricate interaction between the hydrodynamic and morphodynamic processes.

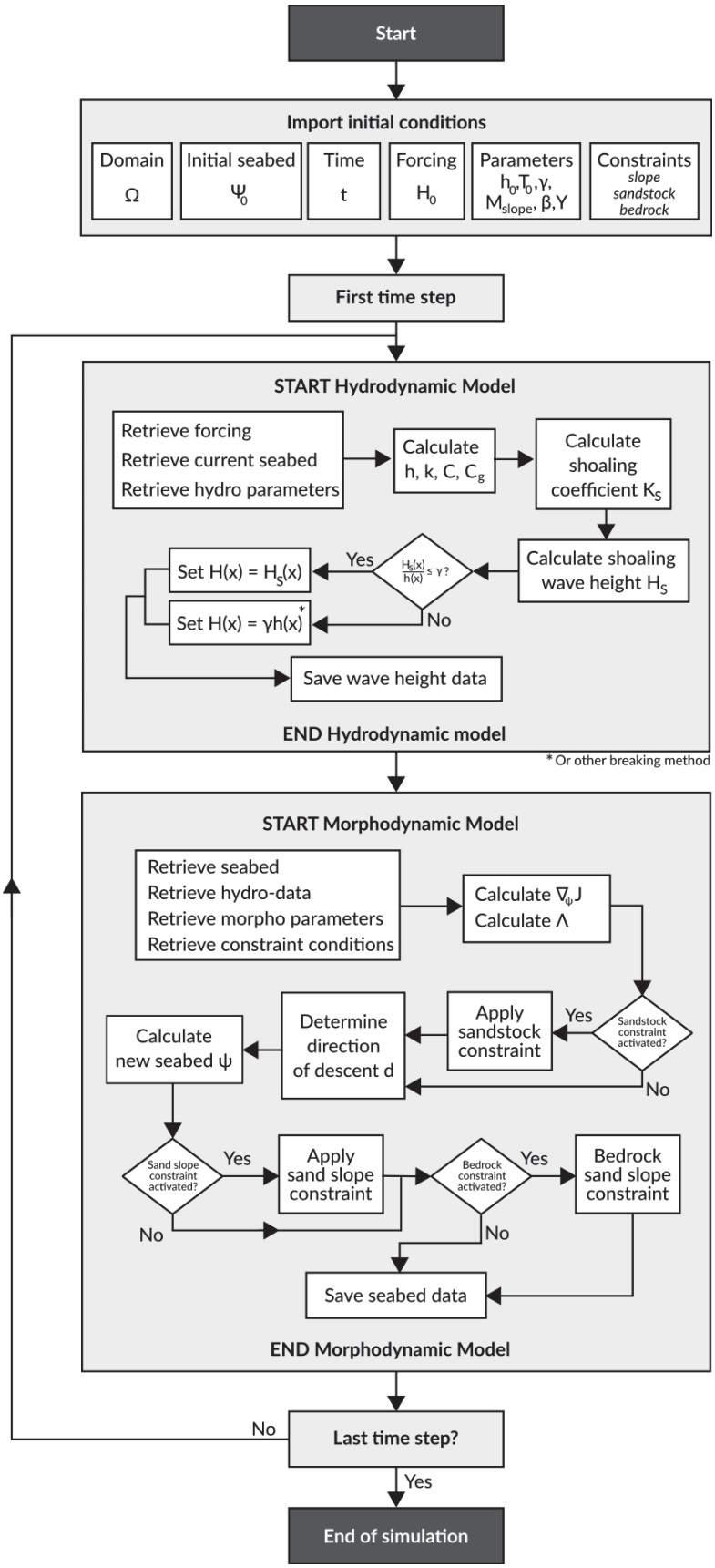

Figure 4.16: Diagram of the workflow of the Opti-Morph model

4.4.1.2 Algorithm Summary

A detailed summary of the algorithm performed by Opti-Morph is provided below.

For each time step t_n, for $n \in [1, N_T]$, the following steps are applied:

➔ **Apply Hydrodynamic model**

Step 1: Import forcing data $H_0(t_n)$

Step 2: Import current morphodynamic data ψ_{n-1}

Step 3: Calculate wave height H_n

Step 4: Save H_n

➔ **Apply Morphodynamic model**

Step 1: Import current wave height H_n

Step 2: Import Υ and Λ parameters

Step 3: Calculate cost function $\mathcal{J}_n$

Step 4: Calculate $\nabla_\psi \mathcal{J}_n$

Step 5: Obtain the direction of descent d_n

Step 6: Apply local a priori constraints (if necessary)

Step 7: Apply global a priori constraints (if necessary)

Step 8: Determine new seabed: $\psi_n = \psi_{n-1} + \Upsilon\Lambda d_n$

Step 9: Apply local a posteriori constraints (if necessary)

Step 10: Apply global a posteriori constraints (if necessary)

Step 11: Save ψ_n

ℹ The sandstock constraint is considered a global a priori constraint whereas the sand slope and the bedrock constraints are considered local a posteriori constraint.

4.4.1.3 Class Organisation

The numerical model Opti-Morph has been implemented using an oriented object structure. Figure 4.17 illustrates the structure of the model using a UML diagram. Structuring

the model using classes was chosen in order to allow flexibility and creativity within the model. Each object can be regarded as a building block which can easily be modified or replaced depending on the user's intentions. For instance, a different hydrodynamic model can be implemented and adapted to the Opti-Morph model with ease. The same applies for the choice of cost function; to introduce a different cost function $\mathcal{J}$, the user simply has to implement the new function as well as its gradient and leave the rest of the Opti-Morph model unchanged.

An abstract class `Model` is used to define the general characteristics of a model. We have two different types of model: a hydrodynamic model and a morphodynamic model. The abstract class model is used because both models share a common structure and methods. For instance, in this model we find the accessors relative to the parameters and variables of the model in question. A model contains both a set of parameters and a set of variables. The parameters are considered constant over the entirety of the simulation and determine the characteristics of the model. As its name suggests, variables vary over the execution of the simulation. For instance, the wave-breaking index γ is considered a parameter of hydrodynamic model whereas wave height H is considered a variable. The accessors relative to this data are respectively `getP`, `setP` and `getV`, `setV`.

The `Domain` class defines the mesh of the domain as well as certain physical characteristics of the configurations such as the mean water level h_0.

The hydro-morphodynamic class `Hydro_morpho_model` is the central component of the Opti-Morph model. This class links the hydrodynamic class `Hydro_model` with the morphodynamic class `Morpho_model`. It is also here where the run method is located. Because of the close relation between the hydrodynamic model `Hydro_model` and the morphodynamic model `Morpho_model`, both classes are associated with each other. Therefore, a hydrodynamic object can be found in the morphodynamic model and vice versa.

The hydrodynamic class `Hydro_model` which inherits from the model class `Model` is used to determine the wave height over the cross-shore profile. To do so, we use the morphodynamic data (such as the seabed) as well as forcing data. The forcing data is stored in a separate class named `Forcing`. Applying the `run` method calculates the wave height and saves the result in a table under the keyword `H`. Each of the hydrodynamic models presented in Section 4.3.2 are sub-classes of `Hydro_model`. A summary of the different keywords is features in table 4.3. Additional tools used by the `Hydro_model` class can be found in the imported file `hydrotools.py`.

The morphodynamic class `Morpho_model` which also inherits from the model class `Model` is used to determine the evolution of the seabed using optimization methods. Applying the `run` method calculates the seabed elevation at that given time step, using the data calculated by the hydrodynamic model `Hydro_model`. The physics is determined by the choice of cost function, whose keywords are summarized in Table 4.2. The constraints associated to this optimization problem are stored in a separate class named

No.	Description	Keyword
1	Shoaling model with decreasing exponential breaking	`shoaling_1run`
2	Shoaling model with decreasing exponential breaking and energy conservation	`shoaling_2run`
3	Global shoaling model with Munk's breaking condition	`shoaling_throughout`
4	Local shoaling model with Munk's breaking condition	`shoaling_incremental`
5	Weighted window local shoaling model	`shoaling_window`
6	Weighted window local shoaling model and improved boundary conditions	`shoaling_window_LC`
7	Weighted window shoaling model with anti-dissipative effect	`shoaling_window_LC_ADT`

Table 4.3: Table of the different hydrodynamic models and their keywords

`Constraints`. The results of the morphodynamic simulation are saved in a table with the seabed stored under the keyword `psi`. Additional tools and methods relative to the morphodynamic model can be found in the imported file `morphotools.py`.

A final class named `plot_data` is called by the `Hydro_morpho_model` class and provides the visual representations of the results. Several methods have been implemented for different graphs depending on the users needs. Numerical data can also be exported if the user wishes to plot the data manually using external tools.

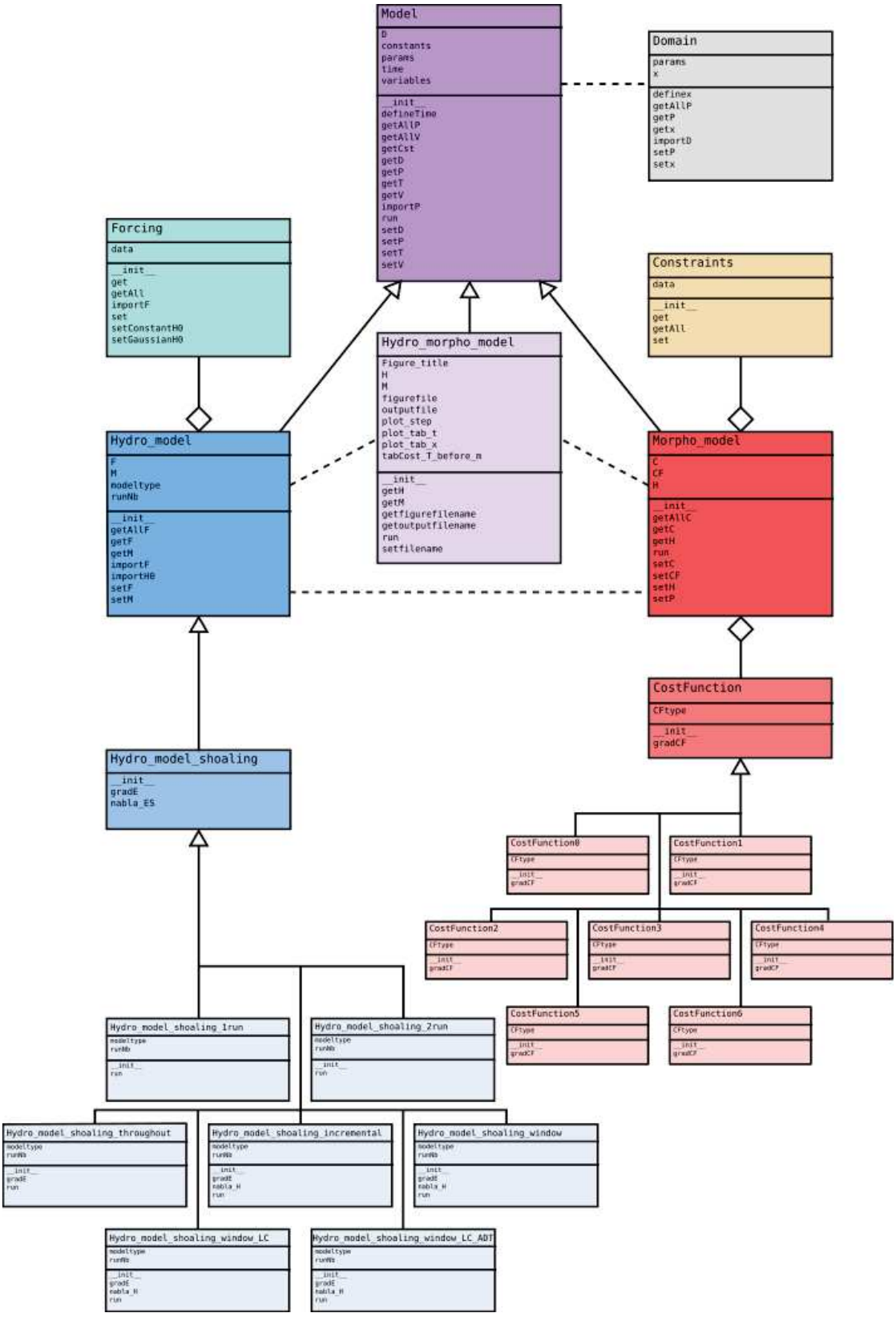

Figure 4.17: UML diagram of the Opti-Morph model

4.4.2 Running Opti-Morph

4.4.2.1 Getting Started

This model was developed in Python 3.5.2. Therefore, in order to execute the Opti-Morph model, the user will need a version of Python compatible with Python 3.5.2 to be installed on their workstation as well as the following packages: `math`, `numpy`, `scipy`, `abc`, `matplotlib`, `netCDF4`.

The files should be organised as follows:

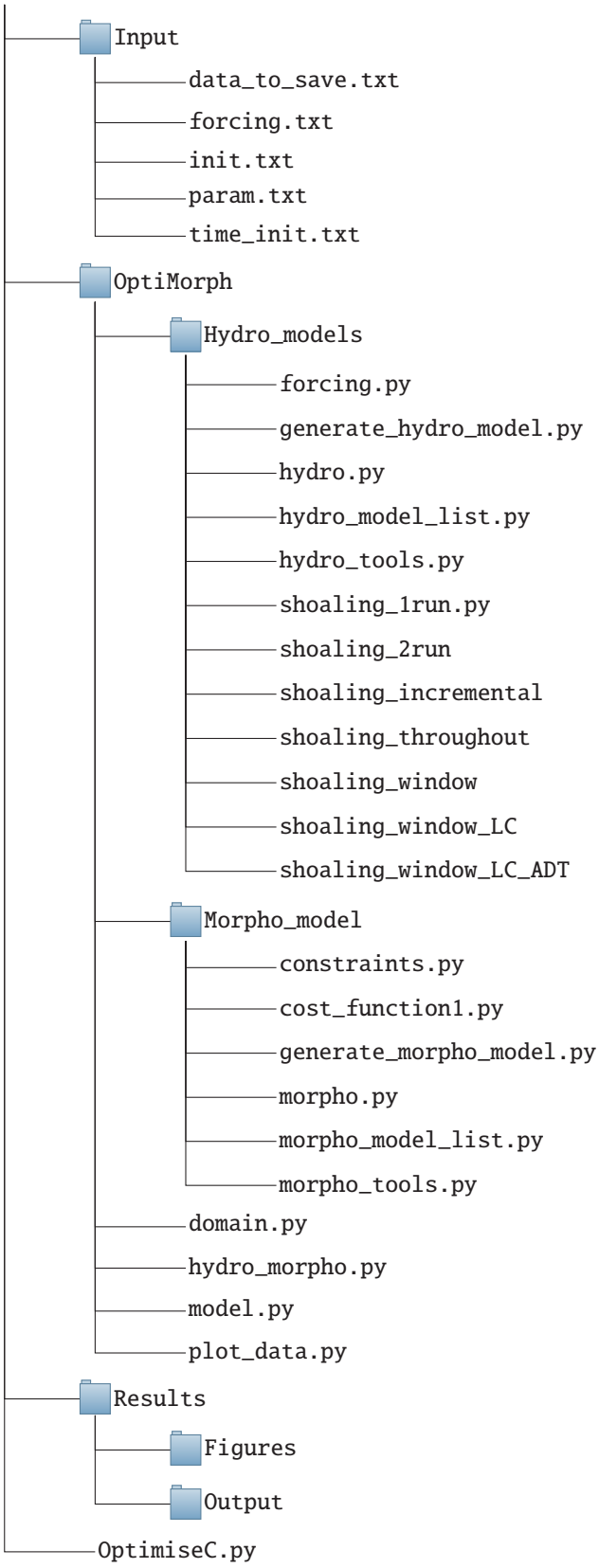
Input
data_to_save.txt
forcing.txt
init.txt
param.txt
time_init.txt
OptiMorph
Hydro_models
forcing.py
generate_hydro_model.py
hydro.py
hydro_model_list.py
hydro_tools.py
shoaling_1run.py
shoaling_2run
shoaling_incremental
shoaling_throughout
shoaling_window
shoaling_window_LC
shoaling_window_LC_ADT
Morpho_model
constraints.py
cost_function1.py
generate_morpho_model.py
morpho.py
morpho_model_list.py
morpho_tools.py
domain.py
hydro_morpho.py
model.py
plot_data.py
Results
Figures
Output
OptimiseC.py

4.4.2.2 Main File

The main file of Opti-Morph that should be run either from the terminal or the chosen development environment is named `OptimiseC.py`.

The `OptimiseC.py` file is organised as followed:

- Import packages
- Import data from `Input` folder
- Figure preparation
- Definition of domain
- Definition of Hydrodynamic model
- Definition of Morphodynamic model
- Definition of Hydro-Morphodynamic model
- Definition of Output
- Run model

Below is an example of `OptimiseC.py` is provided below. The sections highlighted in yellow are modifiable by the user. In particular, the choice of hydrodynamic model (line 52) and cost function (line 67). This will no longer be the case once a graphical user interface (GUI) is built.

```
1  from OptiMorpho.domain import *
2  from OptiMorpho.model import *
3  from OptiMorpho.Hydro_models.hydro import *
4  from OptiMorpho.Morpho_model.morpho import *
5  from OptiMorpho.hydro_morpho import *
6  from OptiMorpho.enum_lists import *
7  from OptiMorpho.enum_generators import *
8
9  from math import pi
10
11 # Import data
12 params = genfromtxt('Input/param.txt')
13 h0 = params[0]
14 T0 = params[1]
15 gamma = params[2]
16 beta = params[3]
17 sandflag = params[4]
18 smoothflag = params[5]
19
20 init = genfromtxt('Input/init.txt')
21 x = init[:,0]
22 psi0 = init[:,1]
23 bedrock = init[:,2]
```

```
mobility = init[:,3]
slopemax = init[:,4]

init_time = genfromtxt("Input/time_init.txt")
time = init_time[:,0]
H0 = init_time[:,1]

dts = genfromtxt('Input/data_to_save.txt', dtype = None)
dtpcpt = int(dts[0])
outargs_x = []
outargs_t = []
inX = True
if int(dts[1]) == 1:
 outargs_x.append('default')
for i in range(2,len(dts)):
 if (dts[i].decode('utf-8') == "END"):
  inX = False
 if inX == True:
  outargs_x.append(dts[i].decode('utf-8'))
 elif (dts[i].decode('utf-8') != 'END'):
  outargs_t.append(dts[i].decode('utf-8'))

# Domain
D1 = Domain()
D1.setx(x)
D1.setP("h0",h0)

# Hydrodynamic model
H1 = generate_hydro_model(Enum_H.shoaling_window_LC_ADT)
H1.setF("T0", T0)
H1.setF("C0", 9.81/(2*pi)*T0 )
H1.setF("sigma0", 2*pi/T0)
H1.setF("theta0", 0)
H1.setP("gamma", gamma)
H1.setP("dwin", 5)
H1.setP("Nwin", floor(dwin/xstep))
H1.setP("aAD", 1)
H1.setP("bAD", 1.2)
H1.setT(time)
H1.setF("H0", H0)

# Morphodynamic model
M1 = Morpho_model()
```

```
67 M1.setCF(Enum_CF.CF0)
68 M1.setC("sand", sandflag)
69 M1.setC("Mslope", slopemax)
70 M1.setP("rho0", mobility)
71 M1.setP("bedrock", bedrock)
72 M1.setV("beta", beta)
73 M1.setP("psi0", psi0)
74 M1.setP("smoothing", smoothflag)
75
76 # Hydro-morphodynamic model
77 HM1 = Hydro_morpho_model(D1, H1, M1)
78 HM1.Figure_title = "Example of simulation with linear seabed"
79 filetag = "Test_1"
80 HM1.setfilename(filetag)
81
82 # Set time-dependent and space-dependent variables to plot
83 to_plot_t(HM1, outargs_t)
84 to_plot_x_during_run(HM1, dtpcpt, outargs_x )
85
86 # Run Opti-Morph
87 HM1.run()
```

Listing 4.1: Example of `OptimiseC.py` file

4.4.2.3 Input Data

The input data is found in a folder named `Input`. Four files should appear in this folder:

- `init.txt`: initial cross-shore data
- `time_init.txt`: forcing data
- `param.txt`: model parameters
- `data_to_save.txt`: requested output data

The `init.txt` file

Let $(x_p)_{p\in[0,N_\Omega]}$ be the discretization of Ω, with N_Ω the total number of points. The `init.txt` file is composed of 5 columns of data:

- the discretization of the domain: $(x_p)_{p\in[0,N_\Omega]}$
- the initial seabed: $(\psi(x_p))_{p\in[0,N_\Omega]}$

- the bedrock: $(B(x_p))_{p\in[0,N_\Omega]}$
- the sand mobility parameter: $(\Upsilon(x_p))_{p\in[0,N_\Omega]}$
- the slope parameter: $(M_{\text{slope}}(x_p))_{p\in[0,N_\Omega]}$

⚠ Ideally, the bathymetric data should ensure that at $x = 0$, we are in deep water. That is, the water depth h is greater than half the wavelength L (cf. [28]).

⚠ For a seabed with the same type of sediment over the cross-shore profile, the mobility parameter and slope parameter will be constant over Ω.

⚠ Setting the bedrock as $B(x_p) = 0$ for all $p \in [0, N_\Omega]$ deactivates the bedrock constraint.

⚠ The user must verify that the initial seabed is consistent with the slope constraint parameter, i.e. that the slope of ψ_0 doesn't exceed M_{slope}. Otherwise, the model will automatically rectify the seabed so as to comply with the slope constraint after the first time step. This may result in a significant and instantaneous change to the seabed.

Examples of the `init.txt` file can be found in Section 4.5, Figures 4.21a and 4.24a.

The `time_init.txt` file

Let $(t_p)_{p\in[0,N_T]}$ be the discretization of the time interval $[0, T]$, with N_T the total number of points.

The `time_init.txt` file is composed on two columns of data and contains the time-dependent data:

- the discretization of the simulated time interval: $(t_p)_{p\in[0,N_T]}$
- the forcing wave height data: $(H_0(t_p))_{p\in[0,N_T]}$

Examples of the `time_init.txt` file can be found in Section 4.5, Figures 4.21b and 4.24b.

The `param.txt` file

The physical and numerical parameters of the model have been grouped together in one file named `param.txt` and organised by type to allow the user to easily modify the different parameters governing the Opti-Morph model. This file should contain the following parameters, in the given order:

```
# Domain parameters
h0

# Hydro parameters
T0
gamma

# Morpho parameters
beta

# Constraint flag
sandc

# Smoothing flag
smoothf
```

Here, `h0` is the still water level (m), `T0` is the wave period (s), here assumed constant over the cross-shore profile and `gamma` is the wave-breaking index defined in Section 4.3.2.2. The parameter `beta` is the precision parameter required for the sandstock constraint (cf. Section 4.3.3.4) and `sandc` is the flag associated with the sandstock constraint. The final parameter is the `smoothf` is a smoothing function, that the user can apply to the seabed to remove noise due to numerical inaccuracies.

⚠ To activate the sandstock constraint, set the flag to 1 and set the associated parameter β to its desired value. To deactivate the constraint, set the flag to 0. The same applied to the `smoothf` flag.

⚠ The slope constraint is permanently activated. In order to locally/temporarily deactivate it, the user can simply increase M_{slope} so that the constraint cannot be triggered (see Section 4.5.2).

Examples of the `param.txt` file can be found in Section 4.5, Figures 4.21c and 4.24c.

The `data_to_save.txt` file

The Opti-Morph model offers the possibility of creating a graphic representation of the different types of data, as well as exporting this data. The user provides the keywords of the data they wish to retrieve at the end of the simulation. The list of the required output Figures_user_guides/data is given in the `data_to_save.txt` file, situated in the `Input` folder.

The `data_to_save.txt` file is separated into 3 sections. The first concerns the number of time steps between each outputs of the space-dependent variables. Then

the list of the space-dependent variables should be given, followed by the list of time-dependent variables.

An example of `data_to_save.txt` file is given below:

```
# Output data
T_out
default_out

# List of space-dependent variables
to export/plot
*List*
END

# List of time-dependent variables to
export/plot
*List*
END
```

where `T_out` is number of time steps between each output for the space-dependent variables. If the user desires a snapshot of the seabed, wave height, or any other space-dependent variable every 50 time incrementations, then they should indicate "50" in the first row of `data_to_save.txt` file.

ℹ This parameter has no impact on the time-dependent Figures_user_guides/exports.

The keyword `default_out` is the flag indicating whether the user requires the default figure to be produced by Opti-Morph. An example of this figure is given in Figure 4.18. The list of space-dependent variables (defined over the cross-shore profile) is then given, with each keyword situated on a different line. The list of keywords can be found in Table 4.4 (left). The keyword `END` is required to mark the end of this first list. The list of time-dependent variables (defined over the time-series) follows, with one keyword per line. The list of keywords can be found in Table 4.4 (right). Once again, the keyword `END` is needed to mark the end of this second list.

Space dependent keywords	time-dependent keywords
• `ADT`[2]: anti-dissipative term • `C`: phase velocity • `Cg`: group velocity • `H`: wave height • `HS`: shoaling wave height • `Lambda`: wave excitation parameter • `h`: water depth • `k`: wave number • `psi`: seabed elevation • `slope`: slope of the seabed	• `E_after`: total wave energy after the seabed response • `E`: total wave energy • `EBS`: energy over Ω_B • `EOB`: energy over Ω_S • `H0`: forcing wave height • `alpha`[1]: breaking parameter • `nbB`: position of x_B in the discretization of the domain Ω • `nbS`: position of x_S in the discretization of the domain Ω • `sandstock`: sandstock • `xB`: location of (first) breaking • `xS`: position of the shoreline

Table 4.4: Table of keywords associated with the spatial (*left*) and temporal (*right*) variables available to plot/export

[1]: only available for `shoaling_1run` and `shoaling_2run`
[2]: only available for `shoaling_window_LC_ADT`

4.4.2.4 Output Data

At the end of the simulation, the requested Figures_user_guides/exports are found in the `Results` folder, with the figures in `Figures` and the exported data in `Output`.

Figure folder

At the end of the simulation, PNG images of the requested variables can be found in the Figure file.

If requested using the `default_out` flag set to 1, Opti-Morph produces a 6-panel

figure detailing the main contributing variables of the simulation at a given time. An example of the default figure is given in Figure 4.18.

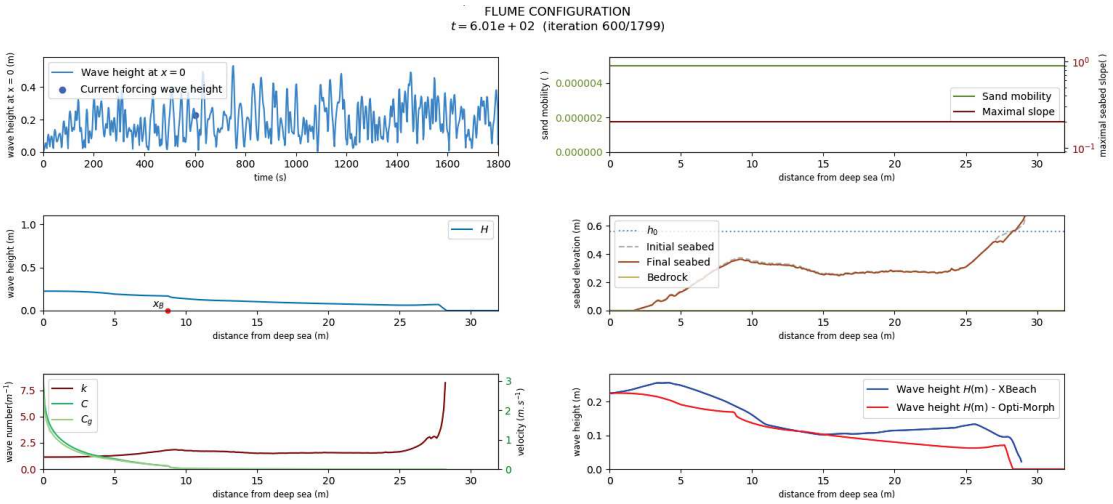

Figure 4.18: Example of the default figure, mid simulation. *Upper left:* Time series of the forcing wave height H_0 with the current forcing indicated with a circular point. *Middle left:* Wave height calculated over the cross-shore profile using the hydrodynamic model no.7. *Bottom left:* Variation of the wavenumber k (red), phase velocity C (green) and group velocity C_g (light green) over the cross-shore profile. *Upper right:* Variation over the cross-shore profile of the two hyper-parameters required by Opti-Morph: sand mobility parameter Υ (green) and the maximal slope parameter M_{slope}. Here constant, these parameters vary when the seabed features different types of sediment over Ω, or in the presence of man-made structures (such as submerged breakwaters, see Section 4.5.2). *Middle right:* Seabed elevation over the cross-shore profile. The initial seabed (grey dashed line), the bedrock (grey solid line) and the mean water height (dotted blue line) have also been specified. *Bottom right:* Comparison of wave height with another hydro-morphodynamic model, if available. Here, a comparison with Xbeach's hydrodynamic module is conducted.

These figures are saved in the folder `Figures` under the title

`Figure_hyd_mor_beta_gamma_time.png`

where `beta`, `Mslope`, `gamma` are the value of the parameters chosen for the simulation and `time` is the time step.

Opti-Morph can also provide simple plots of the quantities involved in the model simulation. Examples of these plots can be found in Figure 4.19, where the wave height, wavenumber and seabed elevation are given mid-simulation.

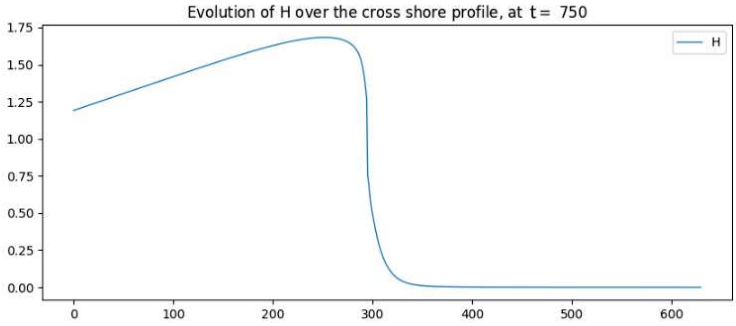

(a) Wave height over the cross-shore profile, mid-simulation

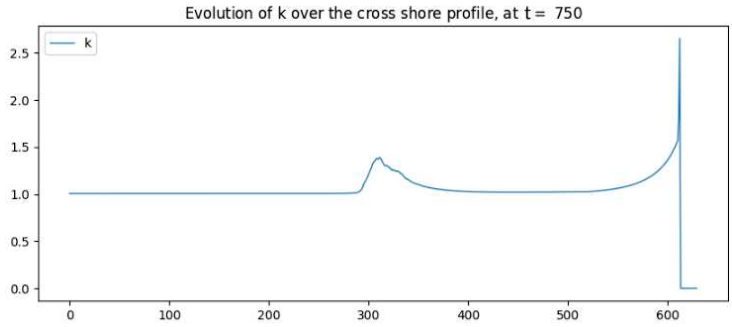

(b) Wavenumber over the cross-shore profile, mid-simulation

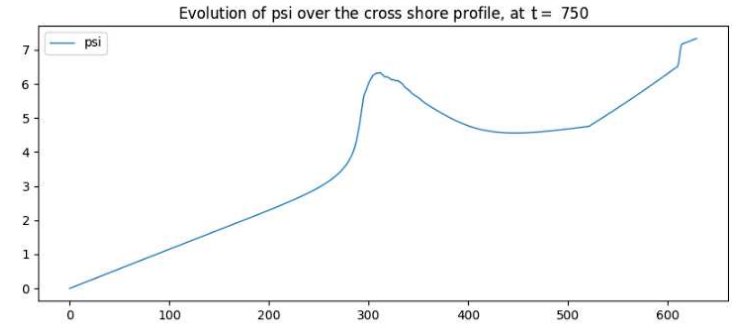

(c) Seabed elevation over the cross-shore profile, mid-simulation

Figure 4.19: Examples of simple plots generated by Opti-Morph during the simulation

Output folder

At the end of the simulation, text files of the requested data can be found in the Output folder. The user can then use this data to perform a more thorough post-processing analysis of the morphodynamic and hydrodynamic processes that took place during the simulation.

4.5 Applications

In this section, the seabed is described as a simple linear function over the cross-shore profile. First, we simulate the results over a homogeneous sandy seabed, then we look at introducing submerged structures designed to limit wave activity at the coast.

4.5.1 Linear Seabed Beach Configuration

4.5.1.1 Setting

The initial cross-shore configuration is given in Figure 4.20: the domain measures $600\,m$, the mean water level is set at $7\,m$ and we apply a storm profile to the seabed, given by the top left graph of Figure 4.20. Here we consider a homogeneous sandy seabed, and therefore the mobility of the seabed Υ and the maximal slope parameter M_{slope} are assumed constant over the cross-shore profile Ω.

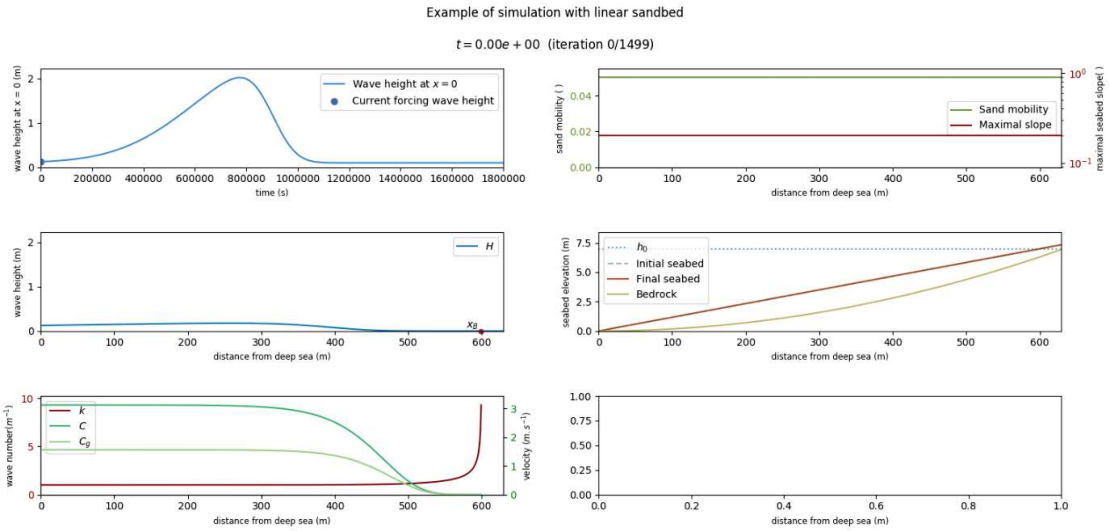

Figure 4.20: Initial sandy beach configuration

4.5.1.2 Input files

The input files have been constructed accordingly, with Figure 4.21 providing an overview of the different files.

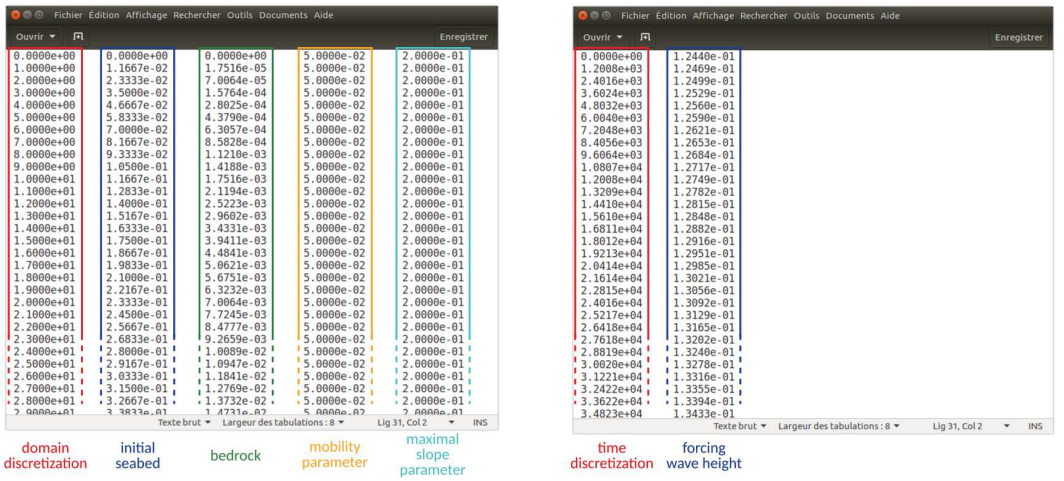

(a) `init.txt` file

(b) `time_init.txt` file

(c) `param.txt` file

(d) `data_to_save.txt` file

Figure 4.21: Input files used in the simulation

4.5.1.3 Results

At the end of the simulation, we get the following results of Figure 4.22. Here, the default figure has been requested, as well as `xB`, `xS`, and `sandstock`.

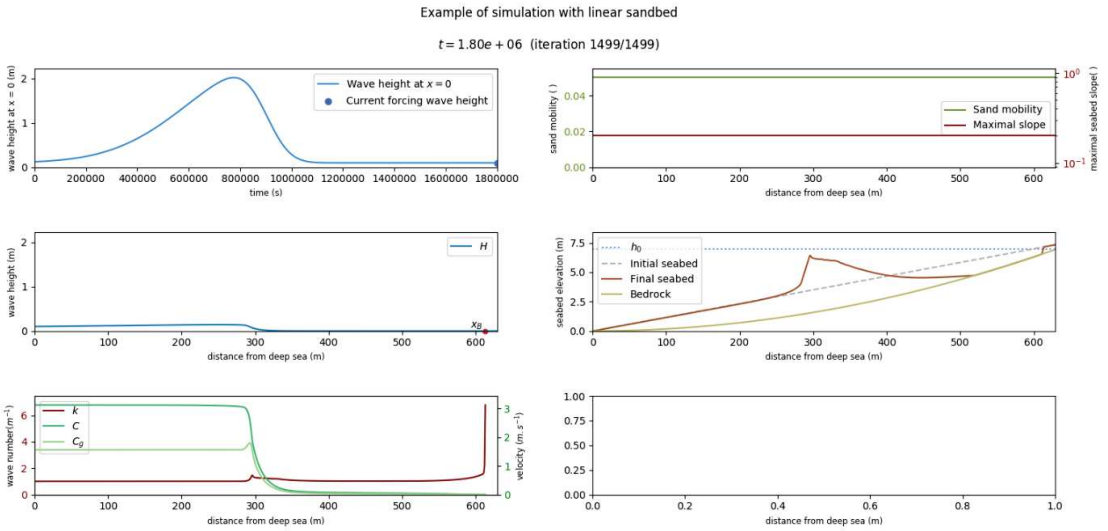

(a) Result of the beach configuration at the end of simulation

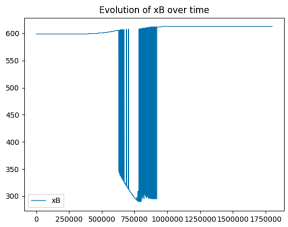

(b) Variation of the breaking point over time

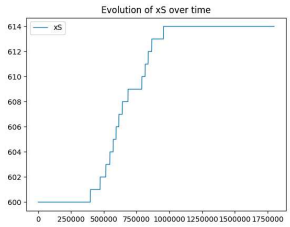

(c) Variation of the shoreline over time

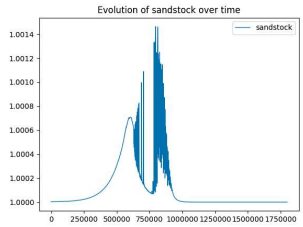

(d) Variation of the sandstock over time

Figure 4.22: Various plots provided by Opti-Morph

A thorough analysis of the results of Opti-Morph can be found in [21] for an experimental flume configuration and [19] for a linear seabed with submerged breakwaters.

4.5.2 Beach Configuration with Submerged Breakwaters

4.5.2.1 Setting

In this simulation, we introduce a solid submerged structure, in the same manner as [19]. To do this, we modify the seabed profile, as well as the sand mobility parameter Υ and the maximal slope parameter M_{slope}, which are no longer constant over the cross-shore profile. In the case of the mobility parameter, no movement can occur at the location of the structures, i.e. $\Upsilon = 0$ where the breakwater is positioned. Similarly, the maximal slope parameter has also been modified to locally deactivate the slope constraint over the structure. Figure 4.23 shows the new initial configuration incorporating a submerged breakwater located at $x = 180\,m$.

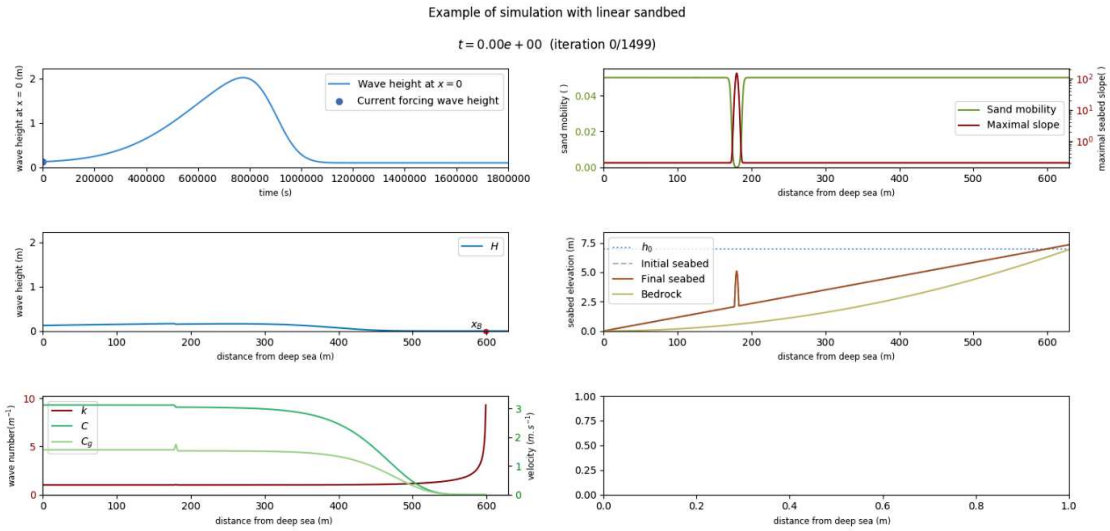

Figure 4.23: Initial sandy beach configuration with a submerged breakwater located at $x = 180\,m$

4.5.2.2 Input files

Similar to before, the input files have been constructed, with Figure 4.21 providing an overview of the different files. Now, the mobility parameter Υ and the slope parameter M_{slope} vary over the cross-shore profile.

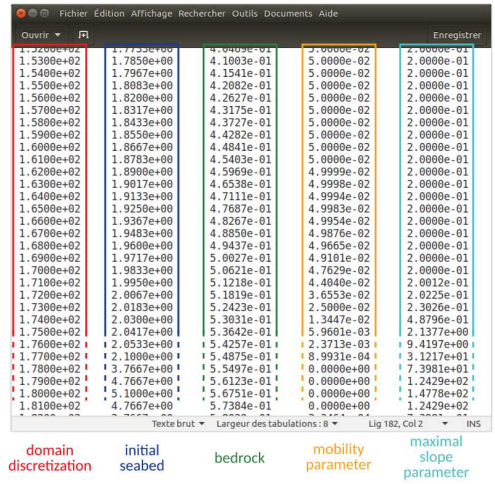

(a) `init.txt` file

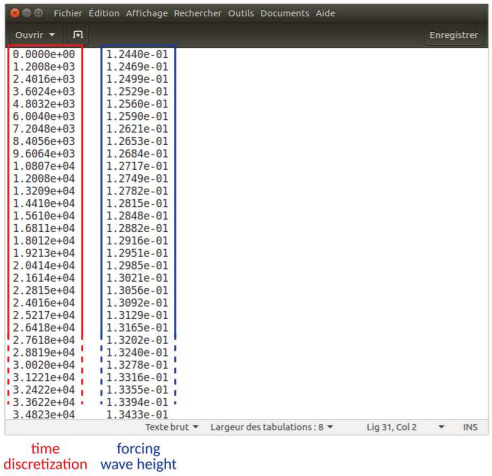

(b) `time_init.txt` file

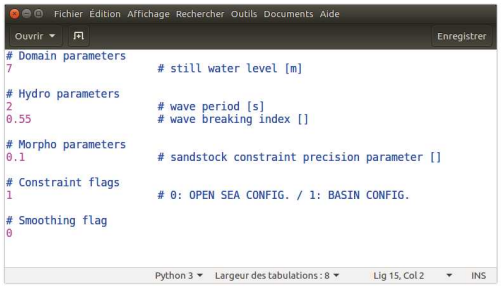

(c) `param.txt` file

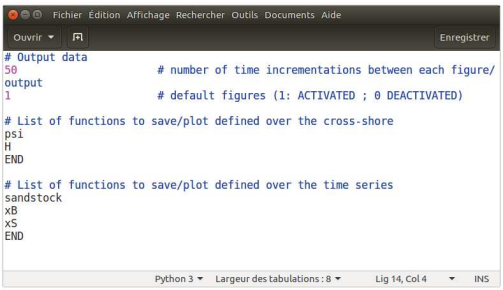

(d) `data_to_save.txt` file

Figure 4.24: Input files used in the simulation

A thorough analysis of the behavior of Opti-Morph in regards to the introduction of geotubes can be found in [19].

4.5.2.3 Results

At the end of the simulation, we get the following results of Figure 4.25. As before, the default figure has been activated (`default_out = 1`), and the graphs of `xB`, `xS`, and `sandstock` were requested.

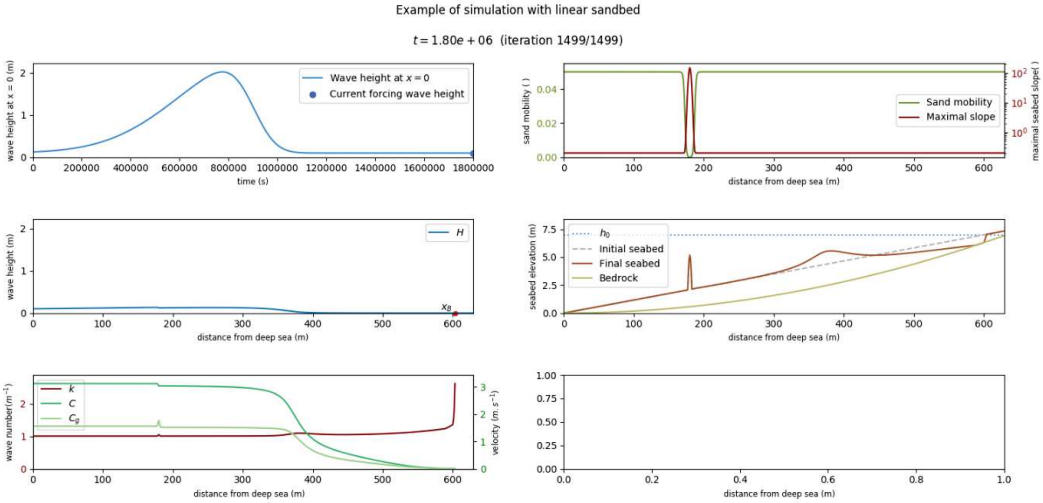

(a) Result of the beach configuration with submerged breakwaters at the end of simulation

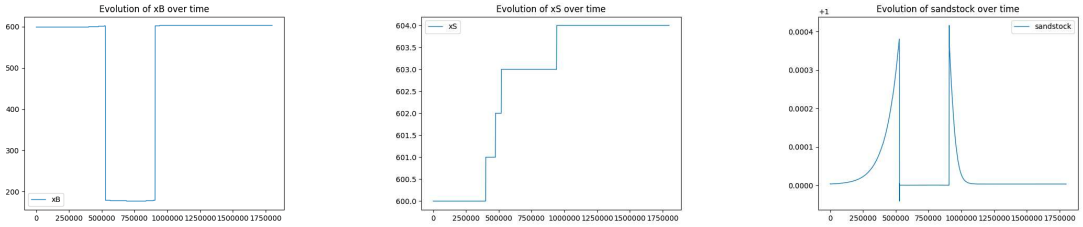

(b) Variation of the breaking point over time

(c) Variation of the shoreline over time

(d) Variation of the sandstock over time

Figure 4.25: Various plots provided by Opti-Morph

4.A List of Symbols

A summary of the notations, variables and parameters used throughout this user guide is provided in the following table.

Name	Keyword	Description	Unit
Ω	`Omega`	domain of the study of the cross-shore profile	m
Ω_S	`Omega_S`	subset of Ω over which the waves shoal	m
Ω_B	`Omega_B`	subset of Ω over which the waves break	m
x_{max}	`x_max`	upper-bound of the domain, situated beyond the shore	m
x_S	`x_S`	shoreline position	m
x_B	`x_B`	location of (first) breaking of the waves	m
Ψ	`Psi`	set of parameters describing the seabed	m
ψ	`psi`	elevation of the seabed	m
ψ_0	`psi_0`	initial seabed (at $t = 0$)	m
ψ_t	-	evolution of the seabed over time	$m.s^{-1}$
B	`bedrock`	bedrock	m
T	`T`	upper-bound of the time series	s
h_0	`h_0`	mean water level	m
h	`h`	water depth	m
T_0	`T_0`	wave period	m
H_0	`H_0`	wave height at $x = 0$	m
H	`H`	wave height	m
C	`C`	phase velocity of the waves	$m.s^{-1}$
C_0	`C0`	initial phase velocity of the waves	$m.s^{-1}$
C_g	`C_g`	group velocity of the waves	$m.s^{-1}$
n	`n`	ratio of phase velocity and group velocity	-
k	`k`	wave number	m^{-1}
L	-	wavelength	m
σ	`sigma`	wave pulsation	s^{-1}
K_S	`K_S`	shoaling coefficient	-
γ	`gamma`	wave-breaking index	-
α	`alpha`	breaking type parameter	-
d_{win}	`dwin`	maximal distance of local spatial dependency of a wave	m
w	-	weighting function	-
H_0^w	-	weighted average of the seaward waves	m
α_w	-	boundary condition transitional parameter	-
a_{AD}	`aAD`	first parameter in the anti-dissipative term	-
b_{AD}	`bAD`	second parameter in the anti-dissipative term	-
χ_{AD}	`ADT`	anti-dissipative term	-
g	`g`	gravitational acceleration	$m.s^{-}2$

ρ_w	`rho_w`	water density	$kg.m^{-3}$
$\mathcal{J}$	`J`	cost function to be minimized	$J.m^{-1}$
$\mathcal{E}$	`E`	Potential wave energy	$J.m^{-1}$
-	`E_after`	Potential wave energy associated with the updated seabed	$J.m^{-1}$
$\mathcal{E}_S$	`E0B`	Potential energy of the shoaling waves	$J.m^{-1}$
$\mathcal{E}_B$	`EBS`	Potential energy of the breaking waves	$J.m^{-1}$
Υ	`Upsilon`	mobility of the sediment	$m.s.kg^{-1}$
φ	-	orbital velocity damping function	-
d	`d`	direction of descent	J
M_{slope}	`M_slope`	angle of repose of the sediment	-
C_{sand}	-	difference in sandstock between the initial and current seabed	
β	`beta`	sandstock constraint precision parameter	-
$\mathcal{J}_{pen}$	-	cost function incorporating the sandstock penalty term	$J.m^{-1}$
N_Ω	`N`	number of points in the discretization of the domain	-
N_T	-	number of points in the discretization of the time series	-
$(x_p)_{p\in[0,N_\Omega]}$	`x`	discretization of the domain Ω	-
$(t_p)_{p\in[0,N_T]}$	`t`	discretization of time interval $[0,T]$ of the simulation	-
-	`nbB`	position of x_B in the discretization of the domain Ω	-
-	`nbS`	position of x_S in the discretization of the domain Ω	-
-	`sandc`	flag activating the sandstock constraint	-
-	`smoothf`	flag activating a smoothing effect on the seabed	-
-	`T_out`	number of time steps between output	-
-	`default_out`	flag activating the creation of the default figure output	-
-	`CF0`	choice of direction of descent	J

Table 4.5: List of symbols used in the Opti-Morph user-guide

Chapitre 5

Conclusion et Perspectives

5.1 Conclusion

Dans ces travaux de thèse, nous avons montré plusieurs applications de la théorie d'optimisation en zone littorale. Dans la recherche de solutions optimales, une fonction de coût fut développée selon les objectifs préalablement définis ainsi que les contraintes imposées pour offrir plus de précision aux résultats finaux. Pour chaque application, la fonction de coût s'appuie sur des quantités relatives à l'hydrodynamisme littoral et ainsi, nous avons développé un modèle hydrodynamique adapté aux besoins du modèle d'optimisation.

Dans un premier temps, nous avons étudié le problème classique d'ingénierie côtière qu'est l'aménagement portuaire. La problématique concerne le réaménagement du port de La Turballe dans le but d'agrandir sa surface exploitable et simultanément réduire l'agitation des vagues. Pour ce faire, l'introduction d'une digue et d'un môle fut proposée, dont leurs dimensions furent l'objet d'une étude par optimisation. La fonction de coût est au cœur de l'étude basée sur l'agitation de l'eau au sein du port. Cette fonction fut alimentée par un modèle hydrodynamique basé sur les équations de Helmholtz et permet de bien tenir compte des conditions aux bords délimitant le domaine d'étude. Plusieurs contraintes furent introduites pour exclure certaines configurations jugées inadéquates. Ces contraintes concernent notamment les dimensions minimales et maximales des structures. Excéder ces valeurs entraînerait des structures trop petites pour les besoins commerciaux ou trop coûteuses en construction. Les résultats montrent l'existence d'une solution optimale qui correspond à un môle d'une largeur de $120\,m$ et une digue mesurant $457\,m$ de longueur.

Dans le Chapitre 2, une seconde étude, indépendante de la première, fut réalisée dans le but de simuler la dynamique littorale des plages sableuses par le biais de la théorie d'optimisation. Un nouveau modèle morphodynamique fut élaboré, basé sur l'hypothèse que le profil bathymétrique d'une plage varie au cours du temps afin de minimiser une

certaine quantité hydrodynamique. À présent, nous utilisons l'énergie potentielle des vagues. Ainsi, la fonction de coût qui est minimisée à chaque pas de temps et qui détermine la nouvelle forme du fond sableux est l'énergie des vagues. Ici, les contraintes sont introduites pour incorporer davantage de physique dans le modèle, tel l'avalanchisme ou l'invariabilité de la quantité de sable en cas de bassin expérimental. Ces processus sont considérés comme des phénomènes secondaires dans le morphodynamisme littoral avec l'action principale provenant de la minimisation de la fonction de coût. Le modèle numérique qui découle de cette théorie fut entièrement conçu lors de la thèse, et est baptisé Opti-Morph. Il permet d'illustrer le potentiel d'un modèle morphodynamique basé sur ce principe d'optimisation. Appliqué sur une configuration expérimentale dont les mesures du profil bathymétrique furent relevées, nous avons analysé les résultats numériques d'Opti-Morph en les comparant avec ces données physiques sur des simulations à court terme. Une analyse de robustesse fut réalisée sur les deux hyperparamètres gouvernant le modèle d'optimisation, ainsi qu'une étude comparative avec un autre modèle hydro-morphodynamique pour montrer le potentiel d'Opti-Morph face aux modèles existants. Des simulations supplémentaires furent également effectuées pour étudier le comportent long terme de ce modèle numérique avec des résultats prometteurs. Ces résultats montrent le potentiel d'un modèle morphodynamique basé sur la théorie d'optimisation, et ce, malgré un modèle hydrodynamique simple. Opti-Morph a aussi l'avantage d'être rapide, robuste et de faible complexité. Un guide d'utilisation, avec une présentation plus détaillée de ce modèle numérique fut rédigé et se trouve au Chapitre 4.

Dans le Chapitre 3, nous avons cherché à déterminer la position optimale d'un géotube le long du profil cross-shore, tout en tenant compte de la réponse morphodynamique de la plage. Pour ce faire, un couplage de deux problèmes d'optimisation fut réalisé : (i) la recherche de l'emplacement optimal d'un géotube et (ii) la réponse morphodynamique littorale par optimisation. Ces deux problèmes d'optimisation ont dû être posés et traités simultanément, chacun nécessitant ses propres fonctions de coût et ensemble de contraintes. La réponse morphodynamique reprend le modèle précédent, Opti-Morph, avec une fonction de coût correspondant à l'énergie des vagues et des contraintes relatives aux phénomènes secondaires précédemment mentionnés. Le deuxième problème cherche à trouver le meilleur emplacement de géotube le long du profil cross-shore qui minimise l'érosion à la côte. La fonction de coût est donc la position du trait de côte et les contraintes concernent les profondeurs minimale et maximale de ce déploiement. Installer un géotube en eaux trop profondes est coûteux en termes d'installation et de maintenance, tandis qu'un géotube installé trop près de la côte encourt le risque d'endommagement. Grâce à la rapidité et faible complexité d'Opti-Morph, ce deuxième problème d'optimisation a pu être traité par méthode directe. Des études supplémentaires ont été menées pour étudier les résultats d'Opti-Morph face à ces structures artificielles, notamment le comportement des vagues et la position du déferlement. Une seconde étude fut réalisée avec une deuxième fonction de coût pour

montrer l'adaptabilité de cette approche.

5.2 Perspectives

Dans la suite, plusieurs perspectives peuvent être considérées pour le modèle numérique Opti-Morph. Nous pouvons être amenés à incorporer d'autres phénomènes physiques dans le modèle, soit en modifiant la fonction de coût, soit en ajoutant des contraintes supplémentaires. Nous apercevons dans les simulations sur le bassin expérimental du Chapitre 2 qu'Opti-Morph ne prédit pas l'avancement de la barre vers la côte. Introduire la notion de courant dans le modèle pourrait mieux simuler cet avancement. Dans ces travaux, nous avons considéré que l'évolution du profil bathymétrique de la plage est gouverné par la minimisation d'une énergie de vagues. Dans les développements futurs, nous pouvons envisager la modification de la fonction de coût pour modéliser d'autres phénomènes, et explorer d'autres physiques observées sur le profil cross-shore. Ceci concerne notamment le changement d'échelle de temps. Dans ce cas, il convient de considérer un modèle hydrodynamique adapté, et il peut être nécessaire d'incorporer la marée et/ou la remontée des eaux dans Opti-Morph.

À présent, un simple modèle hydrodynamique, basé sur la théorie linéaire des vagues fournit Opti-Morph avec les données requise. Une possible piste d'étude serait d'adopter un modèle hydrodynamique plus complexe. L'avantage du modèle actuel est son temps d'exécution rapide et sa capacité d'exprimer analytiquement la hauteur des vagues en fonction du fond, ce qui réduit considérablement le temps de calcul d'Opti-Morph. En effet, ce dernier requiert le gradient de la hauteur des vagues par rapport au fond. Ainsi, adopter d'autres modèles hydrodynamiques peut nécessiter des outils supplémentaires en calcul différentiel, comme les différences finies ou la différenciation automatique.

Actuellement, Opti-Morph s'opère dans une configuration 1D. Cependant, la théorie dont Opti-Morph est basée s'adapte facilement à des configurations 2D. Nous pouvons ainsi envisager d'étendre le modèle numérique à des étendues de plages. Ceci nécessitera des modifications du modèle hydrodynamique, qui devra aborder en outre la réfraction des vagues. Le traitement du transport sédimentaire long-shore est un autre aspect à prendre en compte lors de l'extension du modèle en 2D. Dès lors qu'Opti-Morph s'opère en 2D, il sera possible de réaliser des études supplémentaires sur les géotubes du Chapitre 3, tel que leur position long-shore ou leur orientation par rapport à la côte.

Un premier couplage entre l'optimisation d'ouvrages et l'optimisation du fond fut réalisé dans ces travaux de thèse au Chapitre 3. Ici, une méthode directe fut utilisée pour des raisons de simplicité, et parce que le contexte le permettait. Dans le cadre d'une étude future, nous pouvons être menés à trouver une stratégie de couplage plus complexe, comme suggéré dans l'Introduction, Section 2.2.

Pour reprendre les 3 axes principaux mentionnés dans l'Introduction, le 3ème concerne la validation du modèle numérique. La thèse a légèrement abordé la notion de

robustesse d'Opti-Morph par rapport aux variabilités des paramètres du modèle. Au Chapitre 2, une analyse de robustesse par rapport aux paramètres de pente maximale et de mobilité sédimentaire fut réalisée. Deux sites pour la vérification et la validation de ce modèle sont envisagés dès à présent : le Grau du Roi et la côte à proximité de Béziers. La validation consistera à lancer des simulations numériques dans ces deux configurations en conditions réelles, avec des conditions de forçages météo-marins variables. Plusieurs questions supplémentaires émergent lors de la discussion de validation. Tout d'abord, la distribution spatiale de mobilité du sable n'est pas nécessairement bien connue, et les conditions de la mer sont incertaines. De plus, le fond naturel et les structures rigides ont des comportements différents vis-à-vis de l'état de la mer. Des travaux précédents [75, 75, 78, 77, 76, 80] donnent des pistes pour adresser, avec une complexité calculatoire raisonnable, ces questions. En particulier, la modélisation et l'optimisation ne seront plus mono-point et seront en partie stochastique. Les incertitudes sur les forçages et la mobilité pourront être traitées en introduisant, d'une part, un traitement par intervalle des quantités et de l'autre, des quantiles de densité de probabilité de la distribution spatiale de la mobilité lors de la dynamique bathymétrique.

Liste des Figures

Liste des Tables

Références

[1] H. M. Al-Hashemi and O. S. Al-Amoudi. A review on the angle of repose of granular materials. *Powder Technology*, 330:397–417, 2018.

[2] A. Alises, R. Sánchez, R. Gomez, P. Pery, and C. Castillo. Overtopping hazards to port activities: Application of a new methodology to risk management (port risk management tool). *Reliability Engineering & System Safety*, 123:8–20, 03 2014.

[3] W. Allsop and S. Hettiarachchi. Wave reflections in harbours: design, construction and performance of wave absorbing structures. Technical report, HR Wallingford, 02 1989.

[4] I. Alvarez, R. Rubio, and H. Ricalde. Beach restoration with geotextile tubes as submerged breakwaters in Yucatan, Mexico. *Geotextiles and Geomembranes*, 25:233–241, 08 2007.

[5] D. G. Andrews and M. E. Mcintyre. An exact theory of nonlinear waves on a Lagrangian-mean flow. *Journal of Fluid Mechanics*, 89(4):609–646, 1978.

[6] Y. Balouin, F. Longueville, and Y. Colombet. Video assessment of nearshore and beach evolution following the deployment of a submerged geotextile wave breaker. *Journal of Coastal Research*, Special Issue(No. 75):617–621, 2016.

[7] J.C.W. Berkhoff. Computation of combined refraction-diffraction. *Coastal Engineering Proceedings*, 1(13):23, Jan. 1972.

[8] N. Booij and L. Holthuijsen. Propagation of ocean waves in discrete spectral wave models. *Journal of Computational Physics*, 68:307–326, 02 1987.

[9] F. Bouchette. Coastal defense strategy along hatzuk beach (northern Tel Aviv, Israel). Insights from the COPTER physical experimentation with moveable bed. Technical Report 17-1, BRL Ingénierie, Nîmes, March 2017.

[10] A. Bouharguane. *Analyse, simulation numérique et optimisation de modèles non-locaux en morphodynamique littorale*. PhD thesis, Université de Montpellier, 2011.

[11] A. Bouharguane, P. Azerad, F. Bouchette, F. Marche, and B. Mohammadi. Low complexity shape optimization and a posteriori high fidelity validation. *Discrete and Continuous Dynamical Systems-series B*, 13, 06 2010.

[12] A. Bouharguane and B. Mohammadi. Minimization principles for the evolution of a soft sea bed interacting with a shallow. *International Journal of Computational Fluid Dynamics*, 26:163–172, 03 2012.

[13] M.-H. Briand and J.W. Kamphuis. Sediment transport in the surf zone: A quasi 3-d numerical model. *Coastal Engineering*, 20:135–156, 07 1993.

[14] N. Bugajny, K. Furmanczyk, J. Dudzinska-Nowak, and B. Paplińska-Swerpel. Modelling morphological changes of beach and dune induced by storm on the southern baltic coast using XBeach (case study: Dziwnow spit). *Journal of Coastal Research*, I:672–677, 01 2013.

[15] E. Castillo, M. A. Losada, R. Mínguez, C. Castillo, and A. Baquerizo. Optimal engineering design method that combines safety factors and failure probabilities: Application to rubble-mound breakwaters. *Journal of Waterway, Port, Coastal, and Ocean Engineering*, 130(2):77–88, 2004.

[16] E. Castillo, M. A. Losada, R. Mínguez, C. Castillo, and A. Baquerizo. Optimal engineering design method that combines safety factors and failure probabilities: Application to rubble-mound breakwaters. *Journal of Waterway, Port, Coastal, and Ocean Engineering*, 130(2):77–88, 2004.

[17] Y. Coeffe and P. Pechon. Modelling of sea-bed evolution under waves action. *Proc. 18th ICCE*, 1, 01 1982.

[18] K. Connell, M. Larson, and N. Kraus. Morphologic modeling of multiple barrier island breaches for regional application. In *Proceedings to the Coastal Sediments 2007 Conference*, pages 2011–2073. American Society of Civil Engineers (ASCE), 05 2007.

[19] M. Cook, F. Bouchette, B. Mohammadi, and N. Fraysse. Application of Opti-Morph: Optimized beach protection by submerged geotextile tubes. Preprint, September 2021.

[20] M. Cook, F. Bouchette, B. Mohammadi, and N. Fraysse. Opti-Morph User Guide. Preprint, September 2021.

[21] M. Cook, F. Bouchette, B. Mohammadi, S. Meulé, and N. Fraysse. Opti-Morph, a new platform for sandy beach dynamics by constrained wave energy minimization. Preprint, June 2021.

[22] M. Cook, F. Bouchette, B. Mohammadi, L. Sprunck, and N. Fraysse. Optimal port design minimizing standing waves with a posteriori long term shoreline sustainability analysis. *China Ocean Engineering*, June 2021. Accepted for publication.

[23] A. Cornett, S. Baker, and B. Weaver. Value of 3D physical modeling in harbor design - gateway harbor chicago case study. In *Proceeding of the 34th PIANC World CongressAt, Panama*, 05 2018.

[24] R. Cox and D. Beach. Floating breakwater performance-wave transmission and reflection, energy dissipation, motions and restraining forces. *Proc 1st Int Conf on the Application of Physical Modeling to Port and Coastal Protection*, pages 371–381, 01 2006.

[25] C. Daly. Low frequency waves in the shoaling and nearshore zone a validation of XBeach. *Erasmus Mundus Master in Coastal and Marine Engineering and Management (CoMEM), Delft University of Technology*, 2009.

[26] H. de Vriend, W.T. Bakker, and D.P. Bilse. A morphological behaviour model for the outer delta of mixed-energy tidal inlets. *Coastal Engineering*, 23:305–327, 07 1994.

[27] R. Dean and R. Dalrymple. Coastal processes with engineering applications. *Cambridge University Press*, 03 2004.

[28] R. G. Dean and R. A. Dalrymple. *Water Wave Mechanics for Engineers and Scientists*. World Scientific, 1991.

[29] H. Diab, P. Lafon, and R. Younes. Optimisation of breakwaters design to protect offshore terminal area. *Proceedings of the IASTED International Conference on Modelling, Simulation and Identification, MSI 2014*, pages 70–75, 01 2014.

[30] Y. Ding, S. Wang, and Y. Jia. Development and validation of a quasi-three-dimensional coastal area morphological model. *Journal of Waterway Port Coastal and Ocean Engineering*, 132:462–476, 11 2006.

[31] N. Droenen and R. Deigaard. Quasi-three-dimensional modelling of the morphology of longshore bars. *Coastal Engineering*, 54:197–215, 03 2007.

[32] G. Elchahal, P. Lafon, and R. Younes. Design optimization of floating breakwaters with an interdisciplinary fluid–solid structural problem. *Canadian Journal of Civil Engineering*, 36(11):1732–1743, 2009.

[33] M. Esteban, H. Takagi, and T. Shibayama. *Handbook of Coastal Disaster Mitigation for Engineers and Planners*. Butterworth-Heinemann, 08 2015.

[34] C.A. Fleming and J.N. Hunt. Application of a sediment transport model. *Coastal Engineering Proceedings*, 1(15):69, Jan. 1976.

[35] A. E. Frey, S. Munger, G. L. Williams, M.J. Wutkowski, and K.B. Conner. Gencade application at Onslow Bay, North Carolina. Technical report, Coastal and Hydraulics Laboratory (U.S.) - Engineer Research and Development Center (U.S.), 2012.

[36] A.E. Frey, J. Rosati, K.J Connell, H. Hanson, and M. Larson. Modeling alternatives for erosion control at Matagorda County, Texas, with Gencade. In *Proceedings to the 33rd International Conference on Coastal Engineering*, 2012.

[37] G. Galappatti and C.B. Vreugdenhil. A depth-integrated model for suspended sediment transport. *Journal of Hydraulic Research*, 23(4):359–377, 1985.

[38] J.-C. Galland, N. Goutal, and J.-M. Hervouet. Telemac: A new numerical model for solving shallow water equations. *Advances in Water Resources*, 14(3):138–148, 1991.

[39] M. González Leija, X. Chavez, E. Alvarez, E. Mendoza, and R. Silva. Experimental study on geotextile tube applications as submerged breakwaters for beach protection in Yucatan, Mexico. *Coastal Engineering Proceedings*, 1:25, 01 2014.

[40] F. Grasso, H. Michallet, and E. Barthélemy. Experimental simulation of shoreface nourishments under storm events: A morphological, hydrodynamic, and sediment grain size analysis. *Coastal Engineering*, 58(2):184–193, 2011.

[41] Mark B. Gravens. An approach to modeling inlet and beach evolution. *Coastal Engineering Proceedings*, 1(25), Jan. 1996.

[42] A. Griewank and A. Walther. *Evaluating Derivatives: Principles and Techniques of Algorithmic Differentiation*. Society for Industrial and Applied Mathematics, second edition, 2008.

[43] R. Groenveld. *Harborsim, a generally applicable harbour simulation model*. TU Delft, Section Hydraulic Engineering, 1983.

[44] H. Hanson, K. Connell, M. Larson, N. Kraus, T. Beck, and A. Frey. Coastal evolution modeling at multiple scales in regional sediment management applications. In *Proceedings to the Coastal Sediments 2011 Conference*, volume 3, pages 1920–1932, 04 2011.

[45] H. Hanson and N.C. Kraus. Genesis: generalized model for simulating shoreline change. In *Proceedings to the 30th International Conference on Coastal Engineering*, volume 4, pages 3762–3773, 01 1989.

[46] G. Harris, M. Anderson, B. Schroer, B. Landrum, and D. Möller. A simulation model for determining container throughput at an expanding seaport. In *Proceedings of the 6th Vienna International Conference on Mathematical Modeling MATHMOD2009At. Vienna, Austria*, 02 2009.

[47] L. Hascoet and V. Pascual. Tapenade user's guide. In *INRIA Technical report*, pages 1–31. INRIA, 2004.

[48] K. Hasselmann, T.P. Barnett, E. Bouws, H. Carlson, D. Cartwright, K. Enke, J.A. Ewing, H. Gienapp, D. Hasselmann, P. Kruseman, A. Meerburg, P. Muller, D. Olbers, K. Richren, W. Sell, and H. Walden. Measurements of wind-wave growth and swell decay during the joint north sea wave project (JONSWAP). Technical report, Deutsches Hydrographisches Institut, Hamburg, Germany, 01 1973.

[49] M. Hattori and R. Kawamata. Onshore-offshore transport and beach profile change. *Coastal Engineering Proceedings*, 1(17):71, Jan. 1980.

[50] J.-M. Hervouet. Hydrodynamics of free surface flows: Modelling with the finite element method. *Hydrodynamics of Free Surface Flows: Modelling with the finite element method*, 05 2007.

[51] C. L. Hewitt and R. B. Martin. Revised protocols for baseline port surveys for introduced marine species: survey design, sampling protocols and specimen handling. Technical report, CSIRO Div. of Marine Research, Hobart, Tas., 01 2001.

[52] H. Hidayat and S. Andrianto. Effectiveness of geotextile tubes as a breakwater core. *Coastal Engineering Proceedings*, 1:80, 12 2018.

[53] L. Holthuijsen, N. Booij, and T.H.C. Herbers. A prediction model for stationary, short crested waves in shallow water with ambient current. *Coastal Engineering*, 13:23–54, 05 1989.

[54] D. Isèbe, P. Azerad, F. Bouchette, B. Ivorra, and B. Mohammadi. Shape optimization of geotextile tubes for sandy beach protection. *International Journal for Numerical Methods in Engineering*, 74(8):1262–1277, 2008.

[55] D. Isèbe, P. Azerad, F. Bouchette, B. Ivorra, and B. Mohammadi. Shape optimization of geotextile tubes for sandy beach protection. *International Journal for Numerical Methods in Engineering*, 74:1262 – 1277, 05 2008.

[56] D. Isèbe, P. Azerad, F. Bouchette, and B. Mohammadi. Design of passive defense structures in coastal engineering. *International Review of Civil Engineering (IRECE)*, 5:75, 03 2014.

[57] D. Isèbe, P. Azerad, B. Mohammadi, and F. Bouchette. Optimal shape design of defense structures for minimizing short wave impact. *Coastal Engineering*, 55(1):35–46, 2008.

[58] D. Isèbe, F. Bouchette, B. Mohammadi, P. Azerad, A. Lambert, N. Bujan, F. Grasso, and H. Michallet. Une nouvelle approche pour la protection des plages : Application à la plage du Lido de Sète. *Revue Paralia*, pages 263–272, 11 2008.

[59] B. Ivorra, D. Isèbe, and B. Mohammadi. Optimisation globale à complexité réduite: Application à divers problèmes industriels. In *Proceedings to the 7e colloque national en calcul des structures*, Giens, France, May 2005. CSMA.

[60] C. T. Jahren and S. Ishii. Emergency ferry landing design. *Journal of Waterway, Port, Coastal, and Ocean Engineering*, 121(4):216–222, 1995.

[61] H. Johnson, I. Brøker, and J.A. Zyserman. Identification of some relevant processes in coastal morphological modelling. *Coastal Engineering Proceedings*, 1(24), Jan. 1994.

[62] F. J. Joubert and L. Pretorius. Design and construction risks for a shipping port and container terminal: Case study. *Journal of Waterway, Port, Coastal, and Ocean Engineering*, 146(1):05019003, 2020.

[63] T. Kana, E.J. Hayter, and P. Work. Mesoscale sediment transport at Southeastern U.S. tidal inlets: conceptual model applicable to mixed energy settings. *Journal of Coastal Research*, 15:303–313, 03 1999.

[64] R. Koerner. *Geotextiles: From Design to Applications*. Woodhead Publishing Series in Textiles. Elsevier Science, 2016.

[65] M. Larson and N. Kraus. SBEACH: numerical model for simulating storm-induced beach change. Report 1. Empirical foundation and model development. Technical report, Department of the Army US Army Corps of Engineers, Washington, DC, USA, 07 1989.

[66] M. Larson, N. Kraus, and M. Byrnes. Sbeach: Numerical model for simulating storm-induced beach change. Report 2. Numerical formulation and model tests. Technical report, Departmeny of the Army US Army Corps of Engineers, Washington, DC, USA, 05 1990.

[67] B. Latteux. Harbour design including sedimentological problems using mainly numerical technics. *Coastal Engineering Proceedings*, 1(17):132, Jan. 1980.

[68] C. R. Lawson. Geotextile containment for hydraulic and environmental engineering. *Geosynthetics International*, 15(6):384–427, 2008.

[69] G.R. Lesser, D.J.A. Roelvink, J.A.T.M. Kester, and G. Stelling. Development and validation of a three-dimensional morphological model. *Coastal Engineering*, 51:883–915, 10 2004.

[70] P. Li and X. Zhou. Mechanical behavior and shape optimization of lining structure for subsea tunnel excavated in weathered slot. *China Ocean Engineering*, 29(6):875–890, dec 2015.

[71] L. Lillycrop and M. Briggs. Capabilities in harbor design and monitoring: A case study. *US Army Engineer Waterways Experiment Station (WES), Coastal Engineering Research Center (CERC)*, page 11, 09 1992.

[72] K. Maruyama and T. Takagi. A simulation system of near-shore sediment transport for the coupling of the sea-bottom topography, waves and currents. *Proc. IAHR Symp. Math. Mod. Sed. Transp. Coastal Zone*, pages 300–309, 01 1988.

[73] A. Masria, M. Iskander, and A. Negm. Coastal protection measures, case study (Mediterranean zone, Egypt). *Journal of Coastal Conservation*, 19, 05 2015.

[74] B. L. McCartney. Floating breakwater design. *Journal of Waterway, Port, Coastal, and Ocean Engineering*, 111(2):304–318, 1985.

[75] B. Mohammadi. Reduced sampling and incomplete sensitivity for low-complexity robust parametric optimization. *Int. J. Num. Meth. Fluids*, 73/4:307–323, 2013.

[76] B. Mohammadi. Principal angles between subspaces and reduced order modeling accuracy in optimization. *Structural and Multidisciplinary Optimization*, 50/2:237–252, 2014.

[77] B. Mohammadi. Uncertainty quantification by geometric characterization of sensitivity spaces. *Compt. Meth. Appl. Mech. Eng.*, 280:197–221, 2014.

[78] B. Mohammadi. Value at risk for confidence level quantifications in robust engineering optimization. *optimal Control: Applications and Methods*, 35/2:179–190, 2014.

[79] B. Mohammadi and F. Bouchette. Extreme scenarios for the evolution of a soft bed interacting with a fluid using the value at risk of the bed characteristics. *Computers and Fluids*, 89:78–87, 01 2014.

[80] B. Mohammadi and F. Bouchette. Extreme scenarios for the evolution of a soft bed interacting with a fluid using the value at risk of the bed characteristics. *Computers & Fluids.*, 89:22–46, 2014.

[81] B. Mohammadi and A. Bouharguane. Optimal dynamics of soft shapes in shallow waters. *Computers and Fluids*, 40:291–298, 01 2011.

[82] B. Mohammadi and O. Pironneau. *Applied shape optimization for fluids*. Numerical mathematics and scientific computation. Oxford University Press, Oxford, 2nd ed. edition, 2010.

[83] B. Mohammadi and J.H. Saiac. *Pratique de la Simulation Numérique*. Dunod, May 2003.

[84] W. Munk. The solitary wave theory and its application to surf problems. *Annals of the New York Academy of Sciences*, 51:376 – 424, 12 1949.

[85] A. B. Murray. Reducing model complexity for explanation and prediction. *Geomorphology*, 90(3):178–191, 2007. Reduced-Complexity Geomorphological Modelling for River and Catchment Management.

[86] I. Na'im, A. Shahrizal, and M. Safari. A short review of submerged breakwaters. *MATEC Web of Conferences*, 203:01005, 01 2018.

[87] R. Nairn and H. Southgate. Deterministic profile modelling of nearshore processes. Part 2. Sediment transport and beach profile development. *Coastal Engineering*, 19:57–96, 02 1993.

[88] J. A. Nelder and R. Mead. A Simplex Method for Function Minimization. *The Computer Journal*, 7(4):308–313, 01 1965.

[89] J. Nicholson, I. Brøker, D.J.A. Roelvink, D. Price, J.-M. Tanguy, and L. Moreno. Intercomparison of coastal area morphodynamic models. *Coastal Engineering*, 31:97–123, 07 1997.

[90] H. Niemeyer, R. Kaiser, and B. Weiler. Design wave evaluation for coastal protection structures in the Wadden Sea. In *Proceedings of the 6th International Workshop on Wave Hindcasting and Forecasting*, 03 2001.

[91] Y. O., E. S., J. K., and J. K. Application of submerged geotextile tubes for erosion prevention in east coast of Korea. *Proceedings of the 8th International Conference on Geosynthetics*, 2006.

[92] US Army Corps of Engineers. *Coastal Engineering Manual, Engineer Manual 1110-2-1100*. US Army Corps of Engineers, Washington, D.C., 01 2002.

[93] Y. Oh and E. Shin. Using submerged geotextile tubes in the protection of the E. Korean shore. *Coastal Engineering*, 53:879–895, 11 2006.

[94] D. Pachakis and A. Kiremidjian. Ship traffic modeling methodology for ports. *Journal of Waterway Port Coastal and Ocean Engineering-asce*, 129, 09 2003.

[95] R. Pelnard-Considère. Essai de théorie de l'évolution des formes de rivage en plages de sable et de galets. In *Journées de l'hydraulique*, volume 4, pages 289–298, 1957.

[96] PIANC. *Criteria for Movements of Moored Ships in Harbours: A Practical Guide*. Rep. Work. Gr. No 24. Perm. Tech. Comm. II, Suppl. to Bull. No 88, 1995.

[97] K. Pilarczyk. Design of low-crested (submerged) structures - an overview. *6th International Conference on Coastal and Port Engineering in Developing Countries*, 01 2003.

[98] M. Quick. Onshore-offshore sediment transport on beaches. *Coastal Engineering*, 15:313–332, 1991.

[99] A. Rabinovich. *Seiches and harbor oscillations*, chapter Chapter 11, pages 243–286. World Scientific Publishing Co Pte Ltd, 12 2017.

[100] H.-E. Reineck and I. B. Singh. *Depositional sedimentary environments; with reference to terrigenous clastics*. Springer-Verlag Berlin, New York, 1973.

[101] Dano J.A. Roelvink. Dissipation in random wave groups incident on a beach. *Coastal Engineering*, 19:127–150, 02 1993.

[102] D.J.A. Roelvink, A. Reniers, A. van Dongeren, J. Thiel de Vries, J. Lescinski, and R. McCall. XBeach model – description and manual. Technical report, Unesco-IHE Institute for Water Education, Deltares and Delft University of Technology, Delft, Netherlands, 01 2010.

[103] D.J.A. Roelvink, A. Reniers, A. van Dongeren, J. Thiel de Vries, R. McCall, and J. Lescinski. Modelling storm impacts on beaches, dunes and barrier islands. *Coastal Engineering*, 56:1133–1152, 11 2009.

[104] D.J.A. Roelvink, G.K.F.M. Van Banning, and A. Verwey. Design and development of DELFT3D and application to coastal morphodynamics, 1st international conference, hydroinformatics 94. In *Proceesings of the 1st International conference of Hydroinformatics*, volume 1, pages 451–456, Rotterdam, 1994. Balkema.

[105] D.J.A. Roelvink, D.J. Walstra, and Z. Chen. Morphological modelling of Keta Lagoon case. *Coastal Engineering Proceedings*, pages 3223–3236, 08 1995.

[106] G. Ruessink and J.H.J Terwindt. The behaviour of nearshore bars on the time scale of years: A conceptual model. *Marine Geology*, 163:289–302, 02 2000.

[107] H. Saghi, D.Z. Ning, P.W. Cong, and M. Zhao. Optimization of baffled rectangular and prismatic storage tank against the sloshing phenomenon. *China Ocean Engineering*, 34(5):664–676, oct 2020.

[108] A. Sawicki, M. Kulczykowski, W. Robakiewicz, J. Mierczyński, and J. Hauptmann. New type of bottom protection in harbors & design method. *Journal of Waterway, Port, Coastal, and Ocean Engineering*, 124(4):208–211, 1998.

[109] M.H. Schrader, E.C. Douglass, and L.S. Lillycrop. Regional sediment management strategies for the vicinity of St. Augustine Inlet, St. Johns County, Florida. Technical report, U.S. Army Engineer Research and Development Center, Coastal and Hydraulics Laboratory, 2016.

[110] O. Shabankareh, M. Ketabdari, and M. A. Shabankareh. Environmental impact of geotubes and geotextiles used in breakwaters and small breakwaters construction. *International Journal of Coastal & Offshore Engineering*, 2017.

[111] C. D. Smith. Outlet structure design for conduits and tunnels. *Journal of Waterway, Port, Coastal, and Ocean Engineering*, 114(4):503–515, 1988.

[112] R. Soulsby. *Dynamics of marine sands*. Thomas Telford Publishing, 1997.

[113] R.L. Soulsby. Calculating bottom orbital velocity beneath waves. *Coastal Engineering*, 11:371–380, 11 1987.

[114] Z.L. Tian, Z.C. Sun, S.X. Liang, and X.G.Wang. Inverse calculation of wave-absorbing structure dimensions based on extended ANFIS model. *China Ocean Engineering*, 32(5):501–513, October 2018.

[115] V. Trbojevic and B. Carr. Risk based methodology for safety improvements in ports. *Journal of hazardous materials*, 71:467–80, 02 2000.

[116] D.K. Walstra, D.J.A. Roelvink, and J. Groeneweg. Calculation of wave-driven currents in a 3D mean flow model. *Proceedings of the 27th International Conference on Coastal Engineering*, 276, 01 2000.

[117] D.T. Wang, L.H. Ju, J.L. Zhu, Z. Wang, T.T. Sun, and W.Q. Chen. Experimental study on mean overtopping of sloping seawall under oblique irregular waves. *China Ocean Engineering*, 31(3):350–356, June 2017.

[118] G. Wang, J.H. Zheng, Q.H. Liang, W. Zhang, and C. Huang. Theoretical analysis of harbor resonance in harbor with an exponential bottom profile. *China Ocean Engineering*, 29(6):821–834, December 2015.

[119] H. Wang, G. Miao, and L.-H. Lin. A time-dependent nearshore morphological response model. *Coastal Engineering Proceedings*, pages 2513–2527, 06 1993.

[120] A. Watanabe, K. Maruyama, T. Shimizu, and T. Sakakiyama. Numerical prediction model of three-dimensional beach deformation around a structure. *Coastal Engineering Journal*, 29:179–194, 12 1986.

[121] J. R. Weggel and N. Rajendran. Optimization of a shore protection scheme for the west coast of India. In W. Kato, B. C. Gerwick, M. Homma, R. Lenschow, O. T. Magoon, C. C. Mei, S. Motora, K. Okamura, and J. Penzien, editors, *Ocean Space Utilization '85*, pages 237–248, Tokyo, 1985. Springer Japan.

[122] J. Williams, L. Esteves, and L. Rochford. Modelling storm responses on a high-energy coastline with XBeach. *Modeling Earth Systems and Environment*, 1, 05 2015.

[123] C.S. Wu and P. L.-F. Liu. Finite element modeling of nonlinear coastal currents. *Journal of Waterway, Port, Coastal, and Ocean Engineering*, 111(2):417–432, 1985.

[124] G.W. Wu, H. Wu, X.Y. Wang, Q.W. Zhou, and X.M. Liu. Tidal turbine array optimization based on the discrete particle swarm algorithm. *China Ocean Engineering*, 32(3):358–364, jun 2018.

[125] Y. Xu, Y. Cai, T. Sun, X. Yin, Q. Tan, J. Sun, and J. Peng. Ecological preservation based multi-objective optimization of coastal seawall engineering structures. *Journal of Cleaner Production*, 296:126515, 2021.

[126] M. Yamaguichi and Y. Nishioka. Numerical simulation on the change of bottom topography by the presence of coastal structures. *Coastal Engineering Proceedings*, 1(19):117, Jan. 1984.

[127] W.C. Zhang, H.X. Liu, L. Zhang, and X.W. Zhang. Hydrodynamic analysis and shape optimization for vertical axisymmetric wave energy converters. *China Ocean Engineering*, 30(6):954–966, dec 2016.

[128] N. Zimmermann, K. Trouw, L. Wang, M. Mathys, R. Delgado, and T. Verwaest. Longshore transport and sedimentation in a navigation channel at Blankenberge (Belgium). *Coastal Engineering Proceedings*, 1, 12 2012.

[129] J. Zyserman and H. Johnson. Modelling morphological processes in the vicinity of shore-parallel breakwaters. *Coastal Engineering*, 45:261–284, 05 2002.